Vol. 299, No. 1, December 20, 1994

ISSN 0003-2670

ANALYTICA CHIMICA ACTA

An international journal devoted to all branches of analytical chemistry

ELSEVIER

ANALYTICA CHIMICA ACTA

Scope. *Analytica Chimica Acta* publishes original papers, rapid publication letters and reviews dealing with every aspect of modern analytical chemistry. Reviews are normally written by invitation of the editors, who welcome suggestions for subjects. Letters can be published within **four months** of submission. For information on the Letters section, see inside back cover.

Submission of Papers

Americas

Prof. Harry L. Pardue
Department of Chemistry
1393 BRWN Bldg, Purdue University
West Lafayette, IN 47907–1393
USA

Tel:(+1-317) 494 5320
Fax:(+1-317) 496 1200

Computer Techniques

Prof. J.T. Clerc
Universität Bern
Pharmazeutisches Institut
Baltzerstrasse 5, CH-3012 Bern
Switzerland

Tel:(+41-31) 6314191
Fax:(+41-31) 6314198

Prof. Sarah C. Rutan
Department of Chemistry
Virginia Commonwealth University
P.O. Box 2006
Richmond, VA 23284-2006
USA
Tel:(+1-804) 367 7517
Fax:(+1-804) 367 8599

Other Papers

Prof. Alan Townshend
Department of Chemistry
The University
Hull HU6 7RX
Great Britain

Tel:(+44-482) 465027
Fax:(+44-482) 466410

Prof. Willem E. van der Linden
Laboratory for Chemical Analysis
Department of Chemical Technology
Twente University of Technology
P.O. Box 217, 7500 AE Enschede
The Netherlands
Tel:(+31-53) 892629
Fax:(+31-53) 356024

Prof. Paul Worsfold
Dept. of Environmental Sciences
University of Plymouth
Plymouth PL4 8AA
Great Britain

Tel:(+44-752) 233006
Fax:(+44-752) 233009

Submission of an article is understood to imply that the article is original and unpublished and is not being considered for publication elsewhere. *Anal. Chim. Acta* accepts papers in English only. There are no page charges. Manuscripts should conform in layout and style to the papers published in this issue. See inside back cover for "Information for Authors".

Publication. *Analytica Chimica Acta* appears in 18 volumes in 1995 (Vols. 297–314). *Vibrational Spectroscopy* appears in 2 volumes in 1995 (Vols. 8 and 9). Subscriptions are accepted on a prepaid basis only, unless different terms have been previously agreed upon. It is possible to order a combined subscription (*Anal. Chim. Acta* **and** *Vib. Spectrosc.*).
Our p.p.h. (postage, packing and handling) charge includes surface delivery of all issues, except to subscribers in the U.S.A., Canada, Australia, New Zealand, China, India, Israel, South Africa, Malaysia, Thailand, Singapore, South Korea, Taiwan, Pakistan, Hong Kong, Brazil, Argentina and Mexico, who receive all issues by air delivery (S.A.L.–Surface Air Lifted) at no extra cost. For Japan, air delivery requires 25% additional charge of the normal postage and handling charge; for all other countries airmail and S.A.L. charges are available upon request.

Subscription orders. Subscription prices are available upon request from the publisher. Subscription orders can be entered only by calendar year and should be sent to: Elsevier Science B.V., Journals Department, P.O. Box 211, 1000 AE Amsterdam, The Netherlands. Tel: (+31-20) 4853 642, Telex: 18582, Telefax: (+31-20) 4853 598, to which requests for sample copies can also be sent. Claims for issues not received should be made within six months of publication of the issues. If not they cannot be honoured free of charge. Readers in the U.S.A. and Canada can contact the following address: Elsevier Science Inc., Journal Information Center, 655 Avenue of the Americas, New York, NY 10010, U.S.A. Tel: (+1-212) 633 3750, Telefax: (+1-212) 633 3990, for further information, or a free sample copy of this or any other Elsevier Science journal.
Advertisements. Advertisement rates are available from the publisher on request.

US mailing notice – Analytica Chimica Acta (ISSN 0003-2670) is published 3 times a month (total 54 issues) by Elsevier Science B.V. (Molenwerf 1, Postbus 211, 1000 AE Amsterdam). Annual subscription price in the USA US$ 3677.75 (valid in North, Central and South America), including air speed delivery. Second class postage paid at Jamaica, NY 11431. *USA Postmasters*: Send address changes to Anal. Chim. Acta, Publications Expediting, Inc., 200 Meacham Av., Elmont, NY 11003. Airfreight and mailing in the USA by Publication Expediting.

ANALYTICA CHIMICA ACTA

An international journal devoted to all branches of analytical chemistry

(Full texts are incorporated in CJELSEVIER, a file in the Chemical Journals Online database available on STN International; Abstracted, indexed in: Aluminum Abstracts; Anal. Abstr.; Biol. Abstr.; BIOSIS; Chem. Abstr.; Curr. Contents Phys. Chem. Earth Sci.; Engineered Materials Abstracts; Excerpta Medica; Index Med.; Life Sci.; Mass Spectrom. Bull.; Material Business Alerts; Metals Abstracts; Sci. Citation Index)

VOL. 299 NO. 1 CONTENTS DECEMBER 20, 1994

ANALYTICA CHIMICA ACTA
VOL. 299 (1994)

ANALYTICA CHIMICA ACTA

An international journal devoted to all branches of analytical chemistry
Revue internationale consacrée à tous les domaines de la chimie analytique
Internationale Zeitschrift für alle Gebiete der analytischen Chemie

Anal. Chim. Acta, Vol. 299 (1994)

ELSEVIER

Amsterdam – Lausanne – New York – Oxford – Shannon – Tokyo

0003-2670/94/$07.00

ELSEVIER

Analytica Chimica Acta 299 (1994) 1–7

ANALYTICA CHIMICA ACTA

Determination of lead in whole blood using a capacitively coupled microwave plasma atomic emission spectrometer

Michael W. Wensing, Don-Yuan Liu, Benjamin W. Smith, James D. Winefordner *

Department of Chemistry, University of Florida, Gainesville, FL 32611, USA

Received 18 May 1994; revised manuscript received 18 July 1994

Abstract

Lead in whole blood was determined with a capacitively coupled microwave plasma atomic emission spectrometer with no dilution or addition of matrix modifiers. The sample was vaporized directly from the plasma-supporting electrode into the plasma, ensuring 100% transfer of the sample into the plasma. Microwaves were used to dry the sample, a low-power plasma was used to ash the sample, and a higher-power plasma was used to atomize and excite the sample. A detection limit of 7 ppb Pb (35 pg Pb) was obtained using 5-μl aliquots. The method was accurate (95% confidence) for blood containing 188 and 573 ppb Pb, but gave a high result with blood containing 48 ppb Pb. The precision was 15%.

Keywords: Atomic emission spectrometry; Blood; Lead; Microwaves; Plasma

1. Introduction

Lead has recently been shown to be more toxic than previously thought. Accordingly, the Centers for Disease Control lowered the level of concern for blood lead to 10 μg/dl in 1991 [1]. As a result, the most popular screening technique that was previously used, the indirect determination of lead in whole blood by the fluorescence of zinc protoporphyrin, was invalidated since this method cannot be used when the blood lead concentration is below 20 μg/dl [2]. Therefore, it is important to characterize new methods that are sufficiently sensitive to determine lead at low levels, yet affordable enough to be used as screening techniques.

Several methods are sufficiently sensitive to determine lead in whole blood at concentrations below 10 μg/dl including anodic stripping voltammetry (ASV), potentiometric stripping analysis (PSA), and electrothermal atomization atomic absorption spectrometry (ETA-AAS). However, all of these methods require dilution of the sample and the addition of chemical reagents, which increases the likelihood of sample contamination. ASV and PSA require the addition of acids to lyse the red blood cells where lead is bound, a buffer solution, and a surfactant that helps to stabilize the solution [3]. Accurate and precise results for the rapid determination of lead in whole blood by ETA-AAS requires dilution of the blood sample with Triton X-100 (a surfactant) and the use of a matrix modifier containing phosphate such as ammonium phosphate, diammonium hydrogenphosphate, or phosphoric acid [4]. The Triton X-100 lyses the red blood cells, while the phosphate-containing salts allow higher ashing temperatures, ensuring the complete removal of carbonaceous material. Using simple dilution procedures, i.e., dilution of the blood sample with Triton X-100 and

* Corresponding author.

SSDI 0003-2670(94)00319-X

water, lower ashing temperatures are used, resulting in carbonaceous deposits which accumulate inside the atomizer. These deposits retain lead and are not completely removed during the atomization step or the cleaning step. This results in a continual decrease in instrumental sensitivity for subsequent analyses [5]. ETA-AAS requires at least a five-fold dilution of the sample for accurate results [6]. In our laboratory, we are evaluating a technique that involves no sample pretreatment. This paper describes the evaluation of a capacitively coupled microwave plasma atomic emission spectrometer (CMP-AES) for the direct determination of lead in whole blood.

The CMP-AES has been evaluated by several authors [7] and differs from the microwave-induced plasma atomic emission spectrometer (MIP-AES) by the way energy is transferred to the plasma. In an MIP-AES, microwave energy is stored in a cylindrical resonator (the Beenakker cavity), and the plasma torch is placed at the center of the resonator cavity where the electric field is at a maximum. The plasma is initiated with a spark [8]. In the CMP-AES, the microwave energy is stored in a rectangular waveguide where the electric component of the microwave field couples to an electrode that is held in the central channel of the plasma torch. The torch, containing the electrode, is placed in the waveguide where the electric field is at a maximum. Because of the small diameter (<3 mm) of the electrode, the magnitude of the electric field strength at the tip of the electrode is great and a plasma will spontaneously ignite. Another major difference between the CMP- and MIP-AES is that the CMP-AES is much less affected by impedance changes. Stable operation of an MIP-AES requires the use of tuning stubs to match the load impedance with the generator and resonator impedance. The CMP-AES does not require tuning elements for stable operation.

In the analysis of lead in whole blood, the Centers for Disease Control have limited the maximum sample size to 200 μl which requires that a discrete sample introduction method be used. Discrete sample introduction is simplified in a CMP-AES because microliter volumes can be deposited directly on the plasma-supporting electrode, resulting in 100% transfer of the sample to the plasma with very little dilution by the plasma gas. The sample is dried at low microwave powers by direct absorption of microwaves and also indirectly through capacitive heating of the electrode. At higher microwave powers, a plasma ignites on the electrode, vaporizing the sample and atomizing and exciting the analyte. The atomic emission is detected as a transient signal. Ali et al. [9,10] used this approach with a tungsten filament loop and with a graphite cup electrode. The graphite cup was used for the direct analysis of solid samples and the determination of several elements in coal fly ash and tomato leaf standard reference materials (SRMs) [9]. The filament electrode was applied to the measurement of several elements in aqueous solutions, and detection limits in the 1–100 pg range were obtained for twelve elements [10]. This introduction of samples directly from the plasma-supporting electrode is advantageous over other electrothermal vaporization techniques where the sample is diluted by the carrier gas, and some of the sample may be retained on the tubing walls leading from the vaporization device to the plasma [11].

A disadvantage of the CMP electrode is that it erodes with time and appears in the emission spectra, so it is necessary to choose an electrode material which will not produce interfering spectral emission lines. However, the rate of erosion of the electrode can be limited to a great extent by reducing air entrainment into the plasma. This was accomplished by purging the torch for at least 30 s, prior to igniting the plasma.

This paper characterizes the CMP-AES for the determination of Pb in whole blood using a tungsten filament electrode and the discrete sampling technique mentioned above. Spectral interferences are characterized, the optimization procedure is described, and the technique is applied to blood analysis. Helium is used as the plasma gas due to its excellent excitation efficiency and low background characteristics.

2. Experimental

2.1. Apparatus

The experimental apparatus has been described previously [12]. Several modifications have been made to the setup. The high voltage, voltage-regulated dc power supply, which was previously used to supply power to the magnetron, was replaced with a current-regulated analog-programmable power supply (Model 106-05R, Bertran High Voltage, Hicksville, NY, USA). The magnetron is a non-linear device which has

a voltage–current response similar to that of a diode. Consequently, a more stable microwave power output is obtained when a current-regulated power supply is used to control the magnetron than a voltage-regulated power supply [13]. In addition, more flexibility is obtained with a programmable power supply. The power supply settings and timing were controlled with a computer and a digital-to-analog converter (DAC) (Model SR 245, Stanford Research Systems, Palo Alto, CA, USA). Software was written using QuickBasic® 4.5 to control the DAC. All reported microwave powers refer to the input power to the microwave magnetron and are simply the product of the current and voltage applied to the magnetron.

2.2. Procedure

Aqueous samples were deposited on the electrode with an air displacement pipet, and dried at 70 W for 90 s. No purge gas was used. Helium could not be used as a purge gas since it would autoignite at 70 W. After the drying step, the power was decreased to 14 W and He was allowed to purge the torch at a flow-rate of 10 l/min for a period of 30 s. The purge removed air from the plasma torch. Oxygen is very detrimental to the tungsten electrode, and removing air from the torch extended the lifetime of the electrode significantly. The purge also removed a spectral interferent which was identified as N_2^+. Lead emission at 405.8 nm could not be resolved from the N_2^+ emission which has a band head at 405.9 nm and is degraded toward the ultraviolet region [14]. The N_2^+ emission spectrum was completely eliminated after a 30-s helium purge. After the 30-s purge, the power was increased to 170 W and a He plasma autoignited. This resulted in the vaporization of the sample and atomization and excitation of the analyte. The transient signal was detected with a monochromator and a time-resolved photodiode-array detector. A second detector, which consisted of a photomultiplier tube and a neutral density filter, was used to determine when the plasma ignited and to synchronize the photodiode-array detector with the ignition of the plasma. The signal from this trigger circuit was used to initiate the photodiode-array data acquisition. The response time of this circuit was less than 6 ms, and the array was triggered before any Pb had vaporized. After the photodiode-array detector was triggered, spectra were integrated for 0.18 s periods a total of 40 times, and a time-resolved spectrum was obtained. For blood samples, whole blood was deposited on the electrode without any pretreatment with a positive displacement pipette. The blood was dried at 70 W for 90 s without any purge gas. Following this, the power was decreased to 55 W and He was introduced at 10 l/min. As soon as the He was introduced a plasma autoignited. This low-power plasma was used to ash the blood sample for 2 min. The power was then increased to 170 W which vaporized the sample and atomized and excited the lead. The diode-array detector was triggered just prior to increasing the power to 170 W. In order to completely remove the carbonaceous residue that remained, it was necessary to further increase the power to 200 W and to add H_2 for 1 min. This left the electrode clean and ready for the next sample.

3. Results and discussion

3.1. Characterization of whole blood spectral interferences

Whole blood has a very complex CMP-AES spectrum; therefore, the emission spectrum of whole blood around 405 nm was characterized. Aqueous standards were used to positively identify the sources of emission in the blood spectrum: 1 part per thousand (ppth) Ca as $Ca(NO_3)$, 1 ppth Mn as $Mn(NO_3)_2$, 1 ppth Cu as $CuSO_4$, 1 ppth K as KNO_3, 0.25 ppth Fe as $Fe(NO_3)_2$, and 10% Na_2CO_3. All aqueous standards contained up to 1 ppth of the interferent to be tested. If emission was not observed in aqueous spectra at a concentration of 1 ppth, then it was concluded that the emission would not be observed in whole blood. Fig. 1A depicts the emission spectrum of 5 μl of whole blood from 385 to 425 nm and represents the spectral region which was viewed by the diode-array detector. The most intense emission features in this spectral region are the CN bands, followed by Ca and K emission. Fig. 1B shows an expanded view of the whole blood emission spectrum from 403 to 409 nm. Pb emission, which was observed at 405.8 nm, lies between the K emission at 404.7 nm and the Fe emission at 406.4 nm. Emission spectra of aqueous solutions of compounds normally found in blood were measured in order to identify potential spectral interferences.

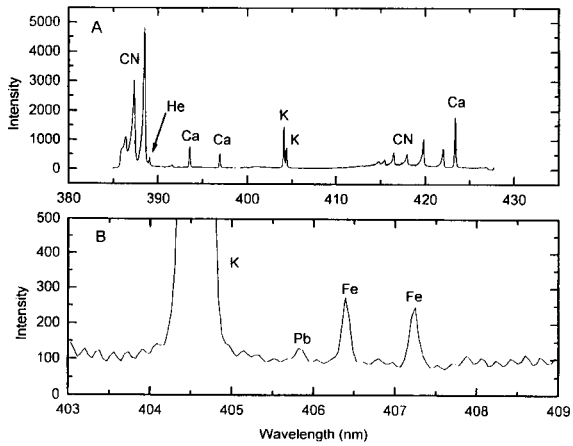

Fig. 1. CMP-AES spectra of whole blood (A) from 385 to 425 nm and (B) from 403 to 409 nm.

3.2. Optimization of the plasma ashing step

As has been reported previously [12], a low-power (55 W) plasma was used to ash blood samples prior to the atomization step. The effect of this ashing step was to remove the more volatile components of blood while leaving the less volatile components behind. It had been determined [12] that potassium chloride was removed at a higher rate than lead chloride, even though lead chloride is generally more volatile than potassium chloride. It is believed that lead chloride is quickly converted to lead oxide during the ashing step by reaction with oxygen from air entrainment. In this report, the duration of the ashing step was optimimized. Aliquots (5 μl) of whole blood which contained 747 ppb Pb were deposited on the electrode, dried, ashed for various periods of time at 55 W, and then atomized at 170 W. If the ashing time was too short, an unstable plasma resulted during the atomization step, and if too long, needless loss of lead resulted. Fig. 2 shows the signal-to-noise ratio obtained for Pb emission during the atomization step versus the ashing time. The maximum signal-to-noise ratio for Pb emission was obtained when the ashing time was about 2 min. Pb emission was not detected when the ashing step was omitted. Instead, only manganese emission was observed. The emission spectrum of whole blood obtained without an ashing step is shown in Fig. 3A, while the emission spectrum of manganese is shown in Fig. 3B. The relative intensities match closely. The emission spectrum of whole blood obtained with the optimum ashing time of 2 min is shown in Fig. 4. The emission spectrum is much simpler, and the Mn emission was greatly reduced. By comparing intensity ratios in the aqueous spectrum of Mn to that observed in the whole blood emission spectrum, it can be predicted that less than 4 counts of the Pb signal in the whole blood emission spectrum is due to Mn emission. An ashing time of 2 min was used in all further experiments.

3.3. Recovery study

The simplest way to calibrate a method is to use aqueous standards. They are readily available, inexpensive, and simple to prepare. Preparing matrix-matched standards or using the technique of standard addition for calibration is much more time-consuming. A direct comparison was made between the emission signal obtained for 3 ppm Pb in an aqueous solution and the emission signal obtained for 3 ppm Pb in a whole blood sample. Volumes of 2 μl of either sample type were deposited on the electrode, dried, ashed for 2 min at 55 W, and atomized at 170 W. The temporal profiles of lead in blood and lead in water are shown in Fig. 5. The percentage recovery, defined as the peak area of the lead signal obtained from whole blood divided by the peak area of the lead signal obtained from an aqueous sample was 90%. Since the recovery was less than 100%, calibration cannot be achieved

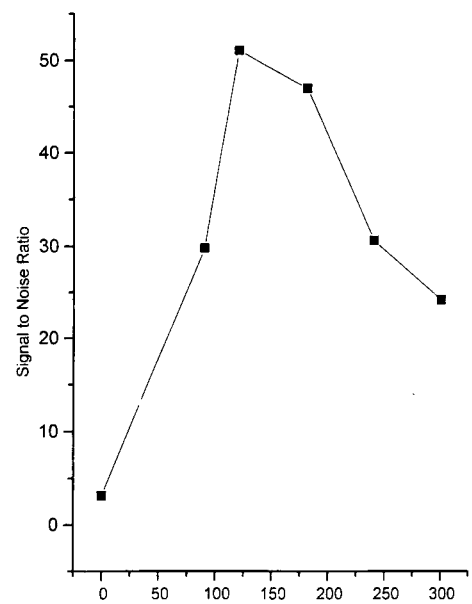

Fig. 2. CMP-AES lead signal-to-noise ratio as a function of the ashing time.

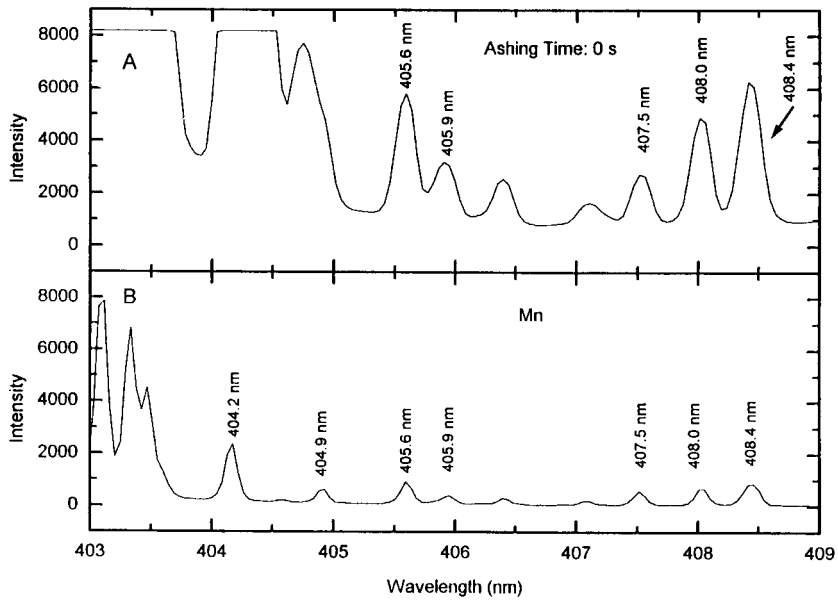

Fig. 3. CMP-AES spectra of (A) 747 ppb Pb in whole blood (the ashing time was 0 s) and (B) an aqueous solution of Mn.

using aqueous samples. However, the high percentage recovery implies that this technique is relatively free from matrix effects. The relative standard deviation (R.S.D.) of the recovery studies was 5% in aqueous solutions and 7% in whole blood.

3.4. Evaluation of the method using whole blood quality control materials (QCMs)

The accuracy of the method was determined using the method of standard additions with QCMs obtained from the Centers for Disease Control Blood Lead Laboratory Reference System. Strict precautions were observed to ensure contamination-free laboratory equipment. Glassware was soaked in a 5% nitric acid bath overnight, rinsed with doubly distilled water, and soaked overnight again to ensure that all lead in the glassware had been completely removed. Pyrex pipettes were used to deliver whole blood into 1-ml Pyrex test tubes which were used to contain the standard addition solutions. The pipettes were all checked for accuracy and precision using standard gravimetric procedures, and all had an R.S.D. less than 0.7% and were within 3% of their certified value. In addition, all components of the standard addition solutions were weighed to ensure accuracy.

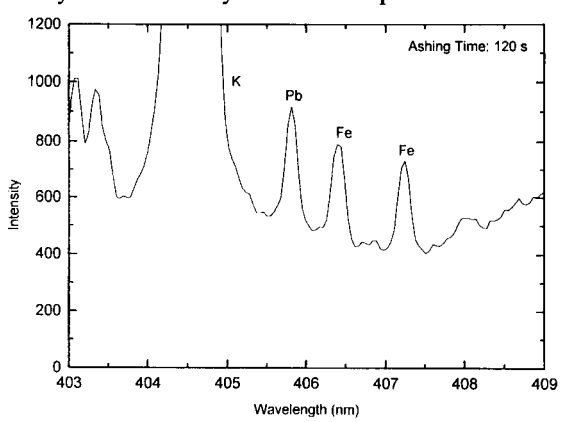

Fig. 4. CMP-AES spectrum of 747 ppb Pb in whole blood. The ashing time was 120 s.

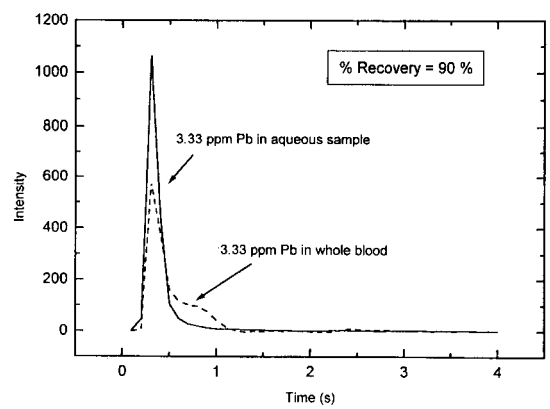

Fig. 5. Temporal emission profile of lead in aqueous and whole blood samples.

Three Centers for Disease Control QCMs were analyzed which contained 573 ppb Pb, 188 ppb Pb, and 48 ppb Pb. Four standard addition solutions were prepared in 1-ml test tubes from each QCM by adding 0.2 ml of the whole blood QCM to 0.25 ml of various concentrations of an aqueous Pb standard. After dilution, the final lead concentration added was 0 ppb Pb, 111 ppb Pb, 333 ppb Pb, and 556 ppb Pb for each standard addition solution, respectively. These solutions were then sonicated for 5 min to ensure that the whole blood mixed with the aqueous lead standard. Aliquots of 5 μl were deposited on the electrode, dried, ashed at 55 W for 2 min, and atomized and excited at 170 W for 10 s. A 1 minute cleaning step, as described above, was used to remove all carbon residue that remained on the electrode.

3.5. Signal analysis

Background correction

The background emission spectrum of blood is fairly complex, especially considering the relatively low spectral resolution (0.2 nm bandpass) that was employed in these studies. Therefore, the first-derivative method was used to zero the background [15,16]. As described previously, the diode-array detector was readout for 0.18-s periods a total of 40 times. Thus, the first spectrum represented the integration time from 0 to 0.18 s, the second from 0.18 to 0.36 s, etc. The first derivative of each individual spectrum was taken. The background-corrected lead signal was then obtained directly from the background − corrected spectrum. From the time-resolved data, the temporal profile of the Pb signal was then obtained. The Pb signal was

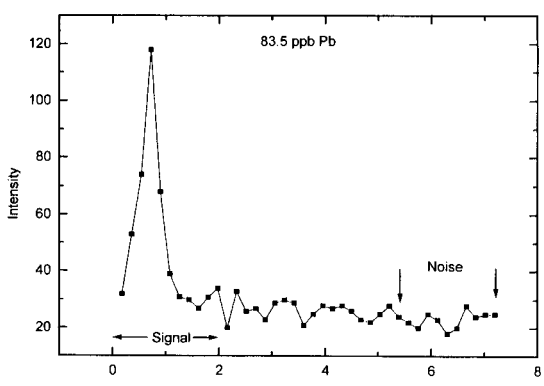

Fig. 6. Temporal emission profile of 83.5 ppb Pb in whole blood.

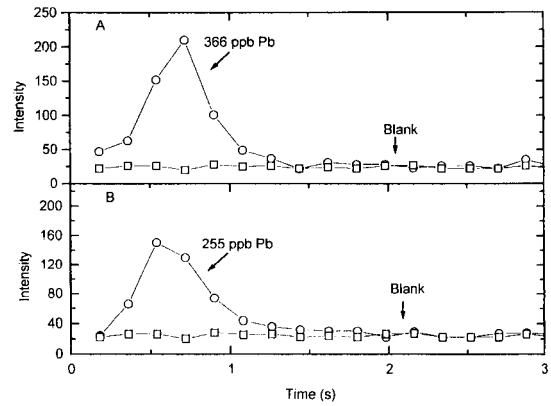

Fig. 7. Temporal emission profiles of (A) 366 ppb Pb and a blank and (B) 255 ppb Pb and a blank.

obtained by integrating the signal from 0 to 1.98 s. The noise on the Pb signal was determined by measuring the fluctuation in the background after the Pb signal had decayed to background level (from 5.4 to 7.2 s) as illustrated in Fig. 6. The Pb had been completely removed at this point, however, the major matrix constituents of blood, K, Ca, etc. remained. In addition, in Fig. 7A and B, the temporal emission profiles of samples containing 366 and 255 ppb Pb, respectively, are shown along with the temporal emission profile of a blank. Fig. 8 shows a spectrum of 83.5 ppb lead in whole blood as a function of wavelength rather than time.

3.6. Analytical figures of merit

The possibility of proportional errors was checked by using standard additions. The *t*-test was performed to determine if the measured concentration was signif-

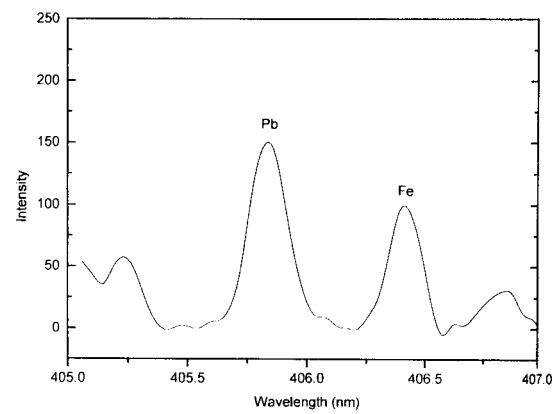

Fig. 8. CMP-AES spectrum of 83.5 ppb Pb.

icantly different from the actual concentration at the 95% confidence level ($n=5$). In the case of the 573- and 188-ppb QCMs, there was no significant difference between the measured (661 ± 91 and 194 ± 19 ppb) and actual concentrations. However, the predicted value for the 48-ppb standard was 81% too high (90 ± 13). The cause could be attributed to sample contamination. Also, since each QCM was diluted 20:45 the zero concentration, before standard addition, contained only 21 ppb Pb, which is within a factor of 3 of the detection limit. It should be noted that in a screening technique, matrix-matched standards would be employed for calibration rather than the standard addition technique. This is beneficial in that sample dilution is not required. Blood standards with certified lead concentrations are commercially available.

The detection limit based on 3 standard deviations (S.D.s) of the background signal was 7 ppb. For the 5-μl aliquots used, the concentration detection limit corresponded to an absolute detection limit of 35 pg. The detection limit of the method meets the requirements set by the Centers for Disease Control (<20 ppb).

The overall precision of the method was determined by averaging the precision values obtained for every sample run. In total, this represented 60 runs. The average precision was approximately 15%. This precision did not quite meet the requirements of the Centers for Disease Control, which require an average precision less than 10%; however, it was close enough to warrant further investigation. The precision was limited by sample loading of the plasma, and could be lowered by increasing the plasma power, decreasing the sample size, or using an internal standard which would behave similarly to lead during the ashing and atomization stages. The analysis time per sample including the cleanup step was just below 5 min and meets the requirements set by the Centers for Disease Control.

4. Conclusions

The CMP-AES method for the determination of Pb in blood is very sensitive (detection limit 7 ppb or 35 pg). The method was not accurate for concentrations below 48 ppb, although it was shown to be accurate at concentrations of 188 and 573 ppb. The method was rapid with an analysis time of less than 5 min per sample.

Future work will involve the study of Pb emission in whole blood from a nickel cup electrode. Preliminary work conducted by the authors has shown that these nickel cups can sustain at least 600 W of plasma power, making the plasma much more robust in the presence of the blood matrix. In addition, oxygen may be added during the ashing step, as nickel oxidizes much less rapidly than tungsten, to assist in the removal of the blood matrix.

Acknowledgements

This publication was supported by Grant No. R08/CCR408614-02 from the Centers for Disease Control (Atlanta, GA, USA). Its contents are solely the responsibility of the authors and do not necessarily represent the official views of the Centers for Disease Control.

References

[1] US Centers for Disease Control (CDC), Preventing Lead Poisoning in Young Children: A Statement by the Center for Disease Control in October, 1991, US Department of Health and Human Services/Public Health Service/Centers for Disease Control, Atlanta, GA, 1991.
[2] D. Noble, Anal. Chem., 65 (1993) 267A.
[3] S.M. Roda, R.D. Greenlan, R.L. Bornschein and P.B. Hammond, Clin. Chem., 34 (1988) 563.
[4] Z. Benzo, R. Raik, N. Carrion and D. Loreto, J. Anal. At. Spectrom., 4 (1989) 397.
[5] K.S. Subramanian, Prog. Anal. Spectrosc., 9 (1986) 237.
[6] B.E. Jacobson, G. Lockitch and G. Quigley, Clin. Chem., 37 (1991) 515.
[7] J. Dahmen, ICP Inf. Newslett., 6 (1981) 576.
[8] A.T. Zander and G.M. Hieftje, Appl. Spectrosc., 35 (1981) 357.
[9] A.H. Ali, K.C. Ng and J.D. Winefordner, J. Anal. At. Spectrom., 6 (1991) 211.
[10] A.H. Ali and J.D. Winefordner, Anal. Chim. Acta, 264 (1992) 327.
[11] J. Alvarado, P. Cavalli, N. Omenetto and G. Rossi, Anal. Lett., 22 (1989) 2975.
[12] M.W. Wensing, B.W. Smith and J.D. Winefordner, Anal. Chem., 66 (1994) 531.
[13] J.R. Brandenberger, Rev. Sci. Instrum., 42 (1971) 1535.
[14] R.W.B. Pearce and A.G. Gaydon, The Identification of Molecular Spectra, Wiley, New York, NY, 4th ed., 1976.
[15] T.C. O'Haver, Anal. Chem., 51 (1979) 91A.
[16] A. Savitzky and M. Golay, Anal. Chem., 36 (1964) 1628.

ELSEVIER

Analytica Chimica Acta 299 (1994) 9–16

ANALYTICA CHIMICA ACTA

An improved method for decontaminating polar snow or ice cores for heavy metal analysis

Jean-Pierre Candelone [a], Sungmin Hong [a], Claude F. Boutron [a,b,*]

[a] *Laboratoire de Glaciologie et Géophysique de l'Environnement du CNRS, 54, rue Molière, Domaine Universitaire, B.P. 96, 38402 St. Martin d'Hères, France*

[b] *UFR de Mécanique, Université Joseph Fourier de Grenoble, Domaine Universitaire, B.P. 68, 38041 Grenoble, France*

Received 23 May 1994; revised manuscript received 20 July 1994

Abstract

An improved method has been developed for the decontamination of Greenland and Antarctic snow or ice cores for heavy metal analysis. The investigated core sections are chiselled while being held horizontal in a polyethylene lathe inside a laminar flow clean bench in a cold room. Each veneer layer and the final inner core are then analysed for Pb, Cd, Zn and Cu by graphite furnace atomic absorption spectrometry in clean room conditions. The procedural blank was found to range from 0.015 pg/g for Cd up to 0.25 pg/g for Cu. The quality of the decontamination was checked by studying changes in heavy metals concentrations from the outside to the center of each core section. In most cases, good plateaus of concentrations were observed in the central parts, then indicating that contamination present on the outside of the cores was not transferred to these central parts. Various Greenland and Antarctic cores were decontaminated, giving new insights into the past and recent occurrence of heavy metals in the atmosphere of both hemispheres.

Keywords: Atomic absorption spectrometry; Heavy metals; Lead; Cadmium; Zinc; Copper; Snow; Ice; Greenland; Antarctica; Global pollution

1. Introduction

The successive well preserved snow and ice layers deposited in the large Antarctic and Greenland ice sheets are unique archives of the past and recent changes in the atmospheric concentrations of heavy metals. Deciphering these archives for heavy metals has unfortunately proved to be very difficult mainly because the concentrations to be measured are extremely low, down to the sub pg/g level.

A key point to obtain reliable data is in the cleanliness of the available samples. For near surface snow, clean samples can be obtained from the walls of clean hand dug pits [1,2] or trenches [3], or by using specially designed clean augers [4]. But deeper layers can only be reached by using large size electromechanical [5] or thermal [6] drills. Such drills provide us with snow/ice cores whose diameters range from about 3 to 5 inches (7.5 to 13 cm), the most frequent diameter being 4 inches (10.2 cm).

A major problem is that the cores are always more or less contaminated on their outside. This contamination originates from various contributions. The main one is the wall retaining fluid (amongst the fluid used are kerosene and freon [7] and *n*-butyl acetate [8]) when such a fluid is required to prevent the closing of the drilling hole at great depths. But other contributions can also originate from the body of the drill, the cable

* Corresponding author.

SSDI 0003-2670(94)00327-0

and the handling, packing and storage of the core.

To obtain reliable heavy metals data from such cores, it is therefore essential to be able to decontaminate them by removing the outside contamination without transferring it to the most central parts and to check the efficiency of the procedure.

Although this problem has already been tackled by a few investigators [9–12], none of them has until now developed a fully satisfying method, i.e. a method which is ultraclean, suitable both for snow or ice cores, not too much time consuming and which allows to check the efficiency of the procedure.

We present here an improved ultraclean mechanical decontamination procedure for snow or ice cores. It has been successfully used for the decontamination of various sections of several snow and ice cores from Greenland and Antarctica.

2. Experimental

The experimental procedure requires two operators. It consists in chiselling successive layers of snow or ice from the outside to the central part of the core using ultraclean stainless steel chisels. The core is kept horizontal, its extremities tightly secured in low density polyethylene (LDPE) tumblers.

2.1. Laminar flow clean bench in a cold room

The whole decontamination procedure takes place in a laminar flow clean bench located inside a cold room at −15°C. The inside of the bench is entirely made out of plastics. Moreover, the working area is covered with a thin LDPE film which is changed regularly. The bench is fitted with a special high efficiency particulate air (HEPA) filter (99.999% efficiency at 0.5 μm) with particulate board frames and plastic separators. It has no rubber or polyurethane compressible gasket: the seal between the HEPA filter frame and the ceiling of the bench is made with silicone cement [13]. The operators wear full clean room garb over their warm clothing. Over their isothermic gloves, they also wear shoulder length LDPE gloves and wrist length LDPE gloves over these. These last gloves are changed as often as required.

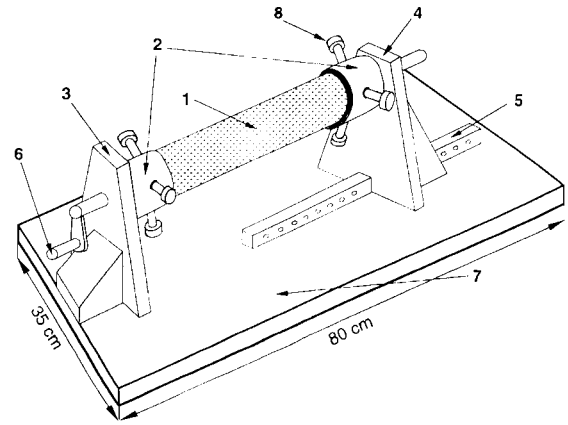

Fig. 1. Schematic diagram of the low density polyethylene (LDPE) lathe used for the decontamination of the snow or ice cores. (1) Snow or ice core (length up to 65 cm); (2) LDPE tumblers; (3) fixed LDPE pillar; (4) movable LDPE pillar which can be slid along the guide rail; (5) LDPE guide rail; (6) LDPE crank used to rotate the core; (7) LDPE heavy base plate of the lathe; (8) LDPE screw.

2.2. Polyethylene lathe

A major improvement is the fact that during the chiselling, the core is not held with the hands of the operator and is not laying on any working surface. Instead, it remains horizontal about 20 cm above the plastic working surface as its extremities are pinched in two LDPE tumblers (Fig. 1). The lathe is designed so that it can be used in order to decontaminate snow or ice cores whose lengths range from 25 to 65 cm. Also, it is suitable not only for cylindrical cores with full section but also for cores for which only part of the cross section is available. This last situation occurs frequently for ice cores obtained as part of international programmes: a given core section is indeed cut into several parts used for different kinds of measurements (Fig. 2). At both extremities, the core is fastened in the

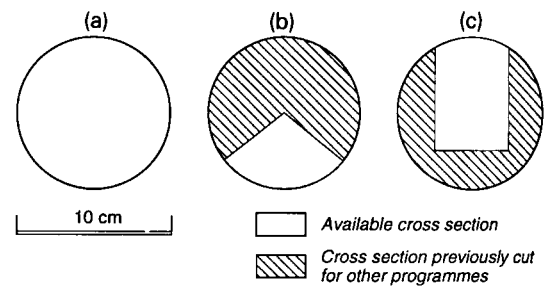

Fig. 2. Greenland and Antarctic snow or ice cores: schematic view of different typical cross sections available for heavy metals investigations.

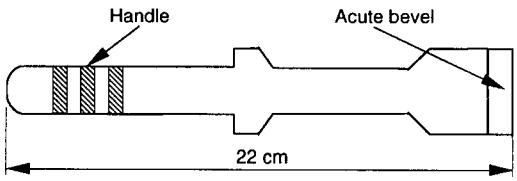

Fig. 3. Stainless steel chisel used for the chiselling of the successive veneer layers.

tumblers using 3 to 6 home made LDPE screws which are screwed, perpendicular to the axis of the core, through threaded holes made in the lateral side of the tumblers (Fig. 1). Depending on the available cross section, several sets of screws of different lengths can be used.

2.3. Chisels

It would have been preferable to make the chisels out of plastics such as LDPE, fluorinated ethylene propylene (FEP) or perfluoroalkoxy (PFA) Teflon. Unfortunately, such plastics are too soft for high density snow and for ice. Therefore, the chisels chosen are similar to those used by Ng and Patterson [9] and Boutron and Patterson [10,11] (Fig. 3). They are made out of a single piece of 2 mm thick plate of stainless steel (ref. 316 L). The cutting edge is 3 cm wide and 4 cm long. It is sharpened to a single acute bevel with an angle of 30°.

Before use, the chisels, cleaned as described in 2.5, are kept horizontal inside a LDPE box, each of them fitted separately in a display rack which prevents any contact between the chisels and allows the cutting edges not to touch the walls of the box.

2.4. Description of the procedure

The core section to be decontaminated is taken out from the LDPE bag inside which it was transported frozen from Antarctica or Greenland back to France. After changing their outer wrist-length LDPE gloves, the two operators introduce the core inside the laminar flow clean bench and put it in the lathe (Fig. 1). The core is then firmly secured between the two tumblers with the LDPE screws, Fig. 1.

A first veneer layer 5 to 10 mm thick is then chiselled as follows. A shallow chord shaving is first made from one end of the core to the other parallel to its axis, the snow or ice chips being allowed to fall directly into a specially designed LPDE tray held by the second investigator. Using the crank, the cut is rotated upward about 30° and another shallow chord shaving is made. The procedure is then repeated until the whole exposed outside surface has been chiselled. The chips obtained from this first layer are then transferred from the tray into an ultraclean 1-l wide mouth LDPE bottle and kept frozen until analysis.

The operators then put on new fresh pairs of LDPE gloves and a second layer is chiselled using another chisel and a new fresh tray. Depending on the initial cross section of the core, this procedure is repeated up to 4 times then giving a maximum of 4 successive layers from the outside towards the center.

The remaining inner core (whose diameter ranges from 2 to 4.5 cm) is then recovered as follows: the first operator holds it firmly with all LDPE home made tongs while the other operator breaks the right end with the last chisel. The right hand pillar of the lathe (part 4 in Fig. 1) is then moved away. An ultraclean [13] 1-l wide mouth LDPE bottle is pushed onto the inner core until about half of it is introduced into the bottle. The inner core is broken in its middle with the chisel and its second half is introduced into a second 1-l bottle. Then the left edge of the inner core is broken with the chisel.

The bottles containing the chips from the successive veneer layers and the two parts of the inner core are then packed into double sealed acid cleaned LDPE bags and brought to the main clean laboratory at 20°C [13].

2.5. Cleaning procedures

They are similar to those described in full detail elsewhere [13]. For the various small size items such as the tumblers, the screws, the trays and the 1-l bottles, the initial cleaning before the first use involved degreasing with $CHCl_3$, then soaking one month in a first acid bath at 50°C (25% Merck "Suprapur" HNO_3 diluted in ultrapure water [13]), one month in a second acid bath at 50°C (0.1% ultrapure HNO_3 from US National Institute of Standards and Technology (NIST) [14] diluted in ultrapure water [13]), and finally one month in a third 0.1% ultrapure NIST HNO_3 bath at 50°C. Transfers from one bath to the next one are made using home made LDPE tongs.

Table 1
Comparative determination of heavy metals in the water used to make the artificial ice core, in the last veneer layer and in the inner core of this artificial core

	Measured concentration (pg/g)			
	Pb	Cd	Cu	Zn
Reference water used to make the core	0.25	0.01	0.2	0.3
Veneer layer adjacent to the inner core	0.42	0.033	0.8	1.25
Inner core	0.36	0.025	0.45	0.5

The cleaning between each core decontamination is similar except that soaking is for only 2 h in the first bath and for 3 days in the other ones.

For the very large size items such as the basement of the lathe, a simplified procedure was used. It however also involved extensive cleaning with HNO_3.

Finally, the cleaning procedure for the chisels involved degreasing with ether, then overnight soaking in 60% HNO_3 bath (Merck "Suprapur" diluted in purest water) and finally soaking in a series of two 0.1% NIST HNO_3 baths for one week (for the initial cleaning, immersions were for a much longer time period).

2.6. Analytical procedures

Inside the clean laboratory [13], each veneer layer and the inner core are melted separately in the 1-l wide mouth LDPE bottle in which they were kept. Various aliquots are then taken in 15- or 60-ml ultraclean [13] LDPE bottles. A 5-ml aliquot is first taken for the direct measurement of Zn, Al and Na by graphite furnace atomic absorption spectrometry (GFAAS) without preconcentration using a Perkin Elmer 2380 spectrometer and HGA 500 graphite furnace (pyrolitically coated graphite tubes) [15]. A 50-ml aliquot is then taken for the determination of Pb, Cd and Cu by GFAAS after preconcentration ($\times 50$) by non boiling evaporation [15].

If necessary, additional aliquots are also made for subsequent analysis of Pb isotopes [16], organo Pb compounds [17], Hg [18] and Bi [19,20]. These last measurements will not be discussed in the present paper.

Table 2
Procedural blank obtained from the analysis of the artificial ice core

	Pb	Cd	Cu	Zn
Veneer layer	0.17	0.023	0.6	0.95
Inner core	0.11	0.015	0.25	0.2

3. Results and discussion

3.1. Determination of the procedural blank

Such determination is essential to obtain fully reliable data. The procedural blank was determined by processing an artificial ice core made out by freezing ultrapure water [13] whose composition (Table 1) was known beforehand. This core was prepared by freezing 2 l of ultrapure water inside a 2-l LDPE ultraclean bottle. The inside diameter of the bottle was about 11.2 cm, then allowing to prepare an artificial ice core whose diameter was similar to that of real Greenland or Antarctic cores.

The bottle was cut using an acid cleaned stainless steel scalpel and the artificial ice core (length about 20 cm) so obtained was chiselled using exactly the same procedure as previously described in 2.4. Three layers were chiselled before getting the final inner core. Each layer and the inner core were analysed separately.

As shown in Table 1, heavy metals concentrations are found to be slightly higher in the last veneer layer and in the inner core than in the reference water used to prepare the core. The differences so observed, listed in Table 2, represent the procedural blank. This procedural blank will then be used for the correction of all the values obtained for Greenland and Antarctic real cores. For the inner core, the blank values are found to range from 0.015 pg/g for Cd up to 0.25 pg/g for Cu (these values include the blank of the non boiling evaporation procedure, which represents a rather small contribution to the total blank). For recent Greenland snow

cores in which the concentrations are relatively high due to very significant anthropogenic contribution, this procedure blank contribution is extremely small, it represents less than a few percent of the measured concentrations. For ancient Greenland or Antarctic ice, on the other hand, it can be very significant (up to about 30% for Cu, 25% for Pb, and 10% for Cd and for Zn) since heavy metals concentrations in such ancient ice are much lower.

It is interesting to mention that the concentrations measured in the veneer layers are significantly higher for all four metals than those observed in the inner core (Table 2). This was expected since the veneer layers are subject to more handling than the inner core: the contact with the chisel is much more extensive; the chips do contact the inner tray; and they are also exposed to the air flow in the clean bench for a much longer time.

The precision of these procedural blanks is difficult to assess, since the artificial core chiselling experiment was done only once because it is very time consuming. It is however interesting to mention that the concentrations measured in the 2nd and 3rd veneer layers of the artificial core were very similar, then suggesting that the precision on the blanks is probably rather good (concentrations measured in the 1st layer were on the other hand found to be significantly higher because of the handling of the core prior to its chiselling).

It is important to emphasize that this artificial core was ice, not snow. We have however used the blank values for Greenland and Antarctic snow cores. It would indeed be extremely difficult to prepare an artificial snow core of known composition. Moreover, it is our feeling that the blank contributions for such a snow core would not be significantly different. If this is not the case, however, it is expected that the blank for the ice might rather be an upper limit of the blank for the snow: this would result into a slight over correction of the snow core data.

3.2. Outside–inside concentration profiles

For each decontaminated core section and each investigated heavy metal, it is essential to study in full details changes in the concentrations from the outside to the inner part of the core. If a clear plateau of concentration is observed in at least two consecutive layers in the central part of the core, it shows that contamination present on the outside has not penetrated to the central part of the core: the plateau value then represents the original concentration in the Antarctic or Greenland snow or ice. If, on the other hand, a continuous decrease of concentration is observed towards the center, it evidences that outside contamination has penetrated to the very center of the core: the concentration measured in the inner part will only represent an upper limit of the real concentration in the original snow or ice.

Very contrasting situations have been obtained for the different snow or ice cores which we have decontaminated in this work. Typical outside-inside profiles are discussed in the following sections.

3.3. Shallow electromechanical snow core from central Greenland

In July 1989, a 70.3 m long snow core covering the years 1772–1989 has been drilled at Summit (72°58′N, 37°64′W elevation 3238 m a.s.l., mean annual temperature −32°C) in central Greenland as part of the european "Eurocore" programme. It was obtained using a 4 inches in diameter electromechanical drill [21]. Such a drill is known to bring significant contamination on the outside of the core sections mainly because of the contact with the knives (2% C and 11.5% Cr steel) and the framework (stainless steel with Teflon coating) of the drill, and the contact of the galvanized steel cable with the walls of the drilling hole. Concentrations

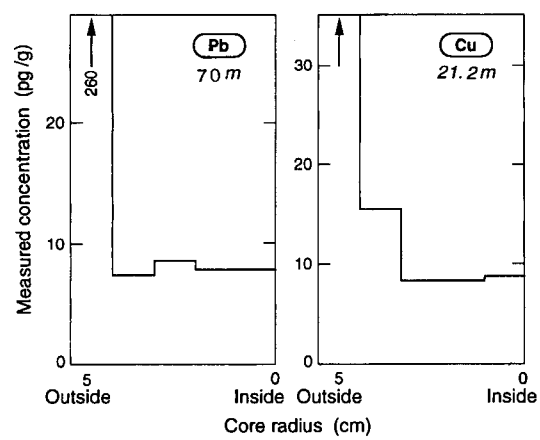

Fig. 4. Changes in Pb and Cu concentrations from the outside to the inside in two sections (depths: 69.88–70.22 and 21.10–21.45 m) of a 70.3-m snow core electromechanically drilled at Summit, central Greenland.

measured in the outermost layer of the core sections were indeed found to range from 10 to 100 pg/g for Cd, 100 to 500 pg/g for Pb and Cu, and 1000 to 5000 pg/g for Zn. It must however be emphasized that these values are for the first 1 cm or so from the outside of the core: the actual contamination present on the very outside of the core was then probably much higher. Also, it is interesting to notice that it is for Zn that the contamination is the most pronounced. This suggests that the cable does contribute a significant fraction of the contamination.

Typical outside–inside concentration profiles are shown in Figs.4, 5 and 6. In most cases, good plateaus of concentrations are obtained as illustrated in Fig. 4 for Pb in the 70-m section and for Cu in the 21.5 m section. This is also the case for the two profiles shown in Fig. 5: for these last two profiles the slight difference observed between the inner core and the next to last layer is indeed within the experimental errors. The fact that good plateaus were observed in most cases was not easy to foretell. It was indeed to be feared that outside contamination could penetrate deeply into such porous snow, which was finally not the case.

In a few cases however, we observed a continuous decrease of concentrations from the outside to the very center of the core as illustrated in Fig. 6 for Zn and Cu in the 52 m section. For these last cases, the concentrations obtained in the inner core must then be considered as upper limits of the original concentrations in the snow. The actual reasons for these few cases are not known, they could however be linked to difficulties

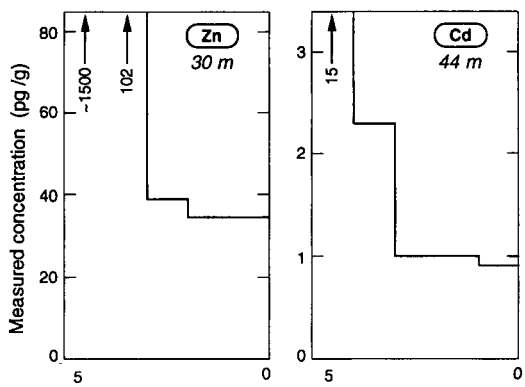

Fig. 5. Changes in Zn and Cd concentrations from the outside to the inside in two sections (depths: 29.77–30.13 and 43.87–44.45 m) of a 70.3-m core electromechanically drilled at Summit, central Greenland.

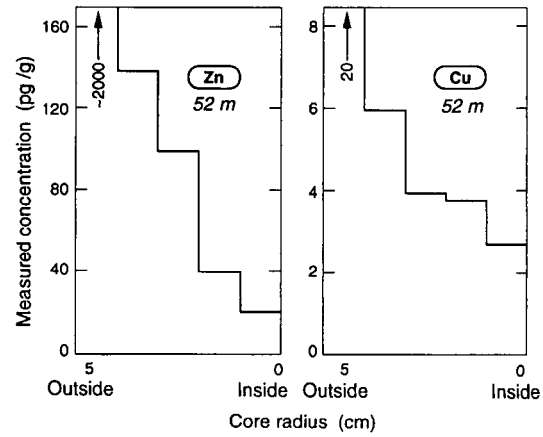

Fig. 6. Changes in Zn and Cu concentrations from the outside to the inside in one section (depth: 51.76–52.23 m) of a 70.3-m snow core electromechanically drilled at Summit, central Greenland.

encountered in the field during drilling operations and/or core handling.

Fig. 7 shows changes in the concentrations of Zn and Cd measured in the inner core as a function of the age of the snow from 1773 to 1965. It can be seen that the concentrations of these two metals have significantly increased from the 1770s, i.e the Industrial Revolution period, to the 1960s. The increase factor is about 5 for Cd and Zn [22]. The causes for these increases are discussed in full detail elsewhere [22]. They are linked to the increasing emissions of these two metals to the atmosphere of the Northern Hemisphere by human activities during this period (fossil fuels burning, mining, non-ferrous metal industry and refuse incineration [23,24]).

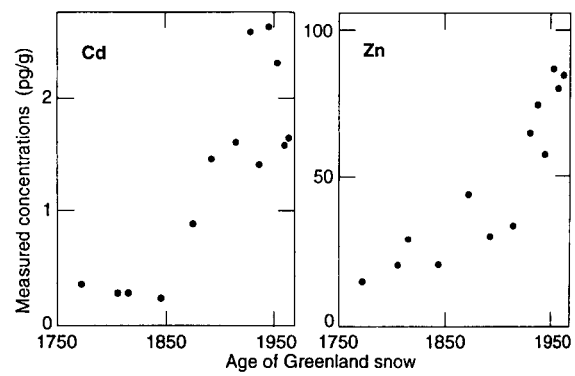

Fig. 7. Summit, central Greenland: observed changes in Cd and Zn concentrations in snow from 1773 to 1965. Each data point integrates one or two years of snow accumulation.

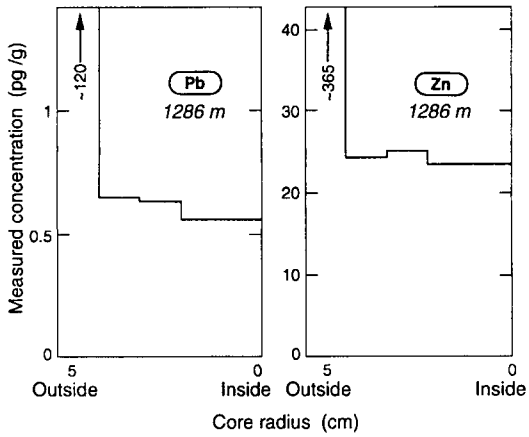

Fig. 8. Measured Pb and Zn concentrations as a function of radius in one section (depth: 1285.90–1286.45 m; estimated age 7760 years BP) of the 3028 m GRIP deep ice core electromechanically drilled at Summit, central Greenland, in a hole filled with a wall retaining fluid.

3.4. Deep electromechanical ice core from central Greenland

At the same location in central Greenland, a 3028.8 m long ice core was recovered by electromechanical drilling in 1990–1992 as part of the joint european Greenland Ice Core Project ("GRIP"). This core covers the last 250,000 years [5].

The electromechanical drill is described in detail in Ref. [25]. Because the depth to be reached was very important, the drilling hole was filled with a wall retaining fluid. The main constituent of the fluid was kerosene. We have decontaminated various sections of this deep ice core. Because many other programmes of investigations were conducted on the same core sections, only a limited part of the core cross section (see Fig. 2b and c) was available.

Significant contamination was found to be present in the outermost layer of the sections. This contamination probably originates at least partially from the fluid. Good plateaus of concentrations were however obtained in most cases as illustrated in Fig. 8 for Pb in the 1286 m section (age: 7760 years BP) and for Zn in the same section. This evidences that the ice acted as a good barrier against transfer of contamination from the outside towards the center of the core, at least for the investigated core sections which were chosen because no visible cracks were seen in them.

Pb concentration, 0.55 pg/g, measured in the inner core of the 1,286 m core section represents the natural concentration level of Pb in Greenland ice before the Greco–Roman times when man started to significantly contaminate the atmosphere of the Northern Hemisphere because of silver–lead mining and smelting [26,27]. As discussed in [27], it mainly originated from rock and soil dust.

3.5. Deep thermal ice core from central Antarctica

In 1977, 1978 a 905-m ice core was thermally drilled at Dome C (77°39′S, 124°10′E; elevation 3240 m a.s.l.; mean annual temperature: −53.5°C) as part of a French–American cooperation. It was thermally drilled in a dry hole which was not filled with a wall retaining fluid [28]. This core covers the past 40,000 years [29] i.e. the whole Holocene interglacial period (the past 10,000 years or so) and part of the last Ice Age. Fig. 9 displays the variations of Pb and Cd concentrations from the outside to the center of the 515 m core section (age: 14,500 years BP). Despite the fact that the core was obtained in a dry hole without fluid, pronounced contamination is present on the outside of the section. This contamination is found to have significantly penetrated to the second layer. Fortunately, a good plateau of concentration is obtained beyond this second layer (Fig. 9).

Pb and Cd concentrations observed in the central part of this core section, 7.8 pg/g and 0.5 pg/g, respectively, are typical for Antarctic ice from the Last Glacial Maximum (LGM), i.e the very cold terminal stage of

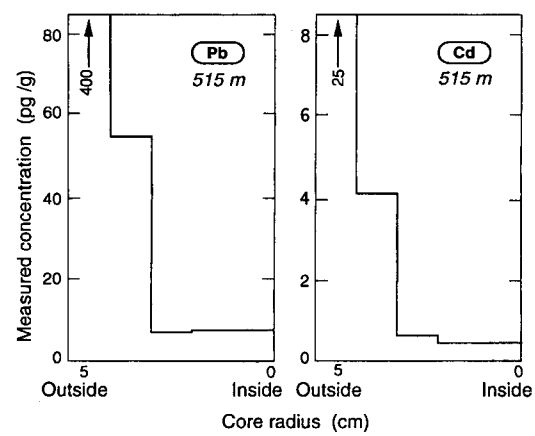

Fig. 9. Measured Pb and Cd concentrations as a function of radius in one section (depth: 514.89–515.07 m; estimated age: 14,500 years BP) of the 905 m deep ice core thermally drilled at Dome C, East Antarctica.

the last Ice Age. They are mainly originating from soil and rock dust: the atmospheric cycles of these two metals were indeed dominated by rock and soil dust during the LGM when the climatic conditions led to increased aridity, stronger winds and enhanced meridional circulations [11,30].

Acknowledgements

This work was supported by the French Ministry of the Environment (Grant No. 92295), the Institut National des Sciences de l'Univers and the University of Grenoble. The Greenland samples were collected as part of the Eurocore and GRIP programmes which were funded by the Commission of European Communities and national funding agencies and organizations in Belgium, Denmark, France, Germany, Iceland, Italy, Switzerland and the United Kingdom. The Antarctic samples were collected as part of a French–American collaboration which was funded by the Expéditions Polaires Françaises, the Terres Australes et Antarctiques Françaises and the Division of Polar Programmes of the US National Science Foundation. We thank C. Rado, R.J. Delmas and F. Maupetit for their participation in the Eurocore field sampling.

References

[1] E.W. Wolff and E.D. Suttie, Geophys. Res. Lett., 21 (1994) 781.
[2] E.D. Suttie and E.W. Wolff, Tellus, 44B (1992) 351.
[3] M. Murozumi, T.J. Chow and C.C. Patterson, Geochim. Cosmochim. Acta, 33 (1969) 1247.
[4] C.F. Boutron, U. Görlach, J.P. Candelone, M.A. Bolshov and R.J. Delmas, Nature, 353 (1991) 153.
[5] W. Dansgaard, S.J. Johnsen, H.B. Clausen, D. Dahl-Jensen, N.S. Gundestrup, C.U. Hammer, C.S. Hvidberg, J.P. Steffensen, A.E. Sveinbjörnsdottir, J. Jouzel and G. Bond, Nature, 364 (1993) 218.
[6] J. Jouzel, C. Lorius, J.R. Petit, C. Genthon, N.I. Barkov, V.M. Kotlyakov and V.N. Petrov, Nature, 329 (1987) 403.
[7] B.B. Kudryashov, V.K. Chistyakov, V.M. Pashkevich and V.N. Petrov, in G. Holdsworth, K.C. Kuivinen and J.H. Rand (Eds.), Proceedings of the Second International Symposium on Ice Drilling Technology, Calgary, Canada, 30–31 August 1982, US Army Cold Regions Research and Engineering Laboratory, Special Report 84-34, Hanover, New Hampshire, 1984, p. 137.
[8] T.A. Gosink, J.T. Kelley, B.R. Koci, T.W. Burton and M.A. Tumeo, J. Glaciol., 37 (1991) 170.
[9] A. Ng and C.C. Patterson, Geochim. Cosmochim. Acta, 45 (1981) 2109.
[10] C.F. Boutron and C.C. Patterson, Geochim. Cosmochim. Acta, 47 (1983) 1355.
[11] C.F. Boutron and C.C. Patterson, Nature, 323 (1986) 222.
[12] E.W. Wolff and D.A. Peel, Ann. Glaciol., 7 (1985) 61.
[13] C.F. Boutron, Fresenius' Z. Anal. Chem., 337 (1990) 482.
[14] P.J. Paulsen, E.S. Beary, D.S. Bushee and J.R. Moody, Anal. Chem., 60 (1988) 971.
[15] U. Görlach and C.F. Boutron, Anal. Chim. Acta, 236 (1990) 391.
[16] K.J.R. Rosman, W. Chisholm, C.F. Boutron, J.P. Candelone and U. Görlach, Nature, 362 (1993) 333.
[17] R. Lobinski, C.F. Boutron, J.P. Candelone, S. Hong, J. Szpunar-Lobinska and F.C. Adams, Anal. Chem., 65 (1993) 2510.
[18] G.M. Vandal, W.F. Fitzgerald, C.F. Boutron and J.P. Candelone, Nature, 362 (1993) 621.
[19] M.A. Bolshov, S.N. Rudniev, J.P. Candelone, S. Hong and C.F. Boutron, Spectrochim. Acta B, in press.
[20] J.P. Candelone, M.A. Bolshov, S.N. Rudniev, S. Hong and C.F. Boutron, J. Phys., C4 (1994) 661.
[21] F. Gillet, D. Donnou, C. Girard, A. Manouvrier, C. Rado and G. Ricou, in G. Holdsworth, K.C. Kuivinen and J.H. Rand (Eds.), Proceedings of the Second International Symposium on Ice Drilling Technology, Calgary, Canada, 30–31 August 1982, US Army Cold Regions Research and Engineering Laboratory, Special Report 84-34, Hanover, New Hampshire, 1984, p. 73.
[22] J.P. Candelone, S. Hong and C.F. Boutron, J. Geophys. Res., submitted
[23] J.O. Nriagu, Nature, 209 (1979) 409.
[24] J.O. Nriagu and J.M. Pacyna, Nature, 323 (1988) 134.
[25] N.S. Gundestrup and S.J. Johnsen, in C.C. Langway Jr., H. Oeschger and W. Dansgaard (Eds.), Greenland Ice Cores: Geophysics, Geochemistry and the Environment, Geophysical Monograph (American Geophysical Union), 33 (1985) 19.
[26] C.C. Patterson and D.M. Settle, Science, 207 (1980) 1167.
[27] S. Hong, J.P. Candelone, C.C. Patterson and C.F. Boutron, Science, in press.
[28] C. Lorius, L. Merlivat, J. Jouzel and M. Pourchet, Nature, 280 (1979) 644.
[29] J. Jouzel, G. Raisbeck, J.P. Benoist, F. Yiou, C. Lorius, D. Raynaud, J.R. Petit, N.I. Barkov, Y.S. Korotkevich and V.M. Kotlyakov, Quat. Res., 31 (1989) 135.
[30] C.F. Boutron, S.N. Rudniev, M.A. Bolshov, V.G. Koloshnikov, C.C. Patterson and N.I. Barkov, Earth Planet. Sci. Lett., 117 (1993) 431.

ELSEVIER

Analytica Chimica Acta 299 (1994) 17–27

ANALYTICA CHIMICA ACTA

Solute–micelle interactions in zwitterionic micellar chromatography

Sigita A. Zibas, L.J. Cline Love *

Department of Chemistry, Seton Hall University, South Orange, NJ 07079, USA

Received 14 September 1993; revised manuscript received 29th June 1994

Abstract

Equilibrium constants relating the solute concentration in the mobile phase and the solute–micelle complex concentration in the mobile phase were determined for two micellar zwitterions, dodecyldimethyl(3-sulfopropyl)ammonium hydroxide (inner salt) (SB-12) and myristyl betaine (MB-14), with a series of substituted benzene derivatives. The chromatographic capacity factors, k', were employed to calculate equilibrium constants (K_{eq}). A rationale is suggested based on experimental results to aid in explaining the zwitterionic micelle–solute intermolecular interactions. Specific attention is given to the polar phenol molecule interactions with SB-12 and sodium dodecyl sulfate (SDS) obtained from membrane equilibrium experiments. Linear Scatchard plots indicate that one phenol molecule is bound to one zwitterion monomer in the micelle.

Keywords: Liquid chromatography; Solute–micelle interaction; Zwitterions

1. Introduction

The increased understanding of amphiphilic molecules that organize to form dynamic aggregates called micelles has allowed researchers to develop a wide variety of analytical applications using these entities. Several of these applications are described in comprehensive reviews [1,2] and more specifically, chromatographic applications are the focus of several other reviews [3–5]. Micellar chromatography has been developed as an extension of conventional reversed-phase chromatography because of the additional partitioning possible between the micelle and both the bulk solvent mobile phase and stationary phase [6–9]. Numerous workers have investigated reversed-phase chromatographic applications using anionic [10,11], cationic [11,12], zwitterionic [13], and non-ionic surfactants [14,15].

A class of micelles that have potentially useful analytical applications have zwitterionic functionalities on their monomeric components, usually a positively charged quaternary nitrogen separated by one or more methylene groups from a negatively charged sulfonate or carboxyl group. Because of earlier interest in the use of micelles as analytical reagents [9,10,16–19], and because of the acknowledged paucity of reported information using zwitterionic surfactants for micellar chromatography [13], results are reported here for two zwitterionic micelles. The first monomeric micelle is dodecyldimethyl(3-sulfopropyl)ammonium hydroxide (inner salt) (sulfobetaine-12 or SB-12) and the second is myristyl betaine (MB-14). The latter has a negatively charged carboxyl endgroup instead of a negatively charged sulfonate group on SB-12. The effect

* Corresponding author.

SSDI 0003-2670(94)00302-5

of variation of the surfactant concentration on the capacity factor, k', was evaluated using the model for determination of solute–micelle equilibrium constants by reversed-phase liquid chromatography (LC) [17]. This model describes the solute partitioning equilibria occurring in a micellar mobile phase with a conventional LC column. Using the following scheme [17], equilibrium constants can be evaluated

$$E_m + L_s \overset{K_1}{\rightleftharpoons} EL_s \quad (1)$$

$$E_m + M_m \overset{K_2}{\rightleftharpoons} EM_m \quad (2)$$

$$EM_m + L_s \overset{K_3}{\rightleftharpoons} EL_s + M_m \quad (3)$$

where the concentrations are in molarity. Here $[E_m]$ is the solute concentration in the bulk solvent, $[L_s]$ is the solute concentration in the stationary phase sites, EL_s is the complex formed in the stationary phase (Eq. 1), $[M_m]$ is the concentration of surfactant as micelles in the mobile phase given by $[M_m] = [\text{total surfactant concentration in mobile phase}] - [\text{critical micelle concentration}]$ and EM_m is the complex formed in the mobile phase containing surfactant. It is understood that only two of the three above equations are independent. The capacity factor of the solute k' is defined by

$$k' = \frac{\phi[EL_s]}{[E_m] + [EM_m]} \quad (4)$$

where the brackets indicate molar concentrations and ϕ is the volume ratio of the stationary to mobile phases. Using Eqs. 1, 2, and 3 in Eq. 4 gives

$$k' = \frac{\phi[L_s]K_1}{1 + K_2[M_m]} \quad (5)$$

or

$$\frac{1}{k'} = \frac{K_2[M_m]}{\phi[L_s]K_1} + \frac{1}{\phi[L_s]K_1} \quad (6)$$

A linear plot of $1/k'$ vs. $[M_m]$ gives K_2 from the slope/intercept, where the intercept is $1/\phi[L_s]K_1$. The value of the equilibrium constant K_2 is a measure of the interaction between the solute and the monomer in the micelle. The equilibrium constant, K_{eq}, is K_2 multiplied by the surfactant's aggregation number [20]. The principal purpose of this exploratory study is to evaluate this interaction.

A comparison between the SB-12 micelles and the anionic surfactant, sodium dodecyl sulfate (SDS), was made because of their structural similarity. SDS contains only the singly negative charged sulfate group and the zwitterionic SB-12 contains its negatively charged sulfate group near the positive quaternary nitrogen group. The three micellar monomers employed are given in Table 1, along with the analytes used. The analytes are non-ionic and vary with respect to the functionalities and hydrocarbon portions of the molecule.

The interaction of phenol with SB-12 was investigated using equilibrium dialysis experiments which allowed quantitative evaluation of the association of phenol with the zwitterionic site. This technique is used extensively to evaluate the interaction between solutes and ionic macromolecules or ionic micelles [21,22], and allows the determination of equilibrium constants for binding of one molecule to another.

2. Experimental

2.1. Instrumental

A modular component liquid chromatographic system consisting of a Spectra Physics SP8700 extended-range ternary pump (San Jose, CA), an LDC UV monitor detector at 254 nm (Riviera Beach, FL) and a Rheodyne sample injector (Cotati, CA) equipped with a 20-μl injection loop was employed. The analytical columns were Shandon (Alltech Associates, Deerfield, IL) ODS Hypersil (25 cm × 4.6 mm). A pre-column (12.5 cm × 4.6 mm) packed with silica gel (Whatman, Clifton, NJ) was placed before the injector to minimize any deleterious effects from impurities in the mobile phase. A Model 5000 Fisher Recordall strip chart recorder (Fisher Scientific Co., Springfield, NJ) was used to record the chromatograms.

The LC system used for analysis of the dialysis solutions consisted of an LDC pump with a Spectra Physics UV variable-wavelength detector at 254 nm and a WISP 712 autosampler (Waters, Milford, MA). Data acquisition and chromatographic integration was carried out on a PE Nelson LIMS system, which allowed accurate quantitation of phenol concentrations inside and outside of the dialysis tubing.

Static light scattering experiments to determine the CMC of SB-12 were performed using a Wyatt Dawn

Model F laser photometer (Wyatt Technology, Santa Barbara, CA).

To ascertain whether the membrane dialysis tubing (Spectrum Medical Industries, 100 MW cutoff) is impermeable to monomer or micelle, monomeric SB-12 was determined by differential refractometry using the Model RF-600 differential refractometer (C.N. Wood, Newtown, PA) after equilibration of the dialysis experiment was established.

2.2. Reagents

The surfactants, SB-12 (Serva Biochemicals, Paramus, NJ) and MB-14 (Lonza, Fairlawn, NJ) were used as received. All solutes were obtained from Fisher Scientific, Springfield, NJ and Aldrich, Milwaukee, WI and are given in Table 1. All micellar mobile phases were prepared using 0.010 M sodium phosphate buffer at pH 6.0 made using appropriate amounts of Na_2HPO_4

Table 1
Surfactant monomers and analytes used in this study

Surfactant monomers	Structure
Dodecyldimethyl(3-sulfopropyl)ammonium hydroxide	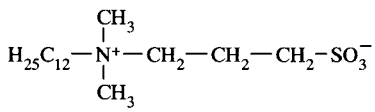
Myristyl betaine	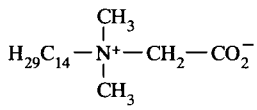
Sodium dodecyl sulfate	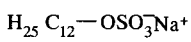

Analytes	Concentration (μg ml^{-1})	Dipole moment (D)	
Phenol	13	1.60 [23]	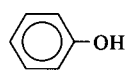
Resorcinol	115	1.56 [23]	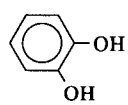
Hydroquinone	148	1.40 [24]	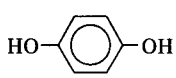
Benzene	290	0 [25]	
Toluene	232	0.36 [25]	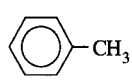
p-Xylene	343	0 [25]	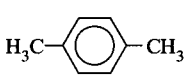
Ethylbenzene	100	0.59 [25]	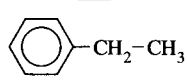
Propylbenzene	100	0.38 [26]	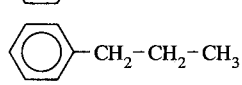
Butylbenzene	100	0.40 [27]	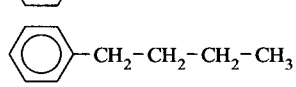

and NaH_2PO_4 and adjusting the pH with H_3PO_4, if necessary (buffer components from Fisher Scientific).

2.3. Procedures

Determination of LC column integrity and surfactant adsorption onto the column. Each LC column was equilibrated with about 50 column volumes of the micellar mobile phases or until a steady baseline was achieved. Subsequent aqueous mobile phases containing increasing surfactant concentrations were passed through the column until a flat baseline was obtained. It is important to note that the SB-12, MB-14 and SDS modified mobile phases each had a dedicated ODS Hypersil column so that three columns were used during this study. Before introducing any surfactant to the C_{18} packing material, the analytical quality of the three columns was verified by comparing chromatographic efficiencies obtained for a test solution containing uracil, phenol, benzaldehyde, *N,N*-diethyl-*m*-toluamide, toluene and ethylbenzene with conventional reversed-phase chromatographic parameters obtained from the manufacturer.

It is well documented that adsorption onto the hydrocarbonaceous column packing material occurs for anionic and non-ionic types of surfactants [14,28–31]. With an anionic surfactant, a constant amount of monomer was adsorbed at all micelle concentrations above the c.m.c. [28], while the amount of non-ionic surfactant adsorbed increases well above the c.m.c. before it finally levels at a constant amount [15]. In the case of zwitterionic micelles, it has been reported that a varying amount of monomer exists in solution above the c.m.c. [32]. Because of these reported results, it was important to determine the adsorption of a zwitterionic monomer on the C_{18} column used in this study.

Using frontal chromatography methods for measuring the cumulative breakthrough volume of the surfactant [29,33], the amount of SB-12 adsorbed onto the Hypersil ODS stationary phase was determined. The column had never been exposed to surfactant, so that there was no bias due to surfactant remaining on the column even after thorough washing. The first baseline plateau was achieved using distilled water which was also used to rinse any organic solvent from the column. The amount of SB-12 adsorbed was 2.1 μm m^{-2} on the C_{18} column as shown in Fig. 1. This value falls in the range previously found for anionic surfactants [29,30]. As is seen with non-ionic surfactants [14], the amount adsorbed continues to increase above the c.m.c. and levels off with 0.20 M SB-12 in the mobile phase (which is about 55 times above the c.m.c. Because the focus of this study is on solute–micelle partitioning represented by chromatographically determined equilibrium constants, it will be shown that deviations from predicted behavior due to the adsorption effect are not apparent in the results.

Determination of the retention data. The equation defining the capacity factor is $k' = (t_R - t_O)/t_O$, where t_R represents the time a solute band takes to elute from the column and t_O is the time it takes for an unretained band to elute through the column [34]. This was conveniently converted to volume units because a constant flow rate of 1.0 ml min^{-1} was used throughout the study. The retention times were corrected for the chromatographic system volume by measuring the elution time of sodium nitrate through the chromatographic setup when the column was replaced with a zero dead volume union. The void times were determined using sodium nitrate as a marker and was confirmed by injecting distilled H_2O with the same results. The average corrected void time for the columns was 2.4 min.

Determination of the c.m.c. of SB-12. It was important to verify the c.m.c. for SB-12, since only one value of 3.6×10^{-3} M was reported [35] (obtained from light scattering experiments). Aqueous SB-12 solutions were filtered several times using 0.1-μm membrane filters (Millipore, Corporation, Marlborough, MA) until no visible scattered light at low angles

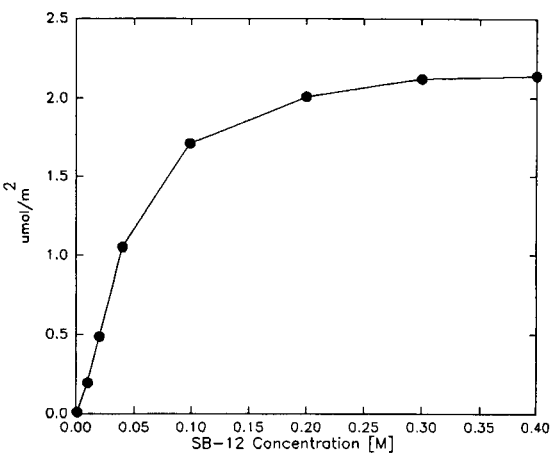

Fig. 1. Adsorption isotherm for zwitterionic SB-12 on ODS Hypersil column packing (the area available for adsorption is 170 m^2 g^{-1} column packing).

was evident to the eye when a light beam was passed through the solution. This is a common procedure for clarifying the solution [36]. The light scattering results were obtained at 90°, where the voltage is proportional to the intensity of scattered light, and a rapid increase in this scattered light indicates a sudden increase in the size of the scattering particle. This is the onset of micelle formation, which occurred at 3.3×10^{-3} M, in close agreement with the previously reported value [35]. The reported c.m.c. for myristyl betaine is 1.7×10^{-4} M [37]. It is to be noted that the c.m.c. for SB-12 is twenty times higher than that of MB-14.

Determination of binding by equilibrium dialysis. Equilibrium experiments using SB-12 and SDS micelles were performed using a conventional equilibrium dialysis setup at 23°C. Dialysis tubing with a molecular weight cutoff of 100 MW was obtained from Spectrum Medical Industries (Houston, TX). This low cutoff was required to prevent the surfactant monomer from dialyzing through the tubing along with any bound low molecular weight analyte. Stock solutions of 0.020 M phenol, 0.20 M SB-12, and 0.20 M SDS were prepared in distilled water further filtered using a Milli-Q system (Millipore). The dialysis solutions were prepared in two ways: (1) a constant concentration of surfactant above the c.m.c. of 3.6 mM was placed inside the dialysis tubing and the tubing was placed in 50-ml centrifuge tubes containing several known concentrations of phenol, and (2) several known concentrations of surfactant in the dialysis tubing were placed in 50-ml glass centrifuge tubes containing a constant, known phenol concentration (0.016 M). The centrifuge tubes were placed on a rotator for 24 h to permit equilibration during dialysis. This was sufficient time to allow equilibration of the phenol between the two phases, i.e., the inside and outside solutions of the tubing. This was confirmed by performing identical experiments, in which dialysis was allowed to proceed for 12 and for 24 h. The same constant values for the equilibrium concentrations of phenol were obtained suggesting that even 12 h would be sufficient for equilibration.

In the phase separation model of micelle formation, the c.m.c. is the saturation concentration of the amphiphile in the monomeric state, whereas the micelles constitute the separated pseudophase [38]. A dialysis experiment was performed which showed that no detectable surfactant concentration (below 2.3×10^{-7} M) penetrated through the dialysis tubing after equilibrating for 24 h. Using differential refractometry for quantitative detection, an SB-12 concentration of 3.3×10^{-2} M was found inside the dialysis bag which is above the c.m.c. (3.6×10^{-3} M). The limit of detection ($S/N=3$) was determined by the detector response for concentrations of SB-12 solutions. This indicates that during dialysis no micelles were detected on the outside of the bag. Also, it was experimentally shown that the solute phenol does not bind to the dialysis tubing. Phenol, dissolved in water at a slightly higher concentration than the concentration used in the dialysis experiment, was placed inside the bag and the same concentration used for the dialysis experiment was placed outside the bag. This enabled phenol to diffuse out of the bag to achieve equilibrium. No volume change of the solutions was observed in any of the experiments after 24 h equilibration time. At equilibration, the phenol concentrations on both sides of the bag were within 1% of each other and >99% of the phenol was recovered from both sides of the membrane experiment. The amount of phenol was quantitated by LC vs. a phenol standard prepared from the stock phenol solution. This showed that the membrane was symmetric and no phenol was adsorbed on the membrane. In addition, attenuated total reflectance (ATR) experiments confirmed that no phenol was on the membrane tubing after equilibration.

3. Results and discussion

The effect of varying the zwitterionic surfactant concentration in the micellar mobile phase on the solute–micelle partitioning equilibria is shown in Table 2. The calculated results are reported based on linear plots of $1/k'$ vs. micelle concentration for several solutes eluted from a C_{18} stationary phase. These are shown in Figs. 2–4. Comparison of the equilibrium constant values can aid in the understanding of interactions between an analyte and surfactant monomer in the micellar mobile phase. It has been shown [39] that use of different stationary phases does not affect solute–micelle equilibrium constants obtained from experimentally determined capacity factor values. Excellent agreement has been obtained when interpreting the results for solute–micelle partition equilibria by equilibrium constants or partition coefficients [12]. The primary focus of the

Table 2
Equilibrium constants and associated error values determined from $1/k'$ vs. $[M_m]$ for various solutes where $[M_m]$ = [molar concentration − c.m.c.] for SB-12. MB-14 and SDS

$[M_m]$	Phenol	Resorcinol	Hydro-quinone	Benzene	Toluene	*p*-Xylene	Ethyl-benzene	Propyl-benzene	Butyl-benzene
SB-12									
Slope	1.17	1.17	2.11	1.01	0.734	0.581	1.43	1.27	1.04
y-intercept	0.0072	0.0085	0.0102	0.0298	0.0132	0.0082	0.0095	0.0030	0.0290
Corr. coeff.	0.9963	0.9980	0.9931	0.9854	0.9770	0.9610	0.9934	0.9987	0.9994
K_2	162.5	137.3	206.9	33.9	54.6	70.8	157.1	477.4	40.5
K_{eq}	10.6×10^3 $\pm2.0\times10^3$	8.9×10^3 $\pm1.0\times10^3$	13.4×10^3 $\pm4.2\times10^3$	2.2×10^3 $\pm0.3\times10^3$	3.6×10^3 $\pm0.7\times10^3$	4.6×10^3 $\pm1.4\times10^3$	9.8×10^3 $\pm2.6\times10^3$	3.1×10^3 $\pm0.9\times10^3$	2.6×10^3 $\pm0.1\times10^3$
MB-14 [M]									
Slope	1.14	1.16	1.22	1.77	0.899	0.584			
y-intercept	0.0080	0.00513	0.0390	0.0279	0.0122	0.00519			
Corr. coeff.	0.9911	0.9895	0.9985	0.9902	0.9900	0.9835			
K_2	142.6	226.1	31.3	63.4	73.7	112.5			
K_{eq}	12.4×10^3 $\pm4.0\times10^3$	19.7×10^3 $\pm10.7\times10^3$	2.7×10^3 $\pm0.1\times10^3$	5.5×10^3 $\pm1.0\times10^3$	6.4×10^3 $\pm1.3\times10^3$	9.8×10^3 $\pm3.5\times10^3$			
SDS [M] [a]									
Slope	0.373			0.419	0.322	0.278			
y-intercept	0.0457			0.0193	0.0078	0.0028			
Corr. coeff.	0.9910			0.9505	0.9613	0.9564			
K_2	8.2			21.7	41.1	99.1			
K_{eq}	0.52×10^3 $\pm0.08\times10^3$			1.3×10^3 $\pm0.55\times10^3$	2.6×10^3 $\pm1.4\times10^3$	6.3×10^3 $\pm1.8\times10^3$			

[a] Ref. 7.

present undertaking is the solute–micelle partitioning equilibria.

Two zwitterionic surfactants, SB-12 and MB-14, were used as the micellar mobile phases. In Table 2, K_2 values for several benzene derivatives are listed which are considered to be neutral at pH 6 buffered solutions. The concentrations were chosen to be above the c.m.c. values for SB-12 and MB-14 (3.3×10^{-3} M and 1.7×10^{-4} M, respectively), but still low enough so that the absorption background due to the zwitterionic micelles in the mobile phase is not significant. Because the SB-12 mobile phase concentrations are lower than for analytical separations using SDS [9,10,16–19], chromatographic sensitivity is improved due to lower background.

Using Eq. 2, K_2 values were obtained by plotting $1/k'$ vs. $[M_m]$ and taking the ratio of slope/intercept as defined by Eq. 6. These values are listed in Table 2. The slope is equal to $K_2[M_m]/\phi[L_s]K_1$ and the intercept given by $1/\phi[L_s]K_1$. The K_{eq} values are calculated by multiplying K_2 values by the surfactants' aggregation number. Reported aggregation numbers are: 65 for SB-12 [40], 87 for MB-14 [41], and 62 for SDS [16]. The K_{eq} values are given with the maximum probable error which was calculated from the uncertainties obtained from the experimental slopes and intercepts. To explain the results, the calculated association constants (K_{eq}) are discussed in terms of intermolecular interactions. This is an often used approach employed in numerous scientific publications discussing chromatographic retention relationships in terms of intermolecular interactions [42–44].

Table 2 and Figs. 2–4 show that the two betaines, SB-12 and MB-14, interact to different degrees with the series of analytes chosen for study. To help explain the trends in k' values, $1/k'$ vs. $[M_m]$ or micelle concentration is plotted. It is important to consider the dominant ion–molecule interactions in conventional reversed phase chromatography [42,43] and recall that k' values are inversely related to the magnitude of the interaction in the mobile phase. As the SB-12 concentration is increased ten-fold from 0.0050 M to 0.040 M, the k' values decrease for all analytes. The plots of $1/k'$ vs. $[M_m]$ are all linear and very similar for the SB-12 and the MB-14 micellar mobile phases for phenol and resorcinol (Fig. 2). The K_2 values for phenol

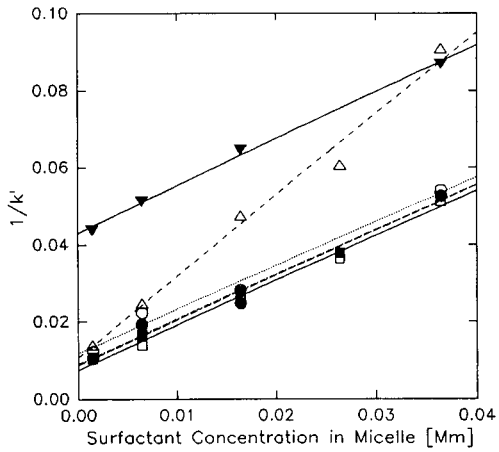

Fig. 2. $1/k'$ vs. SB-12 or MB-14 concentration in the mobile phase for (□) phenol in SB-12, (○) phenol in MB-14, (■) resorcinol in SB-12, (●) resorcinol in MB-14, (△) hydroquinone in SB-12 and (▼) hydroquinone in MB-14.

and resorcinol closely approximate one another, which may indicate that the degree of hydroxyl substitution does not affect these analytes' retention mechanism with SB-12 or MB-14 surfactants. The experimental K_2 values and equilibrium constants are smaller for the partitioning between these hydroxy group substituted benzene derivatives and MB-14 than for SB-12. Hydroquinone behaves differently in the two zwitterionic surfactants and gives results which are more difficult to explain. Based on K_2 values, one may surmise that there are weaker solute–micelle interactions in SB-12 solutions than in MB-14 solutions.

The dipole moments of phenol and resorcinol are 1.60 and 1.56 debyes, respectively, and their sizes are approximately the same. One might expect that their interactions with SB-12 would be similar. The slopes of their $1/k'$ vs. $[M_m]$ plots and their K_2 values in Table 2 are similar and unlike those of hydroquinone. This is seen to a lesser degree for MB-14.

The solute–micelle equilibria for benzene and toluene are stronger in the two betaines, shown by higher K_{eq} values. This may be due to electrostatic differences in the headgroups of the anionic SDS as compared to the headgroups of the zwitterionic SB-12 and MB-14. If the structure of the micelle assembly is idealized so that the charged layer is on the outer edge of a sphere, then the SDS headgroup will have a single negatively charged layer and zwitterionic SB-12 and MB-14 will have doubly charged headgroups containing both positive and negative charges. A more neutral headgroup layer is created on SB-12 than on the headgroup of the SDS micelles because the negative charge on the SB-12 is electrostatically affected by the presence of the positively charged quaternized nitrogen. Then, the charged layer formed by the zwitterionic headgroups of the SB-12 is partially electrostatically compensated and this indicates that the apolar interaction of benzene and its methylated derivatives with the hydrophobic portion of SB-12 is more favored than with SDS micelles.

From Table 2 and Fig. 3, the order of the K_2 values for the methylated hydrocarbons is *p*-xylene > toluene > benzene, which indicates the order of affinity of these molecules for the polar portion of the micelle. Since the dipole moments of benzene and *p*-xylene are zero, ion–dipole interactions alone cannot explain the order. Because the order is that of size, it suggests that the polarizability of the analytes is involved and that the dominant interaction is ion–induced dipole, where the energy is given by [21]

$$E = -q^2\alpha/2\epsilon^2 r^4 \quad (7)$$

where the negative sign indicates attraction, q is the charge on the ion, α is the molecular polarizability of the analyte, ϵ is the dielectric constant of the medium and r is distance between the ion and the molecule. The larger the K_2 value, the more favorable is the ion–induced dipole energy and the stronger is the interaction. The trend in K_2 is observed for both betaines and appears to be more pronounced for SB-12.

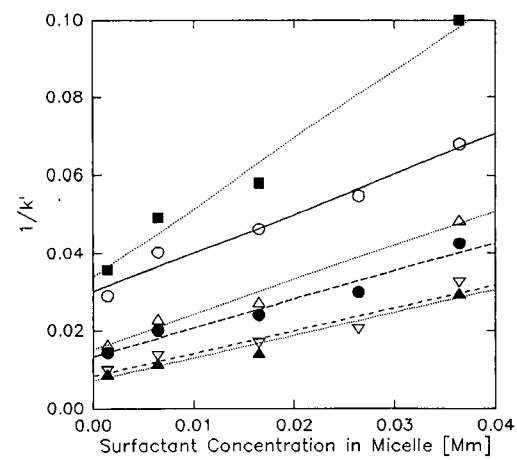

Fig. 3. $1/k'$ vs. SB-12 or MB-14 concentration in the mobile phase for (■) benzene in SB-12, (○) benzene in MB-14, (△) toluene in SB-12, (●) toluene in MB-14, (▲) *p*-xylene in SB-12 and (▽) *p*-xylene.

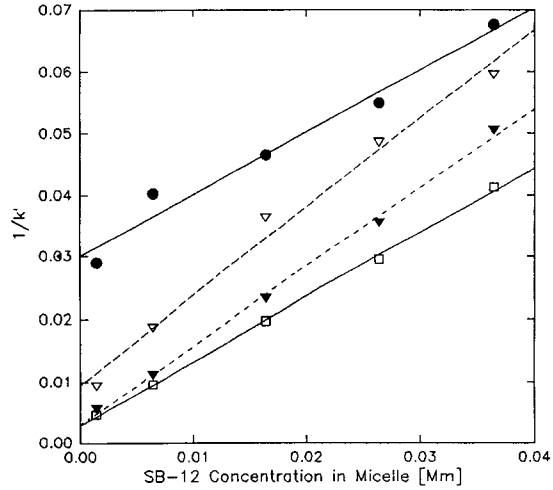

Fig. 4. $1/k'$ vs. SB-12 concentration in the mobile phase for: (●) benzene, (▽) ethylbenzene, (▼) propylbenzene and(□) butylbenzene.

Comparison of the K_2 values at constant SB-12 concentration obtained from Fig. 4, reveals that the K_2 order is benzene > ethylbenzene > propylbenzene < butylbenzene. In this hydrocarbon series, the polarity and the size of the molecules increase slightly from toluene to butylbenzene. It is expected that two intermolecular interactions are operative: ion-polarizability and ion–dipole interactions given by Eqs. 7 and 8, respectively [22,40–42]

$$E = -q\mu/\epsilon r^2 \tag{8}$$

where μ is the dipole moment of the hydrocarbon. Whenever an ion–dipole interaction takes place, an ion–induced dipole interaction is present according to Eq. 7, which depends on the polarizability or size of the hydrocarbon. The discontinuity in the series (lower K_2 value for butylbenzene) has been previously observed for non-ionic surfactants [15]. The reported explanation is the inability of the micelle to completely solubilize butylbenzene. This may explain this deviation from expected behavior.

Comparison of the K_2 values of each of the analytes at the same concentrations of SB-12 and MB-14 show that they are generally lower for the carboxyl betaine as compared to the sulfonated one. This may be rationalized based on the effective charge density of the smaller carboxyl group as compared to the larger sulfonate group [45]. It is understood that the charge density of the sulfonate group is stabilized to a greater extent because the charge can be distributed over a larger volume. This argument has been used extensively to rationalize ion binding to polyelectrolytes [45].

A previous publication by Berry and Weber [13] using zwitterionic micellar chromatography reported using several substituted phenols and other benzene derivatives with SB-12 as the micellar mobile phase. The data treatment, involving partition coefficients, permits a few general observations. Chromatographic selectivity was considered as the ratio of $k'_{\text{solute}}/k'_{\text{benzene}}$ for benzene and toluene, our results for k' and $k'_{\text{solute}}/k'_{\text{benzene}}$ are in close agreement, based on extrapolations from their published graphs [13]. In the discussion of solute orientation with the SB-12 micelle, the observation that the hydroxyl group of the phenol will orient itself in the vicinity of the ammonium group on the SB-12 monomer also has been reported by others (see below). The general conclusion from their work was that hydrophobic interactions were more significant than other interactions including electrostatic effects, polarizability, and hydrogen bonding. The data in the present study as well as another study using anionic micelles [16] also supports this interpretation.

Results from equilibrium dialysis. While the binding of ions to colloids and micelles is known [46], little or no data exists on the interaction of small molecules with zwitterionic micelles. We report a study of the interaction of phenol, a polar molecule, with SB-12, which contains a quaternized positive nitrogen group in close proximity (separated by three methylene groups) to a negatively charged sulfonate group. It is most probable that the polar phenol (1.45 D) molecule interacts simultaneously with both charged groups of the monomers of the micelle, i.e., the $-SO_3^-$ and $-^+N(CH_3)_2(CH_2)_2$. It is plausible to define a complex PL as the only bound state which dissociates according to

$$PL \rightleftharpoons P + L_f \tag{9}$$

and is depicted in Fig. 5 with L_f the free (or unbound) phenol, P the unbound zwitterion head group of each monomer of the micelle, and PL the primary bound state. This is reasonable based on NMR results which found that more benzene is solubilized close to the SB-12 micelle–water interface [47]. From models, the distance between the nitrogen and sulfur atoms can vary from 2.0 to 6.0 Å. So, the phenol molecules with an

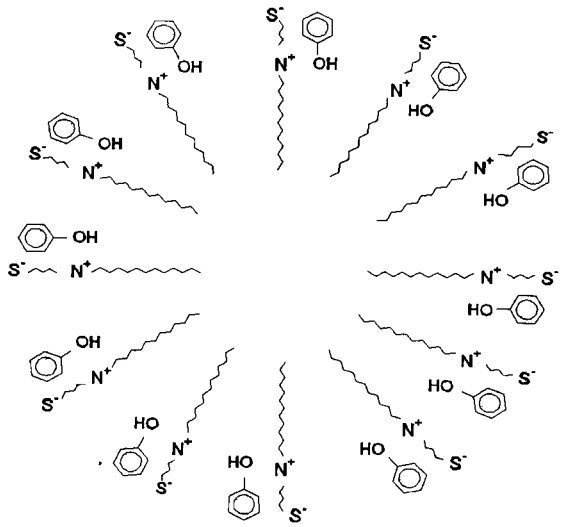

Fig. 5. Pictorial representation of spherical SB-12 micelle interacting with phenol.

average length of 4.2 Å and 0.8 of a unit charge at each end of the dipole can be accomodated. Others have shown by NMR studies [48] that pyridine, a polar molecule with its negative end near its nitrogen atom, and with a dipole moment of 2.19 D, is bound to the micelle SB-12 with the positive end of the polar pyridine bound end toward the negative SO_3 group and the negative end of the polar pyridine bound toward the positive quaternized group of each monomer of the SB-12 micelle. It is plausible to write a dissociation constant K_D for Eq. 9,

$$K_D = \frac{[P][L_f]}{[PL]} \tag{10}$$

where K_D is the reciprocal of the association constant K_b. If the binding sites are identical and independent in interacting with the ligand phenol, then the single equilibrium constant K_D could be determined. To determine either K_D or K_b, it is convenient to define R as the ratio of bound ligand concentration $[L_b]$ to total concentration of all forms of P, represented by $[P_T]$,

$$R = \frac{[L_b]}{[P_T]} = \frac{[PL]}{[P] + [PL]} \tag{11}$$

To evaluate R, a known concentration of L is added to a known concentration of micelle. As has been often reported [49–51] for micelle solutions, concentrations rather than activities are commonly used in evaluating the equilibrium constants. The total concentrations of bound ligand and free ligand are then determined experimentally. This is accomplished by using a thermodynamic technique, equilibrium dialysis, where only the small molecules, in this case phenol and water, can equilibrate between two phases, one containing micelles and the other being micelle free. The membrane is permeable only to the phenol and the solvent water and the cut-off molecular weight of the membrane used does not permit monomer permeation, as discussed previously.

The saturation curve for phenol binding to the zwitterionic SB-12 micelle is shown in Fig. 6. In principle, the number of equivalent sites n on each monomer and K_D can be evaluated from Fig. 6 and the combination of Eqs. 10 and 11 to give

$$R = \frac{n[L_f]}{K_D + [L_f]} \tag{12}$$

However, to obtain n and K_D from Fig. 6 and Eq. 12 is not recommended in favor of a linear equation [21,22,50].

To analyze the data, the total ligand concentration $[L_T]$ is given by [52]

$$[L_T] = [L_f] + R[P_T] \tag{13}$$

where $[L_f]$ is the equilibrium concentration of free ligand, $[P_T]$ is the total concentration of surfactant and R is usually defined as the average number of bound ligands per total molar concentration of macromolecules, from which one obtains

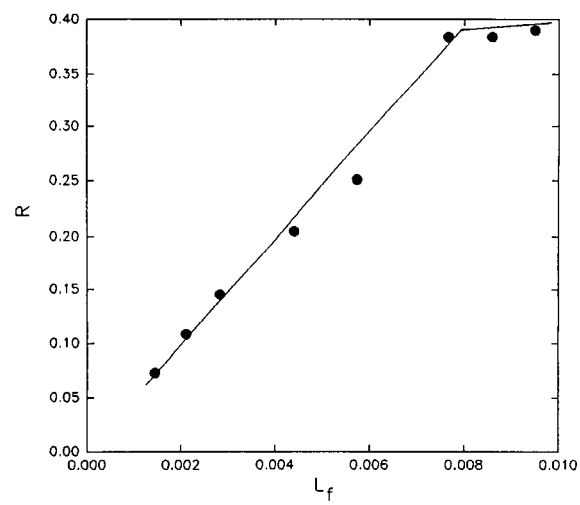

Fig. 6. Saturation curve for phenol bound to SB-12 according to Eq. 12.

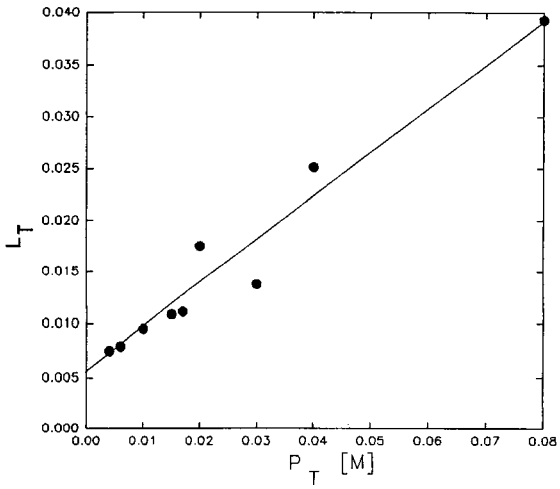

Fig. 7. Dependence of the total ligand concentration, $[L_T]$, on the total concentration of surfactant, $[P_T]$, obtained from equilibrium dialysis of phenol with SB-12.

$$R=\frac{[L_b]}{[P_T]} \tag{14}$$

To evaluate R in this study, the $[P_T]$ represents surfactant concentration which is varied and $[L_T]$ and $[L_f]$ are determined from equilibrium dialysis experiments. A plot of these results for phenol and zwitterionic SB-12 in water at 25°C is shown in Fig. 7. The linear plot obtained is represented by Eq. 13, where the slope R was found to be 0.40 by least squares analysis and at $R=0$ the value of $[L_f]$ is found to be 0.00766. Analysis of binding data is commonly obtained from a Scatchard plot [53] where $R/[L_f]$ is plotted versus R based on Eq. 12 where

$$\frac{R}{[L_f]}=\frac{n}{K_D}-\frac{R}{K_D} \tag{15}$$

The graphs are shown in Fig. 8 for phenol binding to SB-12 and for phenol binding to SDS. The respective slopes and intercepts for SB-12 and SDS are -59.2 and -41.8 and 58.7 and 13.7, respectively. The linearity obtained according to Eq. 15 is indicative of identical and equivalent binding sites on each micelle [21,22,50]. The values of K_D obtained for SB-12 and SDS are 1.69×10^{-2} and 2.39×10^{-2}, respectively, indicating that the phenol molecule is more strongly bound to the betaine compared to the sulfonate. From the values of the slopes and intercepts of Fig. 8, Eq. 15 gives unity as the number of equivalent sites per monomer for SB-12 and 1/3, or one site per three monomers, for SDS. The value of unity for n for the betaine further substantiates treating the two nearby charges on betaines as a single site.

Further experiments varying the pH of the zwitterionic surfactant mobile phases are in progress.

4. Conclusion

The zwitterionic surfactants, SB-12 and MB-14, show behavior consistent with other types of surfactants used in mobile phases, including anionic and non-ionic. In general, the addition of zwitterionic surfactants has greater association with benzene and its methylated derivatives than with an anionic surfactant, but the retention trends are similar. This indicates that the zwitterionic surfactant behaves more like an anionic surfactant with some non-ionic character. The calculated equilibrium constants for resorcinol and hydroquinone with the zwitterionic surfactants SB-12 and MB-14, are slightly lower than those reported in a system with anionic micelles in the mobile phase [54]. This is expected because the zwitterionic headgroups show anionic behavior which can be described effectively as partially neutralized by the ammonium portion of the headgroup. Chromatographic selectivity using these zwitterionic micelles show retention behavior which is not purely like that of mobile phases containing anionic micelles, but a combination of anionic and non-ionic micelles.

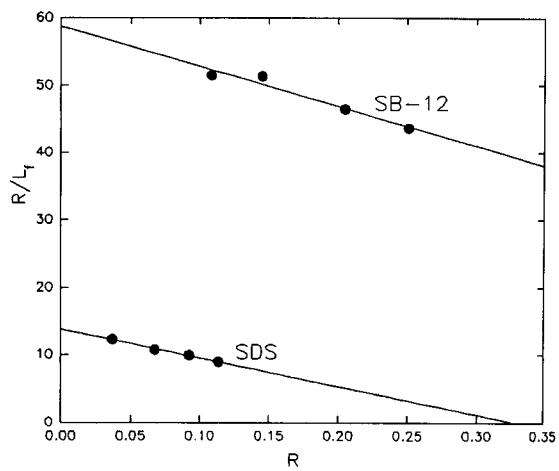

Fig. 8. Scatchard plots of Eq. 15 for (●) phenol interacting with SB-12 (top) and (●) phenol interacting with SDS.

Acknowledgements

The authors would like to thank Dr. Paul Ander for his helpful suggestions in preparing this manuscript. Mr. Michael Cerchio is gratefully acknowledged for performing the light scattering experiments. Helpful suggestions by the reviewers were also appreciated.

References

[1] L.J. Cline Love, J.G. Habarta and J.G. Dorsey, Anal. Chem., 56 (1984) 1132A.
[2] G.L. McIntire, Crit. Rev. Anal. Chem., 21 (1990) 257.
[3] D.W. Armstrong, Sep. Purif. Methods, 14 (1985) 213.
[4] W.L. Hinze, in W.L. Hinze and D.W. Armstrong (Eds.), Ordered Media in Chemical Separations, Vol. 342, American Chemical Society, Washington, DC, 1987, p. 2.
[5] J.G. Dorsey, in J.C. Giddings, E. Grushka and P.R. Brown (Eds.), Advances in Chromatography, Vol. 27, Marcel Dekker, New York, 1987, p. 167.
[6] D.G. Herries, W. Bishop and F.M. Richards, J. Phys. Chem., 68 (1964) 1842.
[7] D.W. Armstrong and S.J. Henry, J. Liq. Chromatogr., 3 (1980) 657.
[8] D.W. Armstrong and F. Nome, Anal. Chem., 53 (1981) 1662.
[9] P. Yarmchuk, R. Weinberger, R.F. Hirsch and L.J. Cline Love, Anal. Chem., 54 (1982) 2233.
[10] P. Yarmchuk, R. Weinberger, R.F. Hirsch and L.J. Cline Love, J. Chromatogr., 283 (1984) 47.
[11] J.S. Landy and J.G. Dorsey, Anal. Chim. Acta, 178 (1985) 179.
[12] M.G. Khaledi, E. Peuler and J. Ngeh-Ngwainbi, Anal. Chem., 59 (1987) 2738.
[13] J. Podcasy Berry and S.G. Weber, J. Chrom. Sci., 25 (1987) 307.
[14] M.F. Borgerding and W.L. Hinze, Anal. Chem., 57 (1985) 2183.
[15] M.F. Borgerding, F.H. Quina, W.L. Hinze, J. Bowermaster and H.M. McNair, Anal. Chem., 60 (1988) 2520.
[16] M. Arunyanart and L.J. Cline Love, Anal. Chem., 56 (1984) 1557.
[17] M. Arunyanart and L.J. Cline Love, Anal. Chem., 57 (1985) 2837.
[18] M. Arunyanart and L.J. Cline Love, J. Chrom. Biomed. Appl., 342 (1985) 293.
[19] F.J. DeLuccia, M. Arunyanart and L.J. Cline Love, Anal. Chem., 57 (1985) 1564.
[20] M.J. Rosen, Surfactants and Interfacial Phenomena, Wiley, New York, 1989, p. 114.
[21] A.G. Marshall, Biophysical Chemistry, Wiley, New York, 1978, p. 70.
[22] C.R. Cantor and P.R. Schimmel, Biophysical Chemistry, Part III, Freeman and Company, San Francisco, CA, 1980, p. 1239.
[23] B. Tinland, Tetrahedron, 24 (1968) 6833.
[24] H. Wollmann et. al., Pharmazie, 29 (1974) 708.
[25] R.C. Weast (Ed.), Handbook of Chemistry and Physics, CRC Press, Cleveland, OH, 1976, E-65.
[26] R. Bittrich and E. Schmack, Z. Phys. Chem., 259 (1978) 179.
[27] D. Cole and P. Michell, Spectrochim. Acta, 20 (1964) 739.
[28] J.S. Landy and J.G. Dorsey, J. Chromatogr. Sci., 22 (1984) 68.
[29] J.G. Dorsey, M.G. Khaledi, J.S. Landy and J. Lin, J. Chromatogr., 316 (1984) 183.
[30] A. Berthod, I. Girard and C. Gonnet, Anal. Chem., 58 (1986) 1356.
[31] A. Berthod and A. Roussel, J. Chromatogr., 449 (1988) 349.
[32] B. Lindman, M.C. Puyal, N. Kamenka, R. Rymden and P. Stilbs, J. Phys. Chem., 88 (1984) 5048.
[33] J.H. Knox and R.A. Hartwick, J. Chromatogr., 204 (1981) 3.
[34] R.J. Hamilton and P.A. Sewell, Introduction to High Performance Liquid Chromatography, Wiley, New York, 1977, p. 16.
[35] K.W. Herrmann, J. Colloid Interface Sci., 22 (1966) 352.
[36] W. Kaye and A.J. Havlik, Appl. Opt., 12 (1973) 542.
[37] P. Mukerjee and K. Mysels, Critical Micelle Concentrations of Aqueous Surfactant Systems, National Standards Reference Data Series, Vol. 36, National Bureau of Standards US, 1971.
[38] B. Lindman, in T.F. Tadros (Ed.), Structural Aspects of Surfactant Micellar Systems in Surfactants, Academic Press, London, 1984, p. 90.
[39] A. Berthod, I. Girard and C. Gonnet, Anal. Chem., 58 (1986) 1359.
[40] P. Lianos and R. Zana, J. Colloid Interface Sci., 84 (1981) 100.
[41] J. Swarbrick and J. Daruwala, J. Phys. Chem., 74 (1970) 1294.
[42] R. Kaliszan, Chromatography, (1987) 19.
[43] L.R. Snyder and J.J. Kirkland, Introduction to Liquid Chromatography, Wiley, New York, 1979, p. 255.
[44] E. sz. Kovats, Chimia, 22 (1968) 459.
[45] V.P. Strauss and Y.P. Leung, J. Am. Chem. Soc., 87 (1965) 1476.
[46] B. Lindman, in T.F. Tadros (Ed.), Structural Aspects of Surfactant Micellar Systems in Surfactants, Academic Press, London, 1984, Chap. 4.
[47] E.J. Fendler, C.L. Day and J.H. Fendler, J. Phys. Chem., 76 (1972) 1460.
[48] M. Petersheim and R. Iannuci, private communication.
[49] K. Shinoda, Colloidal Surfactants, Academic Press, New York, 1963, Chap. 1.
[50] K.E. Van Holde, Physical Biochemistry Second Edition, Prentice Hall, Englewood Cliffs, NJ, 1985, p. 52.
[51] D. Myers, Surfactant Science and Technology, VCH Publishers, New York, 1988, p. 97.
[52] C.R. Cantor and P.R. Schimmel, Biophysical Chemistry, Part III, Freeman and Company, San Francisco, CA, 1980, p. 1242.
[53] R.F. Steiner and L. Garone, The Physical Chemistry of Biopolymer Solutions – Application of Physical Techniques to the Study of Proteins and Nuclei Acids, World Scientific Publishing, Singapore, 1991, p. 53.
[54] D.W. Armstrong and F. Nome, Anal. Chem., 53 (1981) 1662.

ELSEVIER

Analytica Chimica Acta 299 (1994) 29–36

ANALYTICA CHIMICA ACTA

Gas chromatographic column for the storage of sample profiles

Jean-Marie D. Dimandja, José R. Valentín *, John B. Phillips [1]

National Aeronautics and Space Administration, Solar System Exploration Branch, Ames Research Center, Moffett Field, CA, 94035, USA

Received 28 September 1993; revised manuscript received 7 July 1994

Abstract

The concept of a sample retention column that preserves the true time profile of an analyte of interest is studied. This storage system allows for the detection to be done at convenient times, as opposed to the nearly continuous monitoring that is required by other systems to preserve a sample time profile. The sample storage column is essentially a gas chromatography column, although its use is not the separation of sample components. The functions of the storage column are the selective isolation of the component of interest from the rest of the components present in the sample and the storage of this component as a function of time. Using octane as a test substance, the sample storage system was optimized with respect to such parameters as storage and readout temperature, flow rate through the storage column, column efficiency and storage time. A 3-h sample profile was collected and stored at 30°C for 20 h. The profile was then retrieved, essentially intact, in 5 min at 130°C.

Keywords:

1. Introduction

The technique developed in this work is based on the concept of a sample storage column that preserves the true time profile of an analyte of interest. This sampling system uses a gas chromatography (GC) column to retrieve chemical information that exhibits a dependence with respect to time for a component of interest. This technique is intended to be applied for the quantitative determination of water in the atmosphere of Mars. Mars is of significant interest in the search for the origin and evolution of extraterrestrial life because it appears to have had substantial liquid water in the past [1–3]. The most accessible clue to the current location and past distribution of water on Mars is its transport through the atmosphere as part of the climatic cycle. To follow the water, we must investigate its distribution in the atmosphere as a function of altitude, location and time. A storage column allows for continuous sampling without the need for continuous detection, an advantage that will be very useful especially during the descent of a probe through the Martian atmosphere when other critically important data are being collected. The storage technique also has potential applications on Earth, such as the study of environmental substances in remote environments, and the replacement of hygrometric instruments.

* Corresponding author.

[1] Permanent address: Department of Chemistry and Biochemistry, Southern Illinois University, Carbondale, IL 62901, USA.

SSDI 0003-2670(94)00306-8

The main advantage of this storage system is the convenience it presents for its use in remote areas. The idea of the storage process is to accumulate the sample for an appropriately long time, and then read it out in as short a time as is conveniently possible. The operation of the storage system can be compared to that of a tape recorder. In a tape recorder, sound (analogous to a concentration profile) is recorded onto a magnetic tape (analogous to the storage column) as a function of time. The signal is stored until it is convenient to play it back (readout time). The playback version of the signal is an accurate reproduction of the original signal.

The goal of the sample storage technique is to capture and store an analyte of interest over a period of time, and then analyze the sample profile later when it is convenient to do so or when the storage column is retrieved from its remote location. To achieve this goal, we take advantage of the temperature dependence of retention on a chromatographic column, as expressed by the Van't Hoff equation [4],

$$\mathrm{d}\ln k' = \frac{\Delta H^\circ}{R\beta}\mathrm{d}(1/T) \qquad (1)$$

where k' is the capacity factor, ΔH° is the change in enthalpy associated with the transfer of solute molecules from the mobile phase to the stationary phase, T is the temperature, R is the gas constant and β is the phase ratio. The equation above shows that retention can be controlled by adjusting the temperature. This is a key relationship that is utilized during the storage process. The storage column operates similarly to adsorption–desorption sampling methods that have been used in gas chromatography [5–8] in the sense that the adsorption (and storage) of the sample is performed at a low temperature and the desorption is done at a high temperature. However, adsorption–desorption techniques are mainly preconcentration methods in which short columns (cm range) are used to trap the compounds of interest before their insertion onto the gas chromatographic column for analysis. In the sample storage technique longer columns (m range) are used for long sampling times, and the storage column itself is the analysis column.

The storage process can be divided into three distinct stages: the sampling stage, the storage stage and the readout stage. During the sampling stage, the sample stream enters the column at a temperature which corresponds to a high k'. During the storage stage, the gas flow is shut off. This stage includes the time during which the sample profile is stored and the time it takes to increase the temperature of the column from the sampling temperature to the readout temperature (heating time). During the readout stage, the flow is reopened and the stored sample elutes to the detector at a high temperature (low k'). The sampling stage and the readout stage are isothermal processes.

The purpose of this paper is to prove the concept of the storage column and to illustrate optimization of performance for a model substance, in this case octane. Octane was chosen because it is non-polar and therefore is easily analysed by chromatography. Alkanes have essentially no risk of interactions with surfaces other than the stationary phase. The boiling point of octane is 125.66°C, putting it in a range between compounds that would not be retained long enough on an ordinary non-polar column (such as methane through pentane) and compounds that would require too high a temperature for their elution (dodecane and higher).

2. Theory

Three important parameters in the operation of the sample storage system need to be determined: the maximum sampling time (how long a profile can be sampled), the maximum storage time (how long a signal profile can be stored before the effects of longitudinal diffusion lead to a significant loss of information) and the sampling resolution time (the minimum amount of time between two distinguishable events in the sample profile).

2.1. Maximum sampling time

The maximum sampling time (t'_{RS}) is the amount of time it takes for the first event in the sample profile to reach the end of the storage column at the sampling temperature and can be determined by

$$t'_{\mathrm{RS}} = t_{\mathrm{R}} - \frac{4\sigma_t}{2} = t_{\mathrm{R}} - 2\sigma_t \qquad (2)$$

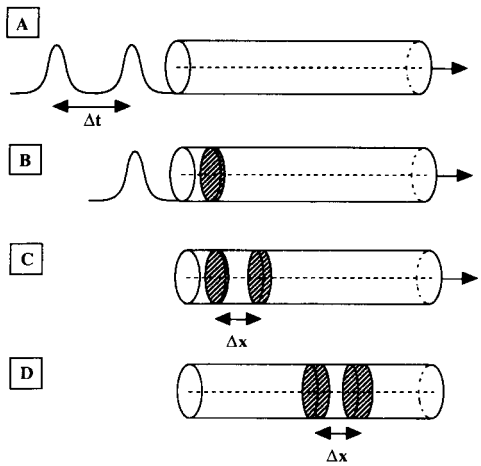

Fig. 1. Effect of band broadening on sample storage. The absence of an arrow in (*D*) indicates that the flow has been shut off.

where t_R is the retention time and σ_t is the bandlength standard deviation (in time units). The assumption is made that a band of analyte, under the influence of diffusion, is Gaussian in nature by the time it reaches the end of the column. $2\sigma_t$ is subtracted from t_R to prevent half of the first "band" (event) to elute from the column during the sampling time.

2.2. Maximum storage time

The maximum storage time depends on the effect of band broadening on the profile stored in the column. Fig. 1 illustrates the sampling process from a band broadening perspective. Two events (Fig. 1A) separated by a time, Δt, enter the column (Fig. 1B) where they are separated in space (Fig. 1C) by a distance, Δx. The distance, Δx, is directly proportional to the time between the events, Δt. Band broadening occurs as the component migrates down the column. In Fig. 1D, although the distance between the centers of two bands (Δx) does not change, the two bands appear to be merging.

Longitudinal diffusion continues to broaden bands even during the storage time with the flow shut off. It is clear that this band broadening limits the amount of time a sample profile can be stored. The resolution between the events in the sample stream at readout depends on band broadening.

A theoretical calculation of the maximum storage time involves the terminal bandlength, or length of a sample concentration pulse by the time it reaches the end of the column. An arbitrary limit for the maximum storage time is set at twice the terminal bandlength of a sample pulse. Beyond this limit, the effects of bandspreading would result in a small loss in information during the storage time. Band variances are additive so the band length would then increase only by a factor of the square root of two. The variance of a band diffusing along a column in the mobile phase is given by [9]

$$\sigma_l^2 = 2D_M t'_S \tag{3}$$

where D_M is the diffusion coefficient of the analyte in the mobile phase, and t'_s is the amount of time the analyte spends in the mobile phase alone. An increase by this factor would be noticeable, but not extreme.

The time t'_s would be the maximum storage time if the column were an open tube, with no stationary phase. The maximum storage time in the storage column, which we define as t_s, includes the amount of time spent in the stationary phase where diffusion rates are insignificant. Therefore the theoretical storage time should be multiplied by the capacity factor at the storage temperature.

$$t_S = t'_S \times k' \tag{4}$$

Beyond the maximum storage time, there will be a loss of information because of the loss of resolution.

2.3. Sampling resolution time

The sampling resolution time is the minimum amount of time between distinguishable events in the sample profile. Statistics tells us that 90% of the area contained in a Gaussian peak falls within 2σ of the mean of the peak (for a resolution $R_s = 1$), if Gaussian bands are assumed. Therefore the minimum distance between two resolved events is $4\sigma_1$ (where σ_1 is the band broadening standard deviation) and the sampling resolution time, t_{SR}, is equal to

$$t_{SR} = \frac{4\sigma_1}{\bar{v}} \tag{5}$$

where $\bar{v}$ is the average velocity of sample substance along the column.

3. Experimental

3.1. Apparatus

The gas chromatography system used in this work is shown in Fig. 2. The gas chromatograph was a Carle Model 111 GC (Carle Instruments, Fullerton, CA) with a thermistor type thermal conductivity detector. The temperature of the gas chromatography oven was monitored by an Omega CN 9000 series miniature microprocessor (Omega Engineering, Stamford, CN). A Brooks Type 5878 Controller and two Model 5850E Brooks mass flow controllers (Emerson Electric, Hatfield, PA) were used to regulate the flow through the reference and sample columns. A Brooks Model 8744 (Emerson Electric, Hatfield, PA) flow controller was used to determine the flow rate of the carrier gas through the headspace sample vial. The gas chromatography injection unit was composed of an 8-port Valco valve with two sample loops (60 μl and 100 μl) and a Valco electric actuator (Alltech, Deerfield, IL) for computer control of the valve. The column was a 3 m $\times$ 1.1 mm i.d. stainless steel tube packed with *n*-octane Porasil C (80–100 mesh). The output signal was digitized by a Nelson Analytical Model 900 analog-to-digital converter (Nelson, Cupertino, CA) and transferred over an IEEE/488 bus (Ziatech, San Luis Obispo, CA) to a System 1800 Model B high-speed microcomputer (Integrated Image Systems, Santa Clara, CA). The data was then transferred to a micro-Vax II computer (Digital Equipment, Santa Clara CA) for data processing using programs written in IDL (interactive data language, version 2.0) (Research Systems, Boulder, CO) The micro-Vax II was connected to a Macintosh II (Apple, Cupertino, CA) computer which was used as a display terminal.

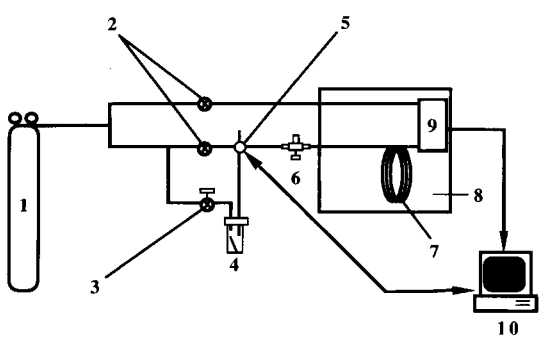

Fig. 2. Storage column apparatus: (1) carrier gas tank; (2) carrier gas flow controllers; (3) sample concentration flow controller; (4) headspace sample vial; (5) injector unit (with vent output); (6) diversion valve; (7) sample storage column; (8) oven; (9) detector; (10) computer.

3.2. Reagents

Analytical reagent grade *n*-octane was purchased from Sigma (St. Louis, MO). The carrier gas was 99.999% helium (Matheson, Newark, CA).

3.3. Headspace sampling

Octane concentration was determined using the evaporation rate of octane and the flow rate of helium through the headspace sample vial. The evaporation rate of octane was experimentally determined to be 7.2×10^{-7} g/min. The helium flow rate through the headspace sample vial was 22.8 ml/min. The octane concentration was then 175 ppm by weight.

3.4. Sampling, storage and readout temperature selection

The sampling temperature was chosen to provide the longest sampling time that could be achieved in the laboratory. The laboratory temperature being 26°C, the lowest oven temperature was set at 30°C. The storage temperature was the same as the sampling temperature to reduce the effects of diffusion and therefore maximize the storage time. The readout temperature was chosen so that octane had a retention time of 2–8 min. This temperature was set at 130°C.

3.5. Storage procedure

A series of sample pulses were input into the column at the storage temperature over a period of time to emulate a sample profile changing with time. Discrete sampling was used as opposed to continuous sampling (i.e., exponential dilution) because it was the easiest way to verify the conservation of the sample profile. The concentration of the sample was determined by the flow rate of the carrier gas through

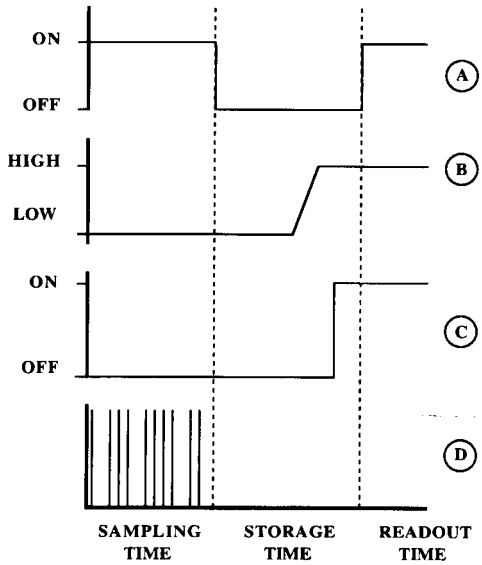

Fig. 3. Timing diagram of the storage procedure. (A) Diversion valve (valve 6); (B) column temperature; (C) A/D data acquisition; (D) injection valve.

the headspace sample vial and the sample evaporation rate. After the sample stream input profile was complete, the flow through the column was shut off using the diversion valve (Fig. 2). The temperature of the gas chromatography oven, and thus of the storage column, was kept at the storage temperature until it was time to elute the profile contained in the column. Fig. 3 is a timing diagram of the storage and readout procedure.

Just before readout, the temperature was increased to the readout temperature. The flow through the column was then reestablished by turning on the diversion valve and the sample profile was eluted to the detector. The analog detector signal was digitized by the analog-to-digital converter and sent to the computer. The data acquisition rate of the computer was selected to be 1 Hz.

The carrier gas flow through the headspace sample vial was controlled manually using the Brooks Model 8744 flow controller. The flow through the storage column and the temperature control of the oven were also controlled manually. A software program supplied by Nelson Analytical generated the injection sequence and acquired the detector signal.

4. Results and discussion

A number of non-polar packed column stationary phases (OV-101, Porapak Q, Porasil C, OPN-Porasil C, *n*-octane Porasil C) were tested for their retention characteristics over the storage temperature to the readout temperature range. Packed columns were used because they are more rugged than capillary columns and thus better suited for the rigors of space flight [10]. *n*-Octane Porasil C showed the best capability for long sampling time at low temperature and short readout time at high temperature.

4.1. Flow rate optimization

The flow rate was optimized at the readout temperature to maximize column efficiency when the sample profile was detected. In practical terms, the optimization of the flow rate was done to reduce the effects of band broadening while the signal profile was read out. The optimum average linear velocity was determined to be 18 cm/s, which corresponded to a volumetric flow rate of 9.2 ml/min. The flow rate was measured before the start of each experiment to confirm this value.

4.2. Determination of maximum sampling and storage times

A single pulse was injected at 30°C to get the information necessary for the determination of the maximum sampling time and the maximum storage time of the column. The void time (t_M) of the peak was 18 s, the retention time (t_R) was 11 062 s, the base width of the peak ($4\sigma_t$) was 1000 s, and k' was 614. The maximum sampling time (t'_{RS}) was 10 562 s (2.9 h).

Calculation of the maximum storage time was done using Eqs. (3) and (4). Eq. (3) requires that σ_l and D_M be known for octane in helium at the storage temperature. σ_t was converted to σ_l by the expression

$$\sigma_l = \bar{v} \times \sigma_t \quad (6)$$

With σ_t equal to 250 s, and $\bar{v} = 2.9 \times 10^{-2}$ cm/s ($k' = 614$), σ_l was 7.3 cm ($\approx 2.4\%$ of column length).

The diffusion coefficient of octane in helium (D_M) was approximated by the value for the diffusion coefficient of octane in air (6.2×10^{-2} cm^2/s) [11]. Eq. (3) gave a t'_s of 430 s. Eq. (4) gave a maximum storage time of 2.6×10^5 s (3.1 days).

4.3. Storage of a simulated sample profile

The storage process is shown in Fig. 4. An injection pattern was input at the sampling temperature through the use of a software program that generated periodic pulses into the column. This injection pattern is a simulation of a changing stream in the sense that the periodic injections are events in time that are occurring in the sample profile. The injection valve is a convenient way to generate a model changing sample stream. The injections should not be looked upon as samples taken from a stream but as the changing stream itself which flows directly into the column.

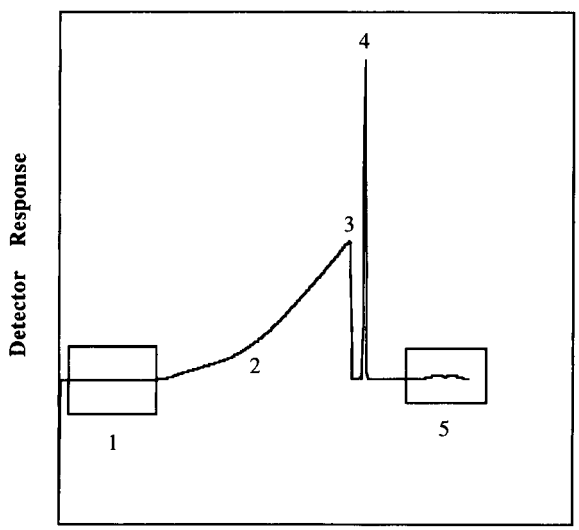

Fig. 4. A typical profile for storage and readout of octane. A sample profile was stored at 60°C and read out at 100°C. The sampling period (1) lasted 2400 s. The storage period (2), during which the flow was shut off, lasted 5400 s. The baseline drift is due to the flow being shut off on the sample line of the thermal conductivity detector while the reference line was left on. The sudden drop (3) corresponds to the moment when the flow is reopened. A small leak was present in the system, thus resulting in air entering the system during the storage period. The air peak (4) corresponds to the time it takes for this accumulated air to reach the detector after the flow has been reestablished in the storage column. Finally, the sample profile (5) elutes through the detector. Note: conditions (such as sampling and readout temperature, sampling period, storage period and readout period) varied with different experiments.

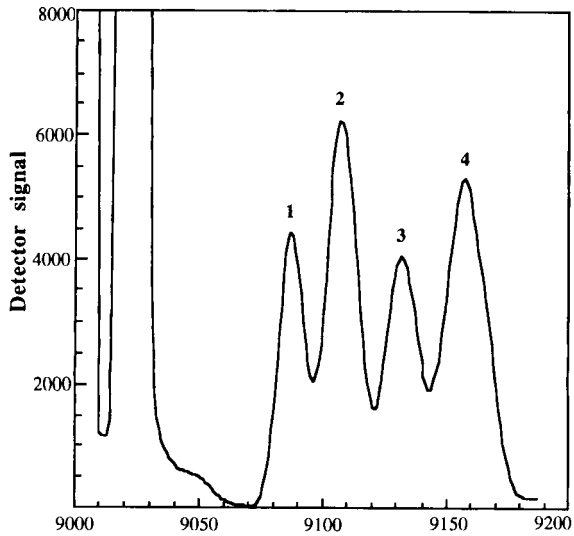

Fig. 5. Octane sample profile. The sampling time was 6200 s (at the sampling temperature of 30°C). The storage time was 2800 s. The storage temperature was the same as the sampling temperature to minimize the effects of diffusion during flow shutoff. The readout time was 200 s at the readout temperature of 130°C. The first and third peak are from the 60-μl injection loop; the second and fourth peak are from the 100-μl injection loop.

In one experiment, four injections were made during the sampling period. The flow through the column was then shut off and the temperature of the oven was raised to 130°C. This was done because it was easier to manually control one flow line instead of having to control both lines. The changing gas flow resulted in a detector baseline drift (marked as zone 2) in Fig. 4. Once the temperature has stabilized at the readout temperature of 130°C, the valve controlling flow through the column was reopened. The detector readout of this response is shown in Fig. 5. The four injections at 30°C were done at 1550, 3100, 4650 and 6200 s. The injector alternates between 60 μl and 100 μl sample loops, thus providing sample peaks of alternating sizes. This pattern is clearly shown in the readout response in Fig. 5.

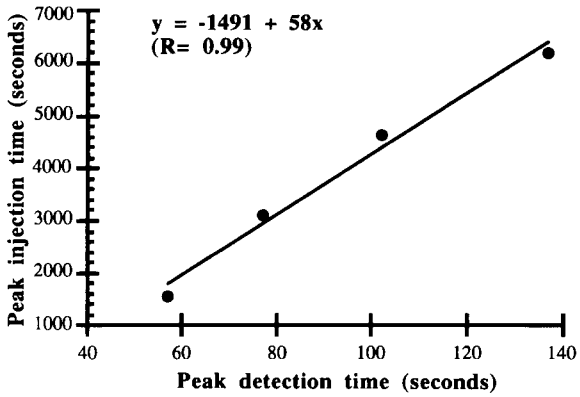

Fig. 6. Correlation between the sampling profile and the detection profile.

The first and third peaks had areas equal to 4.06 and 4.10 (arbitrary units). The areas of peaks 2 and 4 were 6.34 and 6.59. This pattern of peak areas is significant because it corresponds to the use of two different size sample loops on the injection valve. The ratio of peaks 1 and 3 over peaks 2 and 4 is 0.63, which is consistent with the loop sizes of 60 μl and 100 μl that were used.

Since the readout temperature is much higher than the storage temperature, sample profiles which had been collected over a period of a few hours could be detected in a matter of minutes. The profile of the stored sample was not lost in the process; it was only read out on a shorter time scale than it would have if the temperature at readout had been the same as the storage temperature. Fig. 6 shows the correlation between the sampling pattern and the detector response. The R value associated with this procedure is 0.99, which indicates that the sample pattern was conserved adequately during the storage process.

4.4. Storage column efficiency

The storage column efficiency is a measure of the sampling resolution time (or "frequency response") of the column with respect to peaks stored in the column. It is dependent upon the storage time and the column peak capacity, defined here as being the column's ability to completely distinguish between separate events in the sample stream profile.

The storage of a more complex sample pattern leads to problems of peak capacity and failure to retrieve the original information. As the interval between consecutive injections decreases, the loss of information due to the overlap of peaks increases. Therefore, it was important to investigate the correlation between injection interval and peak resolution. The peak sequence is a model signal to simulate a changing sample stream. The storage column has limited peak capacity which is related to the sampling resolution time.

A series of experiments were run at 130°C in which the interval between injections varied from 20 to 40 s. The experimental sampling resolution time was 21 s at 130°C. The extrapolated value of the sampling resolution time at storage temperature was 1093 s (18.2 min). This sampling resolution time, given the sampling time of 10562 s (2.9 h) at 30°C, would allow for 9.7 peaks to be stored in the column with unit resolution. The theoretical sampling resolution time calculated from Eq. (5) was 1000 s for a peak capacity of 10.6.

5. Conclusions

The storage column concept has been proven, and improvements in hardware will be made for better storage column characteristics (longer sampling and storage times, better frequency response) as research moves on to non-model substances. The possibility of using open-tubular columns to improve column efficiency will also be investigated for non-space flight applications. Other improvements involve the sophistication of the storage procedure. Future studies will utilise non-linear continuous sampling systems instead of the linear discrete sampling procedure that was described in this paper to move from the simulation of a component profile to the actual sampling and storage of a component of interest in a remote location.

Acknowledgments

We thank Norishige Takeuchi for his help with experimental design. We also acknowledge the late Dr. Thomas W. Scattergood, whose editorial comments were greatly appreciated. This work was

funded by a research grant from the National Aeronautics and Space Administration (NGT-70233).

References

[1] S.W. Squyres, Ann. Rev. Earth. Planet. Sci., 12 (1984) 83.
[2] M.H. Carr, Icarus, 68 (1986) 187.
[3] M.W. Schaefer, Geochim. Cosmochim. Acta 57 (1993) 4619.
[4] E. Heftmann, Chromatography: Fundamentals and Applications of Chromatographic and Electrophoretic Methods. Part A: Fundamentals and Techniques, Journal of Chromatography Library, Vol. 22, Elsevier, Amsterdam, 1983.
[5] H.-J. Schaeffer, J. High Resolut. Chromatogr., 12 (1989) 69.
[6] B.J. Hopkins and V. Pretorius, J. Chromatogr., 158 (1978) 465.
[7] M. Phillips and J. Greenberg, J. Chromatogr., 564 (1991) 242.
[8] B.A. Ewels and R.D. Sacks, Anal. Chem. 57 (1985) 2774.
[9] G. Guiochon and C. Pommier, Gas Chromatography in Inorganics and Organometallics, Ann Arbor Science Publishers, 1973.
[10] F. Raulin, E. de Vanssay, L. Do and P. Paillous, LC–GC Int., 5 (1992) 22.
[11] G.A. Lugg, Anal. Chem., 40 (1968) 1072.

ELSEVIER

Analytica Chimica Acta 299 (1994) 37–42

ANALYTICA CHIMICA ACTA

Ammonium–hydrogen exchange on two carboxylate resins

Ivan Dobrevski [a], Maria Dimova-Todorova [a], Nadezda Dimitrova [a], Erik Högfeldt [b,*]

[a] *Department of Water Technology, Higher Institute of Chemical Technology, 8010 Bourgas, Bulgaria*

[b] *Department of Inorganic Chemistry, the Royal Institute of Technology, S-100 44 Stockholm, Sweden*

Received 21 February 1994; revised manuscript received 9 May 1994

Abstract

Equilibrium data for the protonation of Wofatit CA-20 at Amberlite IRC-50 are measured at three NH_4Cl concentrations. The data are used, via a three-parameter model, to estimate limiting values of the protonation constants.

Keywords: Ion exchange; Carboxylates; Resins

1. Introduction

Ion exchangers in ammonium form are used for condensate purification as well as purification of waste waters from metal ions such as Cu^{2+}, Cd^{2+} and Zn^{2+}. Knowledge of the ammonium–hydrogen equilibrium is required for optimizing the purification process.

In this paper data on this equilibrium are presented for two temperatures, 303 and 343 K and three ionic strengths, 0.1, 1.0 and 4.0 mol l^{-1} NH_4Cl. A simple three-parameter model allowing for non-ideal behaviour in the ion exchanger is used to summarize the experimental data.

2. Experimental

The resins. Wofatit CA-20 is a macroporous acrylate resin. The samples supplied in hydrogen form contained 6% divinylbenzene (DVB) with a capacity of 10.0 meq g^{-1} and 40% relative humidity.

Amberlite IRC-50 is a methacrylate resin. Here also the samples were delivered in hydrogen form with 5% DVB, a capacity of 11.1 meq g^{-1} and 45% relative humidity. Both resins contain carboxylate groups.

Experiments. The batch method was employed. To samples in hydrogen form with a capacity of 1 meq the required amount of ammonia was added to ensure the conversion of the desired fraction of resin in ammonium form. At the same time 1.00 mol dm^{-3} NH_4Cl autoclaved at either 303 or 343 K was added to make the final volume 100 cm^3. After equilibration for about 4 h measurements commenced and continued until no further change in composition was observed. Separate tests showed that temperature equilibrium had been reached and that the required degree of dissociation, α, was obtained to within a few percent. The glass electrodes were calibrated with standard buffers. The equilibrium constants obtained are thus mixed constants.

3. The model

Applications have been described elsewhere [1,2]. According to the model the equilibrium constant is

* Corresponding author.

SSDI 0003-2670(94)00325-4

dependent upon the kind of nearest neighbours. If the two ionic forms are denoted AR and BR three possibilities can be recognized. If the nearest neighbours are only AR the equilibrium is denoted k_1. If the nearest neighbours are only BR the equilibrium constant is denoted by k_2. If both kinds are present we call the equilibrium constant k_m. We assume random distribution giving the following value for the measured equilibrium constant k.

$$\log k = \log k_1 x^2 + \log k_2 (1-x)^2 + 2\log k_m x(1-x) \quad (1)$$

Here x is the equivalent fraction of one component.

It should be noted that the model corresponds to the well-known fact that an acidity constant has one value in a certain solvent, another in another solvent and a third value in their mixture.

It is practical to use the following equation, which is a second-order polynomial equivalent to Eq. 1.

$$\log k = \log k_1 x + \log k_2 (1-x) + Bx(1-x) \quad (2)$$

where B is an empirical constant. By non-linear regression estimates of the constants in Eq. 2 are found. The parameters k_1 and k_2 are obtained directly, while the third parameter k_m is computed from

$$\log k_m = (1/2)[\log k_1 + \log k_2 + B] \quad (3)$$

4. The equilibrium constant

The reaction studied is

$$H^+(aq) + NH_4R \rightleftharpoons HR + NH_4^+(aq) \quad (4a)$$

The equilibrium quotient k is defined by

$$k = [HR][NH_4^+]/[NH_4R][H^+] \quad (4b)$$

If it is a variable the system behaves non-ideally. With knowledge of the parameters of the three-parameter model the equilibrium constant K of reaction (4a) is computed from

$$\log K = \int_0^1 \log k(x)\,dx$$

$$= (1/3)[\log k_1 + \log k_2 + \log k_m] \quad (5)$$

Finally, we define

$$x = [NH_4R]/([NH_4R] + [HR]) \quad (7)$$

5. Goodness of fit

In order to get an idea of how well the model describes the experimental data the following statistical criteria using the residuals are given. The residual squares sum U:

$$U = \sum_1^n r_i^2 = \sum_1^n (\log k_{exp} - \log k_{calc})^2 \quad (8)$$

where n = number of experimental points.

The standard deviation $s(\log k)$:

$$s(\log k) = \pm\sqrt{U/(n-c)} \quad (9)$$

where c = number of components.

The Hamilton R-factor in per cent, $R(\%)$:

$$R(\%) = 100\sqrt{U/\Sigma \log k_{exp}^2} \quad (10)$$

6. Results

In Table 1 the parameters found are recorded. For Wofatit CA-20 at 303 K and $I = 0.1$ a straight line gives an acceptable fit as seen in Table 2. That only two constants are needed is seen from the value of log k_m being the average of log k_1 and log k_2 and equal to log K. For $I = 1.0$ at the same temperature a straight line also gives an acceptable fit. For $I = 4.0$ a constant value is satisfactory. At 343 K a constant value is satisfactory for $I = 0.1$ and 1.0 M, while $I = 4.0$ requires a straight line. The titration curves are illustrated in Fig. 2.

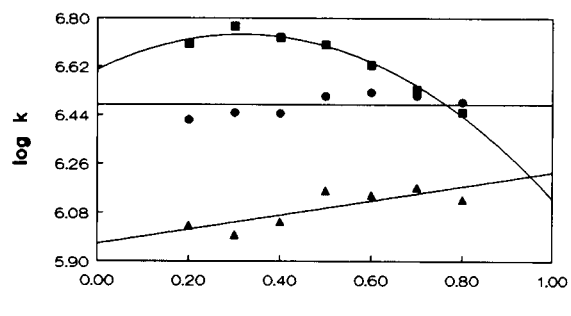

Fig. 1. Reaction: $H^+ + NH_4R \rightleftharpoons HR + NH_4^+$. log k plotted versus x for Amberlite IRC-50 at 343 K and the three ionic strengths. (▲) $I = 0.1$ M NH_4Cl, (●) $I = 1.0$ M NH_4Cl, (■) $I = 4.0$ M NH_4Cl. The curves are those of the model with parameters given in Table 1.

Table 1
Parameters of the model obtained by least-squares fitting to Eq. 2

Resin	T(K)	I	log k_1	log k_2	log k_m	log K	log K_p
Wofatit CA-20	303	0.1	5.419	4.804	5.112	5.112	6.112
Wofatit CA-20	303	1.0	5.290	4.996	5.143	5.143	5.143
Wofatit CA-20	303	4.0	5.315	5.315	5.315	5.315	4.713
Wofatit CA-20	343	0.1	5.509	5.509	5.509	5.509	6.509
Wofatit CA-20	343	1.0	5.717	5.717	5.717	5.717	5.717
Wofatit CA-20	343	4.0	5.453	6.034	5.744	5.744	5.142
Amberlite IRC-50	303	0.1	5.420	5.269	5.345	5.345	6.345
Amberlite IRC-50	303	1.0	5.750	5.750	5.750	5.750	5.750
Amberlite IRC-50	303	4.0	5.886	5.886	5.886	5.886	5.284
Amberlite IRC-50	343	0.1	6.228	5.966	6.097	6.097	7.097
Amberlite IRC-50	343	1.0	6.479	6.479	6.479	6.479	6.479
Amberlite IRC-50	343	4.0	6.131	6.608	7.025	6.588	5.986

For Amberlite IRC-50 at 303 K (Table 3), for $I=0.1$ a satisfactory fit is found with a straight line, for $I=1.0$ and 4.0, a constant value. At 343 K straight lines are sufficient for $I=0.1$ and 1.0 while $I=4.0$ is the only system that requires a second degree polynomial. This is illustrated in Fig. 1 where examples are given for all three kinds of curves.

The experimentally measured pH values can be compared with those computed by using the equation

$$pH_{calc} = \log k_{model} - \log(1/x - 1) - \log I \qquad (11)$$

which is obtained by taking the logarithm of Eq. 4b.

The goodness of fit illustrated by the Hamilton R-factor in percent ($R\%$) is less than unity for all systems studied, which is most satisfactory.

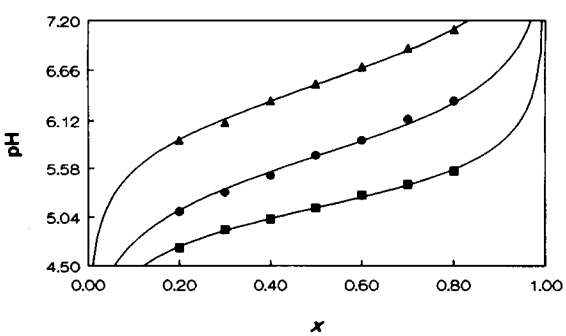

Fig. 2. pH plotted versus x for Wofatit CA-20 at 343 K and the three ionic strengths. (▲) $I=0.1$ M NH_4Cl, (●) $I=1.0$ M NH_4Cl, (■) $I=4.0$ M NH_4Cl. The curves have been computed from Eq. 11 with the parameters given in Table 1.

7. Discussion

The regular mixture. Recently the protonation of the two resins used in this study was investigated. It was shown that at 303 and 343 K and $I=1$ M NaCl straight lines were sufficient to give an acceptable fit to the experimental log $k(x)$ plots [3]. It has been shown elsewhere [2] that $\log k = a + bx$ corresponds to a regular mixture, i.e. the activity coefficient expressions become

$$\log f_1 = 0.5bx^2 \quad \log f_2 = 0.5b(1-x)^2 \qquad (12a,b)$$

The constant b is related to the enthalpy of mixing by

$$\Delta H = 0.5bx(1-x) \qquad (13)$$

With knowledge of b the temperature dependence of the mixing process can be predicted, but this is only true if b itself is independent of temperature. Guggenheim [4] calls b the interchange energy. From the expression

$$\log k = a + bx \qquad (14)$$

it is seen that an interchange energy independent of temperature gives parallel log $k(x)$ curves at different temperatures. This is found practically to be the case for the protonation of Amberlite IRC-50 in our previous publication but not for Wofatit CA-20. In the present study no parallel curves are found implying that b is a function of the temperature.

Table 2
Comparison of experimental and computed log k values for Wofatit CA-20

x	$I=0.1$		$I=1.0$		$I=4.0$	
	log k (exp.)	log k (calc.)	log k (exp.)	log k (calc.)	log k (exp.)	log k (calc.)
$T=303$ K						
0.2	4.912	4.927	5.002	5.055	5.304	5.315
0.3	4.998	4.989	5.088	5.084	5.290	5.315
0.4	5.036	5.050	5.136	5.114	5.278	5.315
0.5	5.130	5.112	5.180	5.143	5.332	5.315
0.6	5.194	5.173	5.214	5.172	5.276	5.315
0.7	5.232	5.235	5.212	5.202	5.394	5.315
0.8	5.278	5.296	5.168	5.231	5.330	5.315
U	1.60×10^{-3}		1.05×10^{-2}		1.04×10^{-2}	
R(%)	0.296		0.753		0.725	
s(log k)	±0.018		±0.046		±0.042	
$T=343$ K						
0.2	5.502	5.509	5.702	5.717	5.904	5.918
0.3	5.468	5.509	5.678	5.717	5.870	5.860
0.4	5.516	5.509	5.676	5.717	5.798	5.802
0.5	5.520	5.509	5.730	5.717	5.742	5.744
0.6	5.524	5.509	5.724	5.717	5.706	5.685
0.7	5.532	5.509	5.772	5.717	5.634	5.627
0.8	5.498	5.509	5.738	5.717	5.550	5.569
U	2.78×10^{-3}		7.11×10^{-3}		1.17×10^{-3}	
R(%)	0.361		0.558		0.225	
s(log k)	±0.022		±0.034		±0.015	

The activity coefficient expressions are still given by Eq. 12.

In this case b can be fitted to

$$b=a'+b'/T \qquad (15)$$

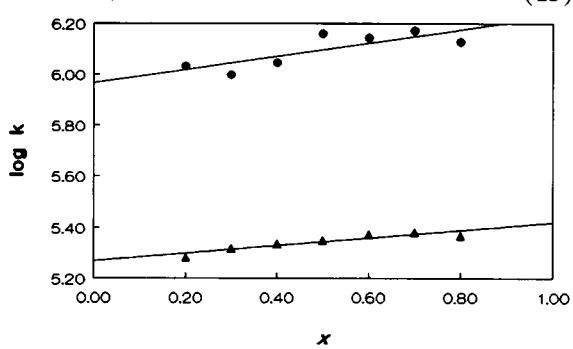

Fig. 3. Reaction: $H^+ + NH_4R \rightleftharpoons HR + NH_4^+$. log k plotted versus x for Amberlite IRC-50 for $I=0.1$ and the two temperatures. (▲) $T=303$ K, (●) T=343 K. The straight lines are those of the model using the parameters in Table 1.

This is illustrated in Fig. 3 where log k is plotted versus x for Amberlite IRC-50 and $I=0.1$ M NH_4Cl and the two temperatures. By fitting to Eq. 15 we get

$$b=1.115-292/T \qquad (16)$$

As might be expected, cases where b is independent of temperature are less common than a temperature-dependent b.

Ionic strength dependence. A plot of the equilibrium constant log K computed from Eq. 5 versus I for both resins and temperatures gives curved plots indicating that a second-order polynomial is needed to fit the data.

For both resins, reaction 4 is shifted towards higher values with I, an illustration of the common ion effect.

Temperature dependence. Rough estimates of the enthalpy for reaction 4 are obtained by plotting log K versus $1/T$. In this way the following values were found: Wofatit CA-20, $\Delta H=8.9\pm1.8$ J mol^{-1};

Table 3
Comparison of experimental and computed log k values for Amberlite IRC-50

x	$I=0.1$		$I=1.0$		$I=4.0$	
	log k (exp.)	log k (calc.)	log k (exp.)	log k (calc.)	log k (exp.)	log k (calc.)
$T=303$ K						
0.2	5.282	5.299	5.712	5.750	5.914	5.886
0.3	5.318	5.314	5.718	5.750	5.900	5.886
0.4	5.336	5.329	5.726	5.750	5.878	5.886
0.5	5.350	5.345	5.750	5.750	5.872	5.886
0.6	5.374	5.360	5.774	5.750	5.906	5.886
0.7	5.382	5.375	5.782	5.750	5.864	5.886
0.8	5.368	5.390	5.788	5.750	5.870	5.886
U	1.11×10^{-3}		6.09×10^{-3}		2.38×10^{-3}	
$R(\%)$	0.235		0.513		0.313	
$s(\log k)$	±0.015		±0.032		±0.020	
$T=343$ K						
0.2	6.032	6.018	6.422	6.479	6.704	6.722
0.3	5.998	6.045	6.448	6.479	6.770	6.740
0.4	6.046	6.071	6.446	6.479	6.728	6.732
0.5	6.160	6.097	6.510	6.479	6.702	6.697
0.6	6.144	6.123	6.524	6.479	6.626	6.636
0.7	6.172	6.149	6.512	6.479	6.534	6.549
0.8	6.128	6.176	6.488	6.479	6.450	6.436
U	1.03×10^{-2}		9.46×10^{-3}		1.79×10^{-3}	
$R(\%)$	0.628		0.567		0.240	
$s(\log k)$	±0.045		±0.040		±0.021	

Amberlite IRC-50, $\Delta H=14.0\pm0.6$ J mol^{-1}. These values are of the same sign and order of magnitude for reaction 4 with NH_4^+ exchanged for Na^+, which might be expected.

Protonation constant. The protonation constant, K_p, of the resin is defined by

$$H^+(aq)+R^-\rightleftharpoons HR \qquad (17)$$

The protonation constant K_p is related to the equilibrium constant of reaction 4 by [5]

$$\log K_p=\log\kappa-\log I \qquad (18)$$

with $[R^-]=[NH_4R]$. Observe that Eq. 25 in [5] should be written as Eq. 18 above. The last column in Table 1 gives log K_p computed from Eq. 18 above. It is found that log K_p plotted vs. I gives a set of straight lines allowing estimates of the protonation constant at infinite dilution. If we compare the protonation constants found in 1.0 M NaCl in our previous publication [3], the influence of ionic medium is found to be appreciable. The protonation constants [6] found from the data of Chatterjee and Marinsky [7] for IRC-50 are consistent with those found here.

8. Conclusions

The three-parameter model allows the estimation of the limiting values of log k with a better certainty than by graphic and similar extrapolations, which sometimes might be of practical value. The titration data show that when hydrolysis of the ammonium is desired as in the Sirotherm process it is better to use methacrylate resins and perform at low I and high T.

References

[1] E. Högfeldt, React. Polym., 11 (1989) 199–219.
[2] E. Högfeldt, in J.A. Marinsky and Y. Marcus (Eds.), Ion Exchange and Solvent Extraction, Vol. 11, Marcel Dekker, New York, 1993, pp. 109–150.
[3] I. Dobrevski, M. Dimova-Todorova, N. Dimitrova and E. Högfeldt, Acta Chem. Scand., 46 (1992) 796.
[4] E.A. Guggenheim, Clarendon Press, Oxford 1952, Chap. 4.
[5] E. Högfeldt, T. Miyajima and K. Yoshida, React. Polym., 20 (1993) 175–180.
[6] A. Chatterjee and J.A. Marinsky, J. Phys. Chem., 67 (1963) 41–47.
[7] E. Högfeldt, E. in M. Streat (Ed.), Ion Exchange for Industry, Horwood, Chichester, 1988, p. 326 and 307–313.

ELSEVIER

Analytica Chimica Acta 299 (1994) 43–57

ANALYTICA CHIMICA ACTA

Modelling complex solution equilibria III. Error-robust calculation of equilibrium constants from pH or potentiometric titration data

Pierre G. Potvin *

Department of Chemistry, York University, 4700 Keele Street, North York, Ontario M3J 1P3, Canada

Received 9 February 1994; revised manuscript received 7 July 1994

Abstract

In calculating unknown equilibrium constants by the least-squares technique from pH (or potentiometric) titration data, errors in the chemical model (initial volume, reactant concentrations, carbonate or other impurities, pK_w and other known equilibrium constants) and measurement errors (electrode calibration, drifts in ionic strength, non-ideal titrant mixing or temperature control) can strongly influence the results. Most of these errors will produce non-randomly distributed pH (or e.m.f.) residuals over some regions of data and thus violate the assumptions of the least-squares method. Simulations and deliberate errors in real data show that fitting the point-to-point changes in pH is less sensitive to such errors than is fitting the raw pH data, producing more trustworthy and reliable refinements of unknown equilibrium constants and more randomly distributed residuals. The refinement results are also insensitive to errors in calibration and more robust with regard to the range of pH spanned by the data. When applied to titrations of glycine–proton and Ni^{2+}–glycine–proton mixtures from one laboratory, the results more closely matched the averages from several laboratories. Further, this approach will actually signal the presence of unsuspected errors.

Keywords: Potentiometry; Titrimetry; pH; Complex solution equilibria; Error calculation; Equilibrium constants

1. Introduction

pH or e.m.f. titration is commonly used to determine the values of unknown equilibrium constants by numerical modelling of the data [1,2]. This usually involves matching, by a least-squares method, the observed or experimental data (y^{expt}) with numbers expected or predicted by a postulated *chemical model* (y^{pred}). Such a model includes the "unknown" equilibrium constants under investigation and *fixed* or "known" parameters such as initial titrate volume, reactant concentrations, and equilibrium constants determined by prior experiment, such as pK_w. One cannot expect a perfect fit between y^{expt} and y^{pred} but statistical theory states that, if the model is appropriate, the mis-match or poorness-of-fit should reflect errors in the measurement of the observable, y. Thus, the *residuals*, $y^{expt} - y^{pred}$, should be of believable size and more-or-less randomly distributed. Unfortunately, one often gets much-less-than-perfect fits where the residuals seem too large and/or are distributed in non-random patterns. This should suggest an inadequacy in the model and one might be tempted to alter it in order to improve the fit, either by expanding it to include previously unsuspected species or by adjusting the values of some of the fixed parameters. Many of the myriad computer programs available for the treatment of titration data allow such adjustments [3–7], and some practitioners do this routinely [8,9], but there are dangers

* Corresponding author.

SSDI 0003-2670(94)00305-X

in both practices and they need justification governed by good judgment.

This paper focuses on systematic error sources as causes of non-random residual distributions. Systematic errors can arise randomly but afflict an entire experiment. Only by repeating the experiment many times can it be hoped that such systematic errors will be averaged out to near-zero, whence the averaged results of many experiments should be less error-sensitive than those of any one experiment. But systematic errors can also arise consistently, with faulty equipment or technique. Only by repeating the experiment with different equipment and operators (i.e. in different laboratories) can consistent errors be similarly reduced. Most experiments are not carried out with this degree of attention to errors and one would welcome any means of avoiding the effects of unsuspected error in treating limited amounts of data. One such means is to anticipate the effects of errors, albeit imperfectly, by weighting the y^{expt} data according to the variance that such errors, given some typical size, can be expected to generate in y^{pred}. This places less weight on those data where the prediction strongly depends on the values of the error-prone parameters.

Nevertheless, non-random residual distributions can persist after weighted treatments. They are common enough (examples can be found in Refs. [3] and [4]), but they are often ignored in spite of two important consequences. Firstly, when the residuals are not random or not normally distributed, the best-fit values of the unknowns, the calculated uncertainties in those values and any statistical test of the aptness of the chemical model all lose validity [10]. Secondly, the best-fit values become sensitive to the *sampling*. That is, the range covered by the data (e.g. of pH), its density within that range, and any neglect of points or regions (such as when precipitation has occurred) can all affect the final, best-fit values. This sampling sensitivity is compounded when non-uniform weights are used, such as when anticipating experimental errors.

In other fields, such as in econometrics with time-series data, non-random residuals are often due to a phenomenon called autocorrelation or serial correlation [10] wherein the residual at one point (in time), r_n, is in some way dependent on the residual at the previous point, r_{n-1}, as well as on some purely random measurement error, ϵ_n, as in

$$r_n = y_n^{expt} - y_n^{pred} = f(r_{n-1}) + \epsilon_n$$

The degree of autocorrelation can be measured and tested [10] for a given set of residuals, and the simplest remedial measure, called the First Differences approach, is to assume a first-order correlation ($r_n = r_{n-1} + \epsilon_n$), the origin of which need not be known. Modelling the point-to-point differences (Δy) should then produce less autocorrelated, more randomly distributed residuals ($\Delta y^{expt} - \Delta y^{pred}$) that approximate the ϵ more closely. Although some non-random character may persist, the model is nevertheless improved. Two additional benefits are possible. One can firstly anticipate that the Δy^{pred} will be much less affected by systematic errors because a pair of neighbouring y^{pred} values are usually affected to similar degrees (which is how non-random residual patterns arise). In the absence of systematic error, of course, fitting Δy^{pred} to Δy^{expt} should be entirely equivalent to the normal regression, i.e. to fitting y^{pred} to y^{expt}. In the presence of error, fitting Δy^{pred} to Δy^{expt} can result in a poorer match of the y^{pred} numbers to y^{expt} than would be obtained by normal regression. Therefore, one can also anticipate that the poorness-of-fit of y^{pred} to y^{expt} resulting from the First Differences treatment will in fact signal the presence of systematic error.

In view of these possible benefits, this paper examines the application of the First Differences approach (herein called the Difference Method or DM) to the treatment of pH titration data, which can be likened to time-series data, in comparison with fitting the raw pH data (herein called the Normal Method or NM). (Though this paper concentrates on pH data, the findings apply equally well to e.m.f. data, which are linearly related.) To assess, in a controlled fashion, the effects of known amounts of error and the biases that they induce, synthetic data sets were extensively used because the desired end results (the perfect models) are known. The effects of both random and systematic errors were examined, as were the influences of data sampling. Both binary and ternary mixtures were modelled but the conclusions that were reached should apply to *any* kind of association. A few synthetic data sets, however varied, cannot mimic all possible titration situations. Nevertheless, the anticipated benefits were indeed realized. To illustrate its use with real data, the Difference Method was also applied to the benchmark Ni^{2+}–glycine system.

2. Methods

All computations were performed using the Fortran program Jacobi [11] after modification as described here to the variance calculation and the Gauss-Newton process.

In a general notation applying to both Methods, the calibrated pH at any nth of N data points is written

$$\mathrm{pH}_n^{\mathrm{expt}} - \rho\mathrm{pH}_{n-1}^{\mathrm{expt}} = \mathrm{pH}_n^{\mathrm{obs}} - \rho\mathrm{pH}_{n-1}^{\mathrm{obs}} + (1-\rho)b \qquad (1)$$

where, normally, $\rho = 0$ and where b is the "intercept" correction related to the Nernst E^0, which can be determined by a Gran plot of the acidic buffer region [1] [12]. Equivalently, with e.m.f. data (E^{obs}),

$$\mathrm{pH}_n^{\mathrm{expt}} - \rho\mathrm{pH}_{n-1}^{\mathrm{expt}} = \frac{RT}{\ln 10 F}(E_n^{\mathrm{obs}} - \rho E_{n-1}^{\mathrm{obs}} - (1-\rho)E^0)$$

With $\rho = 1$, neither b nor E^0 is needed. One seeks to minimize the residuals

$$r_n = \mathrm{pH}_n^{\mathrm{expt}} - \rho\mathrm{pH}_{n-1}^{\mathrm{expt}} - (\mathrm{pH}_n^{\mathrm{pred}} - \rho\mathrm{pH}_{n-1}^{\mathrm{pred}})$$

These would normally be random and of small, constant variance if only random error in the pH measurement were present. Other sources of error give them a non-constant but *quasi*-predictable variance. To obtain estimates of the unknown equilibrium constants that are not biased by any particular pH point in such cases, each nth datum must be weighted by a factor w_n such that the weighted residuals $r_n' = w_n^{1/2} r_n$ will have constant variance. Thus,

$$\sigma^2(r_n') = \sigma^2(\epsilon) = \text{a constant}$$
$$= \sigma^2(w_n^{1/2} r_n) = w_n \sigma^2(r_n)$$

One cannot know $\sigma^2(\epsilon)$ in advance, but this will be estimated by $\mathrm{SWSR}/(N-\rho-N_\beta)$ where the *s*um of the *w*eighted *s*quared *r*esiduals (SWSR) is given by

$$\mathrm{SWSR} = \sum_{n=1}^{N} w_n r_n^2$$

and where $N-\rho-N_\beta$ is the number of degrees of freedom left from estimating N_β unknown equilibrium constants β with $N-\rho$ data. Summing over all the data,

$$\sum_{i=1}^{N} w_i \sigma^2(r_i) \approx \sum_{i=1}^{N} \frac{\mathrm{SWSR}}{N-2} = \frac{N}{N-2}\mathrm{SWSR}$$

then the *w*eighted *m*ean *e*rror (WME) is

$$\mathrm{WME} = \sqrt{\sum_{i=1}^{N} w_i \sigma^2(r_i) \Big/ \sum_{i=1}^{N} w_i}$$
$$\approx \sqrt{\frac{N}{N-2}\mathrm{SWSR} \Big/ \sum_{i=1}^{N} w_i} \qquad (2)$$

The WME is a measure of the poorness-of-fit independent of the weighting scheme, relating the estimated size expected of a residual of unit weight. Setting $w_n \propto 1/\sigma^2(r_n)$ ensures a fairly constant variance if $\sigma^2(r_n)$ reflects the variance in the data owing to all sources of error.

Since $\mathrm{pH}_n^{\mathrm{expt}}$ is independent of $\mathrm{pH}_n^{\mathrm{pred}}$, $\sigma^2(r_n)$ is first divided into two terms:

$$\sigma^2(r_n) = \sigma^2(\mathrm{pH}_n^{\mathrm{expt}} - \rho\mathrm{pH}_{n-1}^{\mathrm{expt}} - (\mathrm{pH}_n^{\mathrm{pred}} - \rho\mathrm{pH}_{n-1}^{\mathrm{pred}}))$$
$$= \sigma^2(\mathrm{pH}_n^{\mathrm{expt}} - \rho\mathrm{pH}_{n-1}^{\mathrm{expt}}) + \sigma^2(\mathrm{pH}_n^{\mathrm{pred}} - \rho\mathrm{pH}_{n-1}^{\mathrm{pred}})$$

The first term is constant:

$$\sigma^2(\mathrm{pH}_n^{\mathrm{expt}} - \rho\mathrm{pH}_{n-1}^{\mathrm{expt}})$$
$$= \sigma^2(\mathrm{pH}_n^{\mathrm{obs}} - \rho\mathrm{pH}_{n-1}^{\mathrm{obs}}) + (1-\rho)\sigma^2(b)$$
$$= (1+\rho)\sigma^2(\mathrm{pH}) + (1-\rho)\sigma^2(b)$$

with $\sigma(\mathrm{pH})$ being an estimate of the electrode's error measuring any one pH and may include an estimate of the error(s) at the pH extrema. An estimate of $\sigma(b)$ can be obtained from the same Gran plot used to determine b [12] but is not needed when $\rho = 1$. It may include an estimate of error due to a drift in ionic strength.

The nature of the second term depends on the method used. With $\rho = 0$, $\sigma(\mathrm{pH}^{\mathrm{pred}})$ is approximated according to error propagation rules by

$$\sigma^2(\mathrm{pH}_n^{\mathrm{pred}}) = \left(\frac{\delta \mathrm{pH}_n^{\mathrm{pred}}}{\delta v}\right)^2 \sigma^2(v) + \sum_{j=1}^{N_p}\left(\frac{\delta \mathrm{pH}_n^{\mathrm{pred}}}{\delta P_j}\right)^2 \sigma^2(P_j) \qquad (3)$$

where $\sigma^2(v)$ represents the expected variance in titrant volume and $\sigma^2(P_j)$ is that expected in the jth of N_p

[1] The Martell group instead adjust the pH of an acidic titrate prior to titration so as to match the pH expected after fully protonating all protonatable species present [9]. This does not allow an estimate of $\sigma(b)$, which is needed for weighting if $\rho = 0$.

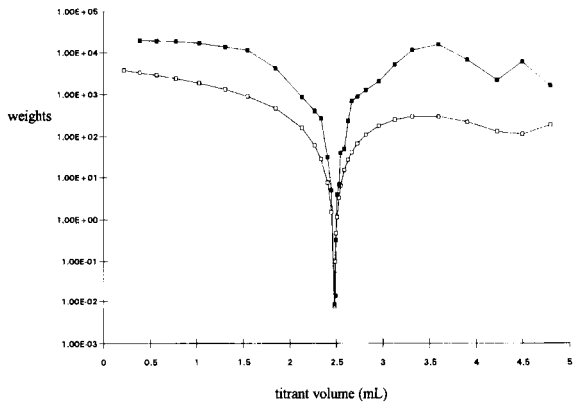

Fig. 1. Weights (presented for clarity on a logarithmic scale) used in treating data set C14 by the Normal Method (open squares) and the Difference Method (filled squares) and calculated as described in the Data section. Note that both Methods place little weight near the equivalence point.

systematic error sources P_j, including initial volume, reactant concentrations and known constants such as pK_w [2]. These variances would be estimated or measured by previous experiment. (Analytical forms of the derivatives are available [11].) On the other hand, if $\rho = 1$, then

$$\sigma^2(\Delta pH_n^{pred}) = \left\{\left(\frac{\delta pH_{n-1}^{pred}}{\delta v}\right)^2 + \left(\frac{\delta pH_n^{pred}}{\delta v}\right)^2\right\}\sigma^2(v)$$

$$+ \sum_{j=1}^{N_P}\left(\frac{\delta pH_n^{pred}}{\delta P_j} - \frac{\delta pH_{n-1}^{pred}}{\delta P_j}\right)^2 \sigma^2(P_j) \quad (4)$$

This follows from the fact that random error in titrant volume at one point is independent of that at the next point, but because a systematic error in one of the parameters P will act in the much same way at each point, their contributions to the total error at neighbouring points will not be independent (i.e. the covariance will be non-zero) but will in fact be smaller in ΔpH^{pred}. Thus, it can be anticipated that the minimization with $\rho = 1$ will be less sensitive to systematic errors in P but be about twice as sensitive to random errors in v. Fig. 1 illustrates the differences in the weights used by the two Methods.

[2] Other authors use less complete descriptions of the expected variance to compute weights [1,3–5,13] or use weighting by the inverse pH–volume slope [6], which amounts to considering only titrant volume as a source of error.

The calculations of species concentrations, of pH^{pred}, of corrections to the estimates of the unknown log formation constants ($\Delta \log \beta$), of the uncertainties in the final, refined log β values and of the correlation coefficients between constants were all as described earlier [11]. With the Difference Method, this requires a modification of the previously described algorithm to repeatedly solve the $N - \rho$ simultaneous truncated Taylor series. In general form,

$$w_n(r_n - \rho r_{n-1})$$
$$= w_n \sum_{k=1}^{N\beta}\left\{\frac{\delta pH_n^{pred}}{\delta \log \beta_k} - \rho\frac{\delta pH_{n-1}^{pred}}{\delta \log \beta_k}\right\}\Delta \log \beta_k$$

can be solved for the corrections to be applied to the current (or initially guessed) estimates of the N_β unknown log β. The scale of the weights has no effect on the values of the logβ but it will affect the uncertainties. The uncertainties in pK_a values were calculated according to the method for derived constants [16].

After achieving the best fit, the WME value should ideally match σ(pH) and thus be ascribable only to electrode error. If WME $< \sigma$(pH), then the σ(pH) estimate was perhaps too high, but if WME $\gg \sigma$(pH), then the data are evidently afflicted with errors that cannot be reduced by adjustment of the variables, either systematic ones in the fixed parameters or as other components to measurement error (drifting ionic strength, poor mixing, slow electrode response, clogging of the membrane, etc.).

A DM model will not be comparable with the NM model for the same data in any test to detect significant difference, because the weights differ not only in using different log β values but also in containing different components. Because the Hamilton R-ratio test [17] (a variant of the F-test for which R factors need never be computed) compares two models that use the same weights, it is not applicable. To equalize the effects of weighting, direct comparisons between competing models were instead made using the WME values (formula 2) that each model generated by the NM. A NM WME′ value was calculated from the DM best-fit log β values. Thus, the hypothesis that the two models are equivalent can be rejected at the $100\alpha\%$ significance level if

$$\frac{WME'}{WME} > \frac{N_P}{N_D - N_P}F_{1-\alpha;\, N_P, N_D - N_P} + 1$$

Table 1
log β_{101} and log β_{102} for glycinate from data set C14 with and various amounts of error in pH and titrant volume and 1% errors elsewhere

$\sigma(v)$	σ(pH) with $\rho=0$			σ(pH) with $\rho=1$		
	0	0.005	0.050	0	0.005	0.050
0	9.6448(40)	9.6448(40)	9.6442(35)	9.6742(112)	9.6697(70)	9.6741(127)
	12.1078(50)	12.1076(50)	12.1033(58)	12.0716(145)	12.0814(157)	12.1125(424)
0.001	9.6448(40)	9.6448(40)	9.6442(35)	9.6744(113)	9.6697(70)	9.6741(126)
	12.1078(50)	12.1076(50)	12.1033(58)	12.0716(144)	12.0815(156)	12.1125(423)
0.010	9.6448(40)	9.6448(40)	9.6442(35)	9.6721(80)	9.6697(67)	9.6743(117)
	12.1078(50)	12.1075(50)	12.1034(58)	12.0764(120)	12.0830(161)	12.1115(386)

in a variant of the Hamilton test. Values of F are available from Tables [10]. This was the case for all the real data sets tested, to a 95% confidence level.

To obtain "experimental" estimates with multiple, real data sets, each ith of N_T data sets were treated separately to afford N_T estimates of each jth of N_β log β values, designated log $\beta_{j,i}$, each with some uncertainty $\sigma(\log \beta_{j,i})$. Weighted average values and standard errors $\sigma(\log \beta_j)$ were then computed with formula 5.

3. Data

Titrations of a binary mixture were simulated to explore most error sources and data sampling effects. In general, 3 ml of a solution that was 0.1 M in NaCl, 0.03 M in HCl and 0.005 M in a hypothetical tetrabasic substance was titrated with 0.1 M NaOH. The cumulative protonation constants were set at 10, 18, 24 and 28. The pK_w (13.78) was taken from Tables [14] and no pH correction was applied (i.e. $b=0$). In one, evenly-stepped data set (SE), 40 titrant increments of 0.03 ml were applied and this brought the expected pH to 12. In another, unevenly-stepped set (SU), also of 40 points reaching to the same pH, smaller increments were applied near the equivalence points and larger increments were used in the H_2O buffer regions, to simulate manual titration. A third, extended set (SX) spanned a broader pH range by using 0.035 M HCl and 50 increments of 0.03 ml. A fourth set (SC) related a titration of a ternary mixture. It was similar to set SE but included 1 mol% of CO_3^{2-} (1 mM) in the titrant. The CO_3^{2-} protonation constants were taken from Tables [14]. To explore the effects of error in known equilibrium constants with a ternary mixture, a data set (SN) was modelled on the Ni^{2+}–glycine system: 3 ml of a titrate that was 0.1 M in NaCl, 7.5 mM in a hypothetical bidentate, 2.5 mM in a hypothetical divalent metal ion and 30 mM in acid was titrated with 0.1 M NaOH. Again, pK_w was 13.78. The ligand's protonation constants [3] were log $\beta_{101}=9.5$ and log $\beta_{102}=13$ and the ideal metal binding constants were set at log $\beta_{110}=5$, log $\beta_{210}=9$ and log $\beta_{310}=13$. For the purposes of data weighting, $\pm 1\%$ errors were allowed in v_0 and in all reactant concentrations, ± 0.005 log units in pH, ± 0.001 ml in titrant volume and ± 0.03 log units in pK_w. For set SC, errors of ± 0.5 mM in $[CO_2^{tot}]$, and ± 0.04 and ± 0.05 log units in the CO_3^{2-} pK_{a1} and pK_{a2} values, respectively, were also allowed. For set SN, these were allowed an error of ± 0.03 log units. Data from the real Ni^{2+}–glycine system were chosen from the literature [15] (referred to, by the authors' numbering, as sets C1, C2 and C7–C14) and also retreated here. The authors' pK_w value of 13.67 (± 0.03) was used and the same errors were allowed as above. To achieve realism in the simulations, all possible error sources were included in the calculation of weights, even if non-existent, but it was verified that the same conclusions could be drawn if non-existent errors were excluded.

For the simulation of errors, random real numbers R_i lying between -50 and $+50$ were used, any ith of which was generated by the central limit theorem with formula

$$R_i = \left(\sum_{j=1}^{100} \mathrm{ran}_j(s)\right) - 50$$

where ran(s) represents evenly distributed, random real numbers lying between 0 and 1, each generated

[3] Here, β_{xyz} refers to $[L_xM_yH_z]/[L]^x[M]^y[H]^z$.

from a seed s by the computer's internal random number generator function. To allow comparisons between numerical approaches for the same, error-containing data, the same seed was used. The numbers R were normally distributed about 0 with a standard deviation, $\sigma(R)$, of 2.8845. For random errors in pH, each nth pH point was altered by the transformation

$$pH_n^{obs} \Rightarrow pH_n^{obs} + \sigma(pH)R_n/\sigma(R)$$

with a given "experimental" $\sigma(pH)$ of 0.005 log units, such that the standard deviation of the induced errors was $\sigma(pH)$. Randomly arising errors in any jth systematic error source P_j were similarly generated according to

$$P_j^{alt} = P_j + \sigma(P_j)R/\sigma(R)$$

allowing standard deviations of 1%, i.e. $\sigma(P_j) = 0.01 \times P_j$. The new pH values expected with these altered volumes or altered parameters (pH^{alt}) were calculated, then the original parameters were restored and the "experimental" pH^{obs} were substituted by the pH^{alt} values. The effects of such errors were examined under conditions where they were either overestimated, accurately estimated or underestimated.

In each experiment, 60–100 trials (depending on c.p.u. time consumption in a time-sharing environment) were carried out in which the log formation constants ($\log \beta$) were recalculated with ρ being 0 or 1. The weighted average $\log \beta$ values and their weighted standard deviations from the ideal values were obtained for N_T trials according to

$$\overline{\log \beta_j} = \frac{\sum_{i=0}^{N_T} \log \beta_{j,i}/\sigma^2(\log \beta_{j,i})}{\sum_{i=0}^{N_T} 1/\sigma^2(\log \beta_{j,i})}$$

$$\sigma(\log \beta_j) = \sqrt{\frac{\sum_{i=0}^{N_T} (\log \beta_{j,i} - \log \beta_j^{true})^2/\sigma^2(\log \beta_{j,i})}{\sum_{i=0}^{N_T} 1/\sigma^2(\log \beta_{j,i})} \frac{N_T}{N_T - 1}} \quad (5)$$

using as weights the inverse of the squared calculated uncertainties in the log formation constants, $\sigma(\log \beta_{j,i})$ [7]. This corresponds to the estimation of experimental error from N_T repeat titrations, each subject to varying amounts of error and each weighted according to how good a fit was obtained.

A weighted average $\log\beta$ value obtained by one Method could be compared with that obtained by the other with a simple t-test of two population means [10], wherein the difference was considered significant at the $100\alpha\%$ level if

$$\overline{\log \beta_j^{DM}} - \overline{\log \beta_j^{NM}} > t_{1-\alpha/2;\, 2N_T-2} \sqrt{\frac{\sigma^2(\log \beta_j^{DM}) + \sigma^2(\log \beta_j^{NM})}{N_T}} \quad (6)$$

where the square root represents the joint error interval. Values of t are available from Tables [10].

4. Results and discussion

4.1. General behaviour

In general, fitting ΔpH^{obs} data (i.e. $\rho = 1$) was well-behaved in that the overall minimum SWSR value was smoothly attained from any direction and, in the absence of systematic errors (vide infra), this coincided with the minimum $\Delta \log \beta$ values. The SWSR–$\log \beta$ profiles with $\rho = 1$ had the same appearance as when ρ was 0, i.e. the calculated $\Delta \log \beta$ corrections increased exponentially with increasingly underestimated $\log \beta$ values but increased linearly with increasingly overestimated $\log \beta$ values [11]. In consequence, the modified Gauss-Newton strategy previously elaborated to avoid overshoot and divergence [11] could be usefully applied here as well.

4.2. Effects of errors in calibration

Errors can arise when, for example, the ionic strength or temperature of the titrate solution is different from those at which the electrode was calibrated. This translates into a systematic shift of the calibrated pH (pH^{expt}) but the observed point-to-point change in pH (ΔpH^{obs}) is entirely unaffected since $\Delta pH^{expt} = \Delta pH^{obs}$. The rigour of the calibration would

no longer be of consequence [4]. Similarly, error occurs when the electrode's response changes during a titration due to a drift in the solution's ionic strength, such that the calibration is no longer valid. Indeed, though it may be possible to maintain a constant ionic strength over some portion of the pH range, it is very difficult to ensure constancy throughout the experiment when dealing with fluctuating and initially unknown concentrations of multiply charged species, even in the presence of tolerably high concentrations of a background electrolyte. But a drifting ionic strength will cause similar errors at neighbouring pH points but a much smaller or even negligible effect on ΔpH^{obs}.

4.3. *Effects of errors in titrant volume (v) and pH measurement*

Error can afflict the titrant delivery and the pH (or e.m.f.) measurement and such is considered random in character. In this context, Baeza et al. [7] have recently tested the performance of a few "best-fit"-seeking algorithms in the presence of random errors in both pH and v. The minimization of a composite SWSR that included residuals in both has even been proposed [13,19] but this is statistically problematic since the residuals are correlated. Least-squares treatments assume random error in one of these and require that the other be totally error-free. (Some programs, such as SCOGS and its descendants [20,21] validly fit the v data instead of pH or E, making the counter-intuitive assumption that the latter are error-free. Indeed, the error in one variable can be considered as belonging to the other.) York's "least-square cubic" method will show that a small random error in the independent variable has a negligible effect on the regression results, in linear systems at least [22]. Further, Berkson [23] has shown that error in an independent variable is admissible when its value is "targeted", as opposed to when it arises randomly (such as when correlating daily sales with unpredictable numbers of customers), so long as that error is independent of the value of either variable. In manual titration, the total volume of titrant delivered at any point is indeed a targeted quantity and any error arising would be independent of the total volume and of the pH. However, machine-driven burets that deliver targeted increments cause the error in the total delivered at any point to be a cumulation of the random errors arising with each increment. If repeat titrations with the same reactant solutions do not differ wildly, if they generally give nearly superimposable titration curves leading to similar results, then this is a non-problem or, at least, not an important one.

A slow electrode response, an incomplete mixing (concentration gradients), temperature gradients, etc. might also contribute non-random character to the measurement error, as can a loss of homogeneity. As well, junction potentials arise with glass electrodes at very high and very low pH. Such errors are difficult to simulate, but estimates might be included in the overall estimate of $\sigma(pH)$. In any case, such non-randomness implies similar errors at neighbouring pH points but a negligible effect on ΔpH^{obs}, whence the DM should be less sensitive.

But just how important are these error contributions to the results from error-prone data? To explore this, the protonation constants of glycinate were evaluated from set C14, described in the Data section, with adjustments of the weighting scheme to allow various amounts of error in v and pH. The results appear in Table 1. The protonation constants obtained by the NM ($\rho=0$) were negligibly affected by the allowance or neglect of random errors in pH or in v, and the allowed value of $\sigma(pH)$ was of no great importance. As expected from a comparison of Eqs. 3 and 4, use of the DM ($\rho=1$) led to more ample influences, with the size of $\sigma(v)$ influencing the results in the third decimal place and $\sigma(pH)$, the second decimal place. Given the uncertainties, these are small effects and, insofar as this data set is typical, v and pH are simply not major contributors to the total variances.

4.4. *Effects of errors in reactant concentrations and titrate volume*

Any error in these parameters introduces an error in the pH expected from the chemical model, pH^{pred}, and the unknown log β will suffer an undesirable adjustment during refinement to force the pH^{pred} to match pH^{expt}. This produces residuals ($pH^{pred} - pH^{expt}$) of consistent (i.e. non-random) sign in certain regions of the data. Impurities in the reactants constitute an important source of error affecting concentrations. Non-titratable impurities cause an overestimation of the

[4] This holds as long as no slope adjustment is made, which theory only allows to correct for temperature changes (cf. Ref. [18]).

concentration of the affected reactant, giving rise to a systematic error. A common titratable impurity is CO_2 absorbed in alkaline solutions. Martell [9] describes a Gran plot-based method of estimating the carbonate content of bases and this estimate can then be included as a fixed parameter in the chemical model under investigation. Another example would be traces of the protonated form(s) of amine bases or of the free base contaminating its salt [6]. Either will affect the total amine content and the total H^+. There is little that can be done with data corrupted by the presence of unknown titratable impurities. Fortunately, one can anticipate a decreased sensitivity in ΔpH^{pred} to such errors because their effects will be very similar at neighbouring pH points and a smaller adjustment in the unknown log β will be required to match ΔpH^{obs} than would be required to match pH^{expt}.

Simulations show that a synthetic, totally error-free data set will provide the same log β values by either Method, with or without weighting. If one Method's results are less sensitive to errors, then the two Methods will lead to differing results in the presence of deliberate errors. By the same logic, if real data give different results when treated by the two Methods, there must be one or more errors in the chemical model, and the effects of those errors on the two sets of logβ results must be unequal. Further, if one Method's results are less sensitive to errors, they will also be less biased by any pre-existing (unsuspected) errors. Thus, a Method's sensitivity to error is a good gauge of the reliability of its results.

Differences in sensitivity are easily assessed. Data set C14 was used to illustrate. The changes in log β values that resulted after introducing deliberate errors in each of the systematic error sources are recorded in Table 2. It was verified that, for small perturbations in any parameter, the changes in log β by either Method increased linearly with the amount of error. Large perturbations sometimes caused heightened sensitivities. Evidently and as expected, the DM was the least sensitive, except when handling errors in pK_w (vide infra). In the absence of evidence of error in pK_w (discussed below), it is reasonable to conclude that the DM results for set C14 are more reliable. Experience with several other data sets has revealed this to be generally true, so long as the point-to-point pH changes are not unusually large. (One contrary instance is a similar data set (C11) from the same authors [15] which gave less sensitive NM results. Part of the difficulty that the DM encounters with set C11 is trying to match the large pH jump (3.3–8.5) that occurs there.) To contrast, the results of applying the NM without weighting (still a common practice) are also reported in Table 2 and these showed much higher sensitivity to most errors.

With the synthetic data sets SE and SU (see the Data section), simulations confirmed the superiority of the DM in the presence of errors in individual parameters and in combinations thereof. Random amounts of deliberate error were introduced in each individual parameter and the log β values and their uncertainties were calculated with each Method. Set SC was similarly used to explore the effect of poor estimates of the carbonate content of the base titrant. After 60–100 tri-

Table 2
Sensitivities of the log formation constants calculated from glycinate (gly) titration data set C14 to deliberate errors in the titration parameters P_j. Without added error, the Normal Method ($\rho=0$) values with weighting (and uncertainties in the least significant digits) were log $\beta_{101}=9.6448(40)$ and log $\beta_{102}=12.1076(50)$, while without weighting, log $\beta_{101}=9.5982(215)$ and log $\beta_{102}=12.1110(433)$ and the Difference Method ($\rho=1$) results were log $\beta_{101}=9.6697(70)$ and log $\beta_{102}=12.0814(156)$

P_j	$\Delta \log \beta_{101}/\Delta P_j$			$\Delta \log \beta_{102}/\Delta P_j$		
	$\rho=0$ All $w_n=1$	$\rho=0$	$\rho=1$	$\rho=0$ All $w_n=1$	$\rho=0$	$\rho=1$
b	1.086	1.055	0.000	3.315	2.614	0.000
v_0	0.0434	0.1941	−0.0096	0.0559	0.9476	0.0352
$[gly^{tot}]_0$	−168.3	−1659	−79.17	−452.5	−8333	−415.8
$[H^{tot}]_0$	262.0	1687	12.86	466.0	8155	332.1
$[OH^-]$	8.614	55.07	−2.000	1.643	211.8	6.943
pK_w	−0.0833	−0.0452	1.000	−0.0832	−0.0447	1.000

Table 3
For data set SE containing random errors in v_0 with $\sigma(v_0) = 0.03$ ml, averages of 100 calculations of cumulative protonation constants and, in brackets, averaged deviations from ideal values in the least significant digits, where the weighting was uniform (unw) or allowed various amounts of error in v_0 given by $f \times \sigma(v_0)$

		unw	$f=0$	$f=1$	$f=10$
$\rho=0$	$\log \beta_{101}$	10.0010(183)	10.0015(208)	10.0015(211)	10.0015(217)
	$\log \beta_{102}$	18.0018(319)	18.0020(333)	18.0021(335)	18.0020(341)
	$\log \beta_{103}$	24.0024(427)	24.0026(434)	24.0026(436)	24.0025(440)
	$\log \beta_{104}$	28.0030(507)	28.0030(516)	28.0031(518)	28.0030(532)
$\rho=1$	$\log \beta_{101}$	10.0003(89)	10.0004(68)	10.0003(61)	10.0001(12)
	$\log \beta_{102}$	18.0007(162)	18.0007(122)	18.0006(113)	18.0001(23)
	$\log \beta_{103}$	24.0010(219)	24.0009(166)	24.0009(156)	24.0000(29)
	$\log \beta_{104}$	28.0013(259)	28.0011(198)	28.0010(185)	28.0001(47)

als, the average log β values, each weighted by its uncertainty, and the similarly weighted average distances from the true values were calculated (Eq. 5). The results of error in v_0 are presented in Table 3 and are typical of those with errors in any parameter except pK_w (vide infra). With equal or unequal titrant increments, with or without weighting, and regardless of whether the errors allowed were grossly overestimated, exact estimates or grossly underestimated, *the Difference Method was consistently more successful and more reliable than the Normal Method.* Moreover, the DM was always most successful with non-uniform weighting whereas the NM was usually better with uniform weighting. As related in Table 4, the same success was obtained with a similar data set (SC) afflicted by random amounts of error introduced in random combinations to *all* the parameters simultaneously including the carbonate content of the base titrant – a situation more akin to real-life titrations.

As evidence of the imperfect anticipation of error in weighting, the exactness of the estimated typical error sizes (standard deviations) used in the calculation of weights did have a bearing on the reliability of the resulting log β values. For instance, with these synthetic data, ten-fold overestimates of $\sigma(v_0)$, $\sigma([H^{tot}]_0)$ and $\sigma([OH^-])$ and underestimates of $\sigma([L^{tot}]_0)$ and $\sigma([CO_2^{tot}]_0)$ even as low as 0 were found to be more useful for the DM than were exact estimates. With the NM, the preferences were exactly opposite though uniform weighting was usually more successful. During a large number of simulations, exact estimates of the typical error sizes are overestimates of the true error for roughly half the trials and underestimates for most of the rest.

Deliberate systematic errors gave rise to two phenomena observed during refinement with the DM. Firstly, the minimum in SWSR did not necessarily coincide with the minimum in Δ log β values, though

Table 4
As with Table 3, results from 60 simulations with set SC containing random errors in v_0, in $[L^{tot}]$, in $[H^{tot}]$, in $[OH^-]$ and in $[CO_2]$, with $\sigma(v_0)$, $\sigma([L^{tot}])$, $\sigma([H^{tot}])$ and $\sigma([OH^-])$ each being 1% of their respective parameter and $\sigma([CO_2])$ being 50% of $[CO_2]$, but where the weighting was uniform (unw) or allowed various amounts of all errors given by $f \times \sigma$

		unw	$f=0$	$f=1$	$f=10$
$\rho=0$	$\log \beta_{101}$	10.0029(673)	9.9975(875)	10.0020(1033)	10.0014(1034)
	$\log \beta_{102}$	18.0032(1194)	17.9963(1565)	17.9926(1639)	17.9904(1602)
	$\log \beta_{103}$	24.0055(1635)	23.9983(2111)	23.9916(2152)	23.9886(2097)
	$\log \beta_{104}$	28.0083(2053)	28.0016(2591)	27.9926(2663)	27.9891(2598)
$\rho=1$	$\log \beta_{101}$	10.0010(248)	10.0028(344)	9.9994(231)	9.9998(196)
	$\log \beta_{102}$	18.0010(446)	18.0043(640)	17.9983(471)	17.9964(426)
	$\log \beta_{103}$	24.0011(610)	24.0054(891)	23.9975(666)	23.9939(577)
	$\log \beta_{104}$	28.0001(750)	28.0052(1110)	27.9963(799)	27.9910(631)

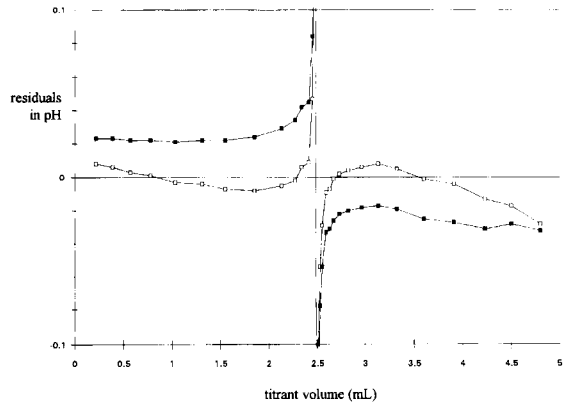

Fig. 2. Residuals $pH^{pred} - pH^{expt}$ from treating data set C14 with the Normal Method (open squares) or the Difference Method (filled squares). Some values near 2.5 ml are offscale.

the differences observed were usually small. Secondly, there were visible effects on the calculated pH curves (pH^{pred}). Consider, for instance, the typical case of deviations from pH^{obs} (or pH^{expt}) caused by deliberate errors in v_0 (Fig. 3). The NM produced residuals that alternated between positive and negative values in attempts to best match pH^{pred} to pH^{obs}, with consistency in sign appearing only at the pH extrema. In contrast, the DM produced larger residuals in pH that were almost all of the same sign, a result of sacrificing the fidelity of pH^{pred} to pH^{obs} so as to best match ΔpH^{pred} to ΔpH^{obs}. Yet there was significantly less corruption of the log β values. Unfortunately, the residual patterns were not particularly distinctive, and one could be misled by combinations of errors and the fact that a pattern

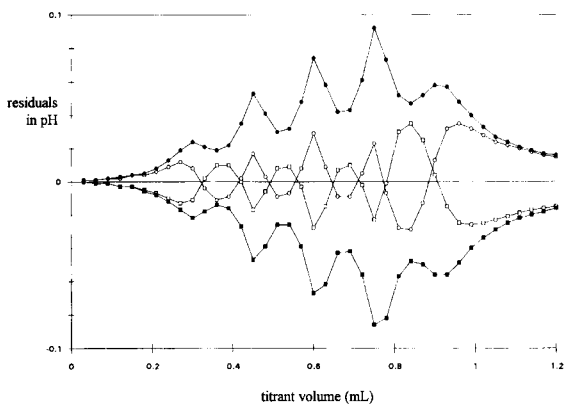

Fig. 3. Residuals $pH^{pred} - pH^{expt}$ from treating data set SE with errors in v_0: Normal Method with +1% (open squares) or with −1% error (open circles), and Difference Method with +1% (filled squares) or −1% errors (filled circles).

from one error source can resemble that of another. For instance, errors in $[OH^-]$ produced patterns that were nearly superimposable with those of Fig. 3.

It is logical that the appearance of such consistently positive or negative residuals in real data probably implies some unsuspected systematic errors. Fig. 2 shows the pattern of residuals in pH obtained upon DM treatment of the real data set C14. The consistency in sign, over certain pH regions, of the residuals could be ascribed to a number of systematic error sources, alone or in combination.

4.5. *Effects of errors in known equilibrium constants*

Fortunately, errors in the operational value of pK_w (and that of b in Eq. 1) are fairly easy to avoid. Titrations can be designed so as to provide a constant ionic strength in the region where the value of pK_w matters most, i.e. beyond the point of neutralization of all added H^+. If carried out in aqueous media, a tabled value of pK_w at that ionic strength can be used [14]. Both the NM and the graphical Gran method [12] can be applied to estimate pK_w from strong acid–strong base titrations at the appropriate ionic strength in the desired solvent. (This could also be done with data from any titration, so long as there exist data in the H_2O buffer regions before and beyond the range of influence of any constant other than pK_w, i.e. at both pH extremes.) The Gran method evaluates both b (or E^0) and pK_w and can be used to standardize the acid, the base and the CO_2 contaminant of bases [9]. The Jameson-Wilson procedure [24] is more approximate and less versatile than the Gran method. With the pK_w, $[H^{tot}]$ and $[CO_2]$ treated as unknowns, the NM gives better somewhat better estimates and is less sensitive to certain errors The DM is not as useful, as $\delta pH/\delta b = 0$ and $\delta pH/\delta pK_w \approx 0$ and the calculation can be quite sensitive to systematic errors.

Nevertheless, the effects of errors in pK_w on other constants were explored. The DM results were generally, though not always, more sensitive to errors in pK_w both in simulations with set SE (data not shown) and in the calculation of the glycinate protonation constants from data set C14 (Table 2). Importantly, the consistent distortions of the log β values from use of the DM produced residuals in pH that cumulated stepwise (Fig. 4), ultimately reaching the amount of error in pK_w (here $\pm 1\%$ or ± 0.1378 log units). This behaviour can

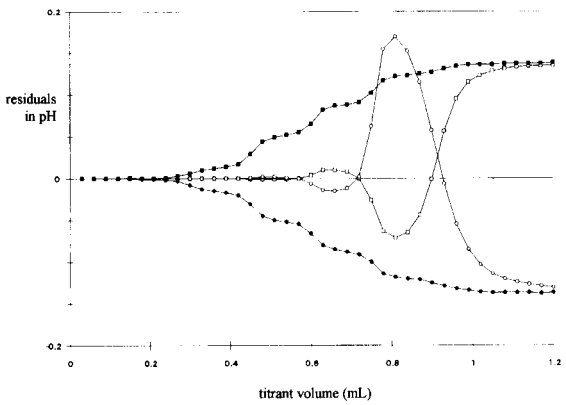

Fig. 4. As with Fig. 3, with errors in pK_w.

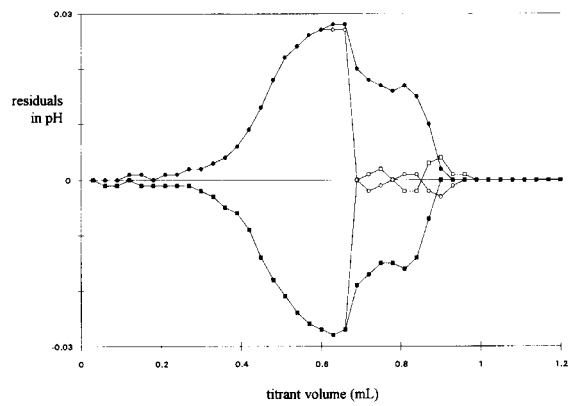

Fig. 5. As with Fig. 3, with data set SN and errors in glycine pK_{a1}.

be understood by considering that a bad pK_w value will cause a miscalculation of $[H^+]$ at the last data point, whence only a similar miscalculation of $[H^+]$ at the previous point will enable ΔpH^{pred} to match ΔpH^{obs}. This residual pattern was easily recognizable as only this error source produced log β results that generated pH residuals that increased with pH, whereas the effects of all other sources petered out at the pH extremes.

The degree of error in an unknown log β that is induced by an error in pK_w depends on the correlation coefficient between these constants. In case of set C14, both glycinate log β_{101} and log β_{102} values were virtually 100% correlated with pK_w and distortions in their values exactly matched the distortion in the pK_w value. With the hypothetical system (set SE), however, the correlation coefficients between pK_w and log β_{10m} were smaller and decreased with increasing m. Consequently, the changes caused by distortions in pK_w followed the order $\Delta \log \beta_{101} > \Delta \log \beta_{102} > \Delta \log \beta_{103} > \Delta \log \beta_{104}$, with the uncertainties increasing with increasingly distorted pK_w, i.e. as occurs with the NM. This result was also found by Baeza et al. [7]. With the NM, the correlation coefficients are a loose function of the pH span (see below).

When treating data from ternary mixtures (e.g. metal–ligand–proton), some equilibrium constants governing binary interactions (e.g. ligand–proton, metal–proton) may be known (or should be determined separately), whence they can be declared as fixed parameters. They therefore constitute systematic error sources (but their errors can be minimized by evaluation with the DM). To explore the sensitivity to errors in other kinds of known constants, a synthetic data set (SN) was constructed bearing a close resemblance to the Ni^{2+}–glycine system. The metal binding constants were evaluated in the presence of random errors in the ligand protonation constants, alone and in combination, all else remaining equal. Table 5 reports some of the results. Except with grossly overestimated $\sigma(\log \beta_{101})$, the NM was somewhat better, even without weighting, if only one protonation constant was in error. With the more realistic scenario of errors in random combinations, however, the DM clearly prevailed. Errors in these protonation constants also left distinc-

Table 5
As with Table 3, results from 100 simulations with set SN containing random errors in one or the other or both ligand pK_a's with $\sigma(pK_{a1}) = \sigma(pK_{a2}) = 0.03$ log units, and where the weighting used exact estimates of the error ($f = 1$)

		pK_{a1}	pK_{a2}	Both
$\rho = 0$	log β_{110}	5.0002(44)	5.0000(4)	4.9960(230)
	log β_{210}	9.0004(89)	9.0000(1)	8.9922(426)
	log β_{310}	12.0011(181)	12.0000(4)	11.9887(888)
$\rho = 1$	log β_{110}	5.0003(76)	4.9998(32)	5.0017(204)
	log β_{210}	9.0006(142)	8.9997(59)	9.0031(387)
	log β_{310}	12.0014(272)	11.9995(111)	12.0077(745)

tive residual patterns (Fig. 5): With both methods, the residuals (in pH) in the acidic portion were large, of consistent sign and overlapping. In that region, i.e. with $[H^+]/[L] \geq 1$, no metal complexes were present and no amount of adjustment of the metal binding constants could correct for the skewed ligand-only equilibria. With $[H^+]/[L] < 1$, free ligand was present and the NM residuals suddenly fell off because adjustments to the binding constants could be made that allowed a better match of pH^{pred} to pH^{expt} while the DM still produced residuals of consistent sign, as before, in order to match ΔpH^{pred} to ΔpH^{obs}. Eventually, the residuals by both Methods fell off to 0 after full deprotonation of the ligand, i.e. beyond the range of influence of the protonation constants.

4.6. *Effects of data sampling*

Data point density and pH span are usually chosen arbitrarily, though they can influence the results of refinement. Fortunately, neither Method was particularly sensitive to the density of data over a given pH span. This was tested with both synthetic (set SE) and real data (set C14) when considering only every second, every third or every fourth data point. The changes in log β that resulted were small (typically affecting the third decimal place) but, not unexpectedly, the uncertainties increased with a decrease in the data density (and in the number of data). Similarly, the simulations with data set SU, with a variable data density, led to the same conclusions as with data set SE, whose data density was constant.

On the other hand, if the pH range is widened or narrowed, the NM results will change the most. This was tested with synthetic data set SX, which is the same as set SE, but with more data at both pH extremes, those which are heavily weighted. In the presence of 1% error in v_0, for instance, the NM produced log β estimates that were 23–28% more deviant and more uncertain, while the DM results, in addition to being truer and more reliable, were more stable (only 13–19% worse and only slightly less certain). In the presence of a 0.03 log unit error in pK_w, the DM results were much more stable (2–6% change) than those by the NM (17–26% change). This sensitivity with the NM originates in the need to compensate for a greater number of error-containing data with a greater change in log β values, whereas the DM can well match the ΔpH^{obs} at the

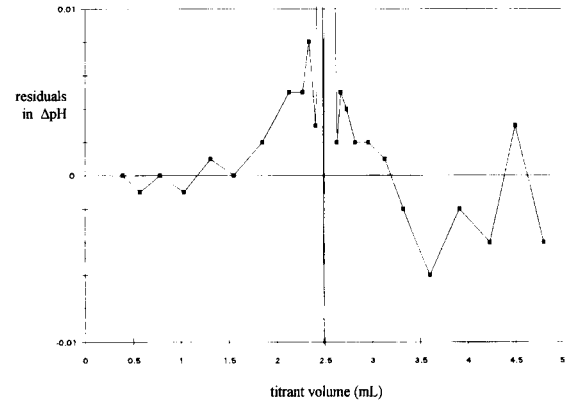

Fig. 6. Residuals $\Delta pH^{pred} - \Delta pH^{obs}$ from treating data set C14 with the Difference Method. Some values near 2.5 ml are offscale.

additional points with the same consistent deviation in pH^{pred} values caused by the same log β distortions. Additional data at the high pH extreme in the presence of transition metal ions may be accompanied by the precipitation of hydroxides and thus may need to be excluded from the refinement of unknown log β. But the data following the consumption of hydroxide due to precipitation will nevertheless allow the detection of errors, e.g. in pK_w, by inspection of the pH^{pred} curves.

4.7. *Effects on residual correlation*

As expected, data fitting with $\rho = 1$, i.e. under the assumption of autocorrelation, generally affords significantly less residual correlation than with $\rho = 0$. To illustrate, Figs. 2 and 6 plot the residuals obtained from data set C14. The NM residuals, $pH^{expt} - pH^{pred}$, were clearly not randomly distributed (Fig. 2), showing a distinctive down-sloping trend in the heavily weighted areas, i.e. those remote from the equivalence point near 2.5 ml (Fig. 1 illustrates the weighting used). The residual correlation coefficient χ from the first-order correlation model

$$r_n = \chi r_{n-1} + \epsilon_n$$

was estimated at 0.89 by formula 7 [10]. The DM residuals, $\Delta pH^{obs} - \Delta pH^{pred}$, were more random, especially in the heavily weighted areas (Fig. 6), and the χ value was much lower (0.36) using formula 7 with $\rho = 1$. (The Durbin-Watson test for autocorrelation [10] cannot be applied to non-linear systems such as this.) The DM cannot, however, eliminate all non-random character.

Table 6
Glycine ($\log \beta_{101}$) and glycinium ($\log \beta_{102}$) formation constants from glycinate, to four decimal places (with uncertainties in the least significant digits in brackets) from four data sets, weighted averages (with weighted standard error in the least significant digit in brackets) and averages reported by the authors [15] and in the group study [25]. WME designates the weighted mean error

Data Set	$\log \beta_{101}$		$\log \beta_{102}$		WME	
	$\rho=0$	$\rho=1$	$\rho=0$	$\rho=1$	$\rho=0$	$\rho=1$
C11	9.6706(15)	9.7007(115)	12.1220(16)	12.1446(126)	0.0048	0.0029
C12	9.6412(23)	9.6495(173)	–	–	0.0102	0.0052
C13	9.6423(23)	9.6535(144)	–	–	0.0088	0.0053
C14	9.6448(24)	9.6696(63)	12.1107(30)	12.0810(141)	0.0066	0.0027
wt. avg.	9.655(8)	9.672(9)	12.119(5)	12.12(3)		
lit. avg.	9.652		12.109			
study avg.	9.654(3)		12.076(3)			

$$\chi \approx \frac{\sum_{n=2+\rho}^{N_d} w_n^{1/2} w_{n-1}^{1/2} (r_n - \rho r_{n-1})(r_{n-1} - \rho r_{n-2})}{\sum_{n=2+\rho}^{N_d} w_n (r_n - \rho r_{n-1})^2} \quad (7)$$

4.8. Benchmark Ni^{2+}–glycine system

In 1982, a group of seven laboratories independently examined glycinate protonation and Ni^{2+}–glycinate complexation by potentiometric or pH titration under the same conditions of temperature (25°C) and ionic strength (1 M NaCl), as part of a study of the reliability of the reported values of equilibrium constants [15]. A later analysis of the inter-laboratory variance was carried out and global averages of data from four of the seven laboratories were proposed [25]. In this work, the four sets of pH data from titrations of glycine (sets C11 to C14) by the group from Catania, Italy were re-treated by both Methods, with the results reported in Table 6. The quality of the fits are represented by the WME calculated according to formula 2. Table 6 also compares the weighted averages provided by each Method (formula 5) and the grand weighted averages reported by the study leaders. Although sets C12 and C13 provided estimates of $\log \beta_{101}$ only, it was verified that these were fairly independent of any value ascribed to $\log \beta_{102}$. The NM and DM results were not very different. According to the *t*-test (formula 6), the NM and DM $\log \beta_{101}$ averages were barely significantly different to a 95% confidence level.

Next, data from six titrations in the presence of Ni^{2+} (sets C1, C2, C7–C10), covering three different metal–ligand ratios, were re-treated using as fixed constants the appropriate set of weighted average protonation constants and uncertainties from Table 6. Sets C1 and

Table 7
As in Table 6, formation constants of glycinate–Ni^{2+} complexes from six data sets

Data Set	$\log \beta_{110}$		$\log \beta_{210}$		$\log \beta_{310}$		WME	
	$\rho=0$	$\rho=1$	$\rho=0$	$\rho=1$	$\rho=0$	$\rho=1$	$\rho=0$	$\rho=1$
C1	5.6058(37)	5.5931(497)	10.3262(61)	10.3783(1114)	–	–	0.0133	0.0177
C2	5.5715(62)	5.6692(182)	10.2603(110)	10.4566(402)	–	–	0.0210	0.0060
C7	5.5754(42)	5.7208(188)	10.2658(44)	10.5521(177)	13.5279(77)	14.0054(358)	0.0117	0.0093
C8	5.5729(29)	5.6623(86)	10.2814(36)	10.4458(94)	13.5501(60)	13.8510(194)	0.0090	0.0053
C9	5.6205(51)	5.6110(54)	10.3814(36)	10.3638(51)	13.8160(51)	13.7828(89)	0.0106	0.0029
C10	5.6959(180)	5.5085(168)	10.5237(183)	10.2242(168)	14.2665(240)	13.6061(335)	0.0376	0.0070
wt. avg.	5.59(1)	5.63(2)	10.31(2)	10.38(3)	13.68(9)	13.79(4)		
lit. avg.	5.60		10.325		13.65			
study avg.	5.631(10)		10.399(10)		13.907(23)			

C2 could not be used to estimate log β_{310} and the authors' average was used as a fixed constant. The results are given in Table 7 and compared with the authors' averages and the study's global results. The two Methods gave significantly different log β_{110} and log β_{210} averages, according to *t*-tests (formula 6), but the log β_{310} averages were not significantly different because of the larger error estimates. A few points merit note. As measured by WME values, the best-fitting data set with the NM was not necessarily the same with the DM. The poorest-fitting sets with the DM resulted in consistent and large residuals in pH, probably signalling the presence of some unsuspected error. All glycinate–Ni^{2+} sets showed a relatively poor fit at the alkaline extremes, leading to a wider variation in the log β_{310} estimates. This was perhaps due to the presence of a hydroxo species, which the authors did not support [15]. This possibility was not explored in this work. Overall, the NM results most closely matched the authors' average values, as expected, while the DM results were closest to the global, inter-laboratory averages [25].

In light of the robustness of the DM toward errors, demonstrated in simulations, and in view of the success with the Catanian data, a complete reprocessing of the Ni^{2+}–glycine data from the entire study might be fruitful.

5. Conclusions

The minimization of residuals in the point-to-point pH changes (the Difference Method) is well-behaved and presents several advantages over the minimization of the residuals in pH (Normal Method), as detailed in the Introduction. In particular, the Difference Method is insensitive toward calibration errors, more robust toward errors in measurement and unsuspected systematic errors in the chemical model, less sensitive to the pH span of the data, and produces residuals that are more randomly distributed. This enhances the validity of the non-linear regression process and any statistical test carried out on it. When carried out with a good estimate of pK_w, obtained as recommended herein, this method assures more trustworthy and more reliable calculations of unknown equilibrium constants, as exemplified by treatment of data for the Ni^{2+}–glycine system. Further, the presence of unsuspected systematic error can be detected by misbehaviour during the calculations, by results that differ significantly from those obtained by the Normal Method and by an inspection of the resultant pH^{pred} curves.

Acknowledgements

The author thanks York University for free computer time and the Natural Sciences and Engineering Research Council for continued funding.

References

[1] F. Gaizer, Coord. Chem. Rev., 27 (1979) 195.
[2] M.T. Beck and I. Nagypál, Chemistry of Complex Equilibria, Ellis Horwood, Chicester, 1990.
[3] P. Gans, A. Sabatini and A. Vacca, J. Chem. Soc. Dalton Trans., (1985) 1195.
[4] A. Izquierdo and J.L. Beltran, Anal. Chim. Acta, 181 (1986) 87.
[5] A. Laouenan and E. Suet, Talanta 32 (1986) 245.
[6] R.J. Motekaitis and A.E. Martell, Can. J. Chem., 60 (1982) 2403.
[7] J.J.B. Baeza, G.R. Ramos and C.M. Fernandez, Anal. Chim. Acta, 223 (1989) 419.
[8] H.C. Smit, L. Meites and G. Kateman, Anal. Chim. Acta, 153 (1983) 121.
[9] A.E. Martell, Determination and Use of Stability Constants, VCH, New York, 1992.
[10] J. Neter, W. Wasserman and M.H. Kutner, Applied Linear Regression Models, R.D. Irwin, Homewood, IL, 1983.
[11] P.G. Potvin, Can. J. Chem., 68 (1990) 2198.
[12] G. Gran, Analyst, 77 (1952) 661; F.J.C. Rossotti and H. Rossotti, J. Chem. Educ., 42 (1965) 375.
[13] Y.L. Sidrak and A. Aboul-Seoud, J. Comput. Chem., 8 (1987) 575.
[14] A.E. Martell and R.M. Smith (Eds.), Critical Stability Constants, Plenum Press, New York, 1975.
[15] E. Bottari, A. Braibanti, L. Ciavatta, A.M. Corrie, P.G. Daniele, F. Dallavalle, M. Grimaldi, A. Mastroianni, G. Mori, G. Ostacoli, P. Paoletti, E. Rizzarelli, S. Sammartano, C. Severini, A. Vacca and D.R. Williams, Anal. Chim. Acta, 68 (1978) 813.
[16] P.G. Potvin, Can. J. Chem., 68 (1990) 2208.
[17] W.C. Hamilton, Statistics in Physical Science, Ronald Press, New York, 1964.
[18] A. Avdeef, J.J. Bucher, Anal. Chem., 50 (1978) 2137.
[19] I. Nagypál, Magyar Kém. Foly. 80 (1974) 49; Acta Chim. Acad. Sci. Hung., 82 (1974) 29.

[20] I.G. Sayce, Talanta, 15 (1968) 1397; Talanta, 18 (1971) 653.
[21] W.A.E. McBryde and J.L. McCourt, Talanta, 19 (1972) 1486.
[22] D. York, Can. J. Phys., 44 (1966) 1079.
[23] J. Berkson, J. Am. Stat. Soc., 45 (1950) 164.
[24] R.F. Jameson and M.F. Wilson, J. Chem. Soc. Dalton Trans., (1972) 2607.
[25] A. Braibanti, F. Dallavalle, G. Mori and B. Veroni, Talanta, 29 (1982) 725.

ELSEVIER

Analytica Chimica Acta 299 (1994) 59–67

ANALYTICA CHIMICA ACTA

Direct determination of cobalt in unpurged oceanic seawater by high speed adsorptive cathodic stripping voltammetry

J.A. Herrera-Melián, J. Hernández-Brito *, M.D. Gelado-Caballero, J. Pérez-Peña

Chemistry Department, Faculty of Marine Sciences, University of Las Palmas de Gran Canaria, P.O. Box 550, Las Palmas de Gran Canaria, Spain

Received 10 March 1994; revised manuscript received 9 May 1994

Abstract

A fast, sensitive method to determine Co(II) in unpurged ocean seawater is presented. The method combines high scan speed staircase voltammetry (HSACSV) and nitrite catalytic effect to enhance Co(II)–dimethylglyoxime reduction currents. The catalytic effect was magnified using high speed adsorptive cathodic stripping voltammetry and peak currents of ca. 0.1 μA were obtained for pM cobalt samples using 30-s deposition times. The effect of buffer, pH, nitrite concentration and scan speed on cobalt sensitivity was studied. Capacitance currents developed at high scan speeds were filtered by background subtraction. The same procedure was successfully applied to remove oxygen interference in unpurged solutions. Blank voltammograms were obtained in different ways yielding similar results without variation in peak reproducibility or accuracy. Nickel and zinc interferences were removed using a cleaning potential before the scan at -1.03 V. Ratios over 10 000 fold were eliminated using more negative cleaning potential steps. Nickel can also be measured by this method. Total analysis time of unpurged seawater (pM levels of cobalt) was decreased to reagents addition time, 30-s adsorption period and 10-s quiescence time. A detection limit of 5.9 pM Co was achieved in seawater. Short analysis time, sensitivity and portable hardware recommend this method for aboard determinations of cobalt. An oceanic profile of cobalt was measured at the Central East Atlantic Ocean.

Keywords: Stripping voltammetry; Cathodic stripping voltammetry; Cobalt ; Nickel; Seawater; Waters

1. Introduction

Several voltammetric methods for trace nickel and cobalt determinations have been proposed using their organometallic complexes adsorbed onto the hanging mercury drop electrode [1–10]. Most of these methods are sensitive enough for the determination of nickel in natural waters and seawater at concentrations as low as 2 nM. However, the oceanic cobalt concentrations are extremely low (10–100 pM) [11,12] and few of these methods appear to have the required sensitivity. Donat and Bruland [6] achieved a very low detection limit (6 pM) using nioxime as ligand but large accumulation times (15 min) were required. The purge and collection periods are the main time consuming steps for these methods. The number of samples that can be analyzed aboard ship and the quality control of the data are limited by the analysis time. The development of fast, sensitive analysis procedures is needed to achieve a better understanding of the cobalt oceanic distributions and its biogeochemical cycle in the ocean.

Recently, sensitive voltammetric techniques based on the catalytic effect of nitrite on the reduction of cobalt complexes have been developed [13–15]. They

* Corresponding author.

SSDI 0003-2670(94)00297-5

are suitable to determine cobalt with detection limits of 40 pM [15] (30 s accumulation time) using dimethylglyoxime (DMG) as ligand in the presence of a large excess of Ni and Zn. The reported technique showed higher sensitivity using linear sweep voltammetry and medium scan speeds (100 mV s^{-1}) compared with a square wave (15 Hz) or differential-pulse wave form. Results without the catalyst [16] have shown that sensitivity for Ni and Co can be drastically increased using higher scan speeds (two or three orders of magnitude) while oxygen interference can easily be avoided. The combination of both features, catalyzed cobalt reduction and high scan speeds, in a single procedure appears as useful way to joint the advantages of both techniques.

The method reported here is based on the procedure described by Bobroski and Bond [15] and the use of high scan speeds [16]. Several modifications are introduced to enhance the analytical sensitivity, reduce contamination risks, and delete the oxygen interference and noise coming from the solution turbulence during the scan. The sensitivity is increased by the fast reduction of the electroactive cobalt complex using a fast potential scan rate and nitrite as catalyst. The stirring of the solution during the scan produces no significant noise. Oxygen interference is also decreased and corrected by blank subtraction. The contamination risk from high concentration of nitrite reagent is avoided by decreasing it one order of magnitude with Chelex-100 cleaning. The total analysis time is drastically shorted by reducing the deposition time down to 30 s and avoiding the 10 min purging time. Detection limit is reduced down to 6 pM in the presence of oxygen and using a 30 s deposition time. The method can be specially valuable for seawater determinations aboard of research vessels and reducing contamination and speciation changes due to the storing of the samples.

2. Experimental

Cobalt and nickel standards were prepared by dilution of Sigma atomic absorption stock solutions to obtain final stock solutions of 4×10^{-7} M Ni and 10^{-8} M Co. Stock solutions of 0.1 M dimethylglyoxime were prepared in Suprapur grade methanol (Merck). Stock buffer solution containing 1 M 4-(2-hydroxyethyl)-1-piperazineethanesulfonic acid (HEPES) and 0.5 M NH_3 (pH 7.8) was also prepared in this way. Milli-Q water was used to dilute reagents and standards. $NaNO_2$ was recrystallized and used to prepare stock solutions. HEPES and $NaNO_2$ solutions were equilibrated over night with Chelex-100 resin (50 g l^{-1}) to remove trace metals.

The oceanic seawater was collected in the Central East Atlantic Ocean (around the Canary Islands) using PTFE-coated Niskin bottles. It was acidified to pH 1.5 and irradiated with a 1 kW UV lamp for 3 h when needed. Potentiostats developed in our laboratory [17,18] were used to provide the high scan speeds required. This equipment was interfaced with an EG&G Princeton Applied Research (PAR) Model 303A static mercury drop electrode in the hanging mercury drop electrode mode (HMDE). Drops with a surface area of 2.8 mm^2 were used.

2.1. Procedure

The direct determination of trace levels of labile cobalt(II) in unpurged seawater samples is described. Samples are prepared in PTFE cups of the polarographic cell, containing 10 ml of water. The solution is made 0.01 M in HEPES, 0.1 M in $NaNO_2$, and 5×10^{-4} M in DMG (100 μl of 1 M HEPES buffer, 200 μl of 5 M $NaNO_2$ and 100 μl of 0.05 M DMG). The adsorption potential (-0.9 V) was applied to the working electrode, while the solution was stirred. After 30 s accumulation time, the stirring is stopped and 10 s is allowed for the solution to become quiescent. The scanning is started at -0.9 V and ended at -1.6 V using staircase modulation with a scan rate of 80 V s^{-1} and a pulse height of 3 mV. The cobalt peak appears at ca. -1.25 V. Background subtraction to remove capacitance and oxygen interferences is made. A blank voltammogram is obtained using the same conditions described before but with 1 s collection time. A standard addition procedure is used to quantify the concentration in the sample. A fast-response potentiostat to achieve high scan speeds is required. The simultaneous determination of nickel can also be carried out by this method. A cleaning potential of 1 s at -1.03 V before the scan at high nickel concentration is recommended.

3. Results and discussion

3.1. The effect of the scan speed in the presence of nitrite

High scan speeds have been avoided, in conventional stripping voltammetry because capacitance components and ohmic drop perturb peak currents. However, adsorptive cathodic stripping voltammetry and computerized instrumentation give a chance to use successfully high scan velocities, since Faradaic currents of an adsorbed electroactive substance should be linearly related to the scan speed and digital background subtraction can remove capacitance components from the polarographic signal.

The relationship between scan speed and I_p (cobalt or nickel peak height) is linear up to velocities around 1 V s^{-1} using a seawater matrix and the DMG complex [15]. Higher scan speeds dampen the relationship as the ohmic drop rises. The cell constant (uncompensated cell resistance × capacitance of the HMDE) depends on several factors such as conductivity of the solution, electrode surface, organic coatings, etc., and fixes the time required to establish the potential between the counter electrode (CE) and working electrode (WE). The practical effect of the ohmic drop on the voltammograms is a lower scan rate than the applied one, a potential shift of the peak potential towards negative values and wider peaks. There are several ways to delay ohmic drop by current feedback compensation or using microelectrodes [19,20]. However, it is possible to quantify the peak height in the presence of ohmic drop using background subtraction to remove capacitance components and standard additions to quantify the peak height.

Fig. 1 gives a voltammogram of a 10 min purged sample, the blank and the difference between them. The blank was measured using the same conditions but before adding DMG. The sample curve shows capacitance and Faradaic currents markedly amplified by the fast scanning. However, the Faradaic- to-capacitance current ratio is very high. The subtraction of capacitance currents is feasible, giving a clean cobalt peak (Fig. 1). Similar results were obtained using a blank made with a 1 s deposition time at −0.9 V. No significant noise is introduced by stirring during the scan, therefore the quiescence time can be avoided. The final

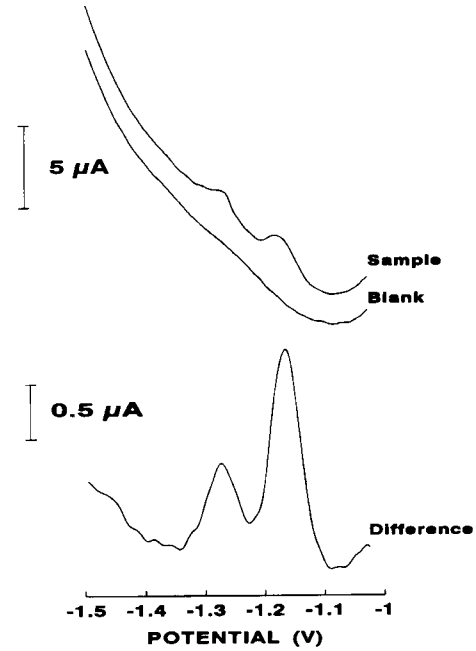

Fig. 1. Background correction procedure in purged solutions. The seawater sample (20 pM Co) was made 5×10^{-4} M DMG, 2×10^{-2} M HEPES and 0.15 M $NaNO_2$. Collection periods of 45 s at −0.9 V, 1 s at −1.01 and 1 s at −0.9 V were used. Scan speed was 45 V s^{-1}.

step (1 s at −0.9 V) was used to fix the initial potential of the scan.

Bobrowski and Bond [15] found a linear relationship between log I_p (cobalt peak height) and log v (scan speed) in the range 10–1000 mV s^{-1} using linear sweep adsorptive stripping voltammetry and in the presence of 0.5 M nitrite. Higher increments of I_p can be achieved by scanning at higher scan speeds and using background subtraction. Fig. 2a shows the relationship between I_p and the scan speed using staircase scanning in the presence of 0.075 M nitrite and without nitrite. The peak heights grow almost linearly with the scan speed giving peaks of 20 μA for 2 nM cobalt using 60 s deposition time and 80 V s^{-1} scan speed. The lack of linearity is caused by ohmic drop distortion, as the plot is made with the potential scan applied. Similar distortion is produced in both samples (catalyzed and non-catalyzed). Kinetic effects also would be involved.

The comparison of both curves shows the catalytic effect of nitrite (Fig. 2a). The catalyzed-to-non-catalyzed current ratio decreases as the scan speed grows. However, peaks 4–5 fold higher are obtained at 80 V s^{-1} in the presence of nitrite, showing the convenience

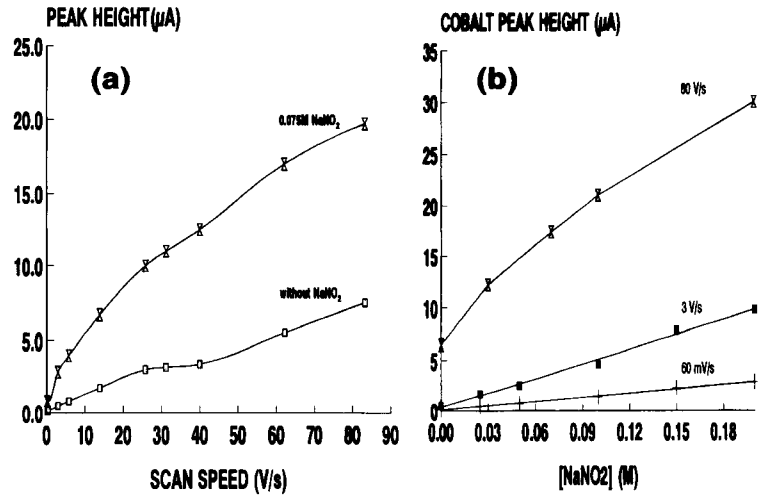

Fig. 2. (a) Relationship between potential scan speed and cobalt peak height with and without the catalyst. (b) Effect of $NaNO_2$ concentration on the cobalt peak height at various scan speeds. The seawater sample was made 5×10^{-4} M DMG, 2×10^{-2} M HEPES and 2 nM Co. Two potential steps were used, 60 s stirred at -0.98 V and 5 s quiescent at -0.8 V.

of working at this scan speed range. The change of the catalyst efficiency under these conditions would be due to kinetic processes where nitrite is involved. Mrzljak et al. [21] suggested the possibility of cobalt regeneration by chemical oxidation on the adsorbed layer.

Nitrite concentration also affects the sensitivity of cobalt determination. Fig. 2b shows an almost linear relationship between nitrite concentration and cobalt peak height. Bobrowski and Bond [15] found a similar increase in the catalytic effect using 0.5 M nitrite and low scan speeds. However, using fast scanning, sensitivity is markedly improved and lower nitrite concentrations can be used to determine cobalt at oceanic water levels. Lower nitrite additions decrease the contamination risk with this reagent. $NaNO_2$ concentrations between 0.05 M and 0.15 M using 30 s accumulation time have provided a detection limit of 5.9 pM cobalt ($n=11$) (see below).

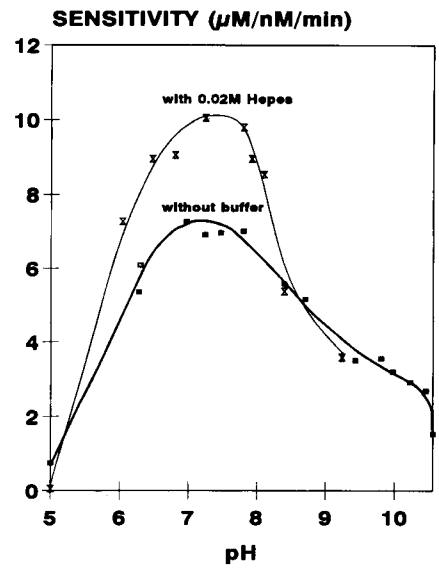

Fig. 3. Effect of pH on the cobalt sensitivity. Sample and collection were the same as in Fig. 2.

3.2. Effect of pH and buffer

The effect of pH and buffer composition has been tested. Fig. 3 shows the best pH range to determine cobalt at high scan speed with and without HEPES. The largest sensitivities have been found at pH between 7 and 8 for the unbuffered solution. The pH was fixed in this sample by adding aliquots of concentrated acid (HCl) or base (NaOH). The presence of HEPES scarcely increases the sensitivity of the determination, keeping the maximum sensitivity at the same pH range but improves cobalt peak resolution, specially in non-irradiated solutions. Concentrations of HEPES above 0.06 M do not affect the peak height. This behaviour is different from that reported by Bobrowski and Bond [14] for his method in differential pulse voltammetry (DPV) and using α-benzil dioxime where the best sensitivity was found at pH 9.

3.3. Unpurged solutions

Using high scan speeds in unpurged samples the metal-to-oxygen current ratio in solution is improved. The whole potential scan lasts a few milliseconds and only the oxygen on the mercury electrode interferes. Oxygen replacement from the bulk solution by diffusion is drastically decreased in this short scan time. The metal-to-oxygen current ratio is enhanced, making feasible a background correction procedure. A blank experiment is carried out without any cobalt–DMG complex adsorbed to measure the oxygen component. This procedure also removes the capacitative components of the signal developed at high scan speeds. The same potential distortion and capacitative currents are produced in both measurements (sample and blank), therefore after blank subtraction only nickel and cobalt peaks appear. Fig. 4 gives voltammograms for an oceanic sample, a blank and several 40 pM standard additions in an unpurged solution using 80 V s^{-1} scan speed. Subchart (a) gives the peak with oxygen and capacitance waves and subchart (b) the same curves after the subtraction of the blank. The peaks obtained are well defined even for concentrations as low as 24 pM. However, the accuracy of the method at this concentration and below starts to depend on the purity of the reagents. Cobalt determination in Milli-Q water (Fig. 4c) gave 10 ± 2 pM Co.

Three main ways to obtain the blank were tested. In the first procedure the blank is obtained using the same conditions but without DMG in the solution to avoid Co–DMG complex formation. This method showed the best baseline in purged solution where the peak resolution is enhanced and capacitance currents removed. The second procedure used the same electrochemical conditions but with a short (1 s) deposition time. This technique improves peak resolution for unpurged seawater. Similar results were also obtained by blanks made with the same drop after the sample scan. Closely similar peak heights ($\pm 2.6\%$, using a 89 pM seawater solution) were obtained using these three methods. There is no significative influence of the adsorbed ligand (DMG) on the HMDE surface at low collection times (30 s).

No improvements were introduced by using a quiescence time in purged solutions. However, the rest period in unpurged solutions can remove part of the peroxide wave. The potential used (-0.9 V) decreases

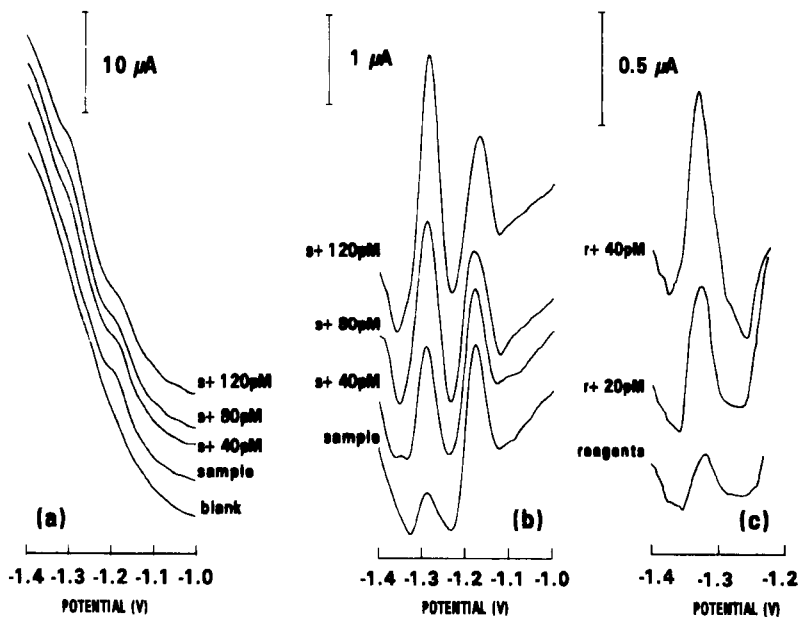

Fig. 4. Background subtraction in unpurged seawater sample of 24 pM Co. The solution was made 5×10^{-4} M DMG, 2×10^{-2} M HEPES and 0.1 M $NaNO_2$. The stirred collection was 40 s at -0.9 V and 10 s quiescent at -1.04 V. The scanning speed was 80 V s^{-1}. Spiking was obtained by standard additions of 40 pM Co. The blank was measured using the same conditions before adding the DMG ligand. (a) Voltammograms before blank subtraction and (b) after blank subtraction. (c) Cobalt determination in a Milli-Q water sample using 90 s deposition time.

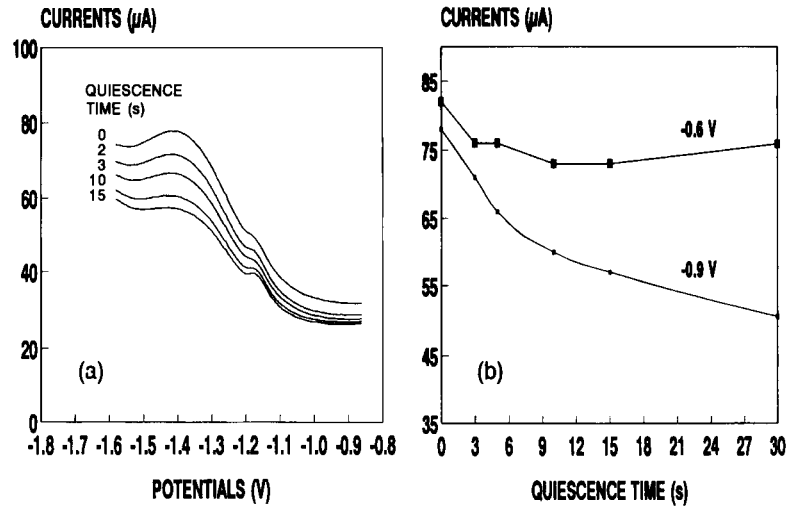

Fig. 5. (a) Effect of quiescence time on the voltammograms of unpurged samples. (b) Relationship between peroxide currents and quiescence time at −0.9 V and −0.6 V deposition potentials.

the hydrogen peroxide generated in the first oxygen reduction step. The oxygen concentration around the electrode surface is depleted with time at this potential as the solution is quiescent. The molecular diffusion from the bulk solution cannot replace the oxygen reduced. Fig. 5a gives voltammograms using several quiescence times. The peroxide wave decreases as the rest period grows, showing the oxygen consumption around the mercury drop. Fig. 5b shows the peroxide maximum currents using two different quiescence potentials (−0.6 and −0.9 V). A partial oxygen depletion takes places at −0.9 V. The same quiescence time for blank and sample must be used in unpurged solution to obtain a good baseline when collection is carried out at −0.9 V. A value around 10 s is suggested for analytical purposes as the current depletion from peroxide begins to plateau at this value.

Blank subtraction in the presence of oxygen without quiescence and keeping the stirrer on during the scan was carried out. Results showed higher noise and lower efficiency for removing the oxygen wave at low scan speed (<10 V s^{-1}). However, no significant differences from the quiescent solutions were obtained when higher scan speeds were utilized. Several stirring speeds were tested (200–1500 rpm) without alteration of the noise level in the voltammogram. The stirring speed was linearly related with the cobalt peak height in the range studied. Higher detection limits could be achieved by increasing the agitation of the solution.

3.4. Interferences

Nickel is always more abundant than cobalt in natural waters. In seawater, nickel concentrations between 1 and 10 nM must be expected while cobalt is present in lower concentrations, between 10 and 100 pM [11,12]. This concentration ratio can hinder the cobalt peak (pM) by nickel overlap. Two procedures to diminish the nickel interference were studied. The first conventional method uses adsorption potentials close to the nickel peak potential. Fig. 6a shows the relationship between collection potentials and metal peaks. An adsorption potential between −1.0 V and −1.05 V can improve the cobalt-to-nickel peak height ratio. However, cobalt sensitivity falls at these adsorption potentials and the procedure is only useful for cobalt concentrations higher than 100 pM. The lack of sensitivity is critical at lower cobalt values.

The nickel interference can also be avoided maintaining the best adsorption potential (−0.9 V) and applying a "cleaning potential" for a short time before scanning. Both metals are accumulated at this potential, keeping the efficiency of the cobalt collection and decreasing the nickel peak height. The Ni peak decrease is controlled by the cleaning potential and time. Fig. 6b gives the relationship between this potential and the peak height for cobalt and nickel in the presence of nitrite. Cleaning potentials of 1 s between −1.0 and −1.05 V improve the Co/Ni peak height ratio by

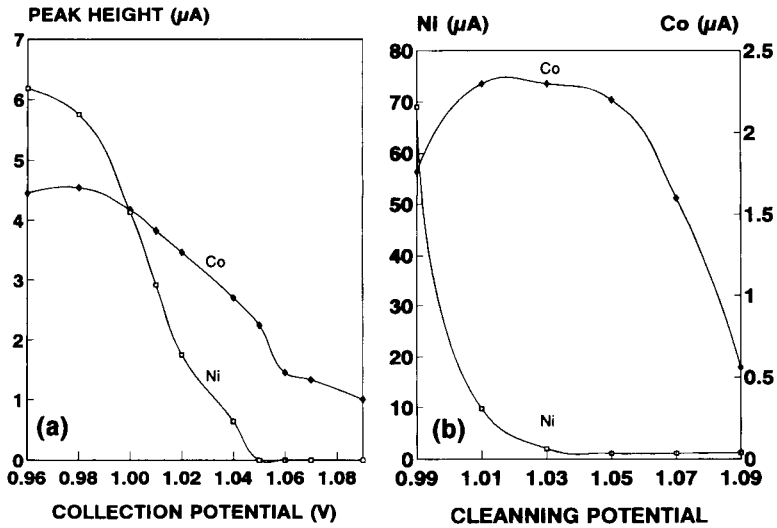

Fig. 6. (a) Relationship between collection potential and peak height. Seawater sample was 3.2 nM in Co and 5.1 nM in Ni, 60 V s^{-1} scan speed and standard chemical conditions. (b) Effect of cleaning potential on cobalt and nickel peak height. The sample was seawater of 89 pM Co and 100 nM of Ni while the scan speed was 100 V s^{-1}.

almost two orders of magnitude without decrease in cobalt sensitivity. The increase in the cobalt peak in Fig. 6b from −0.99 to −1.03 V arises from decreasing nickel overlap.

Fig. 7 shows nickel and cobalt peaks using several cleaning potentials before the scan. The nickel peak is almost two orders of magnitude higher using a cleaning potential of −0.99 V. However, they become similar at −1.03 V while the concentration of nickel in solution is almost 1000 times higher. The cleaning potential method is very effective for eliminating the nickel peak even at larger nickel concentrations. The effect of an excess of 10 000 fold of nickel on the cobalt sensitivity without losing sensitivity for cobalt has been tested. The cleaning period was 1 s at −1.04 V under quiescent conditions during this time. Higher [Ni]/[Co] ratios require more negative cleaning potentials. This procedure would be useful for enriched aquatic matrix.

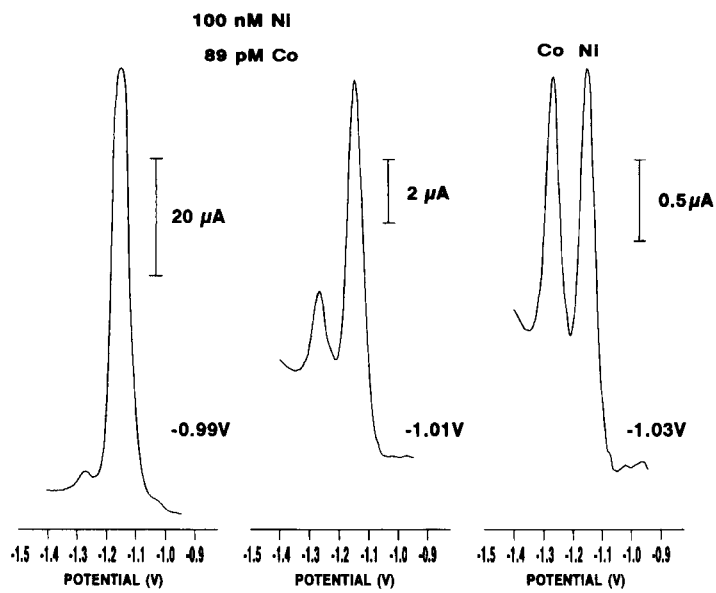

Fig. 7. Voltammograms obtained after using several cleaning potentials.

Table 1
Standard deviation and detection limit ($n=11$)

Metal	Concentration (pM)	Standard deviation (%)	Detection limit (pM) [a]
Cobalt	48 ± 1.9	4.1	5.9
Nickel	2550 ± 0.14	5.5	420

[a] 3σ.

Table 2
NASS-4 reference seawater analysis ($n=5$)

	HSACSV (purged)	HSACSV (unpurged)	Accepted value
Nickel (nM)	4.19 ± 0.19	4.08 ± 0.2	3.88 ± 0.157
Cobalt (pM)	156 ± 4	154 ± 5	152.7 ± 17

Results are mean $\pm \sigma$, $n=5$.

The cleaning potential can change with the pH of the solution since there is a relationship between pH and peak potential.

Zinc could interfere in the cobalt determination when its concentration is very high, e.g. in industrial polluted waters. The method proposed combined with background subtraction also avoids zinc interference at [Zn]/[Co] ratios higher than 10^6. The method was tested by adding a 150 μM zinc standard to a 120 pM cobalt coastal seawater. Blanks were measured using the same electrochemical conditions, but adding one step of 1 s at -1.2 V to remove cobalt and 5 s at -0.9 V to start scanning. The selective complexation of zinc with EDTA has also been tested for higher zinc concentrations showing successful results. The sensitivity of the catalytic method at high scan speeds is not decreased by any of these procedures.

3.5. Reproducibility, detection limits and field measurements

The reproducibility of the procedure for cobalt and nickel was tested by replicate determinations in an unpurged oceanic sample (48 pM Co and 2.55 nM Ni). The results are shown in Table 1. The analytical precision (standard deviation, σ) of this method for cobalt was 4.1% ($n=11$). Detection limits of 5.9 pM cobalt and 0.4 nM nickel were obtained. Blank values of 10 ± 2 pM Co were estimated from determinations in Milli-Q water. The accuracy of the method was tested on open ocean seawater (NASS-4) reference materials (National Research Council, Canada). Table 2 shows the accepted and obtained values in purged and unpurged samples, attesting to the accuracy of the technique.

Fig. 8 shows the distribution of cobalt versus depth at station 40 (29°14'N 13°55'W) sampled in Poseidon P189/1B cruise (around the Canary Islands oceanic waters). The surface layer seems well mixed and constant values of temperature and cobalt were obtained. The beginning of seasonal thermocline explains the cobalt increase between 200 and 400 m. These higher values can be explained by lateral advection of water

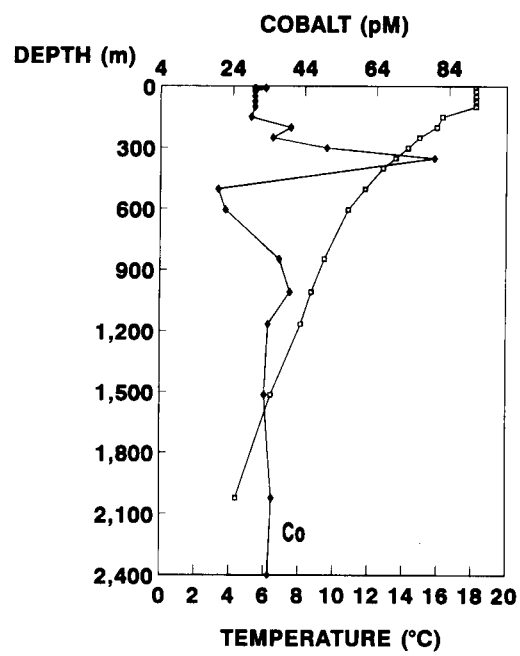

Fig. 8. Cobalt profile in the water column of the Canary Islands Oceanic Waters.

masses cobalt enriched or by earlier aeolian inputs in the area. Saharan dust accounts for significant inputs of metals in the Central Atlantic. Lower concentrations at higher depths were obtained, showing a scavenging behaviour. Below 1200 m, almost constant concentrations were obtained at this water mass. A detailed study of the atmospheric inputs of cobalt in the area is in preparation.

Acknowledgements

This research was supported by a grant from the CICYT (Spanish Commission for Science and Technology) under the Project number NAT90-1070. The authors thank Dr. T.J. Müller from Institut für Meereskunde an der Universität Kiel for his support during the field determinations.

References

[1] C.J. Flora and E. Nieboer, Anal. Chem., 52 (1980) 1013.
[2] B. Pihlar, P. Valenta and H.W. Nurnberg, Fresenius Z. Anal. Chem., 307 (1981) 337.
[3] L. Huynh-Ngoc and N.E. Whitehead, Oceanol. Acta, 9 (1986) 433.
[4] P. Ostapczuk, P. Valenta and H.W. Nurnberg, J. Electroanal. Chem., 214 (1986) 51.
[5] B. Pihlar, P. Valenta and H.W. Nurnberg, J. Electroanal. Chem., 214 (1986) 157.
[6] J.R. Donat and K.W. Bruland, Anal. Chem., 60 (1988) 240.
[7] H. Zhang, J.C. Vire, G.J. Patriarche and R. Wollast, Anal. Lett., 21 (1988) 1409.
[8] L. Huynh-Ngoc, N.E. Whitehead, M. Boussemart and D. Calmet, Mar. Chem., 26 (1989) 119.
[9] C.M.A. Brett, A.M.O. Brett and J.L.C. Pereira, Electroanalysis, 3 (1991) 683.
[10] Z.Q. Zhang, S.Z. Chen, H.M. Lin and H. Zhang, Anal. Chim. Acta, 272 (1993) 227.
[11] G.A. Knauer, J.H. Martin and R.M. Gordon, Nature, 297 (1982) 49.
[12] J.H. Martin and G.A. Knauer, Nature, 314 (1985) 524.
[13] A. Bobrowski, Anal. Lett., 23(8) (1990) 1487.
[14] A. Bobrowski and A.M. Bond, Electroanalysis, 3 (1991) 157.
[15] A. Bobrowski and A.M. Bond, Electroanalysis, 4 (1992) 975.
[16] J. Perez-Peña, J.J. Hernandez-Brito, J.A. Herrera-Melián, C. Collado-Sánchez and C.M.G. van den Berg, Electroanalysis, (1993) in press.
[17] J.J. Hernández-Brito, J. Perez-Peña, V. Siruela-Matos and P. Cardona-Castellano, Electroanalysis, (1994) in press.
[18] J.J. Hernández-Brito, P. Cardona-Castellano, J. Perez-Peña and M.D. Gelado-Caballero, Electroanalysis, 2 (1990) 401.
[19] H. Yamagishi, J. Electroanal. Chem., 326 (1992) 129.
[20] D. Garreau, P. Hapiot and J.M. Saveant, Electroanal. Chem. Interf. Electrochem., 281 (1990) 73.
[21] R.I. Mrzljak, A.M. Bond, T.J. Cardwell, R.W. Cattrall, R.W. Knight, O.M.G. Newman, B.R. Champion and J. Hey, Anal. Chim. Acta, 281 (1993) 281.

ELSEVIER

Analytica Chimica Acta 299 (1994) 69–74

ANALYTICA CHIMICA ACTA

Enzyme microelectrodes for choline and acetylcholine and their applications

Kenji Kano *, Kazuo Morikage, Bunji Uno, Yukihiro Esaka, Masashi Goto

Gifu Pharmaceutical University, 5-6-1 Mitahora-Higashi, Gifu 502, Japan

Received 31 May 1994; revised manuscript received 11 July 1994

Abstract

Hydrogen peroxide based amperometric microsensors have been developed for choline (Ch) and acetylcholine (Ach) by coimmobilization of acetylcholinesterase (AchE) and choline oxidase (ChO) on platinum disk microelectrodes using glutaraldehyde vapor. The sensor was applied in micro flow injection and micro liquid chromatographic analyses. The chromatographic peak heights were linearly proportional to the amounts of Ach and Ch over the range of 0.05 to 10^3 pmol (8×10^{-7} to 1.5×10^{-2} M, 0.06 μl) with correlation coefficients > 0.99. Immobilization of ChO was used for the selective determination of Ch with a response time of 5 s. This electrode was used for activity measurements of AchE down to 0.25 U ml^{-1} in a 1 μl volume in a batch method at a total volume of 5.0 ml.

Keywords:

1. Introduction

Acetylcholine (Ach) plays an important role as a neurotransmitter in the central and peripheral nervous systems. Choline (Ch) serves as a precursor and a metabolite of Ach. Recent advances in neurochemistry have produced a substantial demand for highly sensitive and selective measurements of Ach and Ch [1]. A number of detection methods has been developed for the determination of Ch and Ach [2–11], of which choline oxidase (ChO)-based amperometric biosensors continue to be a topic of interest [5–11]. The determination of Ch is based on the following reaction:

$$\mathrm{Ch} + 2\mathrm{O_2} + \mathrm{H_2O} \xrightarrow{\mathrm{ChO}} \text{betaine} + 2\mathrm{H_2O_2}$$

$$\mathrm{H_2O_2} \xrightarrow{\text{electrode}} \mathrm{O_2} + 2\mathrm{H^+} + 2\mathrm{e^-} \qquad (1)$$

The detection of hydrogen peroxide is an established approach to the construction of biosensors involving immobilized oxidases and such hydrogen peroxide detecting sensors are more easily fabricated. In addition this type of sensor was reported to provide the best sensitivity for Ch [6]. On the other hand, acetylcholinesterase (AchE) converts Ach into Ch:

$$\mathrm{Ach} + \mathrm{H_2O} \xrightarrow{\mathrm{AchE}} \mathrm{Ch} + \text{acetic acid} \qquad (2)$$

Such Ch sensors would be useful for activity measurement of AchE also, if the response is fast com-

* Corresponding author: K. Kano, (present address) Department of Agricultural Chemistry, Faculty of Agriculture, Kyoto University, Sakyo-ku, Kyoto 606, Japan.

Elsevier Science B.V.
SSDI 0003-2670(94)00318-1

pared with the enzymatic reaction. Furthermore direct incorporation of AchE into the Ch sensors enables Ach to be determined.

In this study, we attempted to fabricate enzyme microelectrodes for the determination of Ch and Ach. Several immobilization methods have been proposed including covalent immobilization on membranes or supports [5], crosslinking with glutaraldehyde [10,11] and physical entrapment in a matrix [6–9]. Although the crosslinking method with glutaraldehyde is the most simple and popular, denaturation during crosslinking would be one of its disadvantages. To minimize the denaturation, glutaraldehyde vapor has been utilized [12]. On the other hand, carbon fiber electrodes are frequently used as microelectrodes. The carbon fiber electrodes, however, might not be suitable for sensitive detection because of its larger background current [9]. Taking these points into account, we attempt to immobilize ChO and AchE on platinum microelectrodes using the glutaraldehyde vapor method.

2. Experimental

2.1. Reagents

AchE (EC 3.3.1.7), Type V-S, from electric eel, ChO (EC 1.1.3.17) from *Alcaligenes* sp., Ach chloride and Ch chloride were purchased from Sigma and used as received. All other chemicals were of analytical grade quality.

2.2. Preparation of enzyme microelectrodes

Micro-disk electrodes were made from 200-μm diameter and 3-cm length platinum wires (Japan Lamp Co., Tokyo), sealed with Aron $\alpha^{®}$ 201 epoxy (Toa Synthetic Chemicals, Tokyo) into fused-silica tubes (GL Science, Tokyo) of 250 μm i.d. and a length of 2 cm. The end of the wire was cut off and the electrode surface was polished with emery papers No. 600 and then No. 1000, and sonicated in distilled water. The micro-disk electrodes were pretreated electrochemically in 0.5 M H_2SO_4 by scanning from 0 to 1.2 V at 100 mV s^{-1} for 10 min, rinsing with distilled water and drying. For electrochemical pretreatment, a Fuso HECS-972 potentiostat, a Fuso HECS-980 function generator and Riken F-35 x–y recorder were used. All potentials were referenced to an Ag/AgCl/KCl(sat) electrode (Bioanalytical Systems).

ChO-immobilized microelectrodes were prepared as follows. A 1-μl aliquot of ChO solution (200 U ml^{-1} unless otherwise stated, pH 8.0 phosphate buffer) was placed on the disk surface of the electrodes in the form of a droplet and allowed to dry in air at room temperature. ChO was crosslinked on the electrode surface by exposing the enzyme-mounted electrodes to glutaraldehyde vapor, which was generated from 1 ml of 25% glutaraldehyde solution in an enclosed 5-ml glass bottle for 20 min at room temperature. The ChO-immobilized electrodes were rinsed in pH 8.0 phosphate buffer overnight to remove free enzyme.

When ChO and AchE were coimmobilized on the micro-disk electrodes, a 1-μl aliquot of mixed enzyme solution containing ChO (200 U ml^{-1}) and AchE (2000 U ml^{-1}) was placed on the disk electrodes, unless otherwise stated. The other procedures were identical with those for the ChO-immobilized electrodes.

2.3. Apparatus and measurements

A Princeton Applied Research 174A potentiostat and a Riken Denshi F-35 x–y recorder or a Yokogawa 3056 chart recorder were used for constant-potential amperometry. In the measurements of current–time characteristics of the immobilized-enzyme sensors (batch method), the sensor was immersed in 5.0 ml or 20.0 ml of 0.1 M phosphate or carbonate buffer (pH 6.5–10), with magnetic stirring. A constant potential of +0.6 V vs. Ag/AgCl/KCl(sat) was applied to detect hydrogen peroxide.

Micro flow injection analysis (micro-FIA) and micro liquid chromatographic (micro-LC) experiments were carried out with a Shimadzu LC-9A pump. A Jasco ML-422 micro-valve injector (0.3 μl) or a Valco CI6W micro-loop injector (0.06 μl) was used for sample injection. The wall-jet-type electrochemical cell was made in-house. The structure is illustrated in Fig. 1. An 0.1 M phosphate buffer pH 8.0 and 0.05 M phosphate buffer pH 7.5 containing 0.3 mM sodium dodecyl sulfate (SDS) and 3 mM tetramethylammonium chloride (TMA) were used as

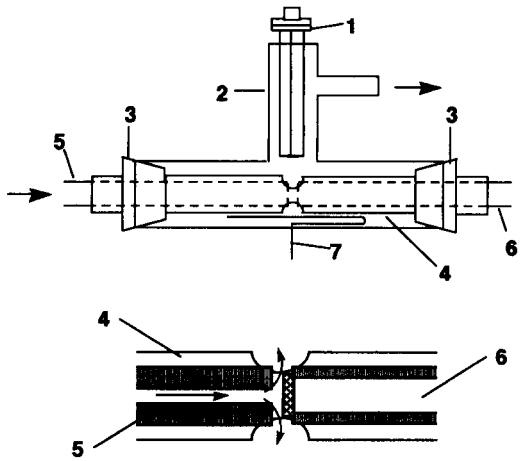

Fig. 1. Schematic diagram of the wall-jet-type electrolysis flow cell. (1) Ag/AgCl reference electrode; (2) acrylic tube; (3) rubber plug; (4) Teflon® tube (250 μm i.d.); (5) fused-silica tube (100 μm i.d.); (6) enzyme microelectrode; (7) Pt wire counter electrode.

mobile phases in micro-FIA and in micro-LC, respectively. These mobile phases were pumped at 30 $\mu l\ min^{-1}$. A Nomura Chemicals ODS-5 micro-column (250 mm × 0.5 mm i.d.) was used for the micro-LC separation.

3. Results and discussion

3.1. Steady state characteristics of Ch sensor

ChO-immobilized microelectrodes (Ch sensors) were characterized electrochemically by the batch method at room temperature. The Ch sensor responded quickly to Ch. The response time was about 5 s to reach 90% of the steady state current, as shown in Fig. 2. A decrease in the time constant of the instrument will decrease the response time further. The superior response time of the Ch sensor is attributed to the thinness of the enzyme layer without an outer membrane. The immobilized ChO exhibited a bell-shape pH dependence over a broad pH range from 6.5 to 10 with its maximum at pH 8–9, whereas the optimum pH of free ChO is pH 7.5–8.5 [6].

The apparent factor of the enzymatic conversion from Ch to hydrogen peroxide was estimated by comparison of the steady state current for a given concentration (1–5 mM) of Ch to that for a double concentration of hydrogen peroxide (see reaction 1). The apparent factor was around 60% at pH 8.0 and it was almost independent of the amount of the pipetted (or immobilized) ChO in the range of 0.1 to 1 U per electrode. Assuming a diffusion-controlled process and a diffusion coefficient of Ch 2.5 times as large as that of hydrogen peroxide, the maximum conversion of 63% ($= 100/2.5^{1/2}$) would be expected for the fast and complete enzymatic reaction. Therefore the above results seem to indicate almost complete conversion by immobilized ChO. In the following work, 0.2 U (200 U $ml^{-1} \times 1\ \mu l$) of ChO was pipetted onto the disk electrode (see Experimental).

3.2. Application of Ch sensor to assay for AchE activity

Measurement of AchE activity is one of the important indices for the studies on the function of a cholinenergic neuron. Although several methods for

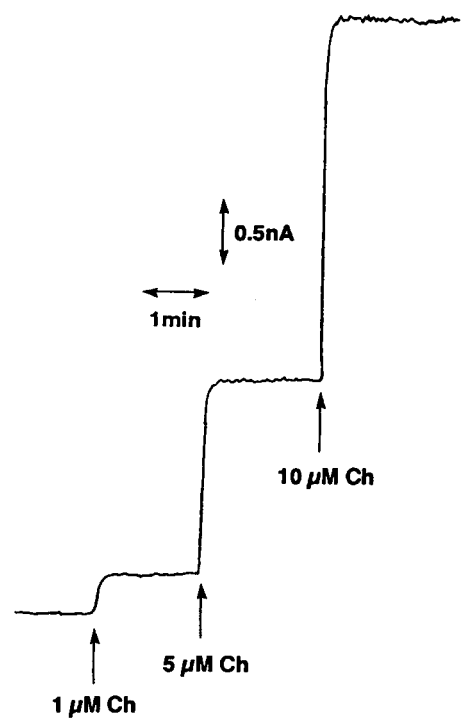

Fig. 2. Typical Ch sensor response to Ch injection in the batch mode.

the measurements have been reported including colorimetry, titmetry, radiometry, fluorometry and immunoassay [for reviews, 13–15] as well as flow injection analysis using an ChO-immobilized electrode [11], development of a new assay system is still desirable.

Taking the quick response of the present Ch sensor into account, the sensor is applicable to measurements of AchE activity. In this work, the activity measurements were performed as follows. In the batch mode, 50 μl of freshly prepared 50 mM Ach solution was added to 5.0 ml of 0.1 M phosphate buffer (pH 8) incubated at 37°C (finally 0.5 mM). The enzymatic reaction was started by the addition of a 1-μl aliquot of AchE solution, after which the current increased with time owing to the enzymatic generation of Ch, which was detected by the Ch sensor. The initial slope (nA min^{-1}) of the current–time response was linear with the concentration of AchE at least up to 5×10^{-3} U ml^{-1} as the final concentration (25 U $ml^{-1} \times 1$ μl sample addition per 5.0 ml of solution). The detection limit ($S/N = 3$) was 5×10^{-5} U ml^{-1} (0.25 U $ml^{-1} \times 1$ μl per 5.0 ml). The measurements of the enzymatic reaction at lower concentrations of AchE was affected by non-enzymatic hydrolysis of Ach. The linear range practically covers the normal range of AchE activity in human serum (1–4 U ml^{-1}) and brain (5–30 U ml^{-1}) [15]. Dividing the slope (nA min^{-1}) by the steady-state response for a given amount of Ch (nA mM^{-1}) gives the initial velocity of the Ch generation (mM min^{-1}). The calculated value was 62% of the labeled value of the commercially available sample.

The presence of bovine serum albumin (50 mg ml^{-1}) or ascorbic acid (0.06 mg ml^{-1}) in the AchE sample solution did not cause any significant change in the slope of the current–time curve, although ascorbic acid, which is oxidized at the same potential (see later), gave rise to an increase in the background current. Considering the micro-scale of this Ch sensor, a decrease in the total volume of the reaction solution will be possible, which would lead to an increase in the sensitivity. These results indicate the potential application of the micro-Ch sensor to AchE assay. Further refinement of the experimental conditions and its application to a chromatographic determination are in progress.

3.3. Steady state characteristics of the Ach / Ch sensor

The AchE/ChO-coimmobilized microelectrodes (Ach/Ch sensors) also showed quick response to Ach as well as Ch with a response time of 10–15 s. The steady state current for Ach was practically independent of the pipetted amount of AchE in the range of 0.5 to 5 U per electrode, although increased amounts of immobilized enzymes caused a decease in the physical stability of the microelectrodes. In the following experiments 2 U (2000 U $ml^{-1} \times 1$ ml) of AchE were pipetted on the micro-disk electrode (see Experimental). The coimmobilization of AchE led to no significant effect on the steady-state response to Ch. The response to Ach increased with increase in pH from 6.5 to 8.5 and then decreased beyond pH 10, giving a maximum response around pH 9. At the optimum pH of the coimmobilized enzymes (pH 9), the apparent factor of the enzymatic conversion from Ach to Ch was as large as 94%, where the apparent conversion factor was estimated by comparison of the response for a given concentration of Ach (1–5 mM) with that for the identical concentration of Ch (see reaction 2).

3.4. Micro-FIA of Ach and Ch with AchE / ChO-coimmobilized electrode

The micro-Ach/Ch sensor was applied to micro-scale flow-through detection of Ach and Ch. Considering the micro-disk shape of the sensor, a wall-jet-configuration was adapted, in which the disk electrode surface was kept as close to the outlet of the fused silica tube as possible to decrease the effective cell volume and increase the current (Fig. 1).

First, micro-FIA was carried out at pH 8.0 (0.1 M phosphate buffer), where a 0.3-μl aliquot of Ach or Ch sample was injected. The relationship between the peak height and the injected amount of Ach and Ch was linear over the range 0.3 pmol to 10^4 pmol (1×10^{-6} to 3×10^{-2} M, 0.3 μl) with correlation coefficients > 0.999. The standard deviations of the peak height were less than 3%.

The current response at the AchE/ChO-coimmobilized electrode was monitored *under continuous flow and close circuit* over an 8-day period. The results are given in Fig. 3. After three days, the peak

heights for Ach and Ch had decreased to 60% of the initial response. After this, however, the decrease in sensitivity slowed down and the response was 40% of the initial value after 8 days. The initial decrease in the sensitivity would be attributable to leaching of unimmobilized enzymes. The S/N ratio was practically constant over the 8-day period, because the decrease in the response was accompanied by a decrease in noise.

3.5. Micro-LC analysis of Ach and Ch

It is well known that ascorbic acid exists in brain in much higher concentration than Ach. Both the Ch and Ach/Ch sensors retained a response toward ascorbic acid, dopa and related compounds, although the immobilized enzyme layer exhibited partial permselectivity toward ascorbic acid. Nafion® coating over the enzyme layer [16] improved the permselectivity drastically: Ch exhibited a steady state current 100 times that of ascorbic acid at the same concentration. The permselectivity, however, does not seem sufficient for in vivo use and the treatment led to significant increase in the response time up to 1.5 min for 90% response. Thus, it would not be preferable to detect Ach or Ch directly and selectively in the batch method or micro-FIA with these electrodes. To overcome this point, we performed micro-LC with a micro-ODS column using the AchE/ChO-coimmobilized microelectrode as a transducer. The optimized mobile phase consisted of 3 mM TMA, 0.3 mM SDS in 0.05 M phosphate buffer (pH 7.5), which was pumped at 30 μl min^{-1}.

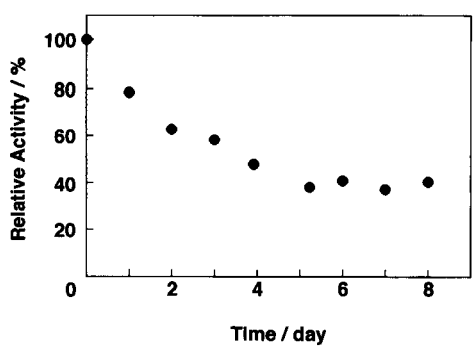

Fig. 3. Stability of AchE/ChO-coimmobilized electrode in micro-FIA under continuous flow and closed circuit at room temperature.

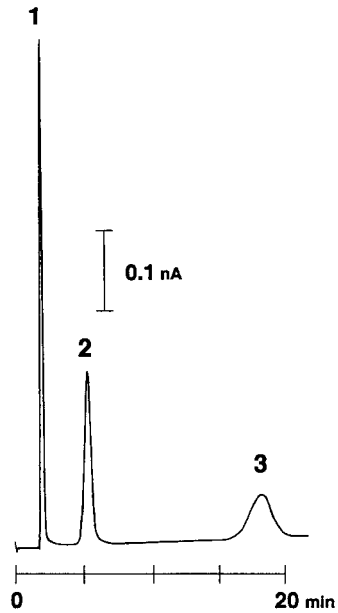

Fig. 4. Chromatogram of a 0.06 μl-injection of a sample mixture of 0.5 mM each of (1) ascorbic acid, (2) Ch and (3) Ach obtained at a AchE/ChO-coimmobilized microelectrode. See text for details.

The injection volume of the sample was 0.06 μl. Under these conditions, the responses from Ch and Ach were well separated from that for ascorbic acid within 20 min. Fig. 4 is a typical chromatogram. Other possible interferences such as dopa and dopac were eluted together with or close to ascorbic acid. An increase in the phosphate buffer concentration up to 0.2 M made the peak of Ach much sharper and concomitantly made the retention times shorter. However, it may not be preferred for practical use because of the too short retention time (3.5 min) for Ch.

The peak heights were in linear relations with the amounts of Ach and Ch over the range of 0.05 to 10^3 pmol (8×10^{-7} to 1.5×10^{-2} M, 0.06 μl) with correlation coefficients > 0.99. The lowest concentrations for the injection were comparable with those in micro-FIA, despite the chromatographic dilution. This is simply attributable to a decrease in the background noise in the micro-LC mode. The mid-range standard deviations were 3.5% for Ach and 1.0% for Ch.

4. Conclusions

Enzyme microelectrodes have been developed for the detection of Ach and Ch. Although the detection and preparative concept is not necessarily original, the proposed method is very simple, low-cost and suitable for micro-disk electrodes. The micro sensors are renewable with ease by polishing and immobilization. Application of micro-LC using the proposed enzyme microelectrode to micro-dialysis for the determination of Ach and Ch in brain is in progress. In addition, it is well known that organophosphorus pesticides inhibit AchE. Therefore, AchE-immobilized sensors can be used for the determination of the pesticides: the inhibition of AchE is directly related to the amount of the pesticides [17]. Although restoration of the activity of the inhibited AchE is a problem, the easy renewal of the present Ach/Ch sensor seems to be convenient for this purpose.

References

[1] K.L. Davis and P.A. Berger (Eds.), Brain Acetylcholine and Neuropsychiatric Disease, Plenum, New York, 1979.
[2] F. Flentge, K. Venema, T. Koch and J. Korf, Anal. Biochem., 204 (1992) 305.
[3] P.C. Gunaratna and G.S. Wilson, Anal. Chem., 62 (1990) 402.
[4] W.B. Stavinoha and S.T. Weintraub, Anal. Chem., 46 (1974) 757.
[5] R.M. Morelis and P.R. Coulet, Anal. Chim. Acta, 231 (1990) 27.
[6] J.-L. Marty, K. Sode and I. Karube, Anal. Chim. Acta, 228 (1989) 49.
[7] M.G. Garguilo, N. Huynh, A. Proctor and A.C. Michael, Anal. Chem., 65 (1993) 523.
[8] R. Rouillon, N. Mionetto and J.-L. Marty, Anal. Chim. Acta, 268 (1992) 347.
[9] E. Tamiya, Y. Sugiura and E.N. Navera, Anal. Chim. Acta, 251 (1991) 129.
[10] T. Yao, M. Sato, Y. Kobayashi and T. Wasa, Anal. Chim. Acta, 165 (1984) 291.
[11] T. Yao, Anal. Chim. Acta, 153 (1983) 169.
[12] D.S. Bindra, Y. Zhang, G.S. Wilson, R. Sternberg, D.R. Thévenot, D. Moatti and G. Reach, Anal. Chem., 63 (1991) 1692.
[13] A.G.R. Loft, J. Clin. Chem. Clin. Biochem., 28 (1990) 893.
[14] M. Masoom and P.J. Worsfold, Anal. Chim. Acta, 179 (1986) 217.
[15] N. Kaneda, Y. Noro and T. Nagatsu, J. Chromatogr., 344 (1985) 93; and references cited therein.
[16] E.W. Kristensen, W.G. Kuhr and R.M. Wightman, Anal. Chem., 59 (1987) 1752.
[17] A.M. Nyamsi Hendji, N. Jaffrezic-Renault, C. Martelet and P. Clechet, Anal. Chim. Acta, 281 (1993) 3.

ELSEVIER

Analytica Chimica Acta 299 (1994) 75–79

ANALYTICA CHIMICA ACTA

Comparison of performances and analytical applications of two immobilized oxalate oxidase sensors

M.A. Saka Amini, J.J. Vallon *

Laboratoire de Biochimie, Toxicologie et Analyse des Traces, Hôpital Edouard Herriot and Laboratoire de Chimie Analytique III, Faculté de Pharmacie, 8 Avenue Rockefeller, Lyon, France

Received 17 December 1993; revised manuscript received 9 May 1994

Abstract

The enzyme oxalate oxidase was immobilized on a pre-activated Nylon membrane or on a collagen membrane after activation of the carboxyl groups with the aid of an acyl–azide reaction. Oxalate was quantitated amperometrically via electrooxidation of the hydrogen peroxide generated in the reaction between oxalic acid and oxygen. The specific activities for the collagen and Nylon membranes were 0.13 and 0.74 U/cm^2, respectively. The enzyme activities for the two membranes were determined as a function of pH and ionic strength. The detection limits of oxalate were 1×10^{-5} M for the collagen sensor and 4×10^{-7} M for the Nylon sensor.

Keywords: Amperometry; Enzymatic methods; Enzyme electrode; Membranes; Oxalate oxidase

1. Introduction

Oxalate ions of endogenous or exogenous origin are present in normal human serum and urine. Their determination in biological fluids is of great importance in diseases with high levels of oxalate which may lead to urinary crystallizations and renal disorders originating from urinary stone formation [1]. Numerous methods have been reported for the determination of oxalate in biological fluids, including colorimetry [2], enzymatic assays [3], flow-injection analysis [4], gas chromatography [5] and liquid chromatography (LC) [6].

The enzymatic methods utilize either oxalate decarboxylase (EC 4.1.1.2) which converts oxalate to formate and carbon dioxide, or oxalate oxidase (EC 1.2.3.4) which converts oxalate stoichiometrically to hydrogen peroxide and carbon dioxide.

In this paper two amperometric biosensors formed by immobilization of oxalate oxidase on collagen and Nylon membranes are presented and their main characteristics are compared. The enzyme electrode consisted of a platinum anode, the potential of which was set at +0.680 V versus Ag/AgCl, connected to an enzymatic membrane maintained in close contact by a screw cap as previously described [7].

The hydrogen peroxide produced is oxidized to oxygen at the platinum disk according to the well known two-electron reaction [8].

2. Experimental

2.1. Apparatus

The amperometric and Ag/AgCl reference electrodes were obtained from Solea Tacussel (France).

* Corresponding author.

SSDI 0003-2670(94)00322-X

The currents were measured on a PRGE polarograph equipped with an Ecoscript recorder (Solea Tacussel). All measurements were performed at an applied potential of +0.680 V versus Ag/AgCl and at 37±0.1°C (Polystat® 86633, Bioblock Scientific, Illkirch, France).

2.2. Reagents

Oxalate oxidase (Ref. No. 567698) was from Boehringer Mannheim (Meylan, France) and all reagents (high grade) were from Merck (Nogent sur Marne, France). The 100-μm-thick collagen film in the dry state was obtained from Centre Technique du Cuir (Lyon, France). The pre-activated Nylon membrane (Immunodyne, 120 μm thick) was obtained from Pall Industries (Saint Germain en Laye, France).

2.3. Enzyme immobilization

For the immobilization of oxalate oxidase on the collagen membrane, its activation and coupling were performed according to the general method of Coulet et al. [9].

The immobilization of oxalate oxidase on the pre-activated Immunodyne membrane was extremely simple and consisted of wetting an 8-mm-diameter pre-activated disk with a 5 U/ml enzyme solution in 0.1 M phosphate buffer, pH 7.0. Of this solution 10 μl were deposited on each side of the membrane and left to react for 1 min at room temperature. After coupling the disk was washed in 1 M KCl for 30 min and stored in 0.1 M citrate buffer, pH 3.6 at 4°C until used.

3. Results and discussion

3.1. Oxalate oxidase purity

Verification of the absence of catalase activity associated with the oxalate oxidase was obtained by recording H_2O_2 calibration graphs in two cases: first with an oxalate oxidase membrane on the sensor and second with a non-enzymatic membrane. Both curves were superimposed, indicating no change in H_2O_2 concentrations, i.e. an absence of catalase activity.

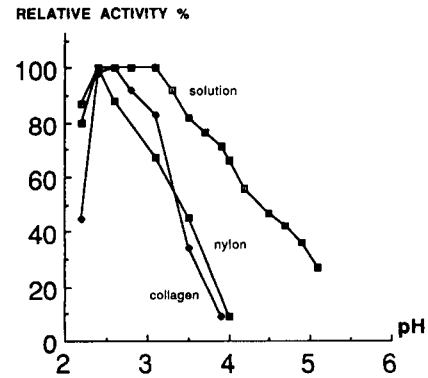

Fig. 1. Enzyme activities as a function of pH in 1 M buffer.

3.2. Soluble and immobilized enzyme activities as a function of pH

Activities were measured between pH 2.2 and 5.0 in 0.1 or 1 M citrate buffer. At the higher ionic strengths (1 M, Fig. 1) the optimum pH was 2.4–2.6 for immobilized oxidase but the collagen-immobilized enzyme showed a narrower pH range than the soluble one. The Nylon probe exhibited greatest activity at pH 2.4–2.5 and a pH range almost identical to that of the collagen-immobilized enzyme. In solution, oxalate oxidase activity showed a plateau between pH 2.4 and 3.4. The absence of a plateau for the probes is probably due to a modification of the active site of the enzyme at high ionic strengths. Indeed, we have observed that the activity of immobilized enzymes is lowered in 1 M buffer compared with 0.1 M buffer (see later).

Fig. 2 (0.1 M buffer) indicates that the optimum pH values are different on collagen (2.6), in solution (3.4–3.6) and on Nylon (3.6). The Nylon probe activity is distributed over the pH range in almost the same way as in solution.

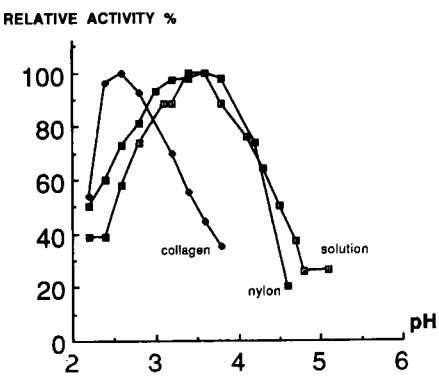

Fig. 2. Enzyme activities as a function of pH in 0.1 M buffer.

It is well known that the behaviour of the enzyme can be modified by an ionic effect of the microenvironment near the immobilized enzyme. We can therefore conclude that the ionic microenvironment of the immobilized enzyme is different on each membrane: in case of the neutral Nylon membrane, the pH of the enzyme microenvironment is identical to that in solution and no pH shift is observed. In contrast, the collagen membrane is polycationic in acidic medium which leads to some repulsion of H^+ ions; thus, the pH in the microenvironment will be more basic than in the bulk of the solution giving rise to a pH shift of one unit. Consequently, a distinct activity of the soluble enzyme can only be maintained after immobilization if the bulk of the solution has a pH that is one unit lower.

3.3. Specific activities of the membranes

Maximum currents corresponding to saturation of immobilized oxidase sites allowed the calculation of specific activities: 129.6 mU/cm^2 for the collagen membrane and 736.6 mU/cm^2 for the Nylon membrane. Thus, the Nylon sensor has a much higher specific activity (more elevated number of binding sites) than the collagen sensor (Fig. 3).

3.4. Michaelis constant of immobilized membranes

The K_m value (a measure of the affinity between oxidase and oxalate) is generally increased by immobilization. The K_m values for oxalate, as determined by the Michaelis–Menten procedure, were as follows: 4.2×10^{-4} M (soluble oxidase) [10]; 0.11 M (collagen sensor); 0.13 M (Nylon sensor). Thus, immobilization alters, to some extent and almost identically for

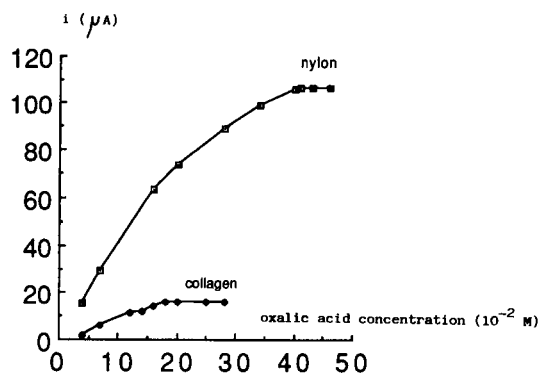

Fig. 3. Measurement of the specific activities of the membranes.

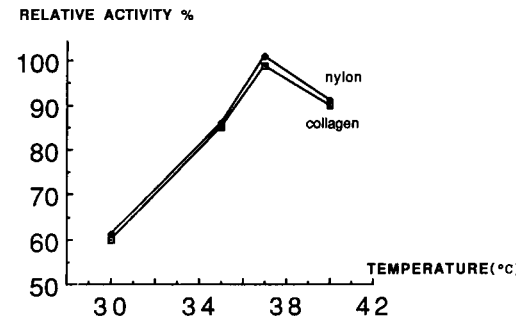

Fig. 4. Effect of temperature on enzyme activity.

Nylon and collagen, the affinity between enzyme and substrate, the reason being probably a modification of the quaternary structure of the binding sites.

3.5. Optimum temperature and detection limit

The enzyme activity of both sensors was studied in 0.1 M citrate buffer in the temperature range 30–40°C. Greatest activity was found at 37°C (Fig. 4). The following values were found for the detection limit (lowest oxalate concentration giving, with optimum settings of instruments, a signal equal to twice the noise): 1×10^{-5} M (collagen); 4×10^{-7} M (Nylon).

The better detection limit observed for Nylon is more likely explained by the higher specific activity (high density of binding carboxyl groups on the Nylon membrane). This performance appears very suitable for the determination of oxalate in biological fluids; for example, in normal human serum the oxalate concentrations range from 1 to 2×10^{-5} M. The detection limit for Nylon is hundred times lower than for collagen.

3.6. Inhibitors

Many inhibitors of oxalate oxidase have been described, including doubly charged cations, ascorbate [11,12], NO_3^-, Cl^-, etc. [13–16]. As we have previously described [17], SCN^- shows irreversible inhibition of the immobilized enzyme. Phthalate, being a very poor inhibitor, can be chosen as a buffer instead of citrate which shows very slight inhibition. The present study was carried out in citrate which allowed working in a wider range of buffering capacity.

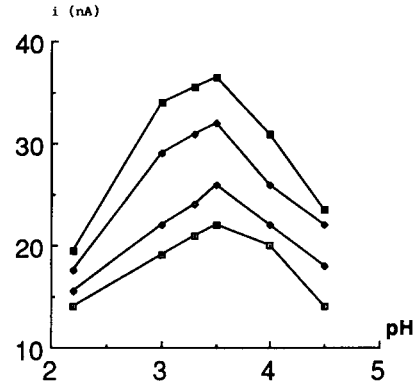

Fig. 5. Influence of the pH of immobilization (□, pH 3.5; ♦, pH 5.0; ■, pH 7.0; ◇, pH 8.0) on activities of the Nylon membrane as a function of pH in 0.1 M buffer.

3.7. Influence of pH on the binding of oxalate oxidase to the Nylon membrane

The immobilization of oxalate oxidase on the Nylon membrane was carried out at room temperature in 0.1 M phosphate buffers of various pH (3.5, 5.0, 7.0, 8.0). Fig. 5 shows that pH 7.0 is the best value for the binding of oxalate oxidase to the Nylon membrane. Oxalate oxidase activities of Nylon membranes were measured in 0.1 M buffer at different pH values ranging from 2.2 to 4.5. As shown in Fig. 5, the optimum pH for all Nylon membranes was near 3.4–3.6.

3.8. Influence of ionic strength on oxalate oxidase activity of Nylon membranes

Fig. 6 shows that the optimum pH for all Nylon membranes in 1 M buffers is 2.4–2.5. Comparison of Figs. 5 and 6 learns that the greater enzyme activity is in 0.1 M buffer.

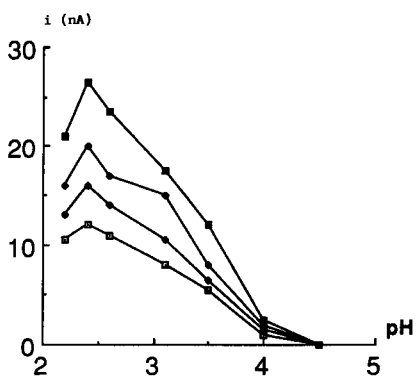

Fig. 6. Influence of the pH of immobilization (□, pH 3.5; ♦, pH 5.0; ■, pH 7.0; ◇, pH 8.0) on activities of the Nylon membrane as a function of pH in 1 M buffer.

4. Discussion

The measurement of oxalate in biological fluids is still a major problem for clinical biochemists.

In this study, we have attempted to compare the main characteristics of two immobilized oxalate oxidase sensors for the determination of oxalate. The Nylon membrane offers significant advantages over the collagen membrane. These advantages include a higher degree of flexibility, mechanical durability, wider pH range for utilisation, greater specific activity and lower limit of detection.

The pre-activated membrane, without further treatment, reacts covalently with the enzyme at an optimum pH of 7. The Nylon sensor has a much lower limit of detection for oxalate (4×0^{-7} M) than the collagen sensor (1×10^{-5} M); thus, it could provide the method of choice to measure oxalate in biological fluids, especially in human serum where the normal oxalate concentration is $1\text{–}2\times10^{-5}$ M. We are currently studying this in our laboratory.

References

[1] A. Hodgkinson, Oxalic Acid in Biology and Medicine, Academic Press, New York, 1977
[2] A. Hodgkinson and A. Williams, Clin. Chim. Acta, 36 (1972) 127
[3] J.E. Buttery, N. Ludvigson, E.A. Braiotta and P.R. Pannall, Clin. Chem., 29 (1983) 700
[4] E. Gaetani, C.F. Laureri, M. Vitto, L. Borghi, G.F. Elia and A. Novarini, Clin. Chim. Acta, 156 (1986) 71
[5] K.Y. Park and J. Gregory, Clin. Chem., 26 (1980) 1170
[6] L. Larsson, B. Libert and M. Asperud, Clin. Chem., 28 (1982) 2272
[7] M.A. Saka Amini, J.J. Vallon and C. Bichon, Anal. Lett., 22 (1989) 43.
[8] J.L. Blum, C. Bertrand and P.R. Coulet, Anal. Lett., 16 (B7) (1983) 525
[9] P.R. Coulet, J.H. Julliard and D.C. Gautheron, Biotechnol. Bioeng., 16 (1974) 1055
[10] J. Chiriboga, Arch. Biochem. Biophys., 116 (1966) 516.
[11] M.F. Laker, A.F. Hofmann and B.J.D. Meeuse, Clin. Chem., 26 (1980) 802.
[12] N. Potezny, R. Bais, P.D. O'Loughlin, J.B. Edwards, A.M. Rofe and R.A. Conyers, Clin. Chem., 29 (1983) 16.

[13] B.J.D. Meeuse and J.M. Campbell, Plant. Physiol., 34 (1959) 583.
[14] M. Sugiura, H. Yamamura, K. Hirano, M. Sasaki, M. Morikawa and M. Tsuboi, Chem. Pharm. Bull., 27 (1979) 2003.
[15] K.L. Goldsack, R.F.A. Ginman and J.M. Wright, Clin. Chem., 30 (1984) 813.
[16] F. Winquist, B. Danielsson, J.Y. Malpote, L. Persson and M.B. Larsson, Anal. Lett., 18 (B5) (1985) 573.
[17] M.A. Saka Amini, J.J. Vallon and S. Lartillot, Anal. Chim. Acta, 245 (1991) 129.

ELSEVIER

Analytica Chimica Acta 299 (1994) 81–90

ANALYTICA CHIMICA ACTA

Comparison of the analytical capabilities of an amperometric and an optical sensor for the determination of nitrate in river and well water

Margaret A. Stanley [a], Joe Maxwell [b], Mairead Forrestal [a], Andrew P. Doherty [a], Brian D. MacCraith [b,*], Dermot Diamond [a], Johannes G. Vos [a,*]

[a] *School of Chemical Sciences, Dublin City University, Dublin 9, Ireland*

[b] *School of Physical Sciences, Dublin City University, Dublin 9, Ireland*

Received 18 February 1994; revised manuscript received 20 July 1994

Abstract

The analysis of nitrate in water has been studied using novel amperometric and optical sensors. A flow-injection analysis system with amperometric detection has been developed in which nitrate is determined as nitrite after reduction in a cadmium column. The working electrode is glassy carbon modified with a crosslinked redox polymer. The linear range is 0.1 to 190 mg/l NO_3-N ($r > 0.999$) and the limit of detection (LOD) is 50 μg/l NO_3-N. A fibre optic sensor based on a dual wavelength absorption approach has also been developed. A signal at 210 nm where nitrate absorbs was referenced against a signal at 275 nm where nitrate does not absorb. Its linear range is from 0.4 to 30 mg/l NO_3-N and its LOD is 400 μg/l NO_3-N. These diverse methods have been applied to the analysis of the same river water samples and good correlations have been observed between the two measurement techniques and a standard ion chromatography method.

Keywords: Amperometry; Flow Injection; Sensors; Nitrate; Waters

1. Introduction

Nitrate enters natural waters from many sources and over the past few decades, its concentration has increased progressively in the environment [1]. The dominant factor in this trend has been the increased usage of nitrate-based fertilisers in agriculture and the consequential leaching of nitrate into freshwater supplies [2–4]. The nitrate anion is quite mobile because of its solubility in water and the predominantly negative charge on soil particles, and so it is readily leached if not utilised by plants. The solubility aspect means that agriculture is a major contributor to nitrate loading in freshwater supplies and consequently in drinking water [3].

Nitrate represents a potential hazard because of its participation in reactions similar to those found in the human stomach which give rise to *N*-nitroso compounds, some of which are carcinogenic [5,6]. It has been suggested that gastric cancer is associated with nitrate intake through this mechanism [7]. Furthermore, certain species of bacteria in humans can enzymatically reduce nitrate to nitrite [8]. The toxic effects of nitrite, vasodilation, lowering of blood pressure and formation of methaemoglobin, are well known [9].

* Corresponding authors.

SSDI 0003-2670(94)00328-9

The European Community Directive on the quality of water intended for human consumption came into effect in August 1985 with a limit of 11 mg/l NO_3-N (nitrate as nitrogen) as the maximum admissible level for nitrate [10].

The standard method for nitrate measurement involves reduction of nitrate to nitrite using a copper activated cadmium catalyst and determination of the nitrite concentration by reaction with sulphanilamide and *N*-1-naphthylethylenediamine in HCl to produce a purple/red azo dye. The absorbance of this dye at 543 nm is measured using a spectrophotometer and this is related to the sample nitrate concentration by means of a calibration curve derived from reference nitrate standards [11].

In view of the increase in interest in the quality of drinking water, sensitive, selective and simple methods for the determination of nitrate are desirable. One approach to this problem is the development of a modified electrode sensor which can be incorporated into a bench-top flow-injection analysis system (FIA) [12]. A second is the development of a fibre optic sensor which has shown itself capable of in situ monitoring [13]. In this contribution both of these types of sensor are investigated in detail. An ion chromatographic system was used to provide a reference method against which these more novel methods of detection could be compared.

Due to the selective detection of the amperometric and the optical sensors described in this paper, the analysis of nitrate can be carried out without the added requirement of mixing the sample with numerous reagents or the expense of chromatographic columns. This allows an added flexibility in the design of these sensors without compromising their sensitivity.

2. Experimental

2.1. Electrolytes and solutions

The electrolyte used was 0.1 mol dm^{-3} H_2SO_4. Nitrite solutions were prepared freshly each day from $NaNO_2$. $NaNO_3$ was used to prepare the nitrate solutions. The carrier solution used with the cadmium column was composed of 0.1 mol dm^{-3} NaCl and 2.5 g/l EDTA. A 2% w/v solution of $CuSO_4 \cdot 5H_2O$ was used to copperise the cadmium. All chemicals described in the text were of A.R. grade and were prepared with Milli-Q water.

2.2. Preparation of $[Os(bipy)_2(PVP)_{10}Cl]Cl$

This material was synthesised according to the procedure described by Forster and Vos [14] except that 2-methoxyethanol was used as the solvent instead of ethanol. A metal loading of one osmium centre per ten vinyl pyridine units was chosen as this loading has been shown to display optimum charge transfer characteristics [15]. PVP (poly-4-vinyl pyridine) of molecular weight 600,000 a.m.u. was used, and bipy = bipyridine.

2.3. Preparation of modified electrode

Modified electrodes were prepared by polishing glassy carbon electrodes with 5 μM alumina as an aqueous slurry on a felt cloth followed by a thorough rinsing with distilled water and methanol. The freshly prepared electrode surfaces were modified by drop coating using a 1% w/v methanolic solution of the polymer. Cross-linking of this polymer was achieved by adding an appropriate volume of 1,10-dibromodecane dissolved in methanol to the polymer deposited on the electrode [16]. These two solutions were then mixed gently and allowed to dry slowly overnight in a methanolic atmosphere.

2.4. Flow injection apparatus

The flow injection apparatus consisted of a Gilson Minipuls 3 peristaltic pump, a six port Rheodyne injector valve (No. 9125) fitted with a 20-μl fixed volume sample loop, a Rheodyne switching valve (No. 0792), an EG and G Princeton Applied Research Model 400 electrochemical detector and a Kipp and Zonen *X–t* recorder. Silicone rubber tubing was used at the peristaltic pump and PTFE 1/16″ o.d. × 1/32″ i.d. tubing for the rest of the system. For the reduction column a 3 mm bore, 50 mm length glass column was used. This was filled with cadmium granules (40–60 mesh) which had been washed in a 2% solution of copper sulphate. The column thus obtained was found to give a stable response over a two week period. A schematic diagram of the FIA apparatus can be seen in Fig. 1. Sample injections were made using a 2 cm^3 glass syringe fitted

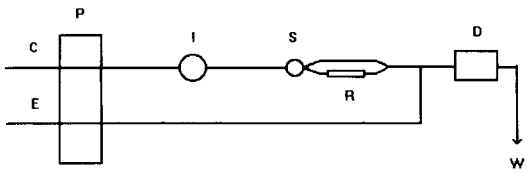

Fig. 1. Manifold of flow injection analysis system. P = Peristaltic pump, I = injection valve, S = switching valve, R = Cu/Cd reduction column, D = electrochemical detector, W = waste. $C = 0.1$ mol dm^{-3} NaCl + 2.5×10^{-3} kg/dm^{-3} EDTA. $E = 0.1$ mol dm^{-3} H_2SO_4.

with a Rheodyne injection needle. In the standard EG and G flow cell, an Ag/AgCl electrode acted as the reference and the auxiliary electrode was the stainless steel cell body.

2.5. Fibre optic sensor

Optical system design

Light from a 30-W Hamamatsu L2196 deuterium lamp was coupled to the optical fibre through two rotating filters. The lamp output beam was collimated by a system of fused silica lenses before passing through a custom-made filter wheel to another lens which focused the UV light into the optical fibre. The optical fibre took light to the absorption cell while another fibre transmitted light from the cell to the photomultiplier and amplifier. The optical fibre used was Fibreguide Industries Superguide G SFS600/660B UV–visible optical fibre with a 600 μm core diameter, a minimum bend radius of 50 mm and a numerical aperture of 0.22. The attenuation at 210 nm was approximately 1.5 dB per metre. The absorption cell shown in Fig. 2 was made at the university. The absorption path length is adjustable but in the work reported here a path length of 1 mm was used.

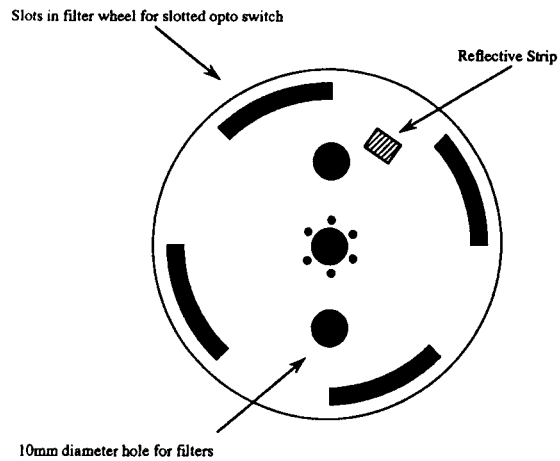

Fig. 3. Filter wheel for fibre optic sensor.

Electronic system

The Hamamatsu R269 photomultiplier tube was mounted directly onto the Hamamatsu C1556 amplifier module to prevent noise pickup from long leads. The amplifier was connected to a 12 bit analogue to digital converter (ADC) via a sample-and-hold circuit (SHA). The AD585 SHA device held the analogue voltage level constant while the AD574 ADC performed a conversion. The ADC was configured to accept a 0–10 V full scale input signal to directly match the output of the amplifier. Spectral selection was accomplished by a custom made filter wheel (see Fig. 3) which was mounted on a Scitec optical chopper which provided a variable speed motor to turn the wheel together with a slotted opto-switch to provide timing pulses. The two interference filters were located diametrically opposite on the wheel. Slots cut along the outer edge of the wheel were used to initiate a "hold" of the optical signal followed by a data conversion on the ADC. Two other slots over opaque areas of the filter wheel enabled subtraction of background light. A small

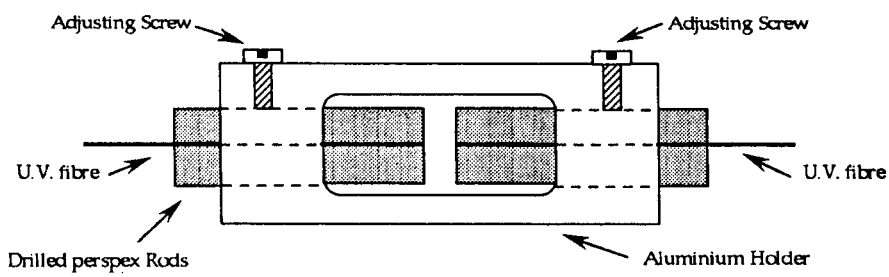

Fig. 2. Absorption cell of the fibre optic sensor. Water is free to move through the hollow inner space.

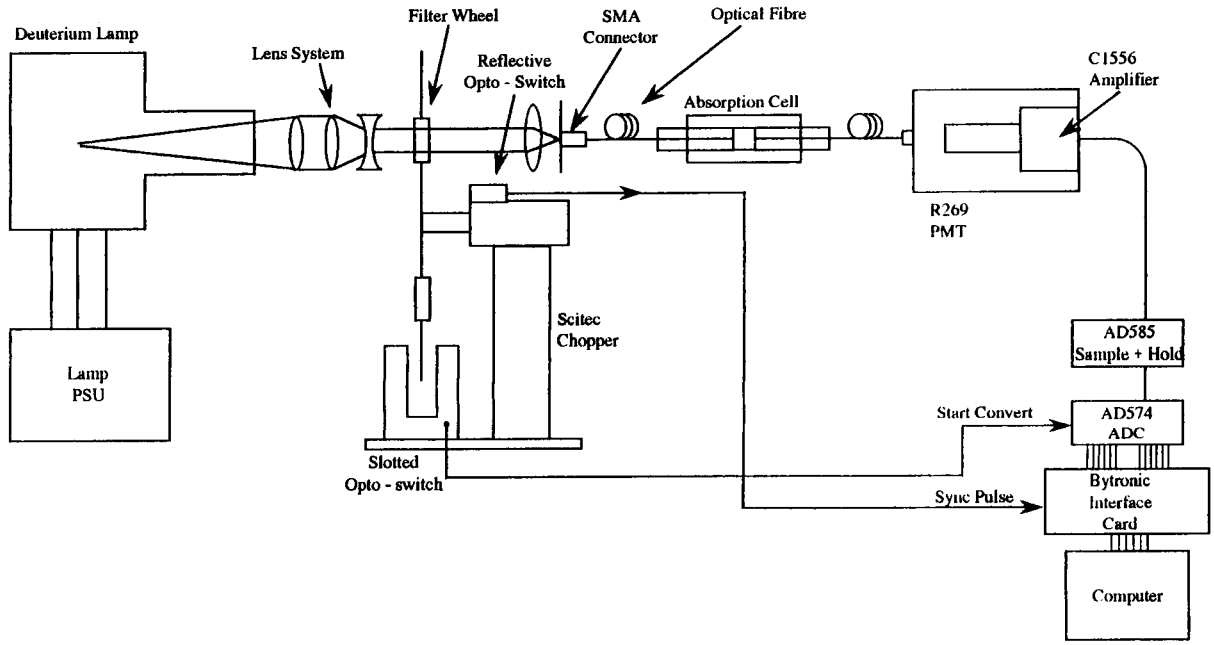

Fig. 4. Manifold of the fibre optic nitrate sensor.

reflective strip placed on the wheel was used to trigger a reflective opto-switch. This provided a synchronisation pulse so that data was collected in the correct sequence on every rotation of the filter wheel.

Nitrate sensor design

A schematic diagram of the prototype optical fibre sensor is shown in Fig. 4. This figure details the layout of the optical and electrical systems in relation to each other. Two narrow band filters were centered on 210 nm and 275 nm in a rotating filter wheel placed between the lamp and the launch fibre. The 210 nm interference filter had a full width at half maximum of 16 nm and a peak transmission of 18% while the 275 nm filter had a full width at half maximum of 9.5 nm and a peak transmission of 19%.

The analogue detection system consisted of a R269 UV-sensitive photomultiplier tube and low noise preamplifier. The output from the preamplifier was fed to an analogue to digital converter via a 'sample and hold' amplifier (SHA) which is synchronised to the rotating filter wheel. The SHA circuit effectively holds the signal at a constant value while an analogue to digital conversion was carried out. Signals corresponding to light levels at 210 nm and 275 nm were stored by a computer. The average of 250 points was then used to provide absorbance factor values for the nitrate solution placed in the absorption cell.

2.6. Sample treatment

All samples were collected in polyethylene containers, which had been washed with Milli-Q water to ensure they were free from contamination. Before filling, the bottles were rinsed three times with the water to be collected. River water samples were collected manually, by dipping the container into the river, a short distance from the riverbank. The samples from the

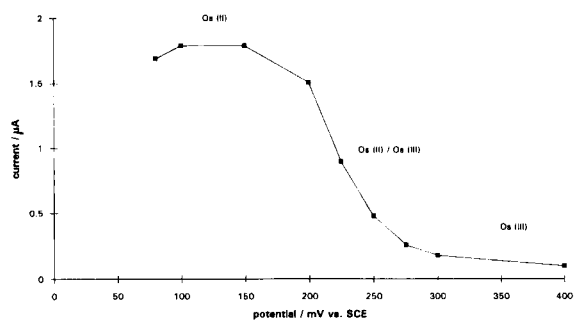

Fig. 5. Hydrodynamic voltammogram for the measurement of 15 mg/l NO_3-N at the modified electrode in the thin layer electrochemical flow cell. Flow rate is 0.5 cm^3 min^{-1}. Other conditions are as described in the text.

wells were collected by means of a pump. These were obtained only after the well was pumped sufficiently to ensure that the sample represented the groundwater source. On collection all samples were sealed, labelled and dated. Samples were refrigerated at 4°C and analysed within 48 h. Repeat measurements were made after several weeks and no loss of nitrate was found to have occurred.

3. Results and discussion

3.1. Modified electrode sensor

Effect of applied potential

An electrode modified with the $[Os(bipy)_2(PVP)_{10}Cl]Cl$ was used to detect nitrate anions after reduction to nitrite by a copperised cadmium column. Fig. 1 shows the layout of the FIA system. It can be used to detect both nitrite and nitrate ions depending on whether the reducing column is bypassed or not.

A hydrodynamic voltammogram of the system's response to nitrate is shown in Fig. 5. At a potential of 0.40 V vs. SCE no response to the reduced nitrate was observed. At this potential, the electrocatalytic sites were in the Os(III) state and therefore could not mediate the reduction of the nitrite. Decreasing the applied potential below 0.4 V vs. SCE resulted in the generation of catalytic Os(II) sites within the polymer and the onset of mediated reduction of nitrite was evident. From these results the optimum potential for detection was found to be 0.120 V vs. SCE and this potential was used for all subsequent measurements.

Sensor response characteristics

A high pH was required for reduction of nitrate by the cadmium column. So the carrier solution was adjusted to pH 9 with sodium hydroxide. However, detection of the reduced nitrate at the redox polymer had previously been found to be dependent on the hydrogen ion concentration [17]. Therefore a low pH was required for optimum detection sensitivity. It was found that at pH 4 the response to a solution containing 14 mg/l NO_3-N was 0.07 μA while at pH 1 the response to the same solution was 2 μA. This demonstrates how altering the pH of the electrolyte at the detector significantly affects the sensor's response. Consequently the flow of carrier from the column was merged with the sulphuric acid electrolyte before reaching the detector.

The peaks obtained using this FIA system were well defined and useful analytically. The precision of the response was found to be excellent with a relative standard deviation of 0.91% ($n=10$). The sample throughput was calculated to be 100 samples/hour from basewidth measurement. At bare electrodes this reaction has been found to cause surface passivation [18]. This passivation was not observed at the modified electrode. No deterioration in the electrode's response was found even after hundreds of determinations. This stability was obtained by crosslinking the metallopolymer with 1,10-dibromodecane. Crosslinking the polymer bestowed greater stability on the electrode without compromising its sensitivity or selectivity. The effect of two weeks of constant electrolyte flow on the sensor's performance was monitored. The peak current of a standard solution of nitrate containing 1.0 mg/l NO_3-N was found to have decreased from 0.135 μA to 0.117 μA over this period, a reduction in signal of only 13%. The precision of this signal slightly decreased to a relative standard deviation of 0.75% for $n=10$. This showed a remarkable improvement in stability compared with the uncrosslinked polymer which was found to have a half-life of only 46 h [17].

At a surface coverage of 1×10^{-9} mol cm^{-2} the sensitivity of the modified electrode in this flow cell was found to be 0.05 $\mu A\ mg^{-1}\ cm^3$. The linear range extends from 0.1 to 190 mg/l NO_3-N with correlation coefficients typically >0.999. The linear range encompassed both the normal nitrate levels and the occasionally excessive levels found in environmental water samples without the need for dilution. The limit of detection, defined as twice the height of the noise ($S/N=2$), was found to be 50 μg/l NO_3-N.

Selectivity

Millimolar concentrations of the cationic species K(I), Na(I), Li(I), Mg(II), Al(III) produced no interfering response at the sensor. The anions Cl^-, SO_4^{2-}, PO_4^{3-} similarly did not interfere. Ascorbic acid, though it is a common interferent in colorimetric procedures, was found to have no interfering effect at the osmium polymer.

A possible interferent is Fe(III) which has previously been shown to be capable of mediation by the osmium polymer [19]. The formal potential of the Fe(II)/Fe(III) couple is 0.46 V vs. SCE therefore the

reduction of Fe(III) can be mediated by the osmium couple (whose $E_{1/2}=0.25$ V vs. SCE). However, formation of the EDTA complex of iron results in a shift in the formal potential to a region negative of the formal potential of the osmium electrocatalyst. The $[Fe(EDTA)]^+$ formal potential being -0.13 V vs. SCE, which eliminates the interference.

Nitrite will of course interfere in the analysis. This can be overcome by comparing the sample's response directly at the sensor and then via the column. Any difference being due to the presence of nitrate.

3.2. Fibre optic sensor

Sensor operation

The principle of operation of the fibre optic sensor was based on the known ultraviolet absorption of the nitrate ion in the 200 nm spectral region. The strong absorbance of nitrate in the 210 nm region was measured relative to the absorbance in a region where nitrate does not absorb. The wavelength 275 nm was chosen for this purpose because nitrate does not absorb at this wavelength and it can be used to compensate for mainly organic interferents when these are present in significant concentrations. This dual wavelength approach was achieved by using two narrow band filters centered on 210 nm and 275 nm in a rotating filter wheel placed between the lamp and the launch fibre. This approach also compensated for spectrally neutral drifts within the system such as ageing of the light source and detector.

The detected signals are processed to yield an absorbance factor A which is defined as

$$A=\log_{10}\left(\frac{I_o}{I}\right) \quad (1)$$

The detected signal at 210 nm was represented by I and the signal at 275 nm represented by I_o. The spectral response of the system at 210 nm was very different to that at 275 nm. Consequently, when A was calculated using Eq. 1 the result was not a true absorbance expressible in absolute absorbance units, i.e. when no nitrates were present the calculated value of A was non-zero due to the fibre itself absorbing more at 210 nm compared to 275 nm. For this reason the calculated result was referred to as an absorbance factor.

Sensor response characteristics

In order to be viable as a groundwater nitrate monitor the sensor must be capable of detecting nitrates at considerable distances from the optical detector and signal processing electronics. With this in mind the sensor was tested using a total length of 40 m of optical fibre, i.e. 20 m between the source and the absorption cell and 20 m between the absorption cell and the detector. A calibration curve obtained with nitrate concentration given in units of mg/l NO_3-N is shown in Fig. 6a. This curve showed a marked levelling off of the slope for concentrations greater than 30 mg/l NO_3-N and hence a great reduction in sensitivity in this region. Consequently the range of this sensor over a total distance of 40 m was limited from 0.4 to 30 mg/l NO_3-N. Experiments carried out on the sensor using only 2 m of optical fibre showed a less marked levelling off of the calibration curve (see Fig. 6b) and the absorbance factor values were much lower than in the case of the 40 m length of fibre. This is a result of the greater total attenuation experienced at 210 nm compared to 275 nm. When the signals at these two wavelengths were

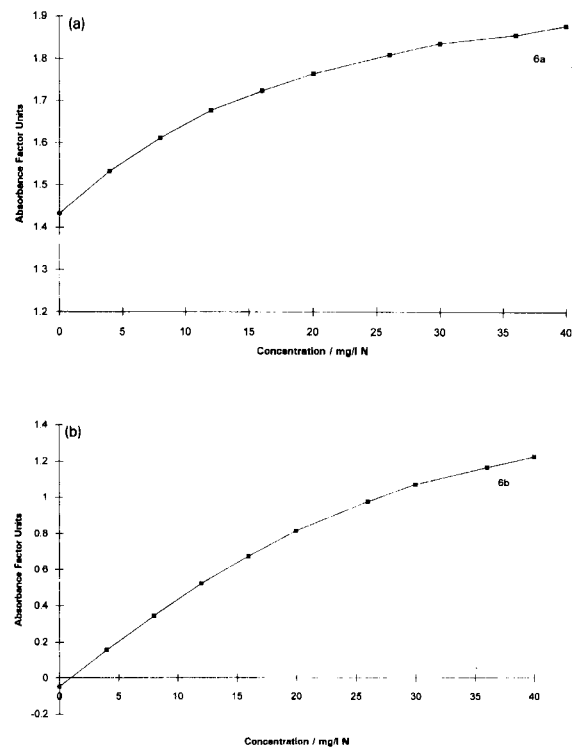

Fig. 6. Calibration curves of the fibre optic sensor. (a) Total fibre length was 40 m; (b) total fibre length was 2 m.

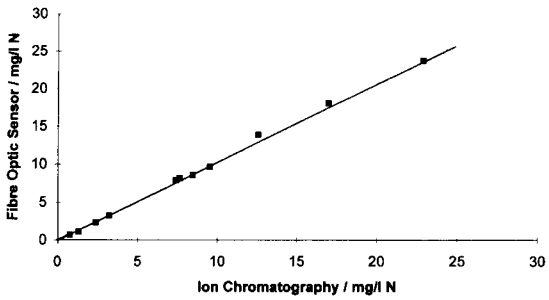

Fig. 7. Comparison of the fibre optic sensor with the standard ion chromatographic method.

ratioed the lower transmission at 210 nm resulted in a larger absorbance factor value. The fibre attenuation was 1.5 dB per metre which means 50% of the light was lost every two metres.

This non-linearity at higher concentrations can also be accounted for by the fact that the Beer-Lambert law is successful in describing the behaviour of dilute solutions only. At high concentrations the refractive index and absorptivity of the solution are not constant but may deviate considerably from their values at low concentrations.

Because the calibration curve for this sensor was not linear over the complete range tested it is not possible to quote an overall sensitivity value. However the sensitivity was approximately 0.04 AFU per mg/l NO_3-N (AFU = absorption factor unit) below 9 mg/l NO_3-N. At higher concentrations the slope gradually decreased and as a result the sensitivity also decreased to approximately 0.02 AFU per mg/l NO_3-N. The resolution of the sensor at lower concentrations was found to be 0.25 mg/l NO_3-N but this rose to 0.55 mg/l NO_3-N in the non-linear region. The repeatability found in consecutive measurements was found to be 1.7% well within the 2.5% specification set down by the UK Water Industry [20].

Selectivity

Although many inorganic anions absorb ultraviolet radiation at wavelengths in the 200 nm region, the majority of the more commonly occurring anions in water such as sulphate and phosphate only show appreciable absorption at shorter wavelengths [21]. Chloride is however expected to interfere and the sensor can therefore only be used for fresh water determinations. A degree of detection selectivity therefore exists for the sensor and this allows nitrate analysis in the presence of relatively high and variable background levels of inorganic ions. This coupled with the fact that direct UV detection is particularly suited to the nitrate ion in view of its relatively high molar absorptivity [22] ensures that the fibre optic sensor is very selective for nitrate determinations in water.

A number of chemical species other than nitrate do absorb in the 210 nm region. These include nitrites, iron(III) species, carbonates and humic acids. Interference from nitrite would be unlikely as nitrite levels in natural waters are extremely low, less than 0.01 mg/l NO_3-N, and any nitrate results due to unusually high concentrations of nitrite would be useful as a pollution indicator.

The effect of carbonates was investigated by using a solution containing 4 mg/l NO_3-N and 300 mg/l carbonate. It was found that the presence of carbonate resulted in a positive 4.5% error. A 4 mg/l iron(III) solution was found to have a maximum absorbance value of only 0.03 AFU. So unless it was present in high concentrations it would not have a large interfering effect. The presence of 40 mg/l of humic acid in a solution of 4 mg/l NO_3-N produced a 10% positive error. However this concentration is much greater than would be expected in most waters and considerably more than that found in groundwater where organic material is negligible.

One way of eliminating these interferents is to prevent them entering the absorption cell. Thompson and Blankley [23] used a conventional dialysis membrane as a filter to prevent iron and large molecules such as humic acids from entering the absorption cell. This technique could be readily applied to the fibre optic sensor's absorption cell. The effect of other interferents such as carbonates depends upon their concentration and this in turn depends upon the geographical location

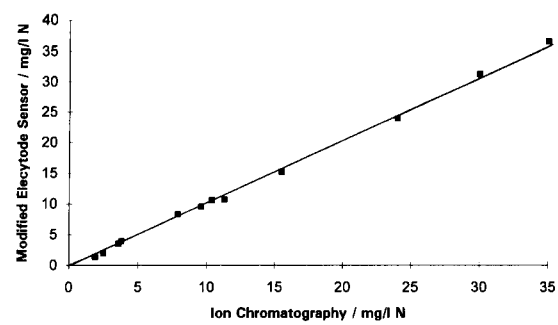

Fig. 8. Comparison of the modified electrode sensor with the standard ion chromatographic method.

of the water source. The interfering effect of nitrite can be discounted as it occurs in extremely small concentrations and any excessive amounts are a clear indication of serious pollution.

3.3. Validation of methods

These two experimental methods of nitrate detection, the modified electrode sensor and the fibre optic sensor, were then compared with an ion chromatographic procedure based on the Dionex Method AU131. The regression graphs (see Figs. 7 and 8) were plotted using the data obtained for both the experimental methods and the standard method. Each point on the graphs represents a single sample analysed by both methods in comparison with the ion chromatographic system. The graphs show only a slight deviation from the ideal with a correlation coefficient of 0.998 for the fibre optic sensor and a coefficient of 0.994 for the modified electrode sensor. This shows that minimum systematic errors occur in the fibre optic sensor and the modified electrode sensor.

Sample analysis

Having established the methods were accurate and precise for the determination of nitrate a number of real samples were collected from rivers in various locations. No sample preparation of any kind was performed on these samples before analysis by any of the systems. The results are shown in Table 1. The matrix concentrations and nature of the different samples are given in Tables 2 and 3 [24]. Good correlation between all three methods can be observed. Interestingly, although the chloride ion is expected to interfere in the fibre optic method the different concentrations of this ion present in the samples (see Table 2) do not adversely affect the results obtained from this sensor.

Use of the ion chromatographic procedure allowed the analysis of the water samples for the presence of other anions apart from nitrate. In the ion chromatographic method, due to the chromatographic process, nitrate is separated from any other anions present thus removing any interferences. Once separation has occurred results depend only on the performance of the

Table 2
Concentrations of a number of anions found in the water samples using ion chromatography (data taken from Ref. [24])

Sample	Concentration of species (mg/l)			
	Chloride	Bromide	Phosphate	Sulphate
Arvagh	23.75	<1	<1	18.56
Boyne	21.85	<1	<1	66.49
Hillcrest	16.3	<1	<1	10.65
Kells	29.79	<1	<1	39.33
Kill (1)	14.73	<1	<1	18.78
Kill (2)	13.86	1.24	<1	17.71
Knockmoylan	50.59	1.22	<1	32.77
Mattock	24.68	<1	<1	14.38
Monasterevin	16.48	<1	1.28	20.05
Stradbally	16.76	1.22	<1	10.84
Tinnock	62.87	1.21	<1	19.62
Ward	45.57	1.14	2.19	11.63

Table 1
Concentration of nitrate in the river and well water samples (NA = not analysed)

Sample	Concentration (mg/l N)		
	Ion chromatographic method	Fibre optic sensor method	Modified electrode method
Arvagh	2.32	2.45	NA
Boyne	0.84	0.73	0.89
Hillcrest	2.43	2.37	2.48
Kells	18.47	17.34	19.83
Kill (1)	<0.1	<0.5	<0.05
Kill (2)	<0.1	<0.5	<0.05
Knockmoylan	2.52	2.71	2.61
Mattock	2.1	2.02	2.41
Monasterevin	3.45	3.29	NA
Stradbally	3.67	NA	3.61
Tinnock	13.12	13.99	13.74
Ward	1.97	2.24	1.99

Table 3
Location of water sampling sites (data taken from Ref. [24])

Sample	Source	County	Well depth (feet)	Additional information
Arvagh	Well	Cavan	25	Agricultural area
Boyne	River	Louth	–	Agricultural area
Kells	Well	Meath	22	Tillage area
Kill (1)	Well	Kildare	85	Limestone area
Kill (2)	Well	Kildare	70	Limestone area
Mattock	River	Louth	–	Agricultural area
Hillcr est	Well	Laois	70	Tillage area
Stradbally	Well	Laois	35	Tillage area
Knockmoylan	Well	Kilkenny	80	Devonian
Monast erevin	River	Kildare	–	Limestone area
Tinnock	Well	Wexford	80	Tillage area
Ward	River	Dublin	–	Agricultural area

conductivity detector and calibration procedures. The fibre optic and modified electrode sensors, however, measure the nitrate in the presence of these ions whose concentrations vary from sample to sample. Despite this these sensors showed good selectivity for nitrate.

4. Conclusions

Two sensors suitable for the detection of nitrate in water samples have been described. A prototype optical fibre sensor for groundwater monitoring has been designed, constructed and tested. At this stage in its development the sensor is semi-portable and further work is being carried out on it to allow it to become a more compact, portable instrument. For example the use of a CCD array instead of the photomultiplier tube would allow the capture of complete spectra thus eliminating filters from the design, with the added bonus of being able to compensate for turbidity. Furthermore this approach would facilitate the development of multiwavelength algorithms which would impart greater selectivity

The electrochemical sensor has been designed for the laboratory environment. It provides a stable detection method housed in an easy to construct manifold. Its main advantages are twofold; first of all no sample pre-treatment is needed and fast sample throughput is possible. Secondly, with this measurement technique the effect of interferences is enormously reduced since with these polymer modified electrodes only species with an appropriate redox potential are detected. This selectivity can be controlled by the choice of the redox potential of the coating. Of all species normally occurring in river and well water, only nitrite and iron could possibly interfere in the reduction process, these can however be dealt with by adapting the measuring technique. Other species present will not interfere at levels up to at least 100 mM. Also the electrodes show a long linear range, fouling of the electrode surface is not observed and the modified electrodes are stable over a long period.

Both sensors approach the problem of nitrate detection but from vastly different approaches. Though not as flexible as the ion chromatography system, which can analyse for the presence of any ion, both sensors are simple to use with short analysis times. Both are reliable methods of detection which show good correlation between each other and with another standardised method. Neither use the costly reagents associated with typical nitrate analyses [11].

Acknowledgements

We thank EOLAS (the Irish Science and Technology Agency) for financial assistance for this work.

References

[1] P. Brimblecombe and D.H. Stedman, Nature, 298 (1982) 460.
[2] D. Forman, S. Al-Dabbagh and R. Doll, Nature, 313 (1972) 620.

[3] H. Moller J. Landt, E. Pedersen, P. Jensen, H. Autrup and O. Moller Jensen, Cancer Res., 49 (1989) 3117.
[4] P.J. Flanagan, Parameters of Water Quality: Interpretation and Standards, Environmental Research Unit, Dublin, 1990,
[5] R. Armijo, A. Gonzalez, M. Orellana, A. H, Coulson, J.W. Sayre and R. Detels, Int. J. Epidemiol., 10 (1981) 57.
[6] C. Cuello, P. Correa, W. Haenszel, G. Gordillo, C. Brown, M. Archer and S. Tannenbaum, J. Natl. Cancer Inst., 57 (1976).
[7] P. Correa, Cancer Surv., 2 (1983) 437.
[8] Assembly of Life Sciences (U.S.). Committee on Diet, Nutrition, and Cancer, Diet, Nutrition, and Cancer, National Academy Press, Washington, DC, 1982.
[9] W. Lijinsky and S. Epstein, Nature, 225 (1970) 21.
[10] D.J. Briggs, The State of the Environment in the European Community 1986, Office for Official Publications of the European Communities, Luxembourg, 1987.
[11] A.E. Greenberg, R.R. Trussel and L.S. Clesceri, Standard Methods for the Examination of Water and Waste Water, American Public Health Association, 1985.
[12] M.D. Imisides, G.G. Wallace and E.A. Wilke, Trends Anal. Chem., 7 (1988) 143.
[13] L.A. Saari, Trends Anal. Chem., 6 (1987) 85.
[14] R.J. Forster, J.G. Vos, Macromolecules, 23 (1990) 4372.
[15] R.J. Forster, J.G. Vos and M.E.G. Lyons, J. Chem. Soc., Faraday Trans., 87 (1991) 3761.
[16] A.P. Doherty and J.G. Vos, Electroanalysis, in press.
[17] A.P. Doherty and J.G. Vos, J. Chem. Soc., Faraday Trans., 88 (1992) 2903.
[18] G. Mengoli and M.M. Musiani, J. Electroanal. Chem., 199 (1989) 99.
[19] A.P. Doherty, R.J. Forster, M.R. Smyth and J.G. Vos, Anal. Chem., 64 (1992) 572.
[20] F. Campbell, Nitrate Measuring Instruments, UK Water Industry Specifications, Information and Guidance Notes, No. 7-11-00, Issue 1, July 1991.
[21] P.R. Haddad and P.E. Jackson, Ion Chromatography – Principles and Applications, Journal of Chromatography Library, Vol. 46, Elsevier, Amsterdam, 1990.
[22] H. Avsec, L. Kosta and I. Janzekovic, Vestn. Slov. Kem. Drus., 33 (1986) 413.
[23] K.C. Thompson and M. Blankley, Analyst, 109 (1984) 1053.
[24] M. Forrestal, M.Sc. Thesis, Dublin City University, 1993.

ELSEVIER

Analytica Chimica Acta 299 (1994) 91–96

ANALYTICA CHIMICA ACTA

Determination of sulphite by use of a fiber-optic biosensor based on a chemiluminescent reaction

József Hlavay [a,*], George G. Guilbault [b]

[a] *Department of Analytical Chemistry, University of Veszprém, P.O. Box 158, 8201 Veszprém, Hungary*

[b] *Department of Chemistry, University of New Orleans, New Orleans, LA 70148, USA*

Received 27 January 1994; revised manuscript received 17 June 1994

Abstract

A fiber-optic biosensor based on the immobilization of sulphite oxidase and peroxidase on different membranes, and subsequent detection of luminol chemiluminescence has been developed. The response was linear in the concentration ranges of 1 to 100 μM and 3.2 to 320 μM, with a detection limit (signal-to-noise ratio = 3) of 0.5 μM sulphite. A Nucleopore polycarbonate membrane proved to be superior to the chemically preactivated ones. The effect of pH, buffer, and immobilization conditions, as well as the elimination of ascorbic acid interference are also discussed. The feasibility of the biosensor developed was demonstrated by assaying the sulphite content of different food samples.

Keywords: Biosensors; Chemiluminescence; Fibre-optic biosensor; Sulphite

1. Introduction

Sulphite is extensively used in the food and the pharmaceutical industry as a preservative, an antioxidant, and an inhibitor of enzymatic reactions. Sulphite can also be found as a pollutant in ground and waste waters. Methods for determination of sulphite in different matrices include the use of techniques such as ion chromatography [1], gas chromatography [2], liquid chromatography [3], and chemiluminescence analysis [4].

In food analysis the AOAC methods are the Monier-Williams and colorimetric methods [5]. The Monier-Williams method comprises distillation, and therefore is time-consuming. The spectrophotometric method is based on colour formation between pararosaniline, formaldehyde and sulphite and has a limited sensitivity [6]. Beutler [7] reported a novel enzymatic technique using sulphite oxidase and measuring the hydrogen peroxide generated by linking it to the oxidation of NADH in the presence of NADH peroxidase. A linear calibration range of 13–205 μM was achieved but the enzymes were not reusable. An enzyme electrode incorporating immobilized sulphite oxidase and an amperometric method for measurement of the hydrogen peroxide produced were also studied [8,9]. Such an electrode was used for determination of sulphite in beer [10]. The enzyme was combined with a gel matrix and applied to the tip of a dissolved oxygen electrode; the paste was covered with a semi-permeable membrane. An enzyme electrode was also fabricated by immobilizing sulphite oxidase in a prewetted Immunodyne membrane and attaching it to a H_2O_2 electrode for determination of sulphite in food products [11]. The electrode exhibited a linear response up to 550 μM with a detection limit of 5 μM. An electrode incorpo-

* Corresponding author.

SSDI 0003-2670(94)00331-9

rating sulphite oxidase immobilized on pig intestine was also developed for determining sulphite; the method involved amperometric detection of H_2O_2 formed in the oxidation reaction [12]. Optimum assay conditions comprised 25 mM Tris buffer of pH 8.76 at 35°C. Pulsed amperometric detection, which retains electrode integrity, with a standard cell consisting of Pt working electrode and Ag–AgCl reference electrode, was used in conjunction with ion-exchange chromatography for the determination of sulphite or total SO_2 in beer [13]. Recoveries of added SO_2 were 95–105%, the rectilinear calibration range was ≤ 12 mg/l with a coefficient of variation of 6.3%. Results agreed with those obtained using the pararosaniline method. Several flow-injection manifolds were tested for the detection of sulphite in samples in the presence of 1 mM EDTA by the suppression effect of sulphite on the reaction between 50 μM H_2O_2, 0.5 mM luminol and 4 U/ml of horseradish peroxidase [14]. The calibration graph was rectilinear from 0.05 to 0.8 mM sulphite; the coefficient of variation ($n=5$) for sulphite in wine was $<4\%$.

In this work, a fiber-optic biosensor was developed for determination of sulphite in foods. Sulphite oxidase (SOD) and peroxidase (POD) were immobilized on different membranes. First, the immobilized SOD was used to generate H_2O_2 as follows:

$$SO_3^{2-} + O_2 + H_2O \xrightarrow{SOD} SO_4^{2-} + H_2O_2 \quad (1)$$

Hydrogen peroxide was detected by a chemiluminescent reaction using luminol (5-amino-2,3-dihydrophthalazine-1,4-dione) at pH > 9:

$$\text{luminol} + 2H_2O_2 + OH^- \xrightarrow{POD}$$

$$3-\text{aminophthalate} + N_2 + 3H_2O + h\nu \quad (2)$$

($\lambda_{max} = 430$ nm).

2. Experimental

2.1. Reagents

Sulphite oxidase (SOD, EC 1.8.3.1) 70 U/mg, bovine serum albumin (BSA), horseradish peroxidase (POD, EC 1.11.1.7) type I 102 U/mg, ascorbic oxidase (AOD, E. 1.10.3.3) 167 U/mg and luminol were purchased from Sigma and used as received. All other chemicals were obtained commercially in the highest obtainable grade and used without further purification. Solutions were prepared with doubly distilled, degassed deionized water. Enzymes were dissolved in phosphate buffer, pH 7.8. The phosphate buffers were prepared using KH_2PO_4 and an appropriate volume of 0.1 M KOH and adjusted to the proper pH. Hydrogen peroxide solution was standardized by titration with potassium permanganate. The working H_2O_2 solutions were prepared freshly every day. The 0.01 M luminol stock solution was made by dissolving 0.177 g of luminol in 0.025 M Na_2CO_3 buffer at pH 7.8. The pH of the final solution was adjusted by 0.1 M KOH to the required value.

2.2. Apparatus

Chemiluminescence measurements were carried out with a Lumac Biocounter Model 2010, which was modified to accommodate a single fiber optic bundle (Oriel, Model 77533). The cell compartment was constructed in such a way that ambient light does not interfere. A hole was drilled through a PVC cylinder and a disposable glass vial of 15×45 mm was placed in the cell body. Two cell configurations were applied in the experiments: in one the end of the fiber optic bundle was embedded and fixed in a removable cover. In the other, the end of one of the two arms of the bifurcated cable was fixed into the cell cover while the other was mounted on the side of the cell 1.5 cm above the bottom of the hole. Details are published elsewhere [15]. Signals were recorded on a Cole-Parmer chart recorder (Cole-Parmer). A Radiometer PHM 84 Research pH meter (Copenhagen) was used for all pH measurements.

2.3. Membranes

SOD and POD were immobilized on different membranes. Nucleopore polycarbonate (NP) membrane (pore size 0.03 μm) is not preactivated. The chemically preactivated membranes used were as follows: Ultrabind US-450 (UB) (Gelman Sciences), with a pore size of 0.45 μm is an unsupported membrane; Immobilon™ AV Affinity membrane (MI) (Millipore, Bedford, MA), is a chemically activated hydrophilic microporous membrane; Immunodyne™ (PI) (Pall BioSupport, New York) is an optically pure white

nylon 66 microporous membrane; and Pall Biodyne Transfer Membrane (PTB) (Pall BioSupport) is an ultra-high purity nylon 66 membrane which offers improved nucleic acid retention and superior handling characteristics over traditional nitrocellulose.

POD was immobilized as published previously [15]. All experiments were performed at room temperature. Various amounts of SOD were diluted by 0.1 M phosphate buffer at pH 7.8. From the preactivated membranes, usually 1.5 × 1.5 cm or 1.5 × 2 cm pieces were cut. In the immobilization methods either 30–50 μl of the SOD solution was placed on both sides of the membranes by micropipette, or the preactivated membrane pieces were immersed into 2 ml of a slowly stirred SOD solution for 0.5 h. The reaction was generally completed in 15 min. The membranes were then immersed in a solution of 0.1 M KCl for 15 min and stored in 0.1 M KH_2PO_4 (pH 7.8) at 4°C. In an other method, SOD solution was injected onto one side of the preactivated membrane and, after the enzyme solution was spread on the surface, 5–20 μl of 2.5% m/v glutaraldehyde (GA) was applied. When the enzyme was coupled (10 min) the membranes were washed and stored in a refrigerator.

For Nucleopore polycarbonate membranes, various amounts of SOD, 2.5% m/v BSA and finally, 2.5% m/v GA were placed on a 1 cm^2 disk and the mixture was gently stirred for 30 s. A total of 80 μl liquid on the membrane was never exceeded. The membranes were allowed to dry at room temperature for 4 h and washed first with distilled water, then with 0.1 M glycine–phosphate buffer solution (pH 7.8) and, last, with 0.1 M phosphate buffer (pH 7.8).

The enzyme membranes were mounted on the top of a PTFE tip by an O ring and secured with parafilm. The PTFE tip fits on the end of the fiber bundle. When not in use the enzyme membranes mounted on the tips were submerged in phosphate buffer solution and stored at 4°C.

2.4. Assay procedure

All measurements were carried out at room temperature by immersing the membranes in the solution of analyte and buffer at the desired pH with constant stirring. Care was taken to keep a constant stirring rate. First, H_2O_2 was generated from a sulphite-containing solution by SOD and then 0.001 M luminol and an appropriate volume of 0.1 M KOH were added and the POD enzyme membrane was immersed into the solution. The total volume was 4.5 ml. The maximum chemiluminescence (CL) intensity was recorded. Before the measurements, the background light intensity was checked by immersing the enzyme membrane into a blank solution; three runs were made and the mean value was calculated.

For the food analysis samples were prepared by the AOAC standard method (colorimetric method 20.126, using *p*-rosaniline as a chromogenic reagent) [5]. Ground dried fruit (10 g) was weighed and transferred to a blender with 290 ml of H_2O. The mixture was blended for 2 min, then 10 ml was withdrawn into a 100 ml volumetric flask.

3. Results and discussion

3.1. Immobilization

The effect of different amounts of immobilized SOD on the sensitivity of the sulphite determination was investigated. The amounts of SOD, BSA and GA were varied. For SOD immobilization on preactivated membranes 12 U per membrane proved to be sufficient along with 5–10 μl of 2.5% m/v GA. The efficiency of SOD immobilization was not the same when using 5–20 ml of 2.5% m/v BSA. As crosslinking reagent, 7.5 μl of 2.5% m/v GA was appropriate for the SOD immobilization both on preactivated and non-treated membranes. Excess of glutaraldehyde can deactivate the enzyme, while less crosslinking reagent resulted in incomplete immobilization. Pall Immonodyne (PI) and Nucleopore polycarbonate (NP) membranes gave superior sensitivity over the other membranes. The effect of different amounts of POD and immobilization conditions on the performance of the fiber optic CL sensor for determination of H_2O_2 was investigated in detail [15].

3.2. Effect of pH

The optimum pH range for determination of H_2O_2 with luminol was found as pH 9.25–9.85 [15]. Therefore, after the sulphite–SOD reaction had been completed, the pH was adjusted to pH 9.5. The effect of pH on the CL intensity when assaying 320 μM sulphite

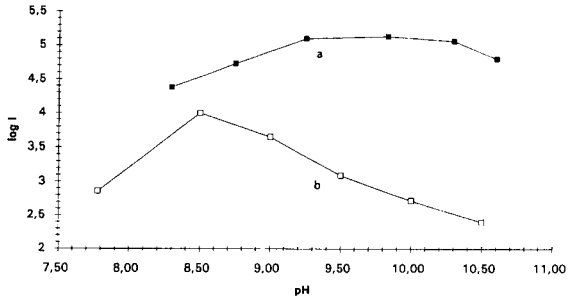

Fig. 1. Effect of pH on the chemiluminescence intensity, *I*. 320 μM sulfite, 0.6 mM TEA–HCl buffer, (a) POD on MI membrane, (b) SOD on NP membrane.

with SOD on a NP membrane and POD on a MI membrane is shown in Fig. 1.

Maximum CL intensity was achieved at pH 8.5 in triethanolammonium chloride buffer. At higher pH the activity of SOD gradually decreased. 10 min was found to be an appropriate reaction time, as explained elsewhere [15].

A main application of the fiber-optic CL sensors is the determination of H_2O_2 generated by highly selective oxidases. However, the pH of the maximum signal is usually lower than that of the optimal pH found for the reaction of luminol and POD. So, experiments were carried out on the coimmobilization of SOD and POD as well as decreasing the reaction time. The analytical performance of the coimmobilized enzyme membrane was not as good as the single-enzyme immobilized membrane; a detection limit of 5 μM H_2O_2 and a linear range of 5–316 μM were obtained [16]. On the other hand, Abdel-Latif and Guilbault [17] reported that by using a surface active agent (CTAB, cetyltrimethylammonium bromide), the pH mismatch of the two reactions could be overcome. However, it was found that the intensity of the CL signal and the activity of the enzymes gradually decreased due to the adsorption of CTAB on the surface of the membranes, so the pH mismatch could not be solved by addition of this surfactant.

3.3. Effect of buffer and storage

For assaying sulphite, 0.1 M phosphate buffer, 10 mM Tris (2-amino-(hydroxymethyl)-1,3-propandiol) and 0.6 mM TEA–HCl (triethanolammonium chloride) were applied at pH 8.5. After the H_2O_2 was generated, the pH of the solution was adjusted to 9.5, luminol was added to the solution and the CL reaction was initiated by immersing the POD membrane in the solution. The CL intensity decreased by about 35% on using phosphate buffer and was only 15% using Tris buffer of the values obtained in TEA–HCl buffer. Therefore, all experiments were performed in 0.6 mM TEA–HCl buffer.

When not in use, the enzyme membranes were stored mounted on a PTFE tip and submerged in different buffer solutions at 4°C. Of the buffers used for assaying the analytes, 0.1 M phosphate buffer (pH 7.8) proved to be superior over the others for this purpose.

Table 1
Analytical characteristics of fiber-optic sensors

SOD	POD	*a*	*b*	*r*	Conc. range (μM)	Det. lim. (μM) [d]
MI [a]	MI	0.62	1.19	0.993	3.2–100	3
PTB [a]	PTB	0.71	1.19	0.996	3.2–320	3
UB [b]	UB	0.89	0.95	0.993	3.2–320	3
PI [a]	PI	1.05	1.32	0.997	3.2–320	3
PI [b]	PI	1.00	1.54	0.990	3.2–320	3
NP [c]	NP	1.21	2.17	0.996	1–100	0.5
NP [b]	NP	1.62	1.77	0.990	1–100	0.5

a = Slope, *b* = intercept, *r* = correlation coefficient for least squares linear regression for log–log plot. MI = Millipore Immobilon, PTB = Pall Transfer Biodyne, UB = Ultrabind, PI = Pall Immunodyne, NP = Nucleopore polycarbonate.

[a] 12 U SOD per membrane.

[b] 12 U SOD + 7.5 ml GA per membrane.

[c] 9 U SOD + 10 ml BSA + 7.5 ml GA per membrane.

[d] Detection limit, signal-to-noise = 3.

3.4. Analytical characteristics of the fiber-optic biosensor

Linear log–log calibration curves up to 320 μM sulphite were obtained by use of the fiber-optic biosensor using the different membranes. Results are summarised in Table 1.

The Nucleopore polycarbonate membrane proved to be the most sensitive for sulphite determination. The CL response was linear in the concentration range of 1–100 μM sulphite with a detection limit of 0.5 μM sulphite. This range compared favourably with other sensors described in the literature [14]. Surprisingly, the preactivated membranes showed poorer sensitivity towards sulphite; linear log–log calibration graphs between 3.2 and 320 μM sulphite were obtained. Using optimum amounts of BSA and GA, SOD was stably immobilized on the Nucleopore polycarbonate membranes. The operational and storage stability of polycarbonate-bound peroxidase was satisfactory; the sensor could reliably be used up to 10 days with almost the same sensitivity as its initial value [15]. The opposite trend was observed for the determination of hypoxanthine and xanthine using xanthine oxidase (XAD) and POD [16].

In an interference study, the biosensor responded to ascorbic acid. It was found that 5 U of ascorbic oxidase (AOD) and 3 min of intensive stirring, before the SOD reaction, eliminated the interference. Control experiments without sulphite were carried out and only the background CL signal was obtained.

Determination of H_2O_2 with POD immobilized on Nucleopore polycarbonate membrane proved to be reproducible; at 100 μM H_2O_2, R.S.D. = 2.3% ($n = 5$). An assay of 100 μM sulphite with the fiber-optic biosensor gave R.S.D. = 9.8% ($n = 5$). The activity of the SOD enzyme membrane slowly decreased; after one week, 78% of the initial activity was measured.

The fiber-optic biosensor developed was used for sulphite measurements in different food samples. Potato flakes (14.4 mg/l), dried raisins (10.2 mg/l), red wine (174 mg/l), beer (9.7 mg/l), and plum (10.5 mg/l) samples were analysed. Five units of AOD (10 μl) was added to 4.5 ml solution and 3 min intensive stirring was used to eliminate any interference due to ascorbic acid. The results were compared with those of a standard spectrophotometric method [5], giving a regression of $Y = 0.12 + 1.12X$ (where Y = sulphite concentration measured by standard method and X = that measured by the fiber-optic biosensor), with a correlation coefficient of 0.954. As can be seen the values obtained by the fiber-optic biosensor were slightly lower than those using pararosaniline.

4. Conclusions

There is an increasing need for the application of a reliable, selective and sensitive sensor for determination of sulphite in food samples. The fiber-optic biosensor based upon the immobilization of SOD and POD on appropriate membranes can fulfil this demand. Using glutaraldehyde as crosslinking agent for immobilization of the peroxide and sulphite oxidases on both sides of the membranes a higher stability can be achieved. With Nucleopore polycarbonate membranes a linear concentration range of 1–100 μM was obtained. The detection limit was found to be 0.5 μM. The sensors should be calibrated every day.

Acknowledgements

This work was partially supported by National Hungarian Science Foundation (OTKA) 2544.

References

[1] C. Anderson, C.R. Warner, D.H. Daniels Jr. and K.L. Padgett, J. Assoc. Off. Anal. Chem., 69 (1986) 14.
[2] T. Hamano, Y. Mitsuhashi, Y. Matsuki, M. Ikuzawa, K. Fujita, T. Izumi and M. Iwaid, Z. Lebens. Unters. Forsch, 168 (1979) 195
[3] N. Imaizumi, K. Hayakawa, N. Okubo and M. Miyazaki, Chem. Pharm. Bull 29 (1981) 3755.
[4] M. Yamada, T. Nakada, Jr. and S. Suzuki, Anal. Chim. Acta, 147 (1983) 401.
[5] AOAC, Official Methods of Analysis, Association of Official Analytical Chemistry, Arlington, 1984, pp. 391–392.
[6] P.K. Dasgupta, K. DeCasare Jr. and J.C. Ullrey, Anal. Chem., 52 (1980) 1912.
[7] H.O. Beutler, Food Chem., 15 (1984) 157.
[8] T. Fonong, Anal. Chim. Acta, 184 (1986) 287.
[9] V.J. Smith, Anal. Chem. 59 (1987) 2256.
[10] D. Fassnidge and E. Van Engel, J. Am. Soc. Brew. Chem., 48 (1990) 122.
[11] A. Mulchandani, C.A. Groom and J.H.T. Luong, J. Biotechnol., 18 (1991) 93.

[12] M.A. Nabirahni and R.R. Vaid, Anal. Lett., 24 (1991) 551.
[13] H.P. Wagner and M.J. McGaratty, J. Am. Soc. Brew. Chem., 50 (1992) 1.
[14] Y.L. Huang, J.M. Kim and R.D. Schmid, Anal. Chim. Acta, 266 (1992) 317.
[15] J. Hlavay and G.G. Guilbault, Acta Chimica Hung., Models in Chemistry, 130 (1993) 83.
[16] J. Hlavay, S.D. Haemmerli and G.G. Guilbault, Biosensors Bioelectron., 9 (1994) 189.
[17] M.S. Abdel-Latif and G.G. Guilbault, Anal. Chim. Acta, 221 (1989) 11–17

ELSEVIER

Analytica Chimica Acta 299 (1994) 97–111

ANALYTICA CHIMICA ACTA

Transformation of polysulfidic sulfur to elemental sulfur in a chelated iron, hydrogen sulfide oxidation process

Eric T. Clarke [a], Touradj Solouki [a], David H. Russell [a,*], Arthur E. Martell [a], Derek McManus [b]

[a] *Department of Chemistry, Texas A and M University, College Station, TX 77843, USA*
[b] *ARI Technologies, Inc., Geneva, IL 60134, USA*

Received 18 April 1994; revised manuscript received 18 July 1994

Abstract

Polysulfides, S_x^{2-}, formed in the oxidative absorption of hydrogen sulfide, are labile, linear polyatomic compounds and readily decompose to elemental sulfur in aqueous solutions. The initial identification of polysulfide species that are found in solutions containing chelated Fe(III) and H_2S using laser desorption Fourier transform ion cyclotron resonance (LD-FTICR) mass spectrometry is described. LD is shown to be a superior ionization method because rearrangement and/or fragmentation product ions that are often observed in electron-impact and chemical-ionization methods are absent in LD mass spectra. The LD-FTICR studies indicate that trisulfide is the dominant polysulfide species in aqueous solution under the experimental conditions employed ([Fe] = 0.018 M and [L] = 0.036 M at pH 8.5, where L = nitrilotriacetic acid), and disulfide, tetrasulfide and pentasulfide are present in lesser proportions.

Keywords: Mass spectrometry; Iron; Polysulfides; Sulfur

1. Introduction

Chelated-iron liquid redox processes are increasingly employed in a variety of industries to concurrently absorb and oxidize the H_2S component of gas streams to elemental sulfur. The hydrogen sulfide is readily removed from the gas stream by absorption in an aqueous solution of chelated ferric iron, Fe(III)L, where L is usually an amino polycarboxylic acid such as nitriloacetic acid (NTA, **1**). In this commercial process, sulfide is oxidized by Fe(III)L to elemental sulfur, and the Fe(III)L is reduced to soluble Fe(II)L near pH 8.5 (Eq. 1). The reduced iron chelate is concurrently oxidized by molecular oxygen derived from air to Fe(III)L (Eq. 2).

$$H_2S + 2Fe(III)L \rightarrow 1/8S_8 + 2Fe(II)L + 2H^+ \quad (1)$$

$$Fe(II)L + 2H^+ + 1/2O_2 \rightarrow 2Fe(III)L + H_2O \quad (2)$$

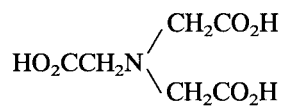

NTA,1

The mechanism by which cyclooctasulfur, S_8, forms via catenation from monoatomic sulfur in H_2S was thought to involve polysulfides but no direct evidence for the presence of these intermediates existed. Knowl-

* Corresponding author.

SSDI 0003-2670(94)00320-3

edge of the persistence and distribution of the various polysulfide homologs may prove valuable in increasing elemental sulfur yields via process modifications that disfavor sulfur oxo-acid by-product salt formation from the air-induced oxidation of polysulfide precursors. For optimal yield of elemental sulfur salts of thiosulfate and sulfate should not form to an appreciable extent in the process.

The unfavorable side-products of the oxidation of H_2S are sulfite (SO_3^{2-}), thiosulfate ($S_2O_3^{2-}$), and sulfate (SO_4^{2-}). Sulfite and thiosulfate are transient products that are eventually oxidized to sulfate. From studies of the kinetics of oxidation of sulfide by molecular oxygen in aqueous solutions, Avrahami and Golding [1] reported that sulfite is the initial oxidation product, and it is readily oxidized to sulfate, more so than thiosulfate. Sulfite can also be consumed by reduction with polysulfides to produce thiosulfate, while thiosulfate concentrations appear to accumulate with time. Commercial yield of sulfur is improved when the production of these sulfur oxy-anions is minimized by any means.

In addition, the combination of H_2S (or Na_2S) with Fe(II)L produces FeS as a side-product or an intermediate product. FeS can be oxidized by bubbling of air or molecular oxygen into the resulting suspension to form $Fe(OH)_3$ in the absence of a chelating agent, or to a soluble Fe(III) complex when NTA is used as the chelating agent. Under reducing conditions, such as those found in the H_2S gas stream line, FeS persists as an insoluble precipitate.

Significant sulfur intermediates formed in the oxidative absorption of hydrogen sulfide are alkali metal polysulfide salts, S_x^{2-}, as can be expected from knowledge of the facile decomposition of polysulfide compounds to elemental sulfur and sulfide, as described by Schwarzenbach and Fisher[2].

Polysulfides are linear, non-branched, polymers of sulfide; crystal structures have been reported for the polysulfides, S_x^{2-}, for $x=2$–7 [3–8]. For tetrasulfide and longer-chain compounds, the terminal S–S bonds have a median reported size of 2.02–2.06 Å while internal S–S bonds have a median length of 2.05–2.07 Å. The dinegative charge of the alkali metal salts is probably distributed evenly along the sulfur chain by p–π bonding or resonance effects; all of the S–S bonds are shorter than 2.08 Å, a value that was calculated by Pauling [9] on the basis of pure p-bonding character.

Polysulfides readily fragment and rearrange in water and organic solvents [10–12], owing in part to their small bond energies, e.g. 35 kcal/mol for tetrasulfide [10] and 70–80 kcal/mol for aliphatic disulfides [11]. Classical methods of analysis [infrared (IR) and ultraviolet–visible (UV–VIS) spectroscopy] cannot be used to distinguish these labile compounds.

Argentimetric potentiometric titration has been used successfully to measure sulfide and thiosulfate in the presence of each other by measuring the difference in their sulfur potentials [13], but application of this titration method to the determination of polysulfides is an interpretive approach and is highly variable. Reliable laser Raman spectrometry [14], proton nuclear magnetic resonance (NMR) spectroscopy [12,15], and reversed-phase liquid chromatography (LC) have been reported for polysulfides, mercaptans, disulfides, and their derivatives [16,17]; however, laser Raman does not fully distinguish chain lengths in polysulfides, functional derivatives of polysulfides cannot be made in the manner of sulfide and mercaptans, and LC does not resolve polysulfide salts.

The exact nature of alkali metal polysulfides prepared as standards and those detected as intermediates in the commercial oxidative absorption process for H_2S and Na_2S has been made with laser desorption (LD) mass spectrometry, that has found earlier application in the study of membrane polymers, peptides, and inorganic compounds [18,19]. In this paper the initial identification of polysulfide species found in solutions containing Fe(III)NTA and H_2S or Na_2S using laser desorption Fourier transform ion cyclotron resonance (LD-FTICR) mass spectrometry is described. The results of supplemental or alternative experiments are reported for purposes of comparison.

2. Experimental

2.1. Synthesis of alkali metal polysulfides

Many synthetic procedures are described in the literature for the preparation of polysulfide salts [20] from the stoichiometric combination of elemental sulfur with sulfide or hydrosulfide in a suitable solvent, e.g., water, ethanol, or condensed ammonia. Among these procedures, only those of Feher and Berthold [21] were found to produce pure potassium salts in

ethanol; all other procedures resulted in mixtures of polysulfides, as shown by LD mass spectral analysis in Table 1. Results of argentimetric potentiometric titration for the characterization of the intended polysulfide salts, and their elemental analysis for metal ion and sulfur (as sulfate), from Galbraith Labs. (Knoxville, TN, USA), also appear in Table 1 for comparison.

K_2S_3 and K_2S_5 were prepared in ethanol by the methods described by Feher and Berthold [21]. For the synthesis of K_2S_3, two molar equivalents of potassium metal were combined with two equivalents of elemental sulfur; the third equivalent of sulfur was supplied by H_2S gas. Metallic potassium (5.24 g or 0.134 mol) was dissolved with stirring in about 50 ml of dry ethanol at room temperature in a three-necked 1-l round-bottom flask. Air was excluded from the flask by introducing a blanket of argon gas within a Schlenk line. Ethanol was slowly added to the dry potassium through a dropping funnel in order to avoid excessive production of hydrogen gas. All of the potassium went into solution within 10–15 min without heating. H_2S gas was next introduced into the flask that contained the resulting potassium ethoxide at a low rate for 1–2 h to make potassium hydrosulfide, KHS, a white precipitate. Additional ethanol was added through the dropping funnel as necessary to keep the KHS in solution.

The excess H_2S was removed from the flask by purging with argon gas for about 0.5 h. Fine pulverized sulfur (4.30 g or 0.134 mol) was added portion-wise (1 g per 15 min) to the KHS solution, and the mixture

Table 1
Characterization of alkali metal polysulfide salts by elemental analysis, argentimetric potentiometric titration, and LD-FTICR mass spectrometry

Polysulfide		Elemental analysis (two sources)				
		Theoretical (%)	Experimental (%)	Probable formula	Argentimetric titration (%)	LD [a] (relative abundance, %)
Na_2S_2	Na	41.82	24.86	$Na_2S_{3.10}$ [b]		S_2 (58)
	S	58.18	51.84–55.83		57	S_3 (100)
	Na	41.82	22.43	$Na_2S_{2.66}$ [c]		
	S	58.18	57.23–57.72			
K_2S_2	K	54.93	29.57	$K_2S_{3.95}$ [c]		S_2 (74)
	S	45.07	47.92		NA	S_3 (100)
K_2S_3	K	44.89	33.18	$K_2S_{3.08}$ [b]		S_3 (100)
	S	55.11	38.19–45.58		87	
Na_2S_4 (Alfa)	Na	26.43	19.16–19.27	$Na_2S_{4.05}$ [b]		S_2 (10)
					93	S_3 (100)
	S	73.56	51.61–58.33			S_4 (23)
						KS_6 (45)
K_2S_4	K	37.86	24.77	$K_2S_{5.85}$ [c]		S_3 (83)
	S	62.14	59.25–59.55		NA	S_4 (23)
						KS_6 (100)
						KS_7 (13)
K_2S_5	K	32.83	30.89–30.96	$K_2S_{4.97}$ [b]		S_5 (100)
	S	67.17	59.30–63.47		92	K_2S_3 (53)
						K_2HS_2 (19)
K_2S_6	K	28.94	31.94–32.18	$K_2S_{4.87}$ [b]		S_2 (84)
	S	71.06	58.50–70.07		NA	S_3 (12)
K_2S_6	K	28.94	30.36	$K_2S_{5.03}$ [c]		S_5 (100)
	S	71.06	62.65–62.69		NA	S_6 (15)
						S_7 (20)
						S_8 (95)
						S_9 (27)

[a] Laser desorption mass spectrometry.
[b] Oneida Research Services.
[c] Galbraith Labs.

was brought to a simmer for 15–20 min. After the mixture was cooled to room temperature, the excess solvent was stripped off by distillation through a side-arm condensor tube and receiving flask under a slight vacuum that was provided by a water aspirator.

Crystals of K_2S_3 with deep yellow color readily precipitated out of ethanol. The crystals were collected in a glass-fritted Schlenk tube and then transferred to a vacuum desiccator for drying over $CaSO_4$ for 24 h. The K_2S_3 crystals were of uniform color and appearance. Yield of K_2S_3 was 8.5 g, or 36.5% of the theoretical yield.

K_2S_5 was prepared in a manner similar to that of K_2S_3 except that four molar equivalents of fine pulverized sulfur (8.66 g or 0.271 mol) were combined with metallic potassium (5.30 g, 0.136 mol) and H_2S in ethanol instead of the two molar equivalents that were used to prepare K_2S_3. Yield of K_2S_5 (deep orange color) was 11.0 g, or 34.0% of the theoretical.

Na_2S_4 was purchased from Alfa, Johnson Matthey (Ward Hill, MA, USA) and also from GFS (Columbus, OH, USA). The tetrasulfide sample from GFS was insoluble in water and was subsequently shown by powder X-ray diffraction to be alpha (orthorhombic) sulfur with characteristic *d*-spacings at 3.85, 3.21, and 3.11 A° [22]. *d*-Spacings reported by Rosen and Tegman [23] for Na_2S_4 were not present in the GFS Na_2S_4 powder spectrum. Elemental sulfur was also present in the Alfa Na_2S_4 sample, to a lesser extent, but the commercial preparation contained a mixture of polysulfides (Table 1). Subsequent efforts to synthesize pure tetrasulfide (and disulfide) salts in this laboratory using ethanol, water, or an aqueous ethanolic mixture as described by Pearson and Robinson [20] also gave mixtures of polysulfides, chiefly with trisulfide. A trial synthesis of K_2S_6 by fusion of K_2S_5 with a molar equivalent of elemental sulfur [21] gave a mixture of disulfide and trisulfide by decomposition (Table 1). Alternative routes of synthesis of K_2S_6 were tried, such as the combination of KHS with five molar equivalents of elemental sulfur in ethanol or the reduction of elemental sulfur with lithium in ethanol, but these attempts gave mostly pentasulfide and trisulfide, respectively. Hence, only K_2S_3 and K_2S_5 could be used as reference compounds in characterization and transformation procedures for alkali metal polysulfide salts.

2.2. Characterization of polysulfide compounds

Laser desorption mass spectrometry

An FTICR mass spectrometer was used to obtain the mass spectra of the sulfide polymers. A detailed description of the mass spectrometer [19] and the use of lasers in mass spectrometry [24] are given in previous publications. Briefly, the spectrometer consists of an Extrel (Madison, WI, USA) FTMS-2001 data system, a 7.0-T, 15-cm, room temperature bore superconducting Oxford Instruments (Oxford, UK) magnet and a home-built cylindrical ion cell. The vacuum chamber was pumped by two cryo pumps (Model RPK 900, Leybold/Heraeus, Cologne, Germany) with a maximum pumping speed of 2600 l s^{-1} and a minimum pumping speed of 300 l s^{-1} for H_2O and He, respectively. The insertion lock used for sample introduction is differentially pumped by a 285 l s^{-1} oil diffusion pump. Typical ion-cell vacuum during the LD event was in the mid 10^{-8} Torr range as measured with a Bayard–Alpert ion gauge.

The analyte samples (polysulfides) were wetted with a drop of a 50:50 mixture of dry methanol and benzene on the sample probe surface to obtain a thin layer of analyte; the polysulfide salts were soluble in methanol, and elemental sulfur could be dissolved in benzene (no LD mass spectra were obtained for these sulfur compounds unless they were wetted with a drop of organic solvent). Tetrahydrofuran (THF) and dimethylformamide (DMF) are unsuitable as solvents for sulfur since THF forms an adduct with the polysulfides [25] and DMF has a low vapor pressure at room temperature.

The sulfur samples were mounted on a brass or stainless-steel probe surface, wetted with a drop of solvent mixture, and irradiated with a beam of N_2 laser (Model VSL-33ND, Laser Science, Cambridge, MA, USA) (337.1 nm) with an energy of 80–120 μJ per pulse, pulsed at 3 ns. At the energy range of 80–120 μJ per pulse fragmentation of the polymeric sulfur chains were not observed. However, at higher laser energies (>150 μJ per pulse) product ions, due to the fragmentation of the intact analyte ions and/or gas phase reactions, were observed (see, for example, Fig. 3). Focusing of the laser beam to an approximate size of 200 μm $\times$ 200 μm was accomplished by using two lenses as a telescope assembly. The laser beam flux densities were measured by placing a power head [Model P25 with a

Scientech (Boulder, CO, USA) D 200 power meter] in the laser beam pathway. Because electronic absorption bands for polysulfides extend to the UV region of N_2 laser (337.1 nm) the use of matrix material to assist desorption–ionization was found to be unnecessary [18]. The laser-desorbed ions were trapped in the ICR cell at a −4-V trapping voltage [19]; trapped ions were excited by chirp excitation with a radiofrequency field, and ion detection was performed at medium resolution (16 000–32 000 data points) in the direct broad-band mode. Results for the LD mass spectral method appear in Tables 1 and 2. Standard K_2S_3 has a characteristic signal at m/z 96 for trisulfide (Fig. 1) and K_2S_5 has a signal for pentasulfide at m/z 160 in the negative-ion mode (Fig. 2). These compounds (Figs. 1 and 2) are pure compounds without any additives but may decompose over time (2–3 months) even if refrigerated. Results from LD-FTICR for the other polysulfide salts, intended as standards, appear in Table 1 and show evidence that these additional compounds are mixtures.

In Fig. 3A and B LD-FTICR mass spectra of S_8 species at low energy laser power (80 μJ per pulse) and high energy laser power (240 μJ per pulse) are shown, respectively. At low laser power (Fig. 3A) the dominant signal at m/z 256 corresponds to S_8 species and lower abundant signals at m/z 160 (S_5) and m/z 288 (S_9) are also present. Notice that at high laser power (Fig. 3B), due to fragmentation and/or gas phase reactions and rearrangements, other S_n ($n=2$–11) species are observed. For this reason, LD-FTICR mass spectral data used in polysulfide analysis were obtained at low laser power (80–120 μJ per pulse).

Results obtained by other methods, e.g., electron impact (EI) and chemical ionization (CI), are compared with those of LD in Table 2 to illustrate the superiority of LD mass spectrometry in obtaining intact polysulfides. The spectra of Na_2S_4 (Alfa), standard K_2S_3, and standard K_2S_5 were obtained by EI on a VG 70-S double-focussing high-resolution mass spectrometer operated under standard conditions and from 110 to 180°C, necessary for the vaporization of the sulfur polymers at 15 eV (15 eV was intended to be a softer treatment for the labile sulfur compounds). For the CI process, charge was transferred to the polysulfide samples dissolved in methanol by ionized methane gas.

Argentimetric potentiometric titration

Methods for the potentiometric titration of polysulfide, sulfide, and thiosulfate with standard $AgNO_3$ in degassed 0.100 M NaOH, all contained within a thermostated cell at 25°C and protected from air with a stream of argon gas that was delivered through gas line fittings, were adapted from Papp and other paper pulp chemists [13]. An Orion Ag/AgS electrode was used

Table 2
Mass spectral analysis for K_2S_3, Na_2S_4 (α), and K_2S_5 by different methods (relative abundances are shown)

Analytical method	K_2S_3	Na_2S_4 (α)	K_2S_5	S_8
Laser desorption	S_3 (100)	S_3 (100)	S_5 (100)	S_8 (100)
		S_4 (23)	K_2S_3 (53)	S_9 (58)
		NaS_6 (45)	K_2HS_2 (16)	S_5 (26)
Electron impact (15 eV)	S_2 (33) [a]	S_2 (100) [b]	S_2 (33) [c]	S_1 (13) [e]
	S_4 (30)	S_4 (17)	S_4 (44)	S_2 (100)
	S_5 (72)	S_5 (40)	S_5 (79)	S_3 (27)
	S_6 (56)	S_6 (33)	S_6 (59)	S_4 (49)
	S_8 (100)	S_8 (100)	S_8 (100)	S_5 (26)
				S_6 (16)
				S_7 (2)
				S_8 (58)
Chemical ionization [d]	–	S_6 (27)	–	–
		S_7 (35)		
		S_8 (100)		

[a] 142°C.
[b] 110°C.
[c] 176°C.
[d] Oneida Research Services.
[e] Ref. [51]

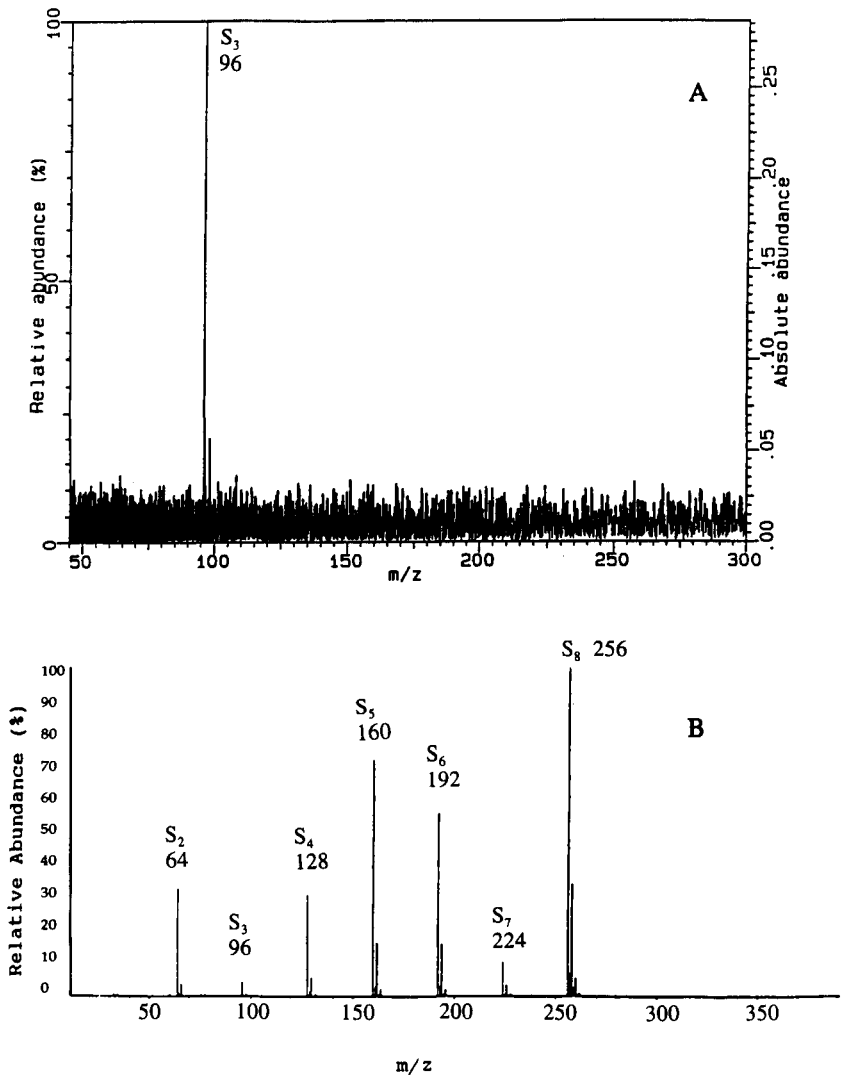

Fig. 1. Mass spectral analysis of K_2S_3 (A) by LD-FTICR mass spectrometry, with sample wetted with a drop of methanol, and (B) by EI, 15 eV at 142°C.

in conjunction with a calomel reference electrode to determine the potentials of sulfide (-600 mV) and thiosulfate ($+100$ mV) in mixtures for concentrations within the range 10^{-2}–10^{-4} M in sulfur. The slope of the Ag/AgS electrode was found, under these conditions, to be -30.67 mV/dec, and was in agreement with the manufacturer's specifications. Sulfide and thiosulfate end-points varied with age of solutions, and fresh standards had to be made daily.

Polysulfide concentrations were estimated from a difference method, for which the polysulfide compounds were oxidized by 3.0 ml of 0.5 M Na_2SO_3 at 60°C for 20 min in 0.100 M NaOH. Excess sulfite was masked by 5.0 ml of 37% formaldehyde, which was added just after the sulfide end-point, and the pH was adjusted to near 7 with 40% acetic acid (to sharpen the end-point). The difference between the thiosulfate concentration generated by reaction of polysulfide with

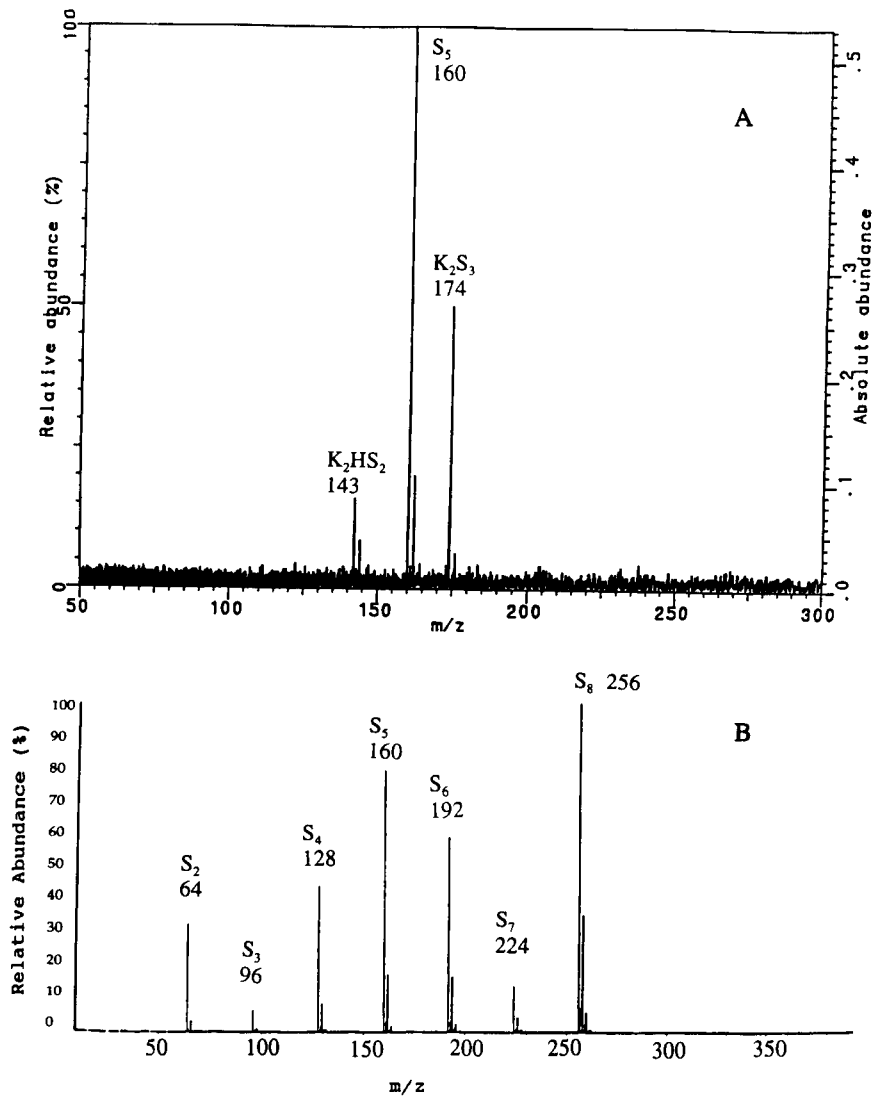

Fig. 2. Mass spectral analysis of K_2S_5 (A) by LD-FTICR mass spectrometry, with sample wetted with a drop of methanol, and (B) by EI, 15 eV at 142°C.

sulfite and that already present in the polysulfide sample was intended to give the amount of polysulfidic sulfur less sulfide [13]:

$$Na_2S_x + Na_2SO_3 \rightarrow Na_2S + (x-1)Na_2S_2O_3$$

However, this theory was shown to be in error, because the concentration of sulfide did not increase in a stoichiometric amount relative to the observed increase in thiosulfate concentration and both concentrations were highly variable. Because estimations of the polysulfidic concentrations were subject to interpretation, argentimetric potentiometric titration was not useful for characterization of polysulfides.

Powder X-ray diffraction

Samples of elemental and polysulfidic sulfur (about 500 mg) were ground and packed on a glass slide for analysis. Acacia gum was used to seal the tetrasulfide sample from air and moisture to limit decomposition. The patterns were run from 15 to 35° 2θ on a Scintag PAD-5 diffractometer equipped with nickel filter for CuKα radiation. Standard powder files [22], reported

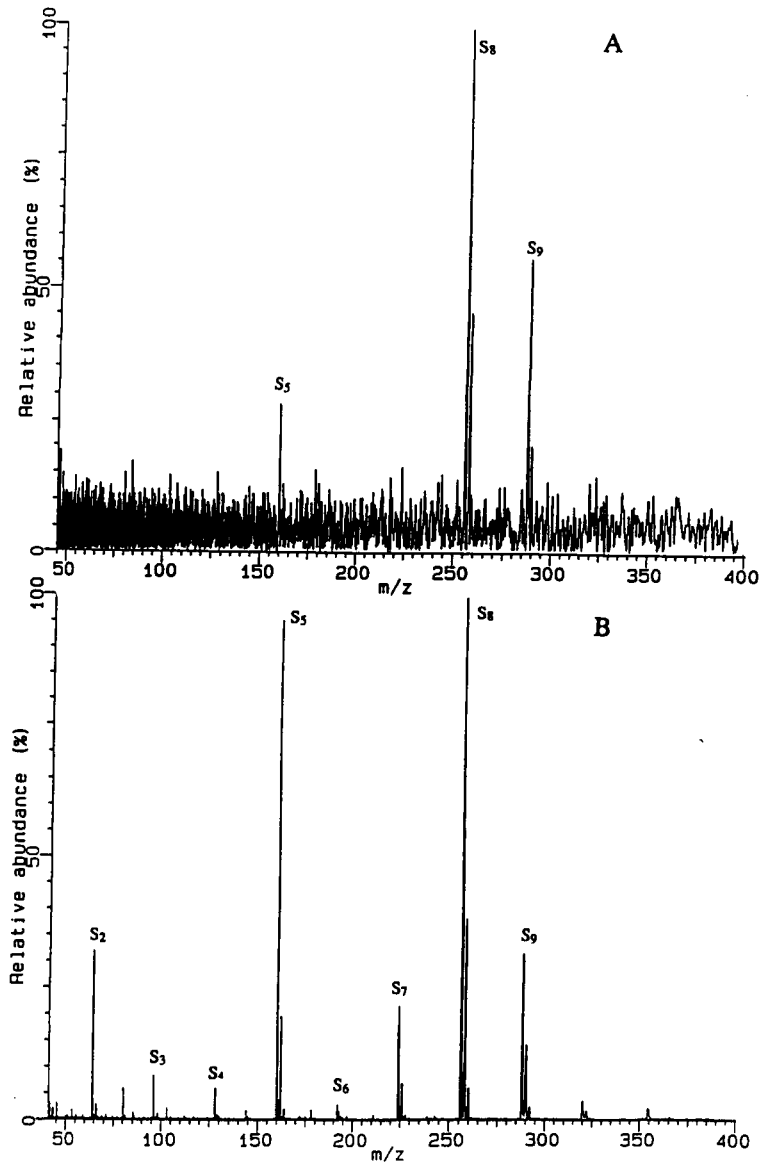

Fig. 3. Mass spectral analysis of S_8 by LD-FTICR mass spectrometry at (A) low laser energy (80 μJ per pulse) and (B) high laser energy (240 μJ per pulse).

in *d*-spacings (Å), were used to identify the spectra (Table 3).

Liquid chromatography of polysulfides

An attempt to separate sulfide and polysulfides mixed together with sulfate, sulfite, and thiosulfate was made with a Wescan Anion R LC column (Alltech) with 10^{-3} M carbonate buffer (about pH 11) and with a Milton Roy (LDC Analytical) Constametric Metering pump and conductivity detector (Conductomonitor III), set at 10 μS. Each of the sulfur anions was found to have a common retention time when using the Wescan column.

Satisfactory separations of sulfur oxy-anions and monosulfide were obtained with carbonate buffer, with tetrapropylammonium hydroxide as counter-ion, and an eluent flow-rate of 1.0 ml/min; however, polysulfidic species were not resolved, as had been noted by

Table 3
Powder X-ray diffraction of elemental sulfur and sodium tetrasulfide (α), with relative intensities

Na_2S_4 [9]	Na_2S_4 (α)	*d*-Spacing (A°) α-sulfur [9]	Absorption [a] product	Transformation [b] product
4.03 (100)	4.15 (60)	3.85 (100)	3.86 (100)	3.86 (100)
3.09 (100)	3.86 (100)	3.44 (40)	3.45 (35)	3.45 (26)
2.90 (100)	3.44 (60)	3.33 (25)	3.34 (21)	3.34 (21)
2.70 (100)	2.86 (80)	3.21 (60)	3.22 (40)	3.22 (32)
2.28 (80)	2.76 (80)	3.11 (25)	3.11 (23)	3.11 (27)
2.23 (80)	2.73 (80)			
2.20 (80)				

[a] Reaction of H_2S with Fe(III)NTA, pH 8.5.
[b] Aeration of K_2S_3 or K_2S_5 in borate buffer, pH 8.5.

Steudel et al. [16]. UV detection was used with an LDC SpectroMonitor variable-wavelength detector set at 215 nm (the maximum wavelength of polysulfides). A change in the type of counter-ion e.g., to tetramethylammonium hydroxide or tetrabutylammonium hydroxide, and with 2.5% acetonitrile, did not effect the resolution of the polysulfide mixture.

From knowledge of separation of mercaptans and dialkylpolysulfides in homologous series with an LC C_{18} column and dry methanol [26,27], attempts were made to derivatize different polysulfide salts with *p*-nitrobenzylbromide [27] in methanol and also acetonitrile (as used for the derivatization of sulfides [28]) for the preparation of bis(*p*-nitrophenyl) thioethers. Derivatives that bear additional charge, such as 2,4-dinitrophenyl thioethers, were also prepared in methanol [28], but it was more desirable to prepare derivatives of polysulfides with uncharged agents, as in benzoyl thioethers (from benzoyl chloride) [29,30]. These derivatives were separated on the PRP-1 column with carbonate buffer and also on the C_{18} column with methanol without adequate resolution; those made with benzoyl chloride and extracted into diethyl ether were non-reproducible. A search of how polysulfides can be alkylated with the intention of separating them by LC revealed that alkylation is too difficult to carry out; the dialkylpolysulfides prepared by Mockel [26] had been synthesized from the corresponding mercaptans by reaction with S_2Cl_2 [31] or by reaction of the mercaptan with elemental sulfur [32].

Liquid chromatography of elemental sulfur

Elemental sulfur, available in a commercial form as fine pulverized sulfur (Spectrum, Gardena, CA, USA or as a product of catenation of H_2S in the oxidative absorption (liquid redox) process, was dissolved in THF and separated with a C_{18} column and methanol. THF has a characteristic peak that does not overlap

Table 4
Liquid chromatography [a] of elemental sulfur with a reversed-phase C_{18} column and THF–methanol

Sulfur	Retention time (min)/peak height [b] (mm)		
	Fine pulverized sulfur (spectrum)	Absorbed sulfur [c]	Absorbed sulfur [d], aged
S_6	4.0/1	4.0/0.5	4.0/0.5
S_7	4.6/7	4.6/3	4.6/3
S_8	5.8/162	5.8/158	5.8/180
Ratio			
S_6/S_7	0.006	0.003	0.003
S_7/S_8	0.043	0.019	0.017

[a] Sulfur was dissolved in tetrahydrofuran (THF) and eluted with dry methanol.
[b] Methanol flux was 2.0 ml/min; UV detection was set at 254 nm.
[c] From reaction of H_2S and Fe(III)NTA, 7 h.
[d] Same as in (c) except that the sulfur was aged for two or more months.

with those of sulfur. The LC pump and UV detector were the same as those described previously for the chromatography of polysulfide anions. The flow-rate of methanol was set at 2.0 ml/min and the detector was set at 254 nm. Retention time of cyclooctasulfur and the other cyclic forms of sulfur (S_6 and S_7) are given in Table 4. Cyclic S_9 and polymeric sulfur dissolved in CS_2 have been separated with a reversed-phase LC column by Steudel and Holz [33].

Proton NMR of protonated polysulfide salts

^{1}H NMR was intended for use in the identification of polysulfide species following their reaction with strong acid to make polysulfanes, H_2S_x, provided that a correspondence between polysulfide and the resulting sulfane could be established. (Direct NMR analysis of sulfur was not considered because only one sulfur isotope, ^{33}S, with spin $I=3/2$, is available for NMR and its use has several disadvantages: ^{33}S has low natural abundance (0.76%); its receptivity to NMR detection is about 10^{-6} that of ^{1}H NMR, ^{33}S has a large quadrupole moment similar to that of ^{14}N; the peaks are often broad, with 10 ppm width; about 5000 transients are required; and the concentration must be high, near saturation [34,35]). Sodium polysulfide salts can be transformed to sulfanes by reaction with 6 M HCl at −10°C [36,37]. The resulting crude oil contains a mixture of polysulfanes that permit NMR spectral characterization in an organic solvent.

Hydrogen chemical shifts have been reported in CS_2 by Hyne et al. [37] for a composite of several mixed sulfane samples. The proton bands are shifted downfield from $\delta=2.84$ ppm (for H_2S_2) to $\delta=4.35$ ppm (for H_2S_5), and the chemical shifts for H_2S_3, H_2S_4, and H_2S_6 are clustered together near 4.3 ppm (Table 5). Additional ^{1}H NMR work for sulfanes was reported by Schmidbaur et al. [38], who obtained mixtures of sulfane compounds from fractional distillation of crude sulfane oil [39] or from the synthesis of sulfanes by combination of H_2S gas with sulfur monochloride (S_2Cl_2) or thionyl chloride [40]. Proton chemical shifts reported by Schmidbaur et al. show a similar trend (originally reported in Hz) (Table 5) but offset by 0.12 ppm. Proton shifts observed for sulfanes were attributed to H–S–H coupling [38].

Table 5
Proton chemical shifts for sulfanes in CS_2 (versus tetramethylsilane)

Sulfur	Hyne et al. [37]	Schmidbaur et al. [38]
H_2S_2	2.84	2.72
H_2S_3	4.20	4.08
H_2S_4	4.22	4.10
H_2S_5	4.35	4.23
H_2S_6	4.44	4.31

Next, Feher and Laue [36] studied the correspondence between sodium polysulfide salts and the polysulfanes that were prepared by the protonation of individual polysulfide compounds with concentrated HCl, and found that for all polysulfide samples tested, from disulfide to pentasulfide, the treated polysulfide salts tended to form higher-chain-length polysulfanes by rearrangement. For a more controlled transformation, Feher and Berthold [41] treated polysulfide salts with fumes of formic acid and found a good correspondence of K_2S_5 to H_2S_5 and Na_2S_4 to H_2S_4, with variation, but K_2S_3 and Na_2S_2 tended to rearrange to higher sulfanes after reaction with formic acid.

In this laboratory, a series of polysulfide salts were treated with trifluoroacetic acid (CF_3COOH) and trifluoracetic anhydride in an attempt to produce polysulfanes with different chain lengths. The immediate reaction of polysulfide with CF_3COOH was the production of a white precipitate, which was removed by centrifugation. The remaining supernatant was dried down in a vacuum desiccator over $CaSO_4$ and then washed with deuterochloroform to complete the removal of residual CF_3COOH. ^{1}H NMR patterns were obtained in deuterochloroform for each of the treated polysulfide samples, but only single bands were obtained in each instance instead of a series or mixture of bands. The single peaks fell in a range of chemical shift from 2 to 9 ppm without resemblance to the literature patterns of chemical shift [37,38] and in an irregular order. Spectra obtained from CS_2 were devoid of any features. A check of the treated polysulfide samples with elemental analysis and LD mass spectrometry revealed that residual fragments of CF_3COOH were present but that the polysulfide chains had been decomposed to sulfide. Thus, the observed single proton chemical shifts were probably caused by H-bonded CF_3COOH residues that had resisted removal in the drying and purification steps.

A more reliable method of production of polysulfanes was sought in the manner of Feher and Berthold [41] by using fumes of dry formic acid to protonate

standard K_2S_3 and K_2S_5 samples and to analyze the products with LD mass spectrometry. The formic acid was dried by refluxing with phthalic acid which was then removed by distillation [42]. About 100 ml of dry formic acid were placed in a 1-l three-necked round-bottom flask, sealed, and cooled with ice-water. A Schlenk tube with a nitrogen gas inlet was placed in horizontal position above the round-bottom flask and was joined to it by a glass column.

About 20 mg of K_2S_3 or K_2S_5 were placed at the far end of the Schlenk tube, and fumes of formic acid were induced to rise up to the small mound of polysulfide sample by gently warming the contents of the round-bottom flask which was transferred to an oil bath. Formic acid fumes were held in contact with the polysulfide sample for 2.5–3 h or until their color had bleached. Contact with the fumes was improved by vibrating the Schlenk tube with an engraving tool. The treated samples were completely dried in a vacuum desiccator for 12 h, and analyses for sulfur were made by LD-FTICR: for treated K_2S_3, disulfide, trisulfide, and tetrasulfide anions were found, indicating that potassium trisulfide had formed H_2S_3 and also H_2S_2 and H_2S_4 by disproportionation. For the treated K_2S_5 sample, a mixture of S_2, S_3, S_4, and S_5 species were obtained by degradation of the potassium pentasulfide. Hence, proton chemical shifts of intended polysulfanes were not useful for the analysis of polysulfide salts.

2.3. *Transformations of sulfide and polysulfide*

H_2S gas was absorbed by Fe(III)NTA solutions in a commercial model apparatus (Fig. 4) which consisted of an absorber column with H_2S inlet fittings and a 1-l vat filled with 0.018 M ferric nitrate and 0.036 M NTA, adjusted to pH 8.5 with NaOH. H_2S gas was delivered to the absorber column at a controlled rate of 2.0 ml/min, while air was forced into the lower reaction vessel at a rate of 1 l/min. The contents of the absorber column and the oxidizer vat were continuously circulated by a peristaltic pump. The pH and redox potential were monitored in oxidizing and reducing zones in order to notice any changes in pH and oxidation state of sulfur and iron (mixed potentials). Samples of the mixture of H_2S and Fe(III)NTA were withdrawn at intervals of 2.0, 3.0, and 3.5 h and were frozen to stop the reaction. Water was removed by lyophilization. LD mass spectral analysis at 2.0-h intervals gave only S_3

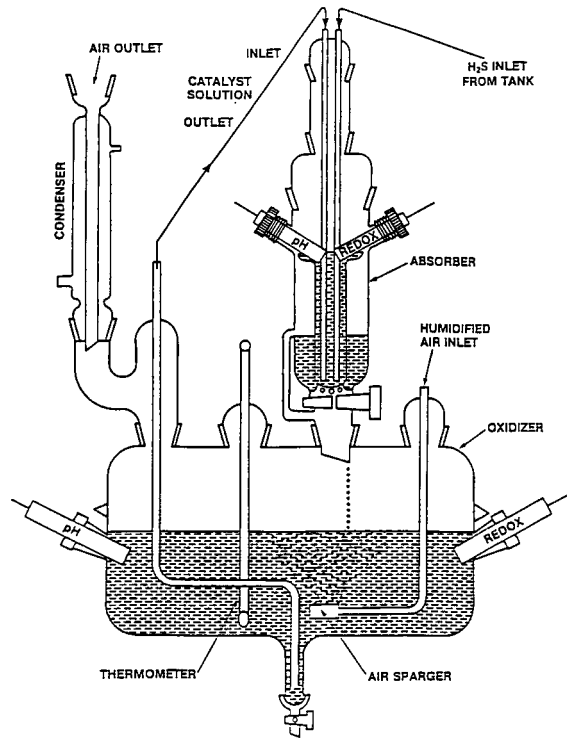

Fig. 4. Drawing of commercial model oxidative absorption or liquid redox apparatus.

species, whereas S_2, S_3, S_4, S_5 and a trace of S_6 species were present in the 3.0-h sample (Fig. 5). The entire suspension was withdrawn from the model apparatus after about 7 h and was filtered over Whatman No. 1 qualitative paper to collect elemental sulfur. The elemental sulfur was washed and dried, then analyzed by powder X-ray diffraction and by LC with a C_{18} column and methanol (Tables 3 and 4).

To determine whether the composition of polysulfides can vary when the pH of the absorbing solution is changed from 7.0 to 8.5 (in increments of 0.5 pH units), about 800 mg or 4 mmol of sulfide (as freshly recrystallized Na_2S) were added portion-wise to 1-l solutions of buffered Fe(III)NTA. The pH of the alkaline Na_2S was adjusted prior to mixing with dilute HCl to the same pH as that of the Fe(III)NTA solution in order to control the pH. Despite this precaution, some alkaline drift in pH was observed with each portion-wise addition of Na_2S, and it was necessary to make additional adjustments with dilute HCl. (The alkaline drift appears to be caused by reduction of Fe(III)NTA where the lower affinity of Fe(II) ion for H_3NTA can

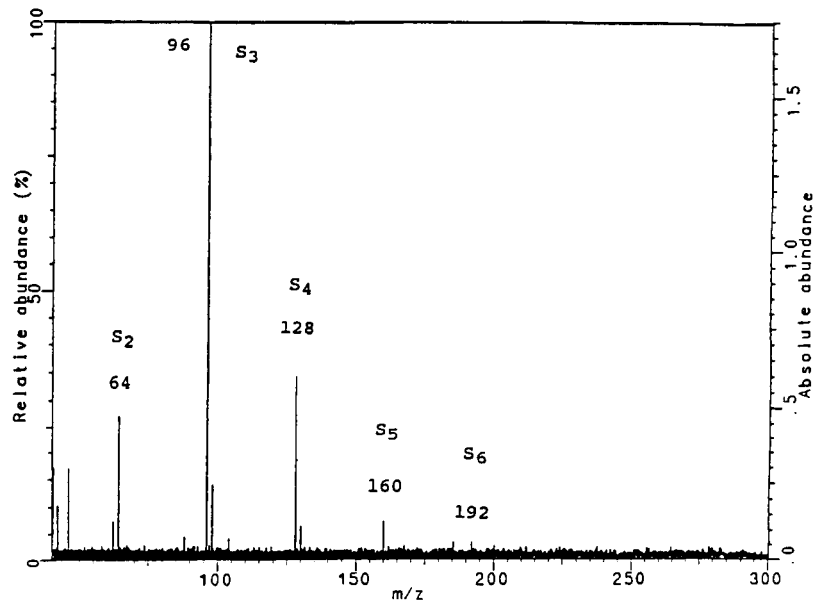

Fig. 5. LD-FTICR mass spectra (negative-ion mode) of polysulfides that are present in the system H_2S + Fe(III)NTA {with [Fe] = 0.018 M and [NTA] = 0.036 M} after 3 h of reaction at pH 8.5. The spectrum was obtained after addition of a drop of methanol to the sample on the probe tip.

result in displacement of fewer equivalents of hydrogen ion from the ligand as the metal complexes are formed.) Table 6 and Fig. 6 give the results of LD mass spectral analysis of polysulfides withdrawn from the Fe(III)NTA–sulfide suspension at different pH values after 3 h of reaction.

Aeration of K_2S_3 and K_2S_5 standard compounds (about 1 g) mixed in 100 ml of borate buffer (pH 8.5) was carried out slowly in 250-ml Erlenmeyer flasks at a gentle bubble rate of one bubble per 2 s. Slow aeration was used deliberately to minimize the accumulation of sulfur oxy-anions, thiosulfate and sulfate, primarily, and to promote the production of elemental sulfur at the expense of polysulfide anion concentrations. Powder X-ray diffraction was used to analyze the transformed elemental sulfur (Table 3). The stability of polysulfide compounds obtained by lyophilization was demonstrated in additional experiments by using labelled K_2S_3. No unusual rearrangements of sulfur were observed in these additional transformation experiments which were collected over a time period of greater than 5 h to produce cyclooctasulfur.

Table 6
Laser desorption analysis of polysulfidic species produced by absorption of Na_2S in Fe(III)NTA solution ([Fe] = 0.018 M; [NTA] = 0.036 M) at different pH values

Polysulfide	Relative intensity			
	pH 8.5	pH 8.0	pH 7.5	pH 7.0
S_2	21.2	1.2	~0	0.0
S_3	100	32.1	12.7	3.6
S_4	30.3	8.5	4.2	1.2
S_5	1.2	3.6		0.0
S_7	0.6	1.2	~0	0.0
S_8	1.2	2.4	~0	0.0
S_9	0.6	1.2	~0	0.0

3. Results and conclusions

LD mass spectrometry has been shown to be a reliable method of analysis for the polysulfide chains with different lengths (Table 1). Trisulfide and pentasulfide potassium salts were synthesized in pure form in ethanol from the combination of potassium hydrosulfide and appropriate equivalent amounts of elemental sulfur. The disulfides and tetrasulfides that were obtained from synthesis by various methods were primarily mixtures with trisulfide. It was not possible to synthesize hexasulfide by any of the attempted methods (see Experimental section). Elemental analysis was not strictly useful for characterization of the polysulfide

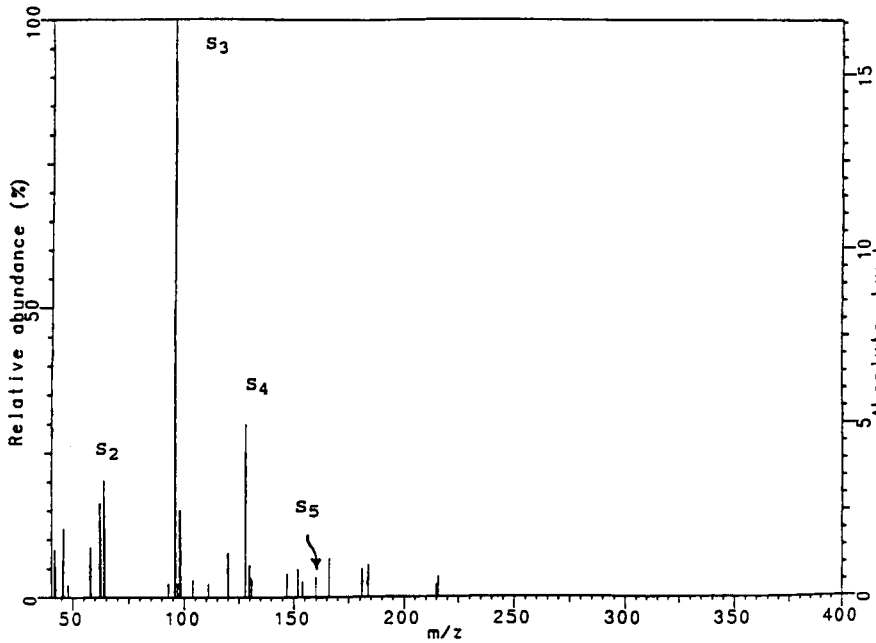

Fig. 6. LD-FTICR mass spectra (negative-ion mode) of polysulfides that are present in the system Na_2S + Fe(III)NTA {with [Fe] = 0.018 M and [NTA] = 0.036 M} after 2 h of reaction at pH 8.5. The spectrum was obtained after addition of a 50:50 benzene–methanol mixture to the sample on the probe tip.

chain lengths, because this analysis is only a ratio of metal and sulfur, and mixtures may give misleading average ratios, as in the example of commercial sodium tetrasulfide. Argentimetric potentiometric titration has been touted by many in the literature [13] as a quantitative measure of polysulfide in mixtures with sulfide and thiosulfate, but this claim has been disproved in the present work, for which polysulfide standards gave variable and inconsistent results.

LD mass spectrometry gives precise and accurate analysis of polysulfides, without fragmentation or rearrangement that is often observed by EI and CI mass spectrometric methods (Table 2). A single peak at *m/z* 96 for trisulfide was observed for K_2S_3 by LD in Fig. 1A, whereas EI at 15 eV gave a range of polysulfide chains, including S_6 and S_8 which were formed by rearrangement (Fig. 1B). Similar results were observed for K_2S_5 in Fig. 2 and Table 2. CI mass spectrometry (Oneida Research Services) gave primarily S_8 by decomposition of commercial Na_2S_4 in methanol, similar to the result obtained by EI at 15 eV. CI and EI were found to be inappropriate when applied to the analysis of fragmentary polysulfide compounds.

The results of characterization of elemental sulfur by powder X-ray diffraction (Table 3) show that the form of sulfur precipitated from the liquid redox apparatus at pH 8.5 (Fig. 3) is α-sulfur (orthorhombic), from the match of *d*-spacing (Å) to well characterized sulfur [22]. Also, it has been conclusively demonstrated that polysulfide salts can be decomposed by gentle aeration to form elemental sulfur with the same composition: elemental sulfur is primarily cyclooctasulfur, S_8, as determined by LC (Table 4). Traces of cyclohexasulfur and cycloheptasulfur are also present. Aging of the precipitated sulfur does not appreciably change the composition of the sulfur.

The proton chemical shifts of sulfanes, H_2S_x [37,38], were not found to be useful in the analysis of intermediary polysulfides that are found in the oxidative absorption process due to the poor correspondence between polysulfide standards and the polysulfanes that were produced by their protonation with weak organic and strong mineral acids (see Experimental section).

Polysulfides have been shown to be reactive intermediates in the catenation of monosulfide to elemental sulfur, or S_8. In Table 5 and Figs. 5 and 6, trisulfide and tetrasulfide appear to be particularly stable species over the pH range studied in Fe(III)NTA solutions, from pH 7.0 to 8.5, and with little variation in their relative proportions. Higher pH, near pH 8.5, tends to

promote higher concentrations of trisulfide and tetrasulfide over those found at neutral pH, and this is correlated with higher rates of production of elemental sulfur at pH 8.5 (data not shown). Alkaline pH retards the decomposition of sulfide and thiosulfate, and may have a similar influence on the stability of polysulfides. The efficiency of the liquid redox process with regard to transformation and precipitation of sulfur is higher at more alkaline pH, to the limit of stability of the Fe(III)NTA chelate (near pH 9.0). The liquid redox performance is expected to be much poorer at acidic pH from these considerations.

4. Discussion

4.1. Catenation process

The immediate result of addition of H_2S or Na_2S to Fe(III)NTA solution is the production of FeS and a labile brown precipitate, suggestive of a possible role of chelated Fe(III) ion in the process of catenation of monosulfide to elemental sulfur. Freshly precipitated FeS is readily oxidized to $Fe(OH)_3$ in the absence of a chelating agent, but the nature of the brown precipitate that is eventually transformed through oxidation with molecular oxygen remains obscure. The transformation of sulfide as FeS in the presence of a chelating agent is yet to be studied by LD mass spectrometry. Speculation as to the formation of a possible sulfido-bridged iron(III) complex $(FeL)_2S$, with NTA as the ligand, has not been borne out by LD-FTICR mass spectrometric studies, although many examples of such dimeric ferric complexes with sulfide have been reported in the literature. N-Hydroxyethylethylenediaminetriacetic acid (HEDTA) [43] can form a μ-sulfido bridge between two Fe(III)HEDTA chelates, and similar structures have been reported for complexes with salicylideneammonium (salen) [44], acetylacetoneimine [45], and macrocyclic tetramethyldibenzo[*b,i*][1,4,8,11]tetraazacyclotetradine [46]. Furthermore, a hydroxo-bridged dimeric Fe(III)NTA complex, $(FeL)_2(OH)$, does not exist at a concentration of 10^{-3} M, from potentiometric titration [47], nor does $Fe(III)L_2(OH)$, when L is NTA. Hence it is unlikely that sulfide or polysulfide could substitute for an hydroxyl anion in a hypothetical bridged dimeric chelate with NTA in the same manner that has been suggested for ethylenediaminetetraacetic acid (EDTA) by DeBerry et al. [48]. The possible role of Fe(III) in the catenation of monosulfide is still to be determined. Polysulfides have been demonstrated as reactive intermediary products in this catenation process.

4.2. Stability of polysulfide species

The special stability of trisulfide observed by LD mass spectrometry is at odds with the report by Schwarzenbach and Fischer [2], who concluded from stopped-flow titration experiments that tetrasulfide and pentasulfide were dominant species in aqueous solution. Also, the virtual invariance of the ratio of trisulfide and tetrasulfide over the pH range 7.0–8.5 in Fe(III)NTA solutions suggests that polysulfides are stable over a broad pH range and do not necessarily interconvert (as has been proposed by Giggenbach and Dudek [49,50]) as a function of sulfide and hydroxide anion concentrations. Teder [49] and Giggenbach [50] have assumed an equilibrium distribution between elemental sulfur and polysulfide solutions based on purely hypothetical considerations. The present work shows that polysulfides can be formed at neutral and alkaline pH without prior combination of sulfide with elemental sulfur, since the polysulfides are formed by catenation of monosulfide in the presence of chelated ferric ion.

Acknowledgements

We would like to thank Dr. I.A. Scott for the use of the lyophilizer. We gratefully acknowledge financial support from the National Science Foundation (No. CHE-9223629), Department of Energy, Division of Chemical Sciences, and Office of Basic Energy Sciences (DE-FG05-85ER-13434).

References

[1] M. Avrahami and R.M. Golding, J. Chem. Soc. A, (1968) 647.
[2] G. Schwarzenbach and A. Fischer, Helv. Chim. Acta, 169 (1960) 1365.
[3] H. Foppl, L.E. Busmann and F.K. Frorath, Z. Anorg. Allg. Chem., 314 (1962) 12.
[4] P. Bottcher, Z. Anorg. Allg. Chem., 432 (1977) 167.

[5] S.C. Abrahams and J.L. Bernstein, Acta Crystallogr. B, 25 (1969) 2365.
[6] B. Kelly and P. Woodward, J. Chem. Soc. Dalton Trans., (1976) 1314.
[7] A. Hordvik and E. Sletten, Acta Chem. Scand., 22 (1968) 3029.
[8] M.G. Kanatzidis, N.C. Baenziger and D. Coucouvanis, Inorg. Chem., 22 (1983) 290.
[9] L. Pauling, Proc. Natl. Acad. Sci. USA, 35 (1949) 495.
[10] I. Kende, T.L. Pickering and A.V. Tobolsky, J. Am. Chem. Soc., 87 (1965) 5582.
[11] J.L. Franklin and H.E. Lumpkin, J. Am. Chem. Soc., 74 (1952) 1023.
[12] T.L. Pickering, K.J. Saunders and A.V. Tobolsky, J. Am. Chem. Soc., 89 (1967) 2364.
[13] (a) J. Papp, Cell. Chem. Tech., 5 (1971) 147; (b) P. Ahlgren and S. LeMon, Sven. Papper., 70 (1967) 160; (c) H. Satake, T. Hisano and S. Ikeda, Bull. Chem. Soc. Jpn., 54 (1981) 1968.
[14] (a) G.E. McMinis and L.E. Gast, J. Am. Oil Chem. Soc., 51 (1974) 198; (b) F.P. Daly and C.W. Brown, J. Phys. Chem., 79 (1975) 350; (c) G.J. Janz, J.R. Downey, E. Roduner, G.J. Wasilczyk, J.W. Coutts and A. Eluard, Inorg. Chem., 15 (1976) 1759.
[15] A.W. Schwab, W.K. Rohwedder and J.S. Ard, Phosphorus Sulfur, 7 (1979) 315.
[16] R. Steudel, G. Holdt and T. Gobel, J. Chromatogr., 475 (1989) 442.
[17] (a) Z. Uddin, l.R. Markuszewski and D.C. Johnson, Anal. Chim. Acta, 200 (1987) 115; (b) E. Singer and H.J. Mockel, Chromatographia, 27 (1989) 27; (c) P. Kokkonen and H. Hyvarinen, Anal. Chim. Acta, 207 (1988) 301.
[18] (a) M. Karas, D. Bachman, D. Bahr and F. Hillenkamp, Int. J. Mass Spectrom. Ion Proc., 78 (1987) 58; (b) R.J. Cotter, Anal. Chim. Acta, 195 (1987) 45; (c) T. Solouki and D.H. Russell, Proc. Natl. Acad. Sci. USA, 89 (1992) 5701.
[19] T. Solouki and D.H. Russell, Appl. Spectrosc., 47 (1993) 211; (b) P.J. Farmer, T. Solouki, D.K. Mills, T. Soma, J.H. Reibenspies and M.Y. Darensburg, J. Am. Chem. Soc., 114 (1992) 4601.
[20] (a) Gmelin Handbuch der Anorganischen Chemie, Vol. 3, Erganzungsbund Literung, 8th ed., 1966, pp. 1049–1188; (b) T.G. Pearson and P.L. Robinson, J. Chem. Soc., (1931) 1304; (c) D.G. Oei, Inorg. Chem., 12 (1973) 438 ; (d) F.W. Kuster and E. Heberlein, Z. Anorg. Allg. Chem., 45 (1905) 53 ; (e) A. Rule and J.S. Thomas, J. Chem. Soc., 105 (1914) 2819 ; (f) F. Feher and H.J. Berthold, Z. Anorg. Allg. Chem., 273 (1953) 144.
[21] F. Feher and H.J. Berthold, Z. Anorg. Allg. Chem., 274 (1953) 223.
[22] Powder Diffraction File, International Center for Diffraction Data, Swarthmore, PA, 1988.
[23] E. Rosen and R. Tegman, Acta Chem. Scand., 25 (1971) 3329.
[24] (a) D.M. Lubman (Ed.), Lasers in Mass Spectrometry, Oxford University Press, New York, 1990; (b) J.E. Campana, in Proceedings of the SPIE Applied Spectroscopy in Material Science, International Society for Optical Engineering, Bellingham, WA, 1991, pp. 138–149.
[25] R.D. Rauh, F.S. Shuker, J.M. Marston and S.B. Brummer, J. Inorg. Nucl. Chem., 39 (1977) 1762.
[26] H.J. Mockel, J. Chromatogr., 317 (1984) 589.
[27] H. Lagenhove, M. Acker and N. Schamp, J. Chromatogr., 257 (1983) 170.
[28] K. Funazo, M. Tanaka and T. Shono, Anal. Sci., 3 (1987) 41.
[29] J. Korolczuk, M. Danielewski and Z. Mielniczuk, J. Chromatogr., 100 (1974) 165.
[30] A.I. Vogel, Qualitative Organic Analysis, Part 2, Wiley, New York, 2nd ed., 1966
[31] A.W. Schwabb, R.D. Gilandi and J.L. Flippen-Anderson, Phosphorus Sulfur, 10 (1981) 123.
[32] B.D. Vineyard, J. Inorg. Chem., 31 (1966) 601.
[33] R. Steudel and B. Holz, Z. Naturforsch., 43B (1988) 581.
[34] R.K. Harris, and B.E. Mann, NMR and the Periodic Table, Academic Press, New York, 1978, pp. 401–402.
[35] H.L. Retcofsky and R.A. Friedel, J. Am. Chem. Soc., 94 (1972) 6579.
[36] F. Feher and W. Laue, Z. Anorg. Allg. Chem., 288 (1956) 103.
[37] J.B. Hyne, E. Muller and T.K. Wiewiorowski, J. Phys. Chem., 70 (1966) 3733.
[38] H. Schmidbaur, M. Schmidt and W. Siebert, Chem. Ber., 97 (1964) 3374.
[39] F. Feher, W. Laue and G. Winkhaus, Z. Anorg. Allg. Chem., 288 (1956) 113.
[40] E. Muller and J.B. Hyne, Can. J. Chem., 46 (1968) 2341.
[41] F. Feher and R. Berthold, Z. Anorg. Allg. Chem., 290 (1957) 251.
[42] D.D. Perrin, W.L.F. Armarego and D.R. Perrin, Purification of Laboratory Chemicals, Pergamon Press, New York, 1966.
[43] C.V. Philip and D.W. Brooks, Inorg. Chem., 13 (1974) 384.
[44] J.R. Dorfman, J.-J. Girard, E.D. Simhon, T.D.P. Stack and R.H. Holm, Inorg. Chem., 23 (1984) 4407.
[45] F. Corazza, C. Floriani and M. Zehnder, J. Chem. Soc. Dalton Trans., (1987) 709.
[46] P. Berno, C. Floriani, A. Chiesi-Villa and C. Guastini, J. Chem. Soc. Dalton Trans., (1989) 551.
[47] R.J. Motekaitis and A.E. Martell, J. Coord. Chem., in press.
[48] D.W. DeBerry, B. Petrinec and T. Trofe, Liquid Redox Recovery Conference, Austin, TX, May 5–7, 1991, Radian Corporation, Gas Research Institute, 1991.
[49] A. Teder, Acta Chem. Scand., 25 (1971) 1722.
[50] (a) W. Giggenbach, Inorg. Chem., 11 (1972) 1201–1217; (b) W. Giggenbach, Inorg. Chem., 13 (1974) 1724.
[51] G. Dudek and E.P. Dudek, J. Chem. Educ., 66 (1989) 304.

ELSEVIER

Analytica Chimica Acta 299 (1994) 113–127

ANALYTICA CHIMICA ACTA

Study on S_2 emission response from sulphur-containing amino acids in molecular emission cavity analysis

Koichi Nakajima [a,*], Kyuji Ohta [a], Takeo Takada [b]

[a] *Faculty of Liberal Arts, Hosei University, 2-17-1 Fujimi, Chiyoda-ku, Tokyo 102, Japan*

[b] *Department of Chemistry, College of Science, Rikkyo University, 3-34-1 Nishi-Ikebukuro, Toshima-ku, Tokyo 171, Japan*

Received 1 June 1994

Abstract

Several factors which affect S_2 emission response from sulphur-containing amino acids are investigated by molecular emission cavity analysis. It is found that multi-peaked responses observed from the amino acids result from heterogeneous gasification of the sample rather than formation of non-volatile compounds. A portion of the sample in a cavity is rapidly gasified by contact with flame gases and the others are slowly and thermally decomposed with temperature rise of the cavity. Thus, sample gasification processes are mainly discussed on the basis of several effects on the emission response, such as sample location within the cavity, addition of acids or bases, cavity temperature and flame composition. It is suggested that the amphoteric property of amino acids suppresses the rapid gasification process by contact with flame gases. Temporary condensed water on the cavity surface on introduction into a flame significantly affects the emission response from the amino acids and a mechanism for the effect is discussed.

Keywords: Gravimetry; Amino acids; Molecular emission cavity analysis; Multi-peak response; S_2 emission; Gasification process

Sulphur and sulphur-containing compounds in a hydrogen-based flame give the characteristic blue S_2 emission, which was first reported by Mulder in 1864 [1]. When a cold object is placed near the flame core, the emission is enhanced near the surface of the object. This phenomenon was first observed by Salet [2], and was called the Salet phenomenon [3]. The S_2 emission, owing to its great sensitivity and selectivity, has been applied to the sulphur-selective gas chromatographic detector (flame photometric detector, FPD) [4] and molecular emission cavity analysis (MECA) [5]. However, the mechanism of S_2 formation and emission has still not be clarified and lots of limitations and enigmas have remained, such as non-linear (exponential) response, variation in the response factor with molecular strength, quenching by other species, and the function of the cold object [6,7].

MECA is a convenient flame spectroscopic technique applicable to the determination of various elements [8]. The characteristic of this technique is the use of a cavity. In conventional MECA, the sample solution is injected into the cavity, which is introduced into a flame after solvent evaporation, i.e., the sample is solid. The sample must be gasified by vaporization or decomposition before formation of an emitting species such as the S_2 molecule. The fact that the emission mechanism involves the gasification process is inevitable for conventional MECA, and thereby, control of the process dominates the analytical usefulness of MECA. A single peak response is usually observed

* Corresponding author.

SSDI 0003-2670(94)00300-9

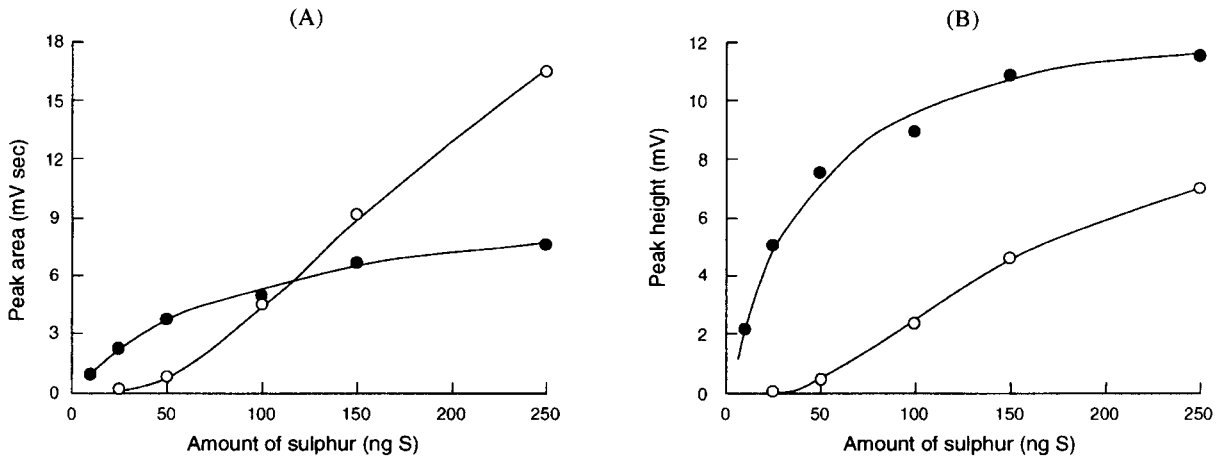

Fig. 1. Variation in S_2 emission response from methionine with the amount. (A) Peak area and (B) peak height of (●) the first peak and (○) the second peak.

when the cavity contains a single chemical species, because of batch operation. If all constituents of a mixture have a different volatility, the emission response observed can be a time-resolved multi-peak. For example, some sulphur anions could be determined simultaneously [9,10]. Carbonyl compounds form sulphite addition compounds in the presence of sodium sulphite, and show a double peak response in MECA, one for excess sulphite and the other peak for the sulphite addition compound [11]. In a similar manner, amines [12] and cyanide react with the formaldehyde–sulphite addition compound and [13] could be determined by the S_2 emission from the products without isolation.

On the contrary, multi-peaked responses have been reported even for a single chemical species. They are dependent on the sample amount [5], incomplete removal of solvent [8], or surface condition of the cavity [14]. In those cases, the accuracy and sensitivity of the technique are decreased and any mixtures are impossible to analyse simultaneously.

In our previous paper [15], heterogeneous gasification was found to be responsible for the multi-peaked response from 1,3-diethyl-2-thiourea. Homogeneous dispersion of the sample within a cavity gave rise to uniform gasification of the sample, and grinding of the inner surface of the cavity was effective for good dispersion of the sample. The multi-peaked response from 1,3-diethyl-2-thiourea became a single peak by using the ground cavity. However, the S_2 emission responses from sulphur-containing amino acids remained split even in the ground cavity, and disappearance of the peak splitting required addition of acid to the cavity. The mechanism of the peak-splitting and the effect of acid could not be clarified. Safavi and Townshend [16] also reported that some organic compounds enhanced the emission from Se or Te and removed the peak splitting, but the mechanism was not clarified.

The shape of the emission response represents the gasification process of the sample, and thereby, peak-splitting and several effects on the response are powerful clues for resolving the gasification process. Elucidation of the process are inherent problems which must be overcome at first in order to clarify the total emission mechanism. This paper describes the mechanism of peak splitting of the S_2 emission responses from sulphur-containing amino acids and several effects on the gasification process.

1. Experimental

1.1. Molecular emission cavity analysis

A silica cavity (5 mm deep, 6 mm I.D.) ground on the inner surface with abrasives is fixed at the end of a rod held in a sample holder assembly. The rod is freely rotatable; it is vertically set up when sample solutions (10 μl) are placed in the cavity with a microsyringe, and the rod is rearranged at 8° below the horizontal after the solvent is evaporated to dryness by using a hot air blower. The cavity is positioned into a nitrogen sheath oxy-hydrogen flame with the centre of the cavity

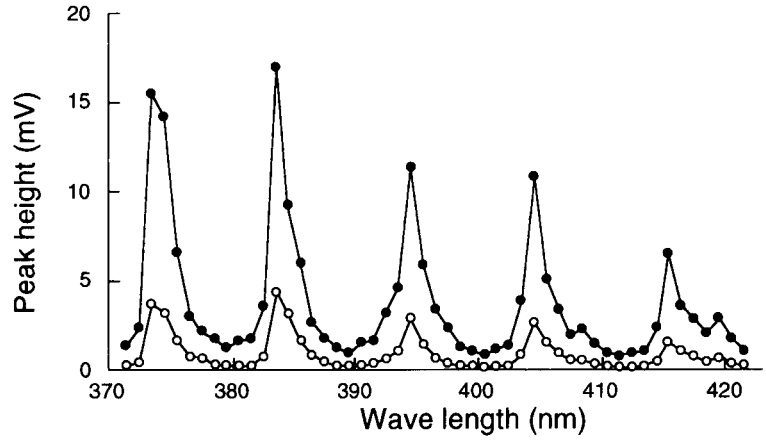

Fig. 2. Spectra of each peak of the double-peak response from methionine (125 ng of sulphur). (●) The first and (○) the second peak.

20 mm above the top of a burner, by sliding the assembly on an optical bench in line with a detector. When gaseous samples (H_2S or SO_2) were measured or when water vapor was introduced into the flame, a silica tube (I.D. 0.5 mm) was fixed in the flame.

Hydrogen (5.0 l min^{-1}) and oxygen (0.15 l min^{-1}) were supplied to a total consumption burner through the fuel (outer) and the nebulizer (inner) inlets, respectively. The burner was modified so that nitrogen (6.0 l min^{-1}) could flow around the oxy-hydrogen

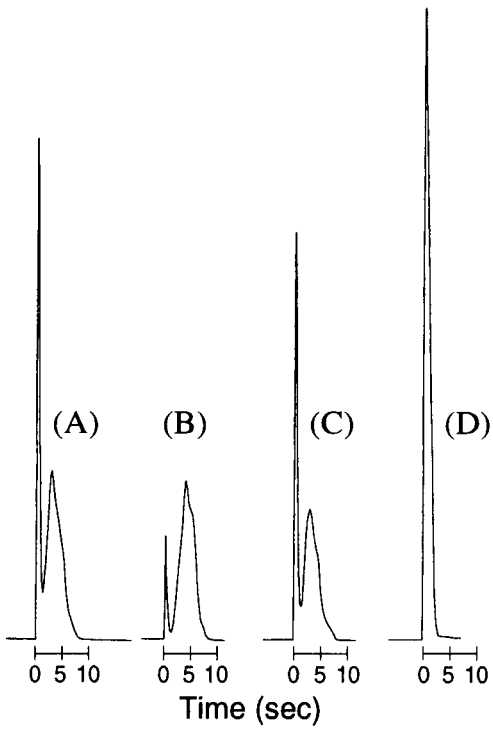

Fig. 3. S_2 emission responses from (A) methionine (250 ng of sulphur), (B) a residue after the 1-s introduction of a cavity, and the residue to which was added (C) 30 μl of water or (D) 30 μl of hydrochloric acid (1 mmol l^{-1}) after the 1-s introduction (water or solvent was evaporated before the cavity was reintroduced into the flame).

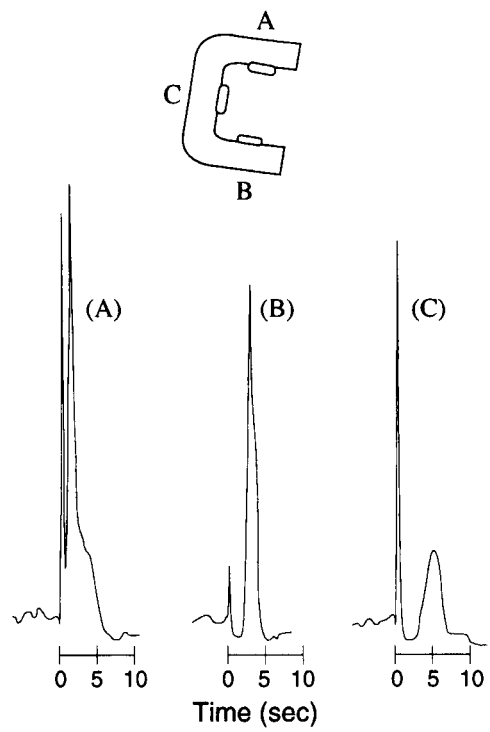

Fig. 4. Effect of sample location within a 3-point polished cavity on S_2 emission response from methionine (0.5 μl of 2 mmol l^{-1} of sulphur) deposited (A) on the A position, (B) on the B position and (C) on the C position.

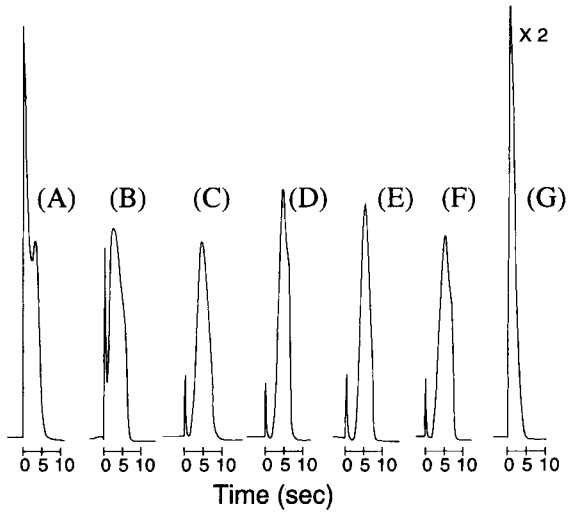

Fig. 5. S_2 emission responses from samples on the C position. (A) 2-Amino-4-thiazoleacetic acid; (B) thiazolidine-4-carboxylic acid; (C) cysteine; (D) *S*-methylcysteine; (E) ethionine; (F) methionine; (G) thiodipropionic acid. Sample amount is 0.5 μl of 250 mg l^{-1} of sulphur.

flame to prevent air entering into the flame from its surrounding [17]. Flow-rates of those gases were controlled with mass flow controllers or a flowmeter with a needle valve.

The S_2 emission was usually measured through an interference filter (half-bandwidth 18 nm) at 394 nm by using a photomultiplier tube (R268, HTV) and the responses were recorded on a Shimadzu Chromatopack C-R3A. A 0.25-m focal length Ebert monochromator with a 100-μm slit and R456 photomultiplier tube (HTV) were used in spectral measurement of the S_2 emission.

In order to estimate the effect of initial temperature of the cavity before introduction into the flame, an apparent cavity temperature was determined as follows. The cavity was exposed for 1 min in an air stream whose temperature was controlled by changing the electric voltage for a blower. The atmospheric temperature around the cavity during the exposure was measured with thermocouples placed in the vicinity of the cavity, and it was regarded as an apparent initial temperature of the cavity.

1.2. Liquid chromatography

Liquid chromatography (LC) was employed for analyses of amino acids in the residue after a cavity was introduced into a flame only for 1 s using the phenylthiohydantoin derivatization technique [18].

A Model LC-9A pump (Shimadzu) was used with a Model RF-535 Spectrofluorimeter; a 12-μl flow cell was used, and the excitation wave length set at 330 nm and the emission at 400 nm. Ten microliters of sample solution were loaded with a Model 7125 injection valve (Rheodyne) with a 20-μl sample loop. A Lichrospher 100 RP-18 (5 μm), 12.5 cm × 4 mm I.D. column was used for separation at 40°C in a column oven (CTO-6A, Shimadzu) with a precolumn heater. A deaerated mixture solution of methanol and 0.0125 mol l^{-1} Na_2HPO_4 solution (1:1, v/v) was employed as a mobile phase and its flow-rate was 1.0 ml min^{-1}. The

Table 1
Gasification temperature and time lag between two peaks

Compound		Peak temperature of DTG (°C)	Time lag in the C-position (s)
2-Amino-4-thiazoleacetic acid	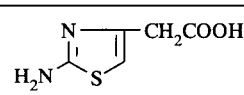	124	2.7
Thiazolidine-4-carboxylic acid	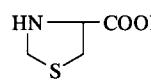	224	3.3
L-Cysteine	$HSCH_2CH(NH_2)COOH$	253	4.5
DL-Ethionine	$C_2H_5SCH_2CH_2CH(NH_2)COOH$	267	4.7
DL-Methionine	$CH_3SCH_2CH_2CH(NH_2)COOH$	274	5.2
Thio-di-propionic acid	$S(CH_2CH_2CHCOOH)_2$	250	-

Sample amount: DTG; 20 μl of 2% solution (0.4 mg), time lag; 0.5 μl of 250 mg l^{-1} of sulphur (125 ng S).

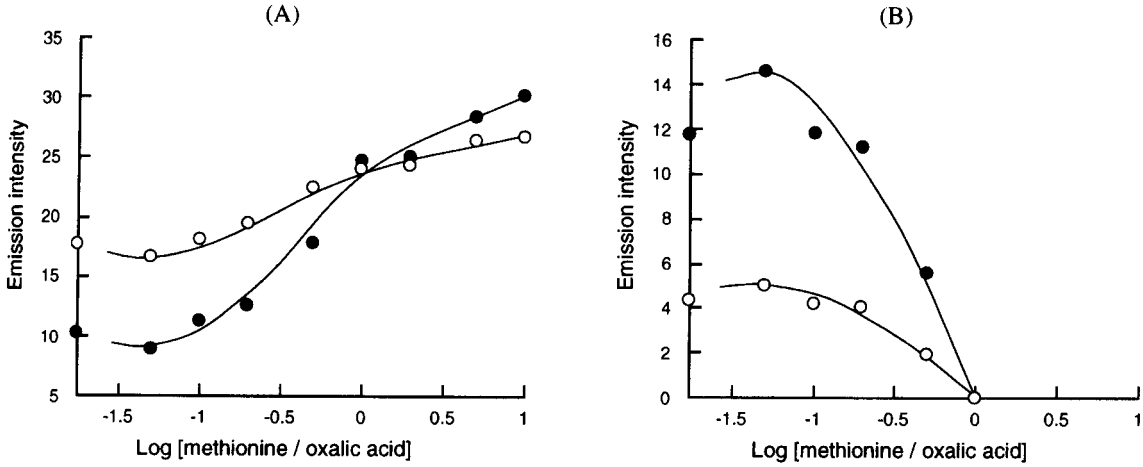

Fig. 6. Effect of concentration of oxalic acid on S_2 emission from 5 nmol of methionine. (●) Peak area and (○) peak height for (A) the first peak and (B) the second peak. Plots on vertical axes are responses in the absence of oxalic acid.

chromatogram was recorded on a Shimadzu Chromatopack C-R2A integrator.

Preparation of the o-phthaldialdehyde–ethanethiol derivatizing solution. A hundred milligrams of *o*-phthaldialdehyde were dissolved in 8 ml of methanol in a 10-ml volumetric flask. Then 0.1 ml of ethanethiol and 1.0 ml of 0.1 mol l^{-1} sodium tetraborate solution (pH 9.5) were added and the solution was diluted to 10 ml with methanol.

Derivatization procedure for amino acid. To a 5.0-ml volumetric flask were added 10 μl or 20 μl of sample solution (methionine standard or the residue), 1.0 ml of 0.1 mol l^{-1} sodium tetraborate solution, and 0.5 ml of the *o*-phthaldialdehyde–ethanethiol derivatizing solution. The mixture was diluted to 5 ml with methanol and allowed to react at room temperature for 1 min. A 10-μl aliquot of the mixture was analysed by LC.

1.3. Thermogravimetric analysis

A Shimadzu TGA-30M was used for thermogravimetric analysis of samples. A 20-μl volume of 2% sample solution was injected into a platinum cell (5 mm deep, 4.5 mm diameter). The sample weight loss and its differential were measured at a heating rate of

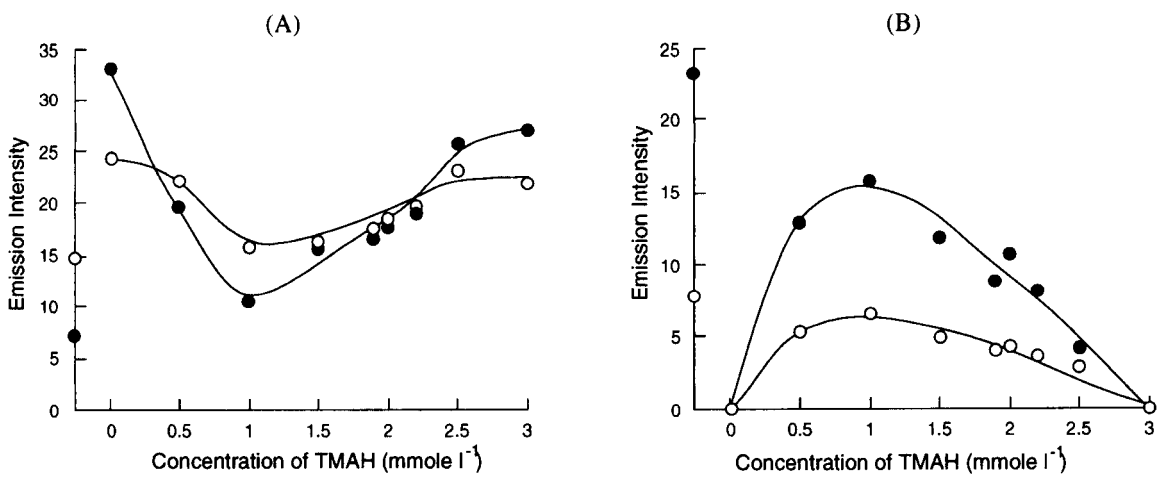

Fig. 7. Effect of composition of additives (TMAH/oxalic acid) on S_2 emission response from 5 nmol of methionine (5 μl of 1 mmol l^{-1}). Methionine was mixed with 5 μl of the mixture solution of oxalic acid (1 mmol l^{-1}, constant) and a certain concentration of TMAH. (●) Peak area and (○) peak height for (A) the first peak and (B) the second peak. Plots on vertical axes are responses from methionine only.

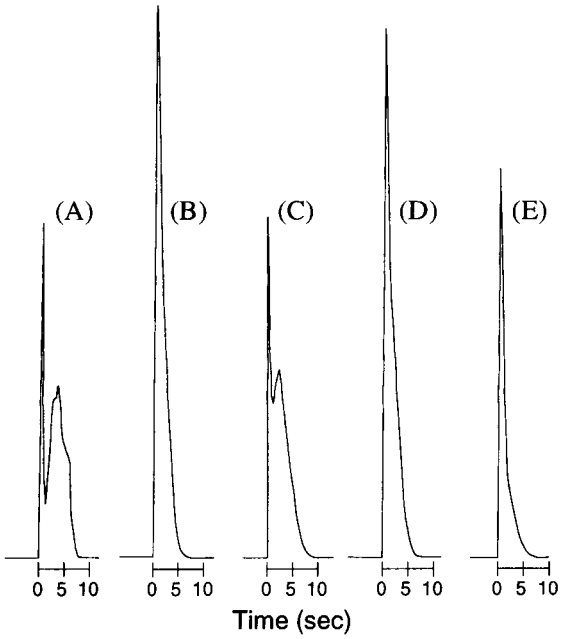

Fig. 8. S_2 emission responses for (A) methionine; (B) *N*-acetylmethionine; (C) cysteine; (D) *N*-acetylcysteine; (E) cysteine methyl ester hydrochloride. Sample amount is 250 ng of sulphur.

10°C min^{-1} in an atmosphere of nitrogen (20 ml min^{-1}), after solvent pre-evaporation at 70°C.

1.4. Reagents

Four sulphur-containing amino acids, DL-methionine (Wako), DL-ethionine (Wako), L-cysteine (Kanto), and *S*-methyl-L-cysteine (Aldrich) were mainly examined for their S_2 emission behavior. These chemicals were dissolved in water which was prepared with an AS-90DF automatic still (Iwaki Glass) with dual ion-exchangers, a carbon filter and a 0.2-μm membrane filter. Other chemicals were guaranteed grade or reagent grade reagents available, and dissolved in water unless specified otherwise in the text.

Hydrogen sulphide and sulphur dioxide [5×10^{-3}% (v/v) in nitrogen] supplied by Takachiho (Tokyo) were used.

2. Results and discussion

When a small amount (less than 25 ng of sulphur) of methionine is introduced into a hydrogen-based flame, a single sharp response is observed, but with increasing amount of methionine a second, new peak appears the intensity of which increases linearly, in contrast to the small increment of the first peak, as shown in Fig. 1. Spectra of both peaks are identical as shown in Fig. 2, and they are undoubtedly the S_2 spectrum [19]. Such multi-peak responses were observed for other sulphur-containing amino acids such as cysteine, ethionine and *S*-methylcysteine.

Burguera et al. [8] suggested that the multi-peak response observed with large amounts of thiourea arose from the interaction of some of the initial decomposition products with undecomposed sample, to form less volatile products. If a less volatile product is responsible for the multi-peak response of amino acids, when the cavity is taken out of the flame before the second peak appears (which is termed as "1-s introduction" because emission of the first peak vanishes within a second), the residue in the cavity should show only a

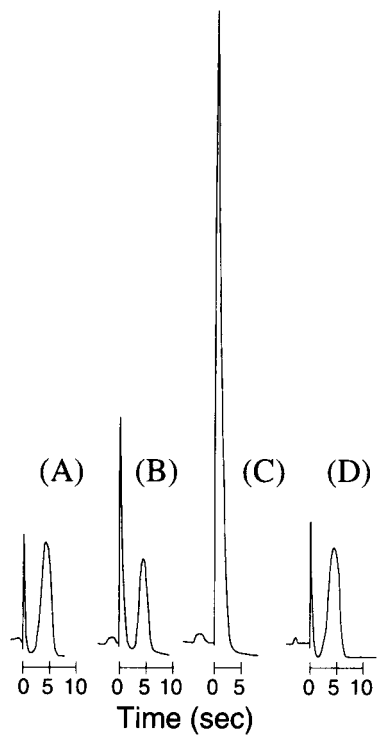

Fig. 9. Effect of oxalic acid on S_2 emission response from methionine. Methionine (0.5 μl of 2 mmol l^{-1}) and additives were deposited separately on the C position and the A position within a 3-point ground cavity, respectively. (A) Methionine only, (B) with 0.5 μl of 20 mmol l^{-1} of the acid, (C) with 0.5 μl of 100 mmol l^{-1} of the acid, and (D) with 0.5 μl of mixture solution of the acid (100 mmol l^{-1}) and TMAH (100 mmol l^{-1}).

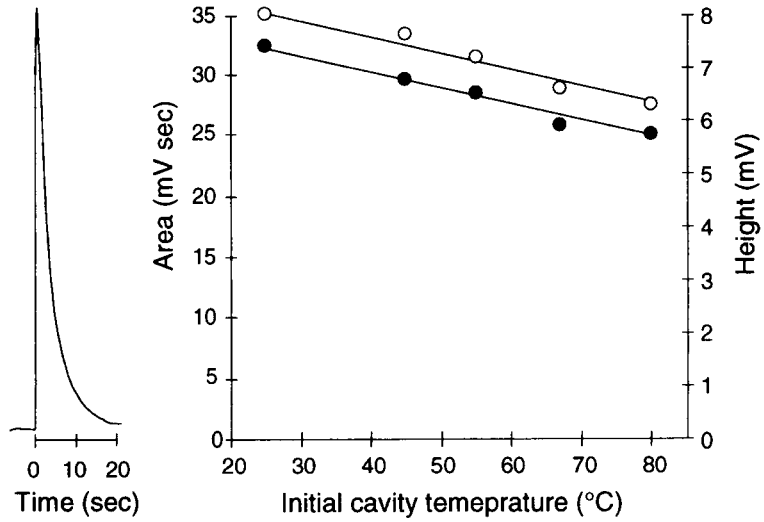

Fig. 10. Typical emission response and effect of initial cavity temperature on S_2 emission observed when a cavity is introduced into a nitrogen sheath oxy-hydrogen flame containing hydrogen sulphide [5×10^{-3} % (v/v), 50 ml min^{-1}]. (●) Peak area and (○) peak height.

single, delayed peak response when the cavity is reintroduced into the flame. The observed signal (Fig. 3B) was a double-peak response, although the first peak was smaller than that normally observed for methionine (Fig. 3A). The result was similar even though the 1-s introduction of the cavity was repeated several times. When 30 μl of water were added to the residue before the cavity was reintroduced into the flame and the sample was dried with a hot air blower, the first peak of the response was enhanced. When acid, instead of water, was added to the residue, only a fast, single-peak response was observed. These results seem to show that the residue is the amino acid itself, not a less volatile product.

In order to confirm the results, we determined the amino acid remained in the cavity after the 1-s introduction into the flame, by using LC with the phenylthiohydantoin derivatization technique [18]. A ground cavity containing 10 nmol of methionine was introduced into the flame and taken out of the flame after 1 s. Forty microliters of water were added to the cavity after cooling for 2 min with a cold air flow, and stirred for a while. A 20-μl volume of the solution was derivatized with *o*-phthaldialdehyde–ethanethiol solution,

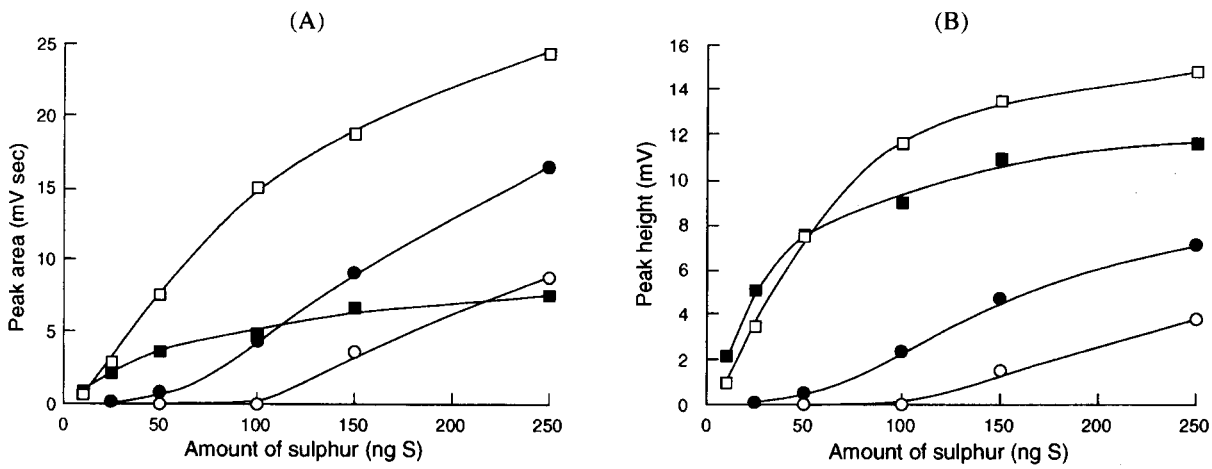

Fig. 11. Effect of cooling of cavity on S_2 emission response from methionine. (A) Peak area and (B) peak height. The first peak with (■) the hot and (□) the cold cavity, and the second peak with (●) the hot and (○) the cold cavity.

and was analysed by LC. From the peak intensity in the chromatogram, 8.8 nmol of methionine was detected. On the other hand, since the residue resulted in a single-peak emission response in the presence of acid (Fig. 3), if the residue is consistent with methionine only, the amount of sulphur of the residue can be determined by MECA by using the calibration graph for methionine mixed with acid, and from the emission intensity it was estimated as 9.1 nmol. It is no doubt that the residue is the amino acid itself and the multi-peak response can be attributed to heterogeneous gasification of the sample.

2.1. *Effect of sample location*

Effect of sample location in the cavity was first investigated for the separate gasification of the sample. The cavity which was ground partially at three positions as shown in Fig. 4 and termed as the 3-point ground cavity, was employed; the diameter of the ground area was about 2–3 mm, and 0.5 μl of sample solution was injected. The results are shown in Fig. 4. In any position, the emission response from methionine consisted of a fast first peak and a delayed second peak. Every first peak occurred immediately after introduction of the cavity into the flame, but the lag of the second peak was dependent on the sample location; time lags between the peaks at the A, B and C position are 1.2, 2.5 and 4.9 s, respectively. These difference in time lags may be attributed to the different temperature rise at each location. Fig. 5 compares emission responses from several compounds in the C position of the 3-point ground cavity. There was no difference among the four α-amino acids, but the response from 2-amino-4-thiazoleacetic acid had a very large first peak compared with other amino acids. Thiodipropionic acid, which is a dicarboxylic acid, not an amino acid, showed a single-peak response in the C position, so the compound was employed as a reference which normally showed a single-peak response in MECA.

Table 1 lists gasification temperatures estimated from thermogravimetric analyses and the time lag between the peaks of the multi-peak responses for six amino acids. From the relationship between the gasification temperature and the time lag, it is expected that the second peak of the multi-peak response is based on thermal decomposition of the compounds. On the other hand, the first peak occurred immediately after introduction of the cavity into a flame, being independent on the gasification temperature and sample location.

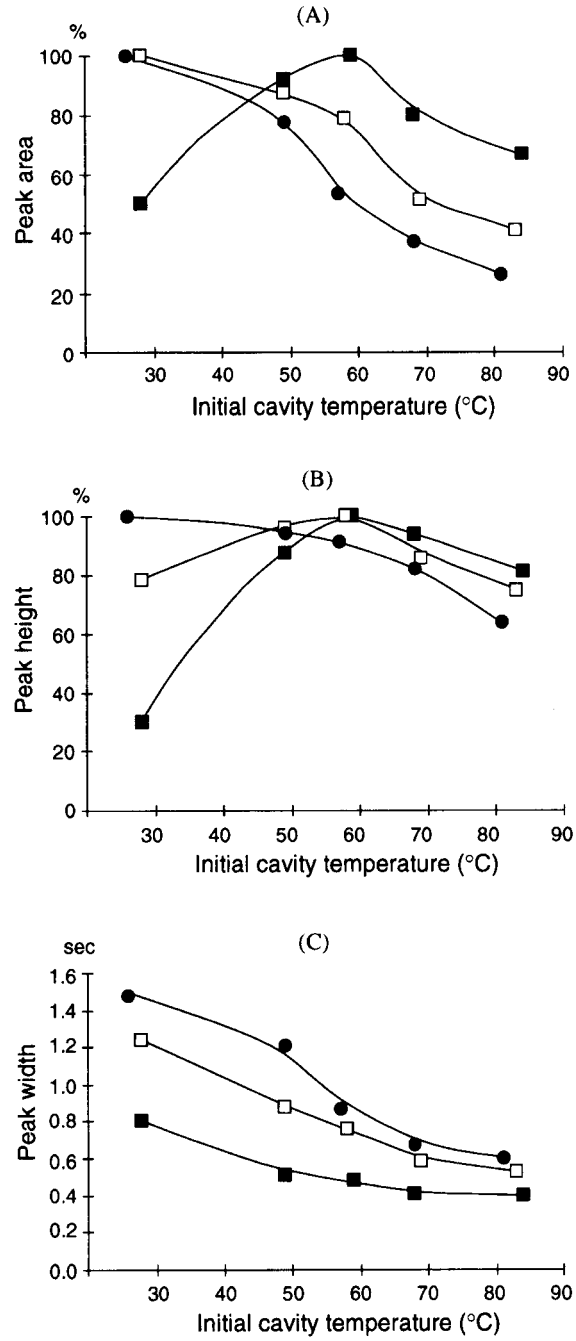

Fig. 12. Effect of initial cavity temperature on S_2 emission from methionine. (A) Peak area, (B) peak height and (C) peak width of (■) the single peak response from 10 ng of sulphur, and the first peak from (□) 50 and (○) 100 ng of sulphur.

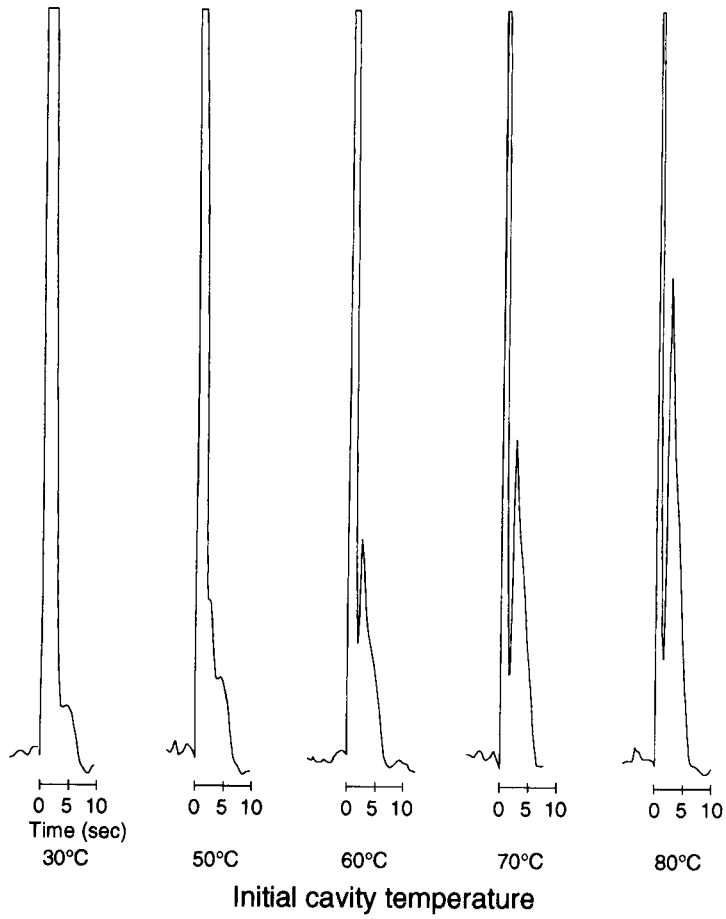

Fig. 13. Variation in the second peak with initial cavity temperature. All the first peaks are out of scale. The sample is 100 ng of sulphur as methionine.

The first peak occurs upon contact with the flame gases and seems to be based on a different process of thermal decomposition for the second peak.

2.2. *Effect of the acid*

Addition of oxalic acid to sulphur-containing amino acids affected the emission response of the amino acids [15,20]: the addition led to an increase in the first peak intensity and a decrease in the second peak, and accordingly, the peak-splitting disappeared. The effect was dependent on the amount of acid, as shown in Fig. 6. The second peak of the emission response from methionine disappeared in the presence of an equimolar amount of oxalic acid, and further addition of the acid led to a further increase in the emission intensity. This enhancement effect was not observed when the sample amount was less than 25 ng of sulphur; with such amounts a single-peak response was observed even in the absence of acid. For gaseous samples such as SO_2 or H_2S, no enhancement of the emission response was observed in the presence of acid. From these results, it is clear that the effect of acid is related to the sample gasification process, not to the excitation mechanism.

A similar effect was observed not only for other acids such as hydrochloric, phosphoric, citric and tartaric acid, but also for some bases such as tetramethylammonium hydroxide (TMAH) and hexamethylenediamine. However, succinic acid and ammonia had hardly any effect, which may be attributed to their weak acidity and basicity, respectively. When a mixture of oxalic acid and TMAH was added to methionine, the emission response drastically varied with the ratio of the acid and the base, as shown in Fig. 7. These results

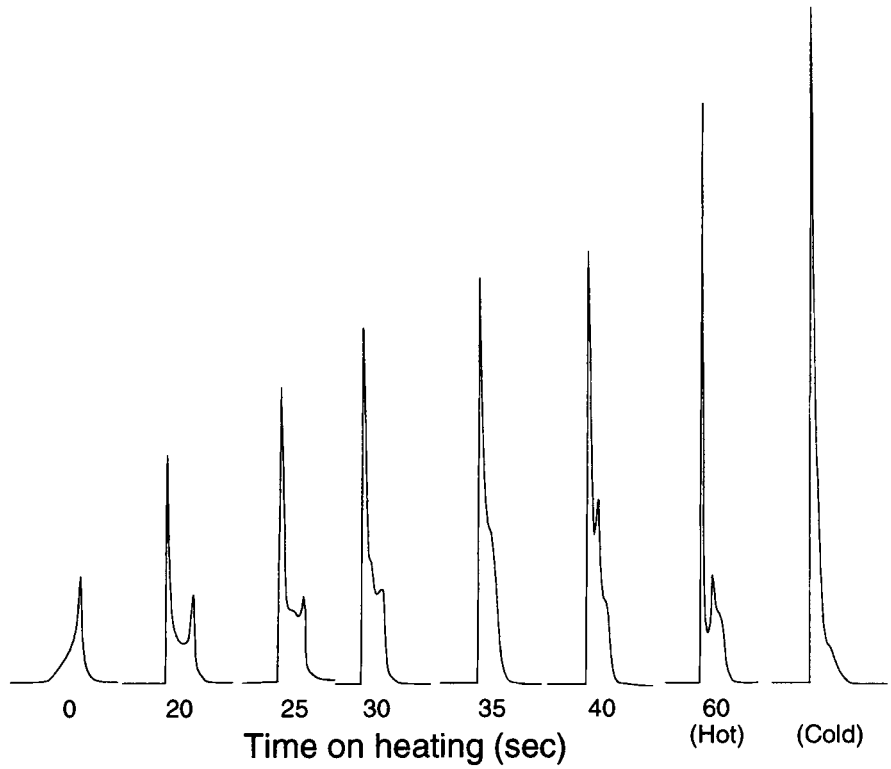

Fig. 14. Effect of water evaporation time on S_2 emission response from methionine (150 ng of sulphur).

lead to the deduction that formation of salts is responsible for the removal of the peak-splitting. That is, the amphoteric property of the amino acids results in the peak-splitting of the emission response, and disappearance of this property due to the formation of salts with the additives brings about changes in the sample gasification process. The difference in the emission responses between 2-amino-4-thiazoleacetic acid and other amino acids shown in Fig. 5 may be explained as follows. All the 4 α-amino acids are amphoteric. Thiazolidine-4-carboxylic acid is also expected to be amphoteric, taking into account its structural analogy with proline. But in the case of 2-amino-4-thiazoleacetic acid, its amphoteric property is considered to be very weak because its dissociation constants, which are estimated from the pK_a of 2-thiopheneacetic acid (3.89) [21] and 2-aminothiazole (8.64) [22], will be smaller than those of the other amino acids; the pK_a values of cysteine, methionine and proline are 1.96 and 10.28, 2.28 and 9.21, and 1.99 and 10.60, respectively [21]. That is, it is considered that the weakness of the amphoteric property for 2-amino-4-thiazoleacetic acid is related to the large first peak of the emission response.

If the amphoteric property of amino acids is responsible for the multi-peak response, modification of functional groups such as esterification of the carboxylic group or acetylation of the amino group would lead to a single response in the emission profiles of amino acids. The results are shown in Fig. 8. The modification led to a single-peak response as expected.

If the effect of addition of acids or bases is based on the formation of salts with sulphur-containing amino acids, the separate location of amino acids and the additives within the cavity would have no effect. When methionine and the additives were separately deposited on the C position and the A position, respectively, in the 3-point ground cavity, the additives, except oxalic acid, had no effect on the emission response. Therefore, it is no doubt that salt formation of amino acids with acids or bases is effective for the removal of the peak-splitting.

Fig. 9 shows that large amounts of oxalic acid promoted the first gasification process of amino acids even when separate locations; oxalic acid was deposited on

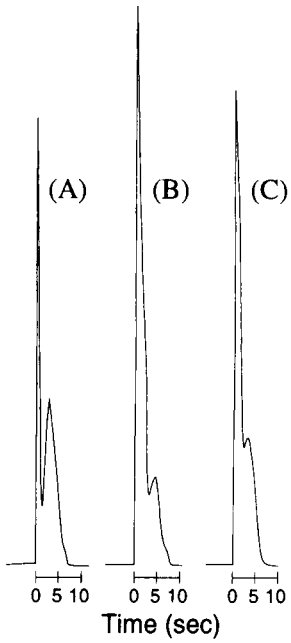

Fig. 15. Effect of a blow of hot water vapor into the cavity on S_2 emission response. Response from methionine (250 ng of sulphur) by using (A) the hot cavity, (B) the cold cavity, and (C) the hot cavity with steam.

the A position and the amino acid on the C position of the 3-point polished cavity. When oxalic acid was deposited on the same location with sulphur-containing amino acids, an equimolar amount was necessary to remove the peak-splitting of the response, but a 50-fold amount was required in the separate location. Although the effect is considered to be based on the vapor or the degradation products of the acid, no effect was observed when a small flow of CO_2 (20–80 ml min^{-1}) was added to the flame or directly blown to the cavity, or when a mixture of oxalic acid and TMAH was deposited. Since oxalic acid is easy to sublime [23], it may be reasonable that the vapor of the acid forms salts with amino acids, and promotes the fast gasification process.

2.3. *Effect of cavity temperature*

When a constant flow (50 ml min^{-1}) of hydrogen sulphide [5×10^{-3}% (v/v) in N_2] was added to a nitrogen sheath oxy-hydrogen flame through a silica needle fixed in the flame, the S_2 emission could not be observed without the presence of the cavity. When a cavity was introduced into the flame, an intense emission was observed in the cavity, which is the Salet phenomenon. However, the emission intensity was not constant, and rapidly decreased with time. A typical emission response is shown in Fig. 10; the intensity decreased to 50% of the maximum after 3 s, and at 20% after 6 s. This rapid decrease is considered to be due to temperature rise of the cavity within the flame. The emission intensity was also dependent on an initial temperature of the cavity at the introduction into the flame, as shown in Fig. 10. In order to change the initial temperature, the cavity before introduction into the flame was heated in a hot air stream, and the temperature of the hot stream around the cavity was regarded as the apparent, initial temperature of the cavity by exposure of the cavity in the stream for 1 min.

In conventional MECA, the solvent of a sample solution is removed in a cavity, before introduction into a flame, with a hot air stream (about 80°C) by using a blower. The solvent pre-evaporation to dryness takes about 1 min, and consequently, the cavity temperature is higher than room temperature at the introduction into a flame (termed a "hot" cavity). When the cavity was cooled with a cold air stream (about 30°C) after the solvent pre-evaporation (termed a "cold" cavity), the observed response was quite different from that without cooling. The results are shown in Fig. 11. Cooling of the cavity leads to an enhancement of the first peak and reduction of the second peak in large amounts of samples. The emission intensity for small amounts (less than 25 ng of S) is greater in the hot cavity, especially the peak height. These emission behaviors were commonly observed among the amino acids examined.

Fig. 12 shows the effect of the initial cavity temperature on the fast emission response; i.e., a single-peak response and/or the first peak of multi-peak responses. The emission response from 10 ng of sulphur showed a maximum at about 60°C, and maximum intensities were shifted to lower temperature with increase in sample amount. The peak width increased with decrease in initial temperature for any amount of sample. It looks reasonable that broadening of the response from sample gasification with decrease in cavity temperature is responsible for the decrease in the emission response from a small amount of sample (10 ng of sulphur), but the reasoning cannot explain the decrease in the peak area. On the other hand, for a large amount of sample (100 ng of sulphur), the peak area at 30°C initial cavity temperature is 3 times greater than that at 80°C. This enhancement could not be explained only by the tem-

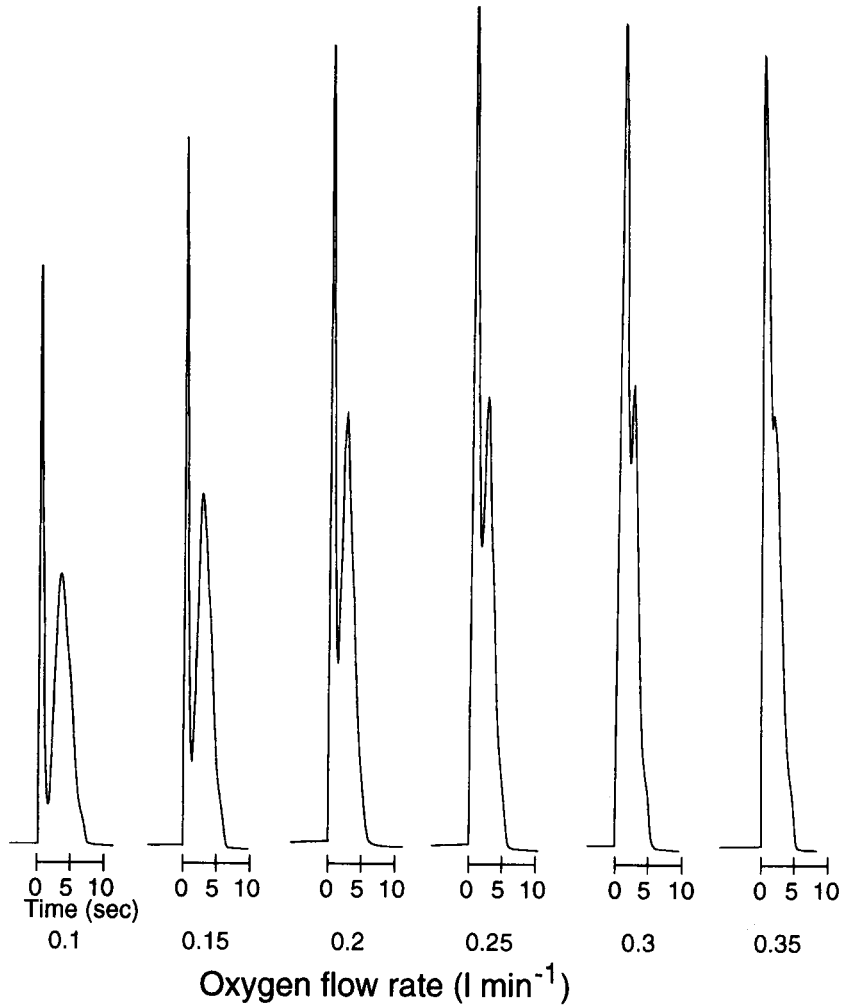

Fig. 16. Variation in S_2 emission response (250 ng of sulphur as methionine) with oxygen flow-rate. Hydrogen flow-rate is 5.0 l min^{-1}.

perature effect of the Salet phenomenon. The intensity of the second peak significantly decreased with decrease in initial cavity temperature, as shown in Fig. 13. The decrease of the second peak is not attributed to overlapping with the first peak due to broadening of the first peak, and means that an amount of sample which is gasified in the fast process increases at lower cavity temperature.

When the cold cavity was introduced into the flame, condensation of water was temporarily observed for a short period of time on the inner surface of the cavity immediately after introduction into the flame. The ground cavity is opaque due to the random reflection of light at the surface, but being wet, the cavity slightly became transparent due to the water adsorbed. The condensation was not observed in the hot cavity, and consequently, the condensed water may be related to the emission behavior, as shown in Figs. 12 and 13. If the condensed water is responsible for the change in emission responses, incomplete pre-evaporation of solvent or addition of water vapor to a cavity would bring about the same variation in the emission responses. Fig. 14 shows the effect of solvent remaining in the cavity on the S_2 emission. Evaporation of a 10-μl volume of sample solution to dryness took about 50 s with a hot air blower, and the cavity was usually heated for 60 s (a hot cavity) in order to make sure of dryness. With decrease in the heating time, i.e., with increase in the amount of solvent remaining in the cavity, the S_2 emission was quenched significantly. But incomplete peak-

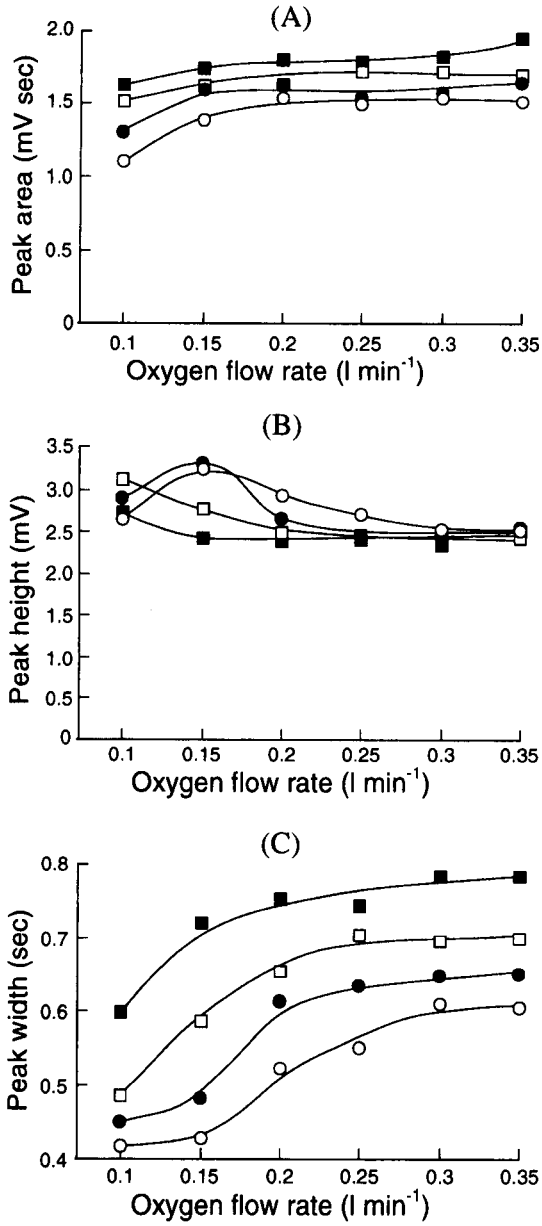

Fig. 17. Effect of flame composition on S_2 emission response from methionine (25 ng of sulphur). (A) Peak area, (B) peak height and (C) peak width. Hydrogen flow-rates: (■) 3.5, (□) 4.0, (●) 4.5 and (○) 5.0 l min^{-1}.

splitting of the response was observed with a certain amount of solvent remaining. When small amounts of hot water vapor (about 90°C) were blown into a hot cavity after the solvent pre-evaporation, the emission response observed consisted of a broad first peak and a small second peak, which looked like the signal with a cold cavity, as shown in Fig. 15. Although it is difficult to determine a quantity of water condensed on the surface and difficult to change quantitatively the amount of steam deposited on the cavity, we suggest that a certain amount of water vapor condensed in the cavity is related to the variation of the emission response, especially to the gasification process of the amino acids.

2.4. *Effect of flame composition*

Fig. 16 shows the variation in the multi-peak response of methionine (250 ng of sulphur) with oxygen flow-rate. The temperature of the flame rises about 100°C with 50 ml min^{-1} of increase in oxygen flow-rate [17]. The rise in temperature of the flame is considered to be responsible for the variation of the emission response; a higher temperature of the flame brings about rapid gasification of the sample, merging of the first and the second peak, and increase in the width of the first peak. However, the results from a small amount of sample (Fig. 17) could not be explained only by the change in flame temperature. The width of the response from 25 ng of sulphur as methionine became broader with increase in oxygen flow-rate and with decrease in hydrogen flow-rate: a decrease in the hydrogen flow-rate (1 l min^{-1}) also resulted in about 100°C rise in the flame temperature [17]. That is, the width became broader with increase in flame temperature. Small amounts of methionine (less than 25 ng of sulphur) showed a single-peak response, which had no peaks merged, and therefore the width could not be broadened by the rapid gasification.

At 0.35 l min^{-1} of oxygen, we observed the temporary condensation of water vapor in the cavity immediately after introduction into the flame, without cooling after solvent pre-evaporation. The condensation was also observed even at lower oxygen flow-rates with a decrease in hydrogen flow-rate; e.g., more than 0.2 l min^{-1} of oxygen at 3.5 l min^{-1} of hydrogen. Excess of hydrogen gas acts as a diluent at the lower part of the flame, because nitrogen gas surrounds the oxy-hydrogen flame. A higher oxygen flow-rate and lower hydrogen flow-rate bring about not only a higher flame temperature, but also a higher concentration of water vapor in the flame. If the increase in concentration of water vapor in the flame is responsible for the variation in the emission responses, the addition of water

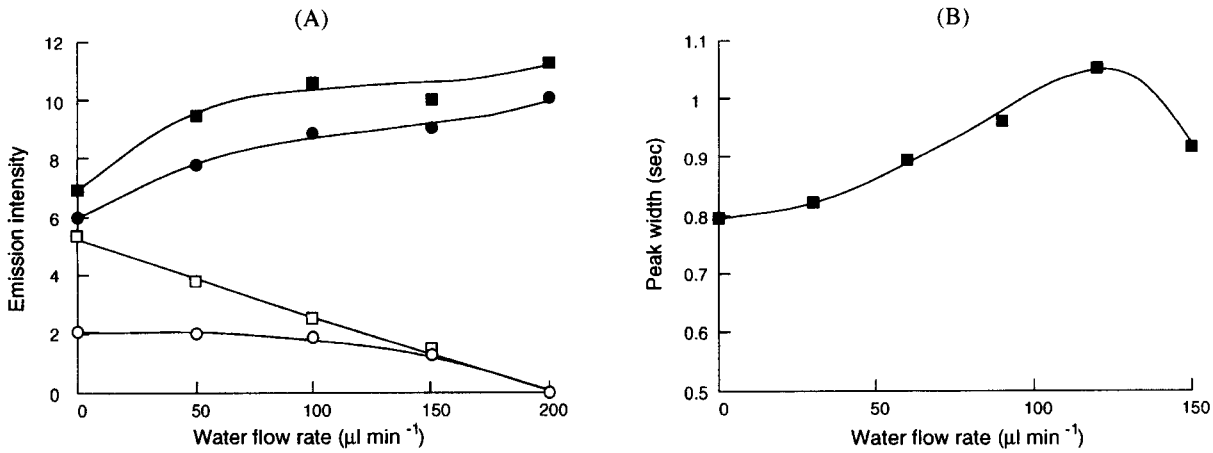

Fig. 18. Effect of addition of water to a flame on S_2 emission response from methionine. (A) (■,□) peak area and (●,○) peak height for the first and the second peak from 125 ng of sulphur. (B) Peak width from 25 ng of sulphur. Gas flow-rates: H_2, 4.0; O_2, 0.15; N_2, 6.0 l min^{-1}.

to the flame would show the same effect. A certain amount of water was added to the flame through a silica needle fixed above the burner head, by using a pump for LC (LC-9A). The results are shown in Fig. 18. The addition of water to the flame clearly intensified the first peak and decreased the second peak for a large amount of the sample, and the single peak response from a small amount of the sample was broadened as expected. It is clear that a high concentration of water vapor, maybe temporary condensed water in the cavity, affects the gasification of the sample, as well as the initial cavity temperature. But the change in the emission response shown in Fig. 16 is clearly different from that in Fig. 13. The second peak shown in Fig. 13 clearly decreases with decreasing initial cavity temperature, i.e., with increase in the amount of condensed water. On the other hand, the second peak in Fig. 16 seems to overlap with the first peak rather than decreasing the intensity with increase in oxygen flow-rate, i.e., with increase in the concentration of water vapor. The time lag between the peaks shown in Fig. 16 became small with increase in the flame temperature, and therefore, we suggest that the variation of the multi-peak response with flame gas flow-rates results from the rapid gasification of the second peak due to the rise of the flame temperature and the broadening of the first peak due to temporary condensation of water vapor.

3. Conclusions

It is clear that the multi-peak response from sulphur-containing amino acids is attributed to heterogeneous gasification of the sample, not to the formation of non-volatile compounds. The first peak of the multi-peak response occurs immediately after introduction of the cavity into the flame, i.e., the first peak is independent on the gasification temperature of the samples. On the contrary, the second peak is dependent on the gasification temperature. These results mean that the first peak is based on a fast gasification process due to contact with flame gases but the second peak is based on thermal decomposition due to temperature rise of the cavity. A portion of sample escapes from the fast gasification process and forms the second peak with its delayed thermal decomposition, i.e., a limitation on the fast gasification process brings about the multi-peak response of amino acids. Since the sample solution was injected into the cavity which was set up vertically, a portion of the sample dispersed within the cavity but other portions of the sample would be deposited as aggregates on the bottom of the cavity (i.e., on the C position) during the solvent pre-evaporation. It was expected that the sample dispersed within the cavity was gasified by contact with flame gases, but on the contrary, the sample deposited on the C position was not rapidly gasified due to slow rise of cavity temperature or difficulty of the flame gases in flowing into the bottom of the cavity. But the residue after the 1-s introduction gave a double peak response and the sample deposited on the C position of the 3-point ground cavity also gave a double peak. These results mean that sample location or aggregate formation cannot explain the limitation on the fast gasification process.

It is no doubt that the amphoteric property of sulphur-containing amino acids results in the multi-peak response, and formation of salts with acids or bases removes the peak-splitting. Since there is strong intermolecular interaction between the amphoteric ions, we could understand the non-volatility of amino acids due to the interaction. Therefore, if the fast gasification process was suppressed completely or the first peak was accompanied by pronounced tailing, the multi-peak response could be attributed to the non-volatility and sample location within the cavity. Although the amphoteric property is related to the limitation mechanism for the fast gasification process, we could not elucidate this mechanism.

The S_2 emission is affected undoubtedly by temporarily condensed water on the cavity surface at introducing into the flame. The enhancement effect of the condensed water on the multi-peak response is considered as the following mechanism. The condensed water vaporizes prior to the second peak emission. A portion of sample dissolves in the condensed water, gasifies with vaporization of water without concentration, and emits the S_2 spectrum which overlaps with the emission response occurring as a result of the fast gasification process. Accelerated sample gasification enhances the intensity of the S_2 emission, because the emission occurs at a lower cavity temperature. On the other hand, the condensed water quenched the S_2 emission from a small amount of sample, and incomplete solvent pre-evaporation also decreased the S_2 emission intensity. These reductive effects would be due to a decrease in concentration of chemical species which concern excitation or formation of the S_2 molecule. Both amounts of sample and condensed water would determine which effect is predominant, i.e., the enhancement effect due to acceleration of sample gasification or the quenching effect due to a decrease in concentration of chemical species. The size of the cavity used is very small compared with the flame and the temperature of the cavity rapidly rises in the flame, so the Salet phenomenon disappears in a short time. Therefore, it is expected that sample gasification at lower cavity temperature brings about higher sensitivity. The condensed water is effective for assisting the producing S_2 emission from a large amount of sample, but undesirable for a small amount of sample. Addition of an acid such as oxalic acid is more effective for the rapid gasification of the sulphur-containing amino acids.

References

[1] M.E. Mulder, Bull. Soc. Chim. Fr., 1 (1864) 453.
[2] G. Salet, Bull. Soc. Chim. Fr., 11 (1869) 302; 14 (1870) 182; 16 (1871) 195.
[3] C. Veillon and J.Y. Park, Anal. Chim. Acta, 60 (1972) 293.
[4] S.S. Brody and J.E. Chaney, J. Gas Chromatogr., 4 (1966) 42.
[5] R. Belcher, S.L. Bogdanski and A. Townshend, Anal. Chim. Acta, 67 (1973) 1.
[6] S.O. Farwell and R.A. Rasmussen, J. Chromatogr. Sci., 14 (1976) 224.
[7] S.O. Farwell and C.J. Barinaga, J. Chromatogr. Sci., 24 (1986) 483.
[8] M. Burguera, S.L. Bogdanski and A. Townshend, CRC Crit. Rev. Anal. Chem., 10 (1980) 185; D. Stiles, A. Calokerinos and A. Townshend (Eds.), Flame Chemiluminescence by Molecular Emission Cavity Detection, Wiley, New York, 1994.
[9] R. Belcher, S.L. Bogdanski, D.J. Knowles and A. Townshend, Anal. Chim. Acta, 79 (1975) 292.
[10] M.Q. Al-Abachi, R. Belcher, S.L. Bogdanski and A. Townshend, Anal. Chim. Acta, 86 (1976) 139.
[11] M.Q. Al-Abachi, R. Belcher, S.L. Bogdanski and A. Townshend, Anal. Chim. Acta, 92 (1977) 293.
[12] A. Safavi and A. Townshend, Anal. Chim. Acta, 128 (1981) 75.
[13] Z.A. Al-Zamil, Y.A. Hassan and S.M. Sultan, Anal. Chim. Acta, 233 (1990) 307.
[14] N.P. Evmiridis and A. Townshend, J. Anal. At. Spectrom., 2 (1987) 339.
[15] K. Nakajima, K. Ohta and T. Takada, Anal. Chim. Acta, 270 (1992) 247.
[16] A. Safavi and A. Townshend, Anal. Chim. Acta, 142 (1982) 143.
[17] K. Nakajima and T. Takada, Bunseki Kagaku, 33 (1984) 183.
[18] D.W. Hill, F.H. Walters, T.D. Wilson and J.D. Stuart, Anal. Chem., 51 (1979) 1338.
[19] R.W.B. Pearse and A.G. Gaydon, The Identification of Molecular Spectra, Chapman and Hall, London, 4th ed., 1976.
[20] K. Nakajima and T. Takada, Anal. Chim. Acta, 199 (1987) 147.
[21] D.R. Lide (Ed.), CRC Handbook of Chemistry and Physics, 71th ed., CRC Press, Boca Raton, FL, 1990.
[22] Hans-G. Boit (Ed.), Beilsteins Handbuch der Organischen Chemie, E III/IV 18, 4063, Springer Verlag, Berlin, 1976.
[23] M. Windholz (Ed.), The Merck Index, Merck, Rahway, 10th ed., 1983.

ELSEVIER

Analytica Chimica Acta 299 (1994) 129–136

ANALYTICA CHIMICA ACTA

Studies on the inhibition of immobilised alkaline phosphatase by metal ions and EDTA in a flow-injection system

J. Marcos, Alan Townshend *

Department of Chemistry, University of Hull, Hull HU6 7RX, UK

Received 24 June 1994; revised manuscript received 19 July 1994

Abstract

Inhibition of immobilized alkaline phosphatase by several metal ions and EDTA was studied in a single-channel flow-injection system. The enzyme was immobilised on controlled pore glass. The same enzyme preparation was used for three months. The inhibition by the tested compounds is reversible, the inhibitors are removed from the enzyme reactor just by passing glycine buffer. The metal ion inhibition response is linear in the range 1×10^{-4}–1×10^{-6} M, while for EDTA the linearity is between 1×10^{-5}–5×10^{-5} M. The relative standard deviation at mid-calibration range is below 5% in all cases. The nature of the inhibition was studied for beryllium and EDTA. Non-competitive inhibition was found at low substrate concentrations, while for substrate concentrations higher than 10^{-3} M inhibitor and substrate compete for the enzyme.

Keywords: Flow injection; Alkaline phosphatase; Inhibition; Metal ions; EDTA

1. Introduction

Alkaline phosphatase (EC.3.1.3.1) is a non-specific enzyme that splits phosphoric acid from phosphate esters, acting at alkaline pH values. It is a dimeric allosteric enzyme [1] with four zinc ions, although only two of them are necessary for activity [2]. This enzyme is associated with bone mineralization, but its function and natural substrate are still unknown [3]. Determination of alkaline phosphatase is important clinically to follow the evolution of bone and hepatobiliary diseases (Paget's disease, osteomalacia, hyperparathyroidism, etc.), and various methods have been proposed for the determination of alkaline phosphatase in serum [4].

Alkaline phosphatase can be used to determine substances that are its inhibitors. These inhibitors can be classified into three groups: metal-chelating agents, metal ions, and orthophosphate and related multicharged anions [5]. Metal-chelating agents, such as EDTA, appear to inhibit the enzyme because they mask the zinc ions that form part of the active sites. Metal ions act by binding or interacting with the enzyme which may be followed by a configuration change or blockage of the active site. The inhibition of alkaline phosphatase by beryllium was detailed in 1949 [6,7]. The toxicity of beryllium can, at least in part, be associated with disturbances of normal ossification due to the interference of beryllium in alkaline phosphatase function in bones. The inhibition of alkaline phosphatase by beryllium, zinc and bismuth ions and some pesticides has been proposed as a method to determine those compounds [8,9]. Zinc has an interesting behaviour. It forms part of the enzyme and is required for the catalysis. When the enzyme loses the zinc the apoenzyme

* Corresponding author.

SSDI 0003-2670(94)00329-7

becomes inactive and it can only be activated by adding zinc. However, zinc at higher concentrations is an inhibitor of the enzyme. This was taken into account by Townshend and Vaughan for different purposes [10,11]. They proposed a method to determine barium that reversed the inhibition by zinc [10], and the determination of zinc and calcium based on their reactivation effect on the apoenzyme [11].

The aim of this work is to investigate the possibilities offered by the inhibition of immobilised alkaline phosphatase by several metal ions and EDTA as a method for their determination. Alkaline phosphatase was immobilised on controlled pore glass (CPG). The enzymatic reactor was placed on a flow-injection system. Thus, the proposed method has the general advantages of such flow systems: high sampling frequency, low cost and versatility [12]. Immobilized enzymes have already been used in FIA to determine inhibitors. Recently, methods have been proposed to determine pesticides. Pesticides are normally strong enzyme inhibitors and this allows their determination in very small concentrations. For example, paraoxon and carbamoylcholine can be determined by their effect on acetylcholinesterase [13,14]. In this case, the inhibition is not reversible, and the inhibited enzyme has to be reactivated by, for example, various oxime derivatives before reuse.

2. Experimental

2.1. Reagents

The enzyme alkaline phosphatase, from bovine intestinal mucosa (10 units/mg solid), was supplied by Sigma (Poole). The CPG (120–200 mesh, mean pore diameter 242 Å) was from Fluka (Glossop). A solution of 1.0×10^{-2} M *p*-nitrophenol phosphate (Lancaster Synthesis, Morecambe) in water was used as substrate stock solution, this solution was always kept refrigerated. The other chemicals were from BDH (Poole). 1.0×10^{-2} M aqueous solutions of the nitrate salts of the following metal ions were prepared: beryllium(II), iron(III), cobalt(II), zinc(II), bismuth(III) (in HCl), calcium(II), barium(II), nickel(II), cadmium(II), aluminium(III) and copper(II). 0.10 M stock solutions of $MgCl_2$ and glycine, in water, were also used. Other aqueous solutions employed were 5% (v/v) HNO_3, 10% (v/v) 3-aminopropyltriethoxysilane, 12% (v/v) glutaraldehyde, 0.1 M sodium phosphate (pH 6.5), 0.1 M diethanolamine, 0.1 M acetic acid–sodium acetate buffer (pH 4.5), 0.1 M sodium carbonate, 0.1 M tris(hydroxymethyl)aminomethane (Tris), 0.1 M sodium chloride and 1.0×10^{-2} M disodium EDTA.

2.2. Immobilisation of alkaline phosphatase

The immobilisation was carried on according to Bowers and Johnson [15] with the modification introduced by Masoom and Townshend [16]. The CPG was boiled with 5% HNO_3 to clean it, washed with water and dried at 90°C. A 10% solution of 3-aminopropyltriethoxysilane in 0.1 M acetate buffer (pH 4.5) was added to the CPG, and the mixture was heated at 90°C for 2 h. After this, the CPG was washed with water, dried and treated with 12% (v/v) glutaraldehyde solution at room temperature for 1 h. The activated CPG was washed with water and let dry at room temperature under a light bulb (240 V, 100 W). 0.2 g of activated CPG was added to a cold solution of 15 mg of alkaline phosphatase in 1 ml of phosphate buffer (0.1 M, pH 6.5), and the mixture was kept in the refrigerator for 6 h. Finally, the CPG-immobilized enzyme was washed with water and stored in glycine buffer (0.1 M, pH 8.0) at 4°C. From it, several enzyme reactors were made by packing the CPG in glass tubes with internal diameter 3 mm and length 1.3–25.0 mm. The enzyme reactors keep their activity at least for three months. After each working day they were filled with glycine buffer (pH 8.0) and kept refrigerated.

2.3. Apparatus and manifold

The detection system was a Cecil Instruments CE272 spectrophotometer (Cambridge) connected to an XY chart recorder. An Ismatec peristaltic pump (Mini 5820), an Anachem rotary-injection valve and a Hellma 178.011-OS flow cell (light path 1.0 cm, volume 30 μl) were also used. PTFE tubing with an internal diameter of 0.5 mm was from Whatman Labsales. The pump tubing was from Elkay (flow-rate, 0.80 cc/m). The manifold used is shown in Fig. 1. A single channel system was used. The carrier was the buffer at the appropriate pH. There were two injection valves: one for the substrate (*p*-nitrophenyl phosphate) and

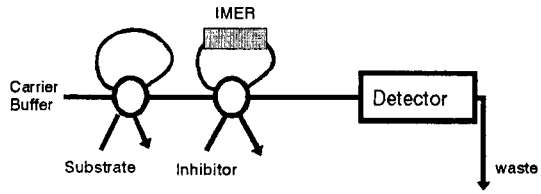

Fig. 1. Manifold used to study the inhibition of immobilized alkaline phosphatase.

another for the inhibitor. The enzyme reactor was placed on the inhibitor loop. The absorbance was measured at 405 nm (wavelength of maximum absorbance for the enzymatic reaction product, *p*-nitrophenol).

3. Results and discussion

Alkaline phosphatase hydrolyses a wide variety of monoesters of phosphoric acid. Typical substrates are phosphate esters of aliphatic alcohols, sugar alcohols, phenols, cyclic alcohols and amines [5]. For this work, *p*-nitrophenyl phosphate was used as substrate. It has often been used as a substrate for this system, and has the advantage of giving a coloured product, so that the reaction can be followed through the formation of the yellow product (*p*-nitrophenol). *p*-Nitrophenyl phosphate also undergoes non-enzymatic hydrolysis at room temperature, but this is very slow compared with the enzymatic reaction. The stock solution of *p*-nitrophenyl phosphate was kept in the fridge (4°C). A fresh working solution was prepared from it every day.

3.1. Metal ion inhibition

As has previously been commented, alkaline phosphatase is inhibited by several metal ions. The purpose of this investigation was to determine metal ions by using their inhibition of immobilised alkaline phosphatase. As beryllium has been reported to be the most potent inhibitor of the soluble enzyme [8,9], beryllium inhibition was studied. The manifold employed was as shown in Fig. 1. The immobilized enzyme reactor (IMER) was initially situated in the carrier stream but no inhibition was seen, probably due to interaction of substrate and beryllium that decreased the inhibition. Therefore, the IMER was placed in the inhibitor loop and inhibition was observed.

To determine the extent of inhibition two peak height measurements were made: one by injecting distilled water (blank, h_b) and the other by injecting a solution of inhibitor (h_i). Thus, $100\times(h_b-h_i)/h_b$ gives the percentage inhibition ($\%I$), which is the parameter used as a measure of the inhibitor effect [17]. When the inhibitor loop is filled, the inhibitor is in contact with the enzyme; then the position of the sample and inhibition injection valves are changed and the carrier stream passes through both loops. The substrate passes through the IMER but the enzymatic reaction is decreased in proportion to the inhibitor concentration. Finally, the buffer passes though the IMER and both substrate and inhibitor are removed. The inhibition is so reversible that if distilled water is injected after the inhibition, the peak signal reaches the initial blank value in one or two injections.

The following variables were studied and optimised: buffer (type, pH and concentration), amount of enzyme, substrate concentration, amount of inhibitor, $MgCl_2$ concentration (see below), incubation time, ionic strength, loop volumes, flow-rate and temperature.

Several buffers have been used with this enzymatic system [18]. Most are amines (diethanolamine, glycine, 2-amino-2-methylpropan-1-ol, ethanolamine, triethanolamine, Tris) although carbonate and borate, for example, have also been employed. Tris, glycine, diethanolamine and carbonate were investigated here. Glycine allowed the greatest inhibition. Inhibition was very poor with the other buffers, so glycine was chosen for further use. The pH of the buffer is also important. pH values between 7 and 10 were studied and greatest inhibition was achieved at pH ca. 8.0. Thus, the optimum pH for the inhibition is different from the optimum pH for the enzymatic reaction (pH 10.0). The effect of buffer concentration between 1.0×10^{-3} and 0.1 M were studied; it was found that the inhibition decreased when the buffer concentration increased. In order to have sufficient buffer capacity a concentration of 5.0×10^{-3} M was selected.

The effect of the amount of enzyme was studied by changing the IMER length. Several reactors with the same diameter (3 mm) and different lengths (between 1.3 and 25.0 mm) were prepared (the density of the reactors was 0.35 mg of solid/mm^3). Fig. 2 shows the influence of the length (enzyme amount) on beryllium inhibition. The inhibition increases with IMER length until it reaches a constant value at $\geq$8.5 mm. As the reactor length increases the dispersion and peak width

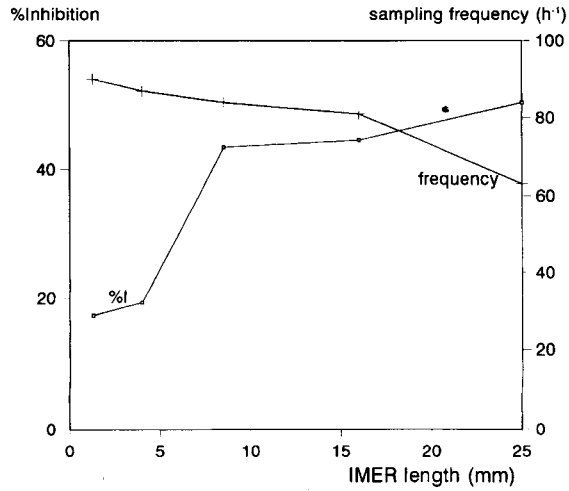

Fig. 2. Influence of the IMER length (enzyme amount) in the percentage of inhibition and the sampling frequency, for 2×10^{-4} M Be^{2+}.

also increase, thus decreasing sampling frequency, so a value of 8.5 mm was chosen for further study.

The substrate concentration was another important variable. No influence on %inhibition was observed below 1.0×10^{-3} M *p*-nitrophenyl phosphate, but above this concentration an increase in the substrate concentration decreased the %inhibition. The peak height increased continuously with increasing substrate concentration. So 1.0×10^{-3} M was selected for further investigation.

Magnesium ions are reported to be an activator for alkaline phosphatase [9,19]. Magnesium interacts with the enzyme and produces a more favourable configuration [20]. Although magnesium is an activator, beryllium still inhibits the enzyme when magnesium is present [14]. It was found that the presence of magnesium enhanced the inhibition of immobilised alkaline phosphatase by beryllium, 1.3×10^{-3} M being the optimum concentration of Mg^{2+} in the carrier. So the carrier stream was established as 5.0×10^{-3} M glycine buffer (pH 8.0) with 1.3×10^{-3} M $MgCl_2$.

The %inhibition (*%I*) increases with increasing amount of inhibitor, but only if the volume of inhibitor solution used to fill the loop is constant is the signal reproducible. Volumes between 0.2 and 3.0 ml were studied, and 1.0 ml was used in further studies. Volumes higher than this did not increase the %inhibition significantly, but the consumption of inhibitor was considerably increased.

The incubation time of enzyme with inhibitor is often important in enzymatic inhibition. An increase in the contact time normally increases the inhibition. In this case, however, the incubation time had no effect, and the incubation time used was only 10 s, the minimum time required to fill the sample loop. This means that there is a rapid interaction between beryllium and enzyme, and agrees with previous studies; in the proposed batch methods for beryllium, incubation was not required, while it is necessary in the determination of pesticides using alkaline phosphatase [8]. Finally, no influence on *%I* was found for ionic strength, loop volume, flow-rate and temperature. The temperature affects the enzymatic reaction itself, but the %inhibition was not affected. Thus, room temperature (18°C) was chosen, and no thermostat was employed.

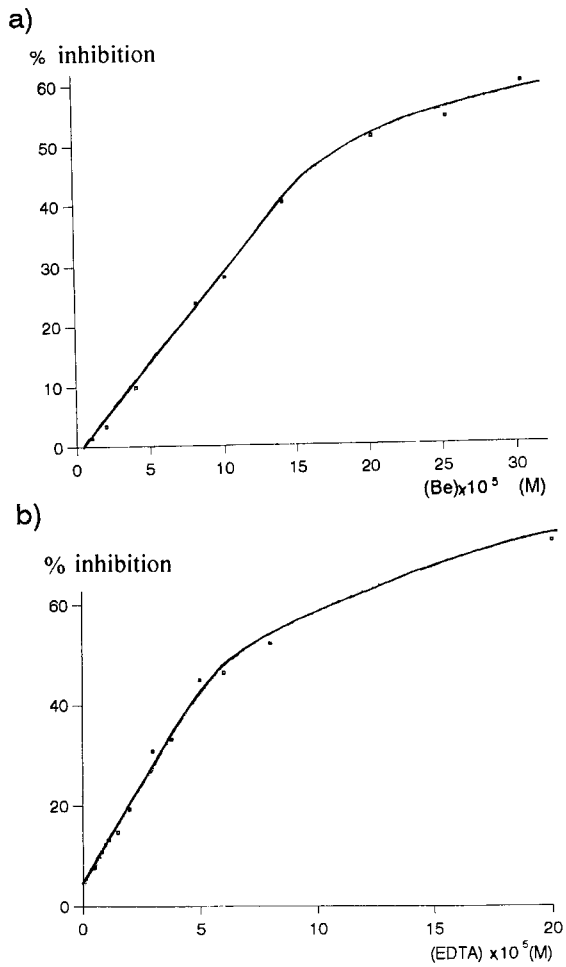

Fig. 3. Plots of percentage inhibition (*%I*) versus inhibitor concentration for (a) beryllium and (b) EDTA.

Table 1
System variables; ranges studied and optimum values

Variable	Initial value	Studied range	Optimum
Buffer	Glycine	Glycine, diethanolamine, Tris, carbonate	Glycine
pH	10.0	7.0–10.0	8.0
Buffer concentration	1.0×10^{-2} M	1.0×10^{-3}–0.1 M	5.0×10^{-3} M
IMER length	4.0 mm	1.3–25.0 mm	8.5 mm
$MgCl_2$	1.0×10^{-3} M	$\leq10^{-2}$ M	1.3×10^{-3} M
Substrate concentration	1.0×10^{-3} M	1.0×10^{-4}–2.0×10^{-3} M	1.0×10^{-3} M
Inhibitor volume	0.2 ml	0.2–3.0 ml	1.0 ml
Incubation time	30 s	10–120 s	10 s
Inhibitor loop volume	60 μl	40–90 μl	60 μl
Substrate loop volume	60 μl	33–80 μl	60 μl
Flow-rate	1.6 ml min^{-1}	0.5–2.5 ml min^{-1}	1.2 ml min^{-1}
Temperature	18°C	18 and 37°C	18°C

The list of variables studied and the optimum values found is shown in Table 1.

3.2. Analytical performance

Working under these optimum conditions, a calibration graph was obtained for beryllium, as shown in Fig. 3a. The graph is linear between 1.5×10^{-5} and 1.5×10^{-4} M, above which the rate of increase of %inhibition decreases, as would be expected. At high concentrations of inhibitor the enzyme approaches saturation by inhibitor, in the same way as it can be saturated by substrate. Therefore, the inhibition graph is similar to a Michaelis-Menten curve. Accordingly, the representation of the inverse of %inhibition versus inverse of inhibitor concentration is a straight line. However, from an analytical point of view, the direct relationship between %inhibition and inhibitor concentration is more useful, because a calibration graph obtained by using the inverses gives larger errors when high concentrations are measured. The following calibration equation was obtained by using 8 standard solutions of beryllium:

$$\%I = (-1.4 \pm 1.6) + (2.94 \pm 0.21)\times10^{5}[\mathrm{Be}]\ (\mathrm{M})$$

where beryllium concentration is expressed in molarity, $r=0.998$, and the 95% confidence limits for the slope and the intercept are depicted. The relative standard deviation (R.S.D.) was 3.0 and 1.4% for 3.5×10^{-5} and 1.0×10^{-4} M beryllium, respectively. The detection limit (calculated concentration for a peak height equal to the blank plus three times the standard deviation of the blank) was 1.5×10^{-5} M (0.14 μg ml^{-1}). As 1 ml was injected, the lowest amount of beryllium detectable was 0.14 μg.

Other metal ions also inhibited alkaline phosphatase. Copper(II), zinc(II), cadmium(II), iron(III), nickel(II), cobalt(II), aluminium(III), bismuth(III), calcium(II) and barium(II) were studied. All of them, except calcium and barium, were found to be inhibitors. In the literature Cu^{2+}, Bi^{3+} and Be^{2+} have been reported as strong inhibitors of the soluble enzyme, but inhibition has also been reported by Zn, Cd, Al, and Co [8,9]. In the system proposed in this paper bismuth was also found to be inhibitor, but owing to the low solubility of its hydroxide, it was only possible to work at concentrations $<1.0\times10^{-5}$ M. A determination limit of 1.0×10^{-6} M was obtained.

The experimental conditions optimised for beryllium inhibition were used for these other metal ions, except that the pH effect was studied in all cases. The optimum pH was always 8.0 or very close to 8.0 (see Fig. 4). In fact, the inhibition decreases quickly if the pH is increased over 8.5. All those metal ions form hydroxides, and this behaviour can be easily explained if the inhibition is due to the free metal ions, and not to the hydroxides. This can also be the reason of a maximum inhibition at a pH lower than the optimum pH for the enzymatic system.

The inhibition reversibility, as well as the incubation time, was studied for each metal ion. The results were the same as for beryllium: reversibility was complete just by passing buffer solution and there was no influence of incubation time. Calibration graphs were estab-

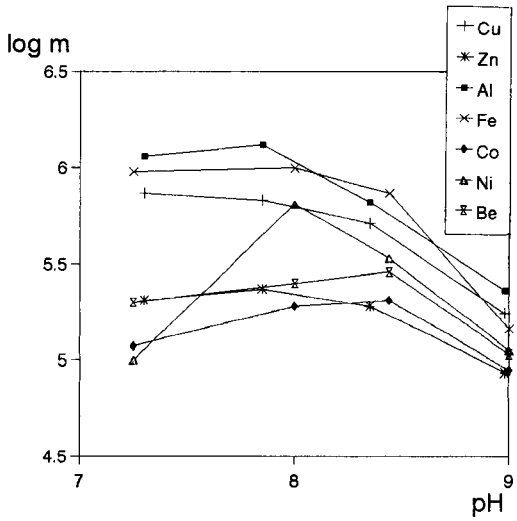

Fig. 4. Influence of pH on the inhibition by some metal ions. The logarithm of the calibration equation slope in the linear range (log m) is plotted versus pH.

lished for all the metal ions. The results are summarised in Table 2. The mid-range R.S.D. was between 1 and 5% in all cases ($n=5$).

3.3. EDTA inhibition

Chelating agents such as EDTA are another type of alkaline phosphatase inhibitor. EDTA is able to mask the enzyme zinc ions, causing the inactivation of alkaline phosphatase. When EDTA is added to a solution of alkaline phosphatase, the enzyme precipitates as a consequence of zinc loss and reactivation only occurs after the addition of zinc or other similar metal ion [11]. In the proposed system, the effect of EDTA was also studied. Inhibition was observed, but it was reversible just by passing buffer. To check whether the apoenzyme was capturing zinc ions present as trace impurities in the buffer, a chelating column (Dowex 50W, 100–200 mesh) was placed in the carrier line before the enzyme. This would remove zinc from the buffer, and prevent reactivation. However the column had no effect on the reversibility. Thus, it could be seen that the immobilised enzyme does not lose the zinc ions, and EDTA is removed just by passing buffer through the IMER. The influence of EDTA concentration on the %inhibition is shown in Fig. 3b. It is linear between 1.0×10^{-6} and 5.0×10^{-6} M. The equation that relates those two variables is:

$$\%I=(3.6\pm1.4)+(8.22\pm0.85)\times10^{5}[\text{EDTA}]\ (\text{M})$$

$r=0.995$ and the concentration of EDTA is expressed in mol l^{-1}. This equation was obtained from 9 results, and the values of slope and intercept 95% confidence limits are also shown. R.S.D. values of 1.3 and 4.5% were obtained for EDTA concentration of 5.0×10^{-5} and 1.5×10^{-5} M, respectively ($n=5$).

3.4. Type of inhibition

The type of inhibition was studied for beryllium and EDTA. Several measurements were made with different concentrations of substrate and inhibitor. The

Table 2
Summary of the results obtained for the metal ions

Metal	n	S_a	S_b	Calibration equation (M)	r	Linear range	
						mol l^{-1}	μg ml^{-1}
Be(II)	7	0.62	8.31×10^{3}	$\%I=-1.60+3.00\times10^{5}$[Be]	0.996	1.5×10^{-5}–1.5×10^{-4}	0.14–1.40
Cu(II)	6	0.88	2.44×10^{4}	$\%I=0.20+5.68\times10^{5}$[Cu]	0.994	1.5×10^{-5}–8.0×10^{-5}	0.95–5.10
Zn(II)	5	0.64	9.19×10^{3}	$\%I=10.8+1.68\times10^{5}$ [Zn]	0.996	1.0×10^{-5}–1.2×10^{-4}	0.65–7.80
Cd(II)	6	1.16	5.16×10^{2}	$\%I=2.00+1.05\times10^{4}$[Cd]	0.992	1.0×10^{-4}–4.0×10^{-3}	11.2–450
Al(III)	6	0.49	4.48×10^{4}	$\%I=-0.70+1.26\times10^{6}$[Al]	0.998	2.0×10^{-6}–3.0×10^{-5}	0.05–0.81
Fe(III)	5	1.71	9.42×10^{4}	$\%I=0.64+1.88\times10^{5}$[Fe]	0.999	3.0×10^{-6}–3.0×10^{-5}	0.17–1.70
Ni(II)	7	0.85	2.48×10^{4}	$\%I=1.50+6.09\times10^{5}$[Ni]	0.996	2.0×10^{-6}–8.0×10^{-5}	0.12–4.70
Co(II)	6	0.70	1.39×10^{4}	$\%I=0.06+3.06\times10^{5}$[Co]	0.996	1.5×10^{-5}–9.0×10^{-5}	0.88–5.30

n = Number of data points used to get the calibration equation; r = correlation coefficient; S_b = standard deviation of the slope, S_a = standard deviation of the intercept. The lower values of the linear ranges are the detection (3σ) limits

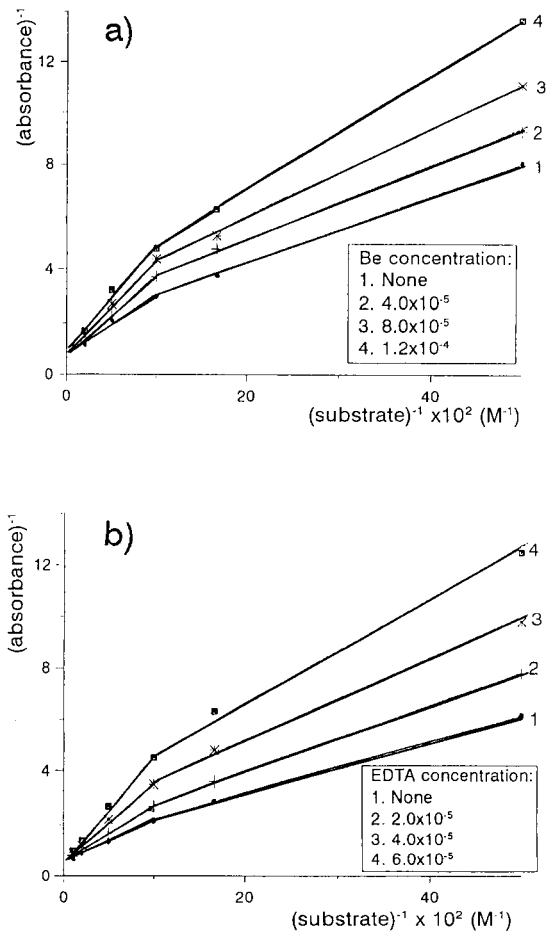

Fig. 5. Lineweaver-Burk graphs obtained for (a) beryllium and (b) EDTA. These graphs show the relationship between the inverse of peak absorbances and the inverse of the substrate concentration. Two linear ranges can be distinguished in both cases. Concentrations in M.

results were represented as Lineweaver-Burk graphs (Fig. 5). As can be seen in the figure, the plots have two parts, which correspond to two different behaviour patterns: one at low concentrations of substrate, and the other one for concentrations $>1.0\times10^{-3}$ M. At low substrate concentrations the lines intersect on the *X*-axis; indicating non-competitive inhibition. Extrapolation of the points above 1.0×10^{-3} M, however, gives a common point on the *Y*-axis, that is, the inhibition is competitive [17].

The change in the inhibition type with substrate concentration can be explained if the enzyme has two active sites, as is described in the literature [21]. If, although the enzyme has two active site, linking with only one substrate molecule is more favourable, the enzyme has an active site free and it can be occupied by the inhibitor. The inhibitor then does not compete with the substrate. When the substrate concentration increases, the enzyme can likely interact with two substrate molecules, so the inhibitor has to compete with the substrate for one of the active sites. This simple explanation seems to explain the experimental facts.

Beryllium and EDTA inhibit alkaline phosphatase in a similar way, although the cause of their inhibition is different. The reason could be that both of them interact with the same active site. Beryllium can interact with negatively charged groups on this site, while EDTA acts by binding with the zinc ion that is an important part of the active site.

The stability of the system is shown by the fact that the same immobilised enzyme preparation was used in the investigation described in this paper over a period of three months.

4. Conclusions

The inhibition of immobilised alkaline phosphatase by several metal ions and EDTA has been studied in a flow-injection system. The %inhibition changes linearly with the concentration of the inhibitor in a certain range so that this system can be employed to determine these metal ions or EDTA. The main problem is selectivity. Because many inhibitors can affect the enzyme, only one of them should be present in the sample at a concentration that can affect the enzyme. However, the method may be able to determine metal ions previously separated by a liquid chromatographic technique.

The type of inhibition by beryllium and EDTA was also studied. Non-competitive inhibition was found at low substrate concentration for both inhibitors, while the inhibition is competitive at substrate concentration over 1.0×10^{-3} M.

Acknowledgements

J. Marcos acknowledges the Basque Country Government (Spain) for financial support through a personal fellowship.

References

[1] D.J. Winzor, Biochim. Biophys. Acta, 200 (1970) 423.
[2] P.D. Boyer, The Enzymes, Vol IV, 3rd edn., Academic Press, New York, 1971, p. 401.
[3] N.A. McCarroll, Anal. Chem., 65 (1993) 388R.
[4] I.M. Christie, P.H. Treolar, Z.B. Koochaki and P.M. Vadgama, Anal. Chim. Acta, 257 (1992) 21.
[5] P.D. Boyer, H. Hardy and K. Myrback, The Enzymes, Academic Press, New York, 1961.
[6] F.W. Klemperer, J.M. Miller and C.J. Hill, J. Biol. Chem., 180 (1949) 281.
[7] R.S. Grier, M.B. Hood and M.B. Hoagland, J. Biol. Chem., 180 (1949) 289.
[8] G.G. Guilbault, M.H. Sadar and M. Zimmer, Anal. Chim. Acta, 44 (1969) 361.
[9] A. Townshend and A. Vaughan, Talanta, 16 (1969) 929.
[10] A. Townshend and A. Vaughan, Anal. Lett., 1 (1968) 907.
[11] A. Townshend and A. Vaughan, Talanta, 17 (1970) 289.
[12] J. Ruzicka and E.H. Hansen, Flow Injection Analysis, 2nd edn., Wiley and Sons, New York, 1988.
[13] I.A. Takruni, A.M. Almuaibed and A. Townshend, Anal. Chim. Acta, 282 (1993) 307.
[14] C. Garcia de Maria and A. Townshend, Anal. Chim. Acta, (1994) in press.
[15] L.D. Bowers and P.R. Johnson, Biochim. Biophys. Acta, 661 (1981) 100.
[16] M. Masoom and A. Townshend, Anal. Chim. Acta, 166 (1984) 111.
[17] P.W. Carr and C.W. Bowers, Immobilized Enzymes in Analytical and Clinical Chemistry, Wiley, New York, 1980.
[18] R.Q. Thompson, M. Parter, C. Stuaver, H.B. Halsall, W.R. Heineman, E. Buckley and H.R. Smith, Anal. Chim. Acta, 27 (1993) 223.
[19] R.A. Morton, Biochem. J., 65 (1959) 1121.
[20] C. Brunel and G. Gathala, Biochim. Biophys. Acta, 309 (1973) 104.
[21] B.I. Kurganov, Allosteric Enzymes. Kinetic Behaviour, Wiley, Chichester, 1982.

ELSEVIER

Analytica Chimica Acta 299 (1994) 137–144

ANALYTICA CHIMICA ACTA

Synthesis of thiacrown ether carboxylic acids and their characteristics as extractants for metal ions

Keiitsu Saito *, Ichiro Taninaka, Satomi Murakami, Akihiko Muromatsu

Division of Natural Environment and Chemistry, Faculty of Human Development, Kobe University, Tsurukabuto, Nada, Kobe 657, Japan

Received 25 May 1994

Abstract

Two thiacrown ethers with pendant carboxylic acid groups, 3,6,10,13-tetrathiacyclotetradec-1-oxyacetic acid (TTCTOAA) and 2-(3,6,10,13-tetrathiacyclotetradec-1-oxy)hexanoic acid (TTCTOHA), were synthesized and their proton dissociation constants (pK_a) were determined potentiometrically at 25 ± 0.1°C and an ionic strength of 0.1. The pK_a values of TTCTOAA and TTCTOHA were 3.97 and 4.05, respectively. The characteristics of thiacrown ether carboxylic acids as extraction reagents for metal ions were examined and compared with those of the neutral thiacrown compound 1,4,8,11-tetrathiacyclotetradecane (TTCT) in the presence of picrate ion for the formation of the ion pair. 1,2-Dichloroethane was used as the extraction solvent. The extractability of metal ions with TTCTOAA was very low. In the case of TTCTOHA, copper(II), silver(I) and copper(I) were extracted into 1,2-dichloroethane. The extractability of silver(I) and copper(I) was lower than that with TTCT and picrate ion. The extraction percentage of silver(I) with TTCTOHA was significantly higher than that of copper(I), whereas hardly any difference in extractability with TTCT was observed between silver (I) and copper(I). Although copper(II), a borderline Lewis acid, was weakly extracted with TTCT and picrate ion, it was extracted well (over 90%) with TTCTOHA into 1,2-dichloroethane. The extraction of copper(II) and silver(I) with TTCTOHA into different organic solvents was examined. The extractability of copper(II) and silver(I) decreased in the order 1-octanol ≈ benzene > 1,2-dichloroethane and 1-octanol > 1,2-dichloroethane > benzene, respectively.

Keywords: Potentiometry; Carboxylic acids; Metal ions; Thiacrown ethers

1. Introduction

As a thioether group acts as a soft Lewis base and reacts selectively with soft Lewis acids, thiacrown ethers have been studied as extraction reagents which are selective for soft metal ions [1–7]. The extractive–spectrophotometric determination of silver and copper with the thiacrown ether 1,4,8,11-tetrathiacyclotetradecane (TTCT) by the use of an appropriate coloured anion has been reported [8]. Some chromogenic thiacrown ethers which have dissociative groups in alkaline media such as hydroxyl and picrylamino groups have been synthesized and their characteristics as extractive–spectrophotometric reagents have been reported [9–11]. However, a thiacrown ether with a dissociative group in acidic media, such as a carboxyl group, has not been synthesized. In the case of a thiacrown ether carboxylic acid, the carboxyl group can donate electrons

* Corresponding author.

SSDI 0003-2670(94)00296-7

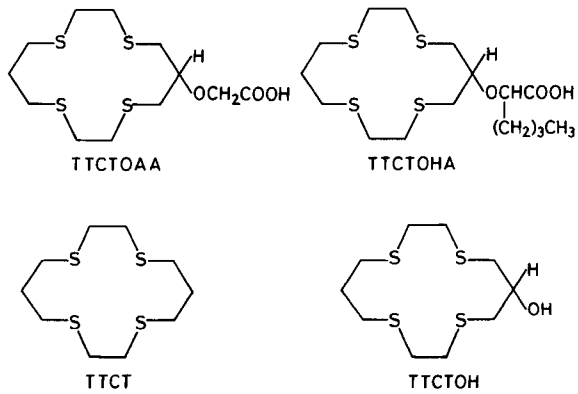

Fig. 1. Thiacrown ethers studied.

to metal ions so that a different selectivity from neutral thiacrown ethers can be expected.

In this study, two new thiacrown ether carboxylic acids which have four sulphur atoms in the 14-membered ring were synthesized and their proton dissociation constants were determined. The characteristics of the thiacrown ether carboxylic acids as extraction reagents for metal ions were examined. The results were compared with those for the neutral thiacrown ether TTCT in the presence of picrate ion for the formation of the ion pair. The interaction of the carboxylate ion and the metal ion is discussed. The thiacrown ethers considered are shown in Fig. 1.

2. Experimental

2.1. Synthesis of reagents

1-Hydroxy-3,6,10,13-tetrathiacyclotetradecane (2, TTCTOH)

Sodium metal (0.9 g, 0.039 mol) was dissolved in absolute ethanol (400 ml) under nitrogen. To this solution, an anhydrous benzene solution (400 ml) containing 3,7-dithianonane-1,9-dithiol (**1**) (4.1 g, 0.018 mol) and 1,3-dibromopropan-2-ol (3.9 g, 0.018 mol) was added dropwise during a 5-h period by cooling in an ice-cold water-bath. After the mixture had been stirred for 12 h at room temperature, the mixture was filtered and the solvent was removed under reduced pressure. The resulting white solid was dissolved in chloroform and washed with water and subsequently dried with anhydrous magnesium sulphate. The solvent was then removed and the residue was chromatographed on a silica gel column with chloroform–ethyl acetate (9 + 1, v/v) as the eluent. The product was recrystallized from ethanol; m.p., 113.5–115.5°C; yield, 1.2 g (23%).

3,6,10,13-Tetrathiacyclotetradec-1-oxyacetic acid (TTCTOAA)

After removal of the protecting mineral oil from 9.6 g (0.24 mol) of sodium hydride by washing it three times with heptane under nitrogen, 100 ml of dry tetrahydrofuran (THF) were added. The hydroxy thiacrown ether **2** (11.4 g, 0.04 mol) dissolved in 500 ml of THF was added with stirring, then the mixture was stirred for 1 h at room temperature. To this mixture, dry THF solution (150 ml) containing bromoacetic acid (11.2 g, 0.08 mol) was added dropwise during a 2-h period and the mixture was stirred for 4 h at room temperature. After addition of water (300 ml) to destroy the excess sodium hydride, the THF was evaporated under reduced pressure. The alkaline aqueous solution was shaken three times with dichloromethane (100 ml) to remove unreacted **2** and was acidified with concentrated hydrochloric acid. The acidic aqueous solution was shaken three times with dichloromethane (100 ml) to extract TTCTOAA and the dichloromethane solution was dried with anhydrous magnesium sulphate. After filtration, the dichloromethane solution was evaporated under reduced pressure. The residue was chromatographed on a silica gel column with ethyl acetate–hexane (4 + 1, v/v) as the element and recrystallized four times from hexane–benzene to give a white crystalline product; m.p., 67.5–69.0°C; yield, 3.5 g (21%). Found, C 42.00, H 6.55; calculated for $C_{12}H_{22}O_3S_4$, C 42.07, H 6.47%. IR (KBr), 3400–2300 (COOH), 2900 (CH), 1720 cm^{-1} (C=O). MS (70 eV) m/z (relative intensity, %) 344 (M + 2, 25), 343 (M + 1, 23), 342 (M^+, 94), 266 (24), 208 (37), 207 (84). ^1H NMR ($CDCl_3$), $\delta = 1.90–1.95$ (2H, m, $CH_2CH_2CH_2$), 2.66–2.95 (16H, m, CH_2CHCH_2, $CH_2CH_2CH_2$, CH_2CH_2), 3.68–3.73 (1H, m, CH_2CHCH_2), 4.28 (2H, s, CH_2).

2-(3,6,10,13-Tetrathiacyclotetradec-1-oxy)hexanoic acid (TTCTOHA)

After removal of the protecting mineral oil from 8.4 g (0.21 mol) of sodium hydride by washing three

times with heptane under nitrogen, 50 ml of dry THF were added. After 10.0 g (0.035 mol) of **2** dissolved in 100 ml of THF had been added with stirring, the mixture was stirred for 1 h at room temperature. To this mixture, dry THF solution (100 ml) containing 2-bromohexanoic acid (10.3 g, 0.053 mol) was added dropwise during a 5-h period and the mixture was then stirred for 24 h. After addition of water (250 ml) to destroy the excess sodium hydride, the THF was evaporated under reduced pressure. The alkaline aqueous solution was shaken four times with hexane (50 ml) to remove unreacted **2** and was acidified with concentrated hydrochloric acid. The acidic solution was extracted with dichloromethane (200 ml) and the dichloromethane solution was dried with anhydrous magnesium sulphate. After filtration, the dichloromethane solution was evaporated under reduced pressure. The residue was chromatographed on a silica gel column with dichloromethane–ethyl acetate (4 + 1, v/v) as the element and recrystallized four times from hexane–benzene to give a white crystalline; m.p., 72.0–73.0°C; yield, 8.3 g (60%). Found, C 48.18, H 7.57; calculated for $C_{16}H_{30}O_3S_4$, C 48.21, H 7.54%. IR (KBr), 3200 (COOH), 2920 (CH), 1735 cm^{-1} (C=O). MS (70 eV), *m/z* (relative intensity, %) 400 (M + 2, 31), 399 (M + 1, 34), 398 (M^+, 98), 267 (65), 266 (57), 264 (23). ^1H NMR ($CDCl_3$), $\delta = 0.88–0.94$ (3H, t, CH_3), 1.33–1.45 (4H, m, $CH_2CH_2CH_2CH_3$), 1.78–1.96 (4H, m, $CH_2CH_2CH_2$, $CHCH_2CH_2$), 2.64–3.16 (16H, m, CH_2CHCH_2, $CH_2CH_2CH_2$, CH_2CH_2), 3.61–3.69 (1H, m, CH_2CHCH_2), 4.18–4.24 (1H, t, $CHCH_2$).

1,4,8,11-Tetrathiacyclotetradecane (TTCT)

The neutral thiacrown ether TTCT was synthesized according to the method of Rosen and Bush [12] and purified as described previously [6].

2.2. Reagents

Metal sulphates (analytical-reagent grade) were used and 1×10^{-2} M stock solutions of metal ions were prepared. The concentrations of metal ions except for silver(I) and palladium(II) were standardized by EDTA titration. The concentrations of silver(I) and palladium(II) were determined by potentiometric titration with sodium chloride and gravimetric analysis with dimethylglyoxime, respectively. 1,2-Dichloroethane was purified as described previously [6]. Octan-1-ol was shaken three times with 2 M potassium hydroxide, 1 M perchloric acid and distilled water, then dried with anhydrous sodium sulphate and distilled in vacuo. Benzene was shaken three times with concentrated sulphuric acid, 2 M sodium hydroxide and distilled water, then dried with anhydrous calcium chloride and distilled. Other reagents were of analytical-reagent grade.

2.3. Apparatus

A Taiyo M-100 incubator was used for shaking the solutions. A Seiko SAS-725 atomic absorption spectrometer was used for the determination of metal ions. IR spectra were measured with a Shimadzu IR-440 infrared spectrophotometer. UV–visible absorption spectra were measured with a Hitachi U-3200 spectrophotometer. pH was measured with a Toa HM-5ES pH meter.

2.4. Proton dissociation constant

The proton dissociation constants were determined potentiometrically at 25 ± 0.1°C and an ionic strength of 0.1. The ionic strength was adjusted with sodium perchlorate. A definite amount of TTCTOAA or TTCTOHA was dissolved in dioxane–water under an atmosphere of nitrogen. The solution was titrated with carbonate-free sodium hydroxide solution in water–dioxane which was kept at an ionic strength of 0.1 under an atmosphere of nitrogen. The nitrogen was passed through a soda-lime tube.

2.5. Liquid–liquid extraction of metal ions

A 10-ml volume of an aqueous solution containing a metal ion (5×10^{-5} M) and a buffer solution were maintained at an ionic strength of 0.1 with sodium sulphate. This solution was kept in a 50-ml cylindrical glass tube equipped with a stopper. The buffer solution was prepared with sulphuric acid (pH < 3.0), acetic acid–sodium acetate (1×10^{-2} M, pH 3.0–6.2) or disodium hydrogenphosphate–potassium dihydrogenphosphate (1×10^{-3} M, pH > 6.4). For the copper(I) solution, hydroxylammonium sulphate or ascorbic acid was added to a copper(II)

solution to give a concentration of 3.3×10^{-2} or 5×10^{-3} M, respectively. To the resulting aqueous solution, 10 ml of 5×10^{-3} M TTCTOAA or TTCTOHA solution were added and the mixture was shaken for 30 min at 200 strokes min^{-1} at 25 ± 0.1°C. The mixture was then centrifuged for 5 min at 2000 rpm. When the two phases were separated, the pH of the aqueous phase was measured and the concentration of the metal ion in the aqueous phase was determined by atomic absorption spectrometry.

The metal ion concentration in the 1,2-dichloroethane or benzene phase was determined as follows: a definite amount of the organic phase was allowed to evaporate, the residue was treated with 1 ml of concentrated nitric acid and diluted to 10 ml with water and the metal ion in this solution was determined by atomic absorption spectrometry. The concentration of copper(II) or silver(I) in the octan-1-ol phase was determined as follows: a definite amount of the organic phase was diluted to 10 ml with ethanol and the concentration of copper(II) or silver(I) was determined by atomic absorption spectrometry. The standard solutions were prepared with 4-cyclohexylbutanoates for atomic absorption spectrometric analysis.

3. Results and discussion

3.1. Synthesis of reagents

The synthesis of TTCTOAA and TTCTOHA proceeded via the steps shown in Scheme 1. The starting compound, **1**, was synthesized according to the method of Rosen and Bush [12]. The hydroxy thiacrown ether **2** was synthesized by the high dilution method by reference to the method of Rosen and Bush [12]. The thiacrown ethers with pendant carboxylic acid groups were synthesized by reference to the method of Bartsch and co-workers [13,14]. The lower yield of TTCTOAA is attributed to a short reaction time.

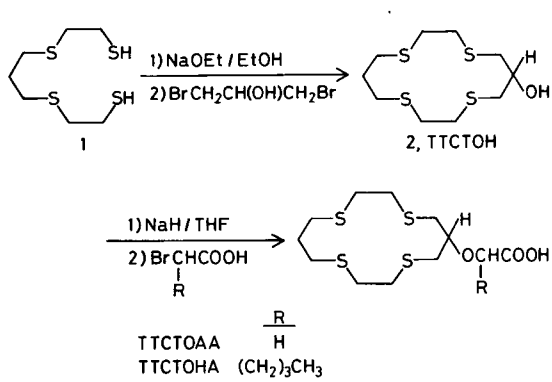

Scheme 1.

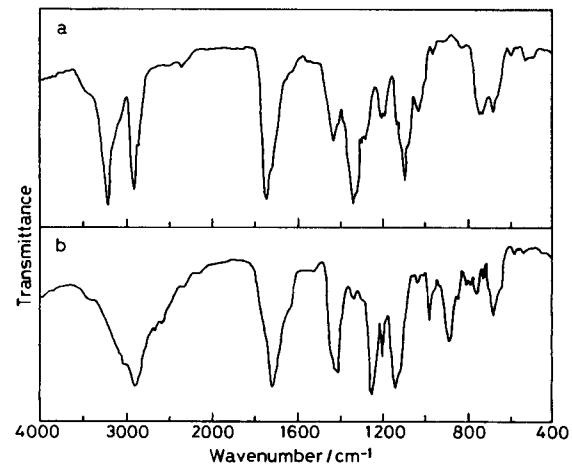

Fig. 2. IR spectra of thiacrown ether carboxylic acids, (a) TTCTOHA; (b) TTCTOAA.

As shown in Fig. 2, the IR spectra of TTCTOAA and TTCTOHA exhibit an interesting difference. The infrared spectra of carboxylic acids usually show broad, ill-defined O–H stretching absorption bands because of the intermolecular hydrogen bonding. Although very broad, ill-defined O–H stretching absorption was observed in the IR spectrum of TTCTOAA and a sharp O–H stretching absorption at 3200 cm^{-1} was noted for TTCTOHA. This spectral change suggests that the intermolecular hydrogen bonding of the carboxylic acid group in TTCTOHA is extremely weakened or absent. This is due to the steric hindrance by a butyl group at the α-position in the carboxylic acid group of TTCTOHA.

3.2. Proton dissociation constant

Proton dissociation constants of TTCTOHA and TTCTOAA were determined by titration with sodium hydroxide solution. As the reagents were slightly soluble in water, the titration was carried out in

aqueous dioxane solution with various mole fractions of dioxane. Values of pH measured in aqueous dioxane solutions were corrected according to the method proposed by Van Uitert and Haas [15]. The apparent pK_a values were estimated from the point of 50% neutralization of the acids on the titration curves. The plots of the apparent pK_a values against mole fraction of dioxane are shown in Fig. 3. The pK_a values in the aqueous solution were estimated by extrapolation. The plot for TTCTOHA was a straight line with a correlation coefficient of 0.998. The pK_a value obtained for TTCTOHA was 4.05. For TTCTOAA, the data points at higher mole fractions of dioxane deviated from a straight line. Therefore, the pK_a value was estimated from three data points at lower mole fractions of dioxane to be 3.97.

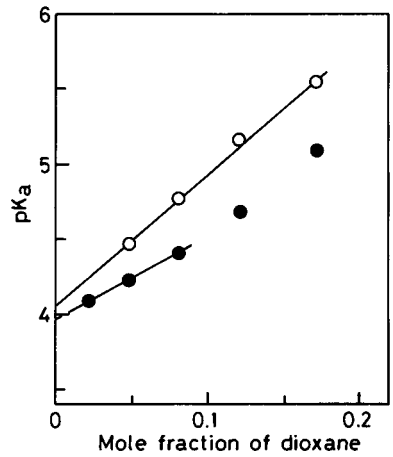

Fig. 3. Proton dissociation constant of (○) TTCTOHA and (●) TTCTOAA as a function of the mole fraction of dioxane.

Table 1
Data for the extraction (%E) of various metal ions with TTCTOAA, TTCTOHA and TTCT into 1,2-dichloroethane

Metal ion	Pearson classification [a] [16]	α [17]	TTCTOAA		TTCTOHA		TTCT [b] [1]	
			pH	%E	pH	%E	pH	%E
Mg(II)	H	0	4.6	4.1	4.6	0	5.4	0
			5.6	3.3	6.3	0		
Mn(II)	H	1.04	4.6	0	4.6	0	5.4	0.8
			5.7	0.5	6.3	0		
Zn(II)	B	1.25	4.6	0	4.6	0	5.4	0.5
			5.7	0	6.3	0		
Co(II)	B	1.39	4.6	0.7	4.6	1.1	5.4	0.8
			5.7	0.7	6.3	1.0		
Ni(II)	B	1.41	4.6	1.8	4.6	1.1	5.4	0.7
			5.7	1.4	6.3	1.7		
					7.9	15.0 [c]		
Cu(II)	B	1.64	4.6	0	4.6	0.6	5.4	5.9
			5.7	2.2	5.8	10.4		
			6.3	6.7	6.2	45.8		
					7.0	91.5		
Cd(II)	S	1.66	4.6	0	4.6	0	5.4	0.8
			5.7	0.5	6.6	0.6		
Ag(I)	S	3.60	4.6	9.8	4.6	68.6	5.4	99.4
			5.7	6.0	6.0	71.3		
					6.4	67.8		
Cu(I)	S	3.92	4.5	1.6	4.6	12.4	5.4	99.4
			5.8	2.9	6.0	13.4		
					6.4	15.0		
Pd(II)	S	5.33	4.5	0	4.5	1.1	5.4	14.3
			5.4	0	5.6	0.7		
					9.6	0 [c]		

[a] H = hard; B = borderline; S = soft.
[b] Presence of picrate ion, 1×10^{-3} M.
[c] The recovery was not quantitative.

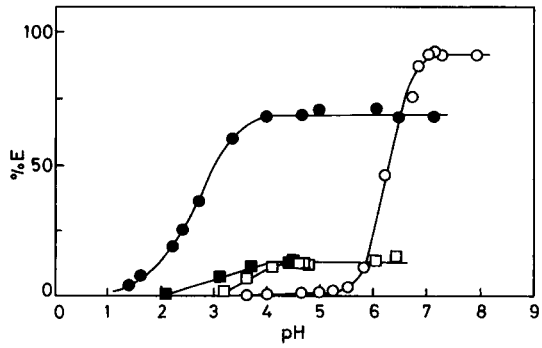

Fig. 4. Relationship between percentage extraction (%E) of copper(II), silver(I) and copper(I) with TTCTOHA and pH. Initial concentrations: metal ion, 5×10^{-5} M; TTCTOHA, 5×10^{-3} M. Metal ions: ○ = Cu(II); ● = Ag(I); □ = Cu(I) (hydroxylammonium sulphate); ■ = Cu(I) (ascorbic acid).

3.3. Liquid–liquid extraction of various metal ions with TTCTOAA and TTCTOHA

The extraction of various metal ions with TTCTOAA into 1,2-dichloroethane was carried out. The results are shown in Table 1, together with those for extraction with TTCT in the presence of picrate ions [1], the Pearson classification for Lewis acids [16] and α values which present the softness of the metal ions [17]. The following metal ions were examined: magnesium(II) and manganese(II) as hard metal ions; cobalt(II), nickel(II), copper(II) and zinc(II) as borderline metal ions; and cadmium(II), silver(I), copper(I) and palladium(II) as soft metal ions.

The extraction behaviour of the hard and borderline metal ions with TTCTOAA is basically similar to that with TTCT and picrate ion. The hard and borderline metal ions except for magnesium(II) and copper(II) were hardly extracted. Although magnesium(II) is a hard Lewis acid, a few per cent of magnesium(II) was extracted with TTCTOAA. This is due to the carboxylic acid group which is a hard Lewis base [16], because magnesium(II) was not extracted at all with TTCT in the presence of picrate. Copper(II) was slightly extracted with TTCTOAA and the extractability was dependent on the pH of the aqueous phase. Among of the soft metal ions, cadmium(II) and palladium(II) were hardly extracted with TTCTOAA. As silver(I) and copper(I) were quantitatively extracted with TTCT in the presence of picrate, it was expected that these metal ions would be extracted well with TTCTOAA. However, the extraction of silver(I) and copper(I) was below 10%.

After the extraction of copper(II) with TTCTOAA, the aqueous phase assumed a deep blue colour and exhibited two absorption maxima at 560 and 390 nm, which are similar to those of the complex of copper(II) with TTCT in methanol–water (80 + 20) reported by Dockal et al. [18]. This suggests that the low extractability of metal ions is attributable to the low lipophilicity of the complexes formed with TTCTOAA. Therefore, TTCTOHA, which has a more hydrophobic group, was synthesized and its characteristics as an extractant for various metal ions were examined. The results are also shown in Table 1.

Although magnesium(II) was slightly extracted with TTCTOAA, it was not extracted at all with TTCTOHA, in spite of the fact that it has a carboxylic acid group. This may be due to the steric hindrance by the butyl group at the α-position in the carboxylic acid group. Manganese(II), classified as a hard metal ion, and cobalt(II), nickel(II) and zinc(II), classified as borderline metal ions, were hardly extracted with TTCTOHA at pH < 6.3. The extraction of nickel(II), which has the largest α value among of the borderline metal ions except for copper(II), was tried at pH 7.9. Nickel(II) was extracted with TTCTOHA to some extent, although the recovery was not quantitative. Copper(II) was extracted with TTCTOHA and the extraction percentage was dependent on the pH of the aqueous phase. The extractability of copper(II) with TTCTOHA was higher than that with TTCTOAA or TTCT. Of the soft metal ions, silver(I) and copper(I) were extracted with TTCTOHA but their extraction percentages were lower than those (over 99%) with TTCT in the presence of picrate ion. A large difference in the extractability between silver(I) and copper(I) was observed, whereas no difference in the extractability between these metal ions could be observed for other thiacrown ethers [1,4,9–11]. Cadmium(II) was hardly extracted with TTCTOHA or with TTCTOAA and TTCT. Although palladium(II), which has the largest α value among the metal ions examined, was extracted with TTCT to some extent, it was scarcely extracted with TTCTOHA or TTCTOAA.

3.4. Dependence on pH for the extraction of copper(II), silver(I) and copper(I) with TTCTOHA

As thiacrown ether carboxylic acids are weak acids, the extractability of copper(II), silver(I) and copper(I) with TTCTOHA should depend on the pH of the aqueous phase. Therefore, the pH dependence of the extraction of these metal ions was examined in detail. Plots of the percentage extraction ($\%E$) against the pH of the aqueous phase are shown in Fig. 4. For copper(II), the extractability is constant at 92% above pH 7 and decreases rapidly in the pH range 5–7. Copper(II) was scarcely extracted below pH 5. Silver(I) was extracted above pH 1. The extractability of silver(I) increases in the pH range 1–4, reaching a constant level of 70% at pH > 4. For copper(I) solution, two reducing agents were tested. When hydroxylammonium sulphate was used as the reducing agent, the extractability increased in the pH range 3.0–4.5, reaching a constant level of 15% at pH > 4.5. On the other hand, when ascorbic acid was used, the extractability increased in the pH range 2.0–4.5, reaching a constant level of 15% at pH > 4.5.

The difference in the extractability is due to the difference in reducing power of these reductants in acidic media. As silver(I) and copper(I) have the same charge and their α values are 3.60 and 3.92, respectively, it was expected that the extractability of copper(I) would be higher than that of silver(I). However, the extractability of copper(I) was lower than that of silver(I). Although copper(II) is classified as a borderline metal ion, its extractability was higher than those of silver(I) and copper(I), classified as soft metal ions. This result is very different from those with neutral thiacrown ethers in the presence of picrate ions [1,4]. The extraction of copper(II) with TTCT and picrate ion was only 6%, so that the interaction between the carboxylate ion and copper(II) seems to affect the extractability.

3.5. Effect of organic solvents

The extraction of copper(II) and silver(I) with TTCTOHA into benzene, octan-1-ol and 1,2-dichloroethane was examined. The results are shown in Table 2. The extraction percentages of copper(II) into benzene and 1-octanol at pH 6.8 were slightly higher than that into 1,2-dichloroethane. On the other hand, the extractability of silver(I) depends closely on the extracting solvent, that is, the extraction of silver(I) into 1,2-dichloroethane, octan-1-ol and benzene at pH > 4.6 was 70, 80 and 45%, respectively. As the dielectric constants of 1,2-dichloroethane, octan-1-ol and benzene are 10.7, 10.3 and 2.3, respectively, the results show that organic solvents having a high dielectric constant are favoured for the extraction of silver(I). Although the dielectric constant of octan-1-ol is lower than that of 1,2-dichloroethane, the extractability of silver(I) into octan-1-ol was higher than that into 1,2-dichloroethane. This may be due to the solvation of the complex with TTCTOHA by octan-1-ol molecules. For the extraction of copper(II), no dependence of the extractability on the dielectric constants of the extracting solvents was observed. Copper(II) was extracted well into benzene, which has a low dielectric constant. As the extractability of ion-pairs generally increases with increase in the dielectric constant of the solvent, in the case of silver(I) the carboxylate ion of TTCTOHA mainly functions as a counter anion. In contrast, it seems likely that for copper(II) the carboxylate ion not only functions as a counter anion but also takes part in the bonding of the copper(II) ion because the extractability is almost independent of the dielectric constants of the extracting solvents.

Table 2
Effect of organic solvent on the extraction of copper(II) and silver(I) with TTCTOH

Metal ion	1,2-Dichloroethane		Octan-1-ol		Benzene	
	pH	$\%E$	pH	$\%E$	pH	$\%E$
Cu(II)	4.6	0.6	4.6	0	4.6	0
	6.2	45.8	6.2	78.2	6.1	70.1
	6.8	87.6	6.8	95.5	6.9	94.2
Ag(I)	2.7	35.6	2.8	58.7	2.7	20.3
	4.6	68.6	4.6	79.9	4.6	46.2
	6.4	67.8	6.3	79.7	6.1	44.6

3.6. Extraction of copper(II) and silver(I) with TTCTOH and / or 1-hexanoic acid

In order to examine how the introduction of a carboxylic acid group into the thiacrown ether molecule affects the extractability of metal ions, the extraction of copper(II) and silver(I) with 5×10^{-3}

Table 3
Extractability of copper(II) and silver(I) with TTCTOH and/or hexanoic acid and TTCTOHA

Reagent (5×10^{-3} M)	Cu(II)				Ag(I)	
	Octan-1-ol		1,2-Dichloroethane		Octan-1-ol	
	pH	%E	pH	%E	pH	%E
TTCTOH	7.4	0 [a]	7.2	0 [a]	5.2	3.3
Hexanoic acid	7.2	2.0	7.2	0 [a]	5.2	0
TTCTOH + hexanoic acid	7.2	4.4 [a]	7.1	3.5 [a]	5.2	4.7
TTCTOHA	6.8	95.5	> 7.0	91.0	4.5	79.9

[a] The recovery was not quantitative.

M TTCTOH and/or 5×10^{-3} M 1-hexanoic acid was carried out. 1-Hexanoic acid and TTCTOH were taken as the carboxylic acid and thioether moieties of TTCTOHA, respectively. Octan-1-ol and 1,2-dichloroethane were used as solvents. The results are shown in Table 3 together with those for extraction with TTCTOHA. Copper(II) was not extracted with TTCTOH alone. Although it has been reported [19] that copper(II) was extracted well with 1-hexanoic acid into octan-1-ol at a high concentration (above 0.5 M) of the reagent, copper(II) was scarcely extracted with 5×10^{-3} M 1-hexanoic acid. Silver(I) was hardly extracted with 5×10^{-3} M 1-hexanoic acid or TTCTOH alone into octan-1-ol. In the extraction with 5×10^{-3} M TTCTOH and 1-hexanoic acid, copper(II) and silver(I) were extracted into the organic solvents to some extent. However, the extraction percentages were very low compared with those with 5×10^{-3} M TTCTOHA. Hence it is clear that the introduction of the carboxylic acid group into the thiacrown ether is very effective for the extraction of metal ions.

Acknowledgements

The authors thank Dr. Motoho Muroi of the Public Health Research Institute of Kobe City for obtaining mass spectra. They thank Miss Masuko Nishinaka of the Department of Chemistry, Faculty of Science, Kobe University, for elemental analyses.

References

[1] K. Saito, Y. Masuda and E. Sekido, Anal. Chim. Acta, 151 (1983) 447.
[2] A. Ohki, M. Takagi and K. Ueno, Anal. Chim. Acta, 159 (1984) 245.
[3] E. Sekido, K. Saito, Y. Naganuma and H. Kumazaki, Anal. Sci., 1 (1985) 363.
[4] E. Sekido, H. Kawahara and K. Tsuji, Bull. Chem. Soc. Jpn., 61 (1988) 1587.
[5] E. Sekido and A. Nakabayashi, Anal. Chim. Acta, 221 (1989) 99.
[6] K. Saito, S. Murakami, A. Muromatsu and E. Sekido, Anal. Chim. Acta, 237 (1990) 245.
[7] K. Chayama and E. Sekido, Anal. Chim. Acta, 248 (1991) 511.
[8] K. Saito, Y. Masuda and E. Sekido, Bull. Chem. Soc. Jpn., 57 (1984) 189.
[9] E. Sekido, K. Chayama and M. Muroi, Talanta, 32 (1985) 797.
[10] M. Muroi, T. Tamiki and E. Sekido, Bull. Chem. Soc. Jpn., 62 (1989) 1797.
[11] M. Muroi and E. Sekido, Anal. Sci., 9 (1993) 691.
[12] W. Rosen and D.H. Bush, J. Am. Chem. Soc., 91 (1969) 4694.
[13] R.A. Bartsch, G.S. Heo, S.I. Kang, Y. Liu and J. Strzerbicki, J. Org. Chem., 47 (1982) 457.
[14] R.A. Bartsch, Y. Liu, S.I. Kang, B. Son, G.S. Heo, P.G. Hipes and L.J. Bills, J. Org. Chem., 48 (1983) 4864.
[15] L.G. Van Uitert and C.G. Haas, J. Am. Chem. Soc., 75 (1953) 451.
[16] R.G. Pearson, J. Am. Chem. Soc., 85 (1963) 3533.
[17] S. Yamada and M. Tanaka, J. Inorg. Nucl. Chem., 37 (1975) 587.
[18] E.R. Dockal, T.E. Jones, W.F. Sockol, R.J. Engerer, D.B. Rorabacher and L.A. Ochrymowycz, J. Am. Chem. Soc., 98 (1976) 4322.
[19] H. Yamada, C. Kato and M. Mizuta, Bull. Chem. Soc. Jpn., 65 (1992) 186.

Analytical Applications of Circular Dichroism

Edited by **N. Purdie** and **H.G. Brittain**

Techniques and Instrumentation in Analytical Chemistry Volume 14

Circular dichroism is a special technique which provides unique information on dissymmetric molecules. Such compounds are becoming increasingly important in a wide variety of fields, such as natural products chemistry, pharmaceutics, molecular biology, etc. The content of this book has been selected in order to feature the unique aspects of circular dichroism, and how these strengths can be of assistance to workers in the field.

Substantial discussions have been provided regarding the particular phenomena associated with dissymmetric compounds which give rise to the circular dichroism effect. Reviews are also given of the type of instrumentation available for the measurement of these effects. A number of chapters cover the wide range of applications illustrating the power of the method.

Owing to its broad appeal, the book will be of interest to workers in all areas of chemistry and pharmaceutical science.

Contents:

© 1994 360 pages Hardbound
Price: Dfl. 355.00 (US $ 202.75)
ISBN 0-444-89508-6

ORDER INFORMATION

For USA and Canada
ELSEVIER SCIENCE INC.
P.O. Box 945
Madison Square Station
New York, NY 10160-0757
Fax: (212) 633 3880

In all other countries
ELSEVIER SCIENCE B.V.
P.O. Box 330
1000 AH Amsterdam
The Netherlands
Fax: (+31-20) 5862 845

US$ prices are valid only for the USA & Canada and are subject to exchange rate fluctuations; in all other countries the Dutch guilder price (Dfl.) is definitive. Customers in the European Community should add the appropriate VAT rate applicable in their country to the price(s). Books are sent postfree if prepaid.

ELSEVIER SCIENCE B.V.

Send your article on floppy disk!

All articles may now be submitted on computer disk, with the eventual aim of reducing production times and improving the reliability of proofs still further. Please follow the guidelines below.

With revision, your disk plus one final, printed and exactly matching version (as a printout) should be submitted together to the editor. **It is important that the file on disk to be processed and the printout are identical.** Both will then be forwarded by the editor to Elsevier.

The accepted article will be regarded as final and the files will be processed as such. Proofs are for checking typesetting/editing: only printer's errors may be corrected. No changes in, or additions to the edited manuscript will be accepted.

Illustrations should be provided in the usual manner and, if possible, on a **separate** floppy disk as well.

Please follow the general instructions on style/arrangement and, in particular, the reference style of this journal as given in the "Guide for Authors".

The preferred storage medium is a 5¼ or 3½ inch disk in MS-DOS or Macintosh format, although other systems are also welcome.

Please label the disk with your name, the software & hardware used and the name of the file to be processed.

For further information on the preparation of compuscripts please contact:

Elsevier Science B.V.
Analytica Chimica Acta
P.O. Box 330
1000 AH Amsterdam, The Netherlands
Phone: (+31-20) 5862 791 Fax: (+31-20) 5862459

ELSEVIER
SCIENCE

PUBLICATION SCHEDULE FOR 1995

	O'94	N'94	D'94	J	F	M	A	M	J	J	A	S
Anal. Chim. Acta	296/2 296/3 297/1–2	297/3 298/1 298/2	298/3 299/1 299/2	299/3 300/1–3 301/1–3	302/1 302/2–3 303/3							
Vib. Spec.		8/1		8/2		8/3		9/1		9/2		9/3

INFORMATION FOR AUTHORS

Detailed "Instructions to Authors" for *Analytica Chimica Acta* was published in Volume 289, No. 3, pp. 381–384. Free reprints of the "Instructions to Authors" of *Analytica Chimica Acta* and *Vibrational Spectroscopy* are available from the Editors or from: Elsevier Science B.V., P.O. Box 330, 1000 AH Amsterdam, The Netherlands. Telefax: (+31-20) 4852 459.

Manuscripts. The language of the journal is English. English linguistic improvement is provided as part of the normal editorial processing. Authors should submit three copies of the manuscript in clear double-spaced typing on one side of the paper only. *Vibrational Spectroscopy* also accepts papers in English only.

Rapid publication letters. *Letters* are short papers that describe innovative research. Criteria for letters are novelty, quality, significance, urgency and brevity. Submission data: max. of 2 printed pages (incl. Figs., Tables, Abstr., Refs.); short abstract (e.g., 3 lines); *no* proofs will be sent to the authors; submission on floppy disc; *no* revision will be possible.

Abstract. All papers, reviews and letters begin with an Abstract (50–250 words) which should comprise a factual account of the contents of the paper, with emphasis on new information.

Figures. Figures should be suitable for direct reproduction and as rich in contrast as possible. One original (or sharp glossy print) and two photostat (or other) copies are required. Attention should be given to line thickness, lettering (which should be kept to a minimum) and spacing on axes of graphs, to ensure suitability for reduction in size on printing. Axes of a graph should be clearly labelled, along the axes, outside the graph itself.

All figures should be numbered with Arabic numerals, and require descriptive legends which should be typed on a separate sheet of paper. Simple straight-line graphs are not acceptable, because they can readily be described in the text by means of an equation or a sentence. Claims of linearity should be supported by regression data that include slope, intercept, standard deviations of the slope and intercept, standard error and the number of data points; correlation coefficients are optional.

Photographs should be glossy prints and be as rich in contrast as possible; colour photographs cannot be accepted. Line diagrams are generally preferred to photographs of equipment. Computer outputs for reproduction as figures must be good quality on blank paper, and should preferably be submitted as glossy prints.

Nomenclature, abbreviations and symbols. In general, the recommendations of IUPAC should be followed, and attention should be given to the recommendations of the Analytical Chemistry Division in the journal *Pure and Applied Chemistry* (see also *IUPAC Compendium of Analytical Nomenclature, Definitive Rules*, 1987).

References. The references should be collected at the end of the paper, numbered in the order of their appearance in the text (*not* alphabetically) and typed on a separate sheet.

Reprints. Fifty reprints will be supplied free of charge. Additional reprints (minimum 100) can be ordered. An order form containing price quotations will be sent to the authors together with the proofs of their article.

Papers dealing with vibrational spectroscopy should be sent to: Dr J.G. Grasselli, 150 Greentree Road, Chagrin Falls, OH 44022, U.S.A. Telefax: (+1-216) 2473360 (Americas, Canada, Australia and New Zealand) or Dr J.H. van der Maas, Department of Analytical Molecular Spectrometry, Faculty of Chemistry, University of Utrecht, P.O. Box 80083, 3508 TB Utrecht, The Netherlands. Telefax: (+31-30) 518219 (all other countries).

0003-2670/94/$07.00

Organic Reactions

Equilibria, Kinetics and Mechanism

By **F. Ruff** and **I.G. Csizmadia**

Studies in Organic Chemistry Volume 50

This book begins with a brief survey of non-kinetic methods, and continues with kinetic methods used for the elucidation of reaction mechanisms. It is method oriented and therefore deals with the following topics: basic principles of reaction kinetics; Structure and reactivity relationships; isotope effects; acids, bases, electrophiles and nucleophiles; and concludes with homogeneous catalysis.

Rigorous mathematical descriptions of the basic principles are provided in a clear and easily understandable form. The book is more comprehensive than many physical organic texts and it is supported by an extensive list of references. It also contains a valuable collection of problems.

Contents: 1. Introduction. 2. Non-kinetic Method for the Elucidation of Reaction Mechanisms. Stoichiometry and reaction mechanisms. Structure of products. Structure of intermediates. Stereochemical experiments. Isotopic labeling experiments. Crossover experiments. **3. Energetics of Chemical Reactions.** Nomenclature of thermodynamic potential functions. Thermodynamic requirements for chemical reactions. Kinetic requirements for chemical reactions. The principle of microscopic reversibility. Kinetic and thermodynamic control. **4. Kinetics of Elementary Reactions.** Basic principles of reaction kinetics. The integrated rate equation. Pseudo-orders of simplified rate equations. Numerical determination of reaction order and rate constants from experimental data. **5. Kinetics of Complex Reactions.** Reversible reactions. Parallel reactions. Consecutive reactions. Approximate methods for analyzing complex reactions. Conclusions. Examples. **6. Theories of Chemical Reactions.** Temperature dependence of chemical equilibria. Temperature dependence of reaction rates. Collision theory. Transition-state theory. Structure of activated complexes. Entropy of activation. Enthalpy of activation. The isokinetic relationship. Volume of activation. **7. Structure and Reactivity Relationships.** The Hammett equation. The linear free-enthalpy relationship. The application of Hammett equation to multistep reactions. The σ^+, σ^-, and σ_0 substituent constants; the Yukawa-Tsuno equation. Separation of inductive and resonance effects. Separation of electronic and steric effects. **8. Isotope Effects.** Isotope effects on equilibria. Theory of kinetic isotope effect. Primary kinetic isotope effect. Secondary kinetic isotope effects. Solvent isotope effect. **9. Environmental Effects.** The structure of liquids. Solvation. Solvent effects in chemical equilibria. Solvent effect in chemical kinetics. Solvent effect on reaction rates. Specific solvation effects on reaction rates. Empirical solvent-polarity parameters. Salt effects. **10. Acids, Bases, Electrophiles and Nucleophiles.** Strengths of Brønsted acids and bases. Structural effects on Brønsted acidity and basicity. Solvent effect on acidity and basicity. Acidity of solvents and acidity functions. Very weak acids. Superacids. Lewis acids and Lewis bases. Nucleophiles and electrophiles. **11. Homogeneous Catalysis.** Acid-base catalysis. Rates of proton-transfer reactions. Brønsted's law of catalysis. Reactions in strongly acidic media. Nucleophilic catalysis. Electrophilic catalysis. Neighboring group participation and intramolecular catalysis. Micellar catalysis. Enzymic catalysis.

ELSEVIER SCIENCE

© 1994 480 pages Hardbound
Price: Dfl. 380.00 (US$ 217.25)
ISBN 0-444-88174-3

ORDER INFORMATION
ELSEVIER SCIENCE B.V.
P.O. Box 330
1000 AH Amsterdam
The Netherlands
Fax: (+31-20) 5862 845

For USA and Canada
P.O. Box 945
Madison Square Station
New York, NY 10159-0945
Fax: (212) 633 3680

US$ prices are valid only for the USA & Canada and are subject to exchange rate fluctuations; in all other countries the Dutch guilder price (Dfl.) is definitive. Customers in the European Union should add the appropriate VAT rate applicable in their country to the price(s). Books are sent postfree if prepaid.

0003-2670(19941220)299:1;1-3